STRUCTURAL DETERMINATIONS OF PENNSYLVANIA ANTHRACITES

Peter J. Pappano, Jonathan P. Mathews, Harold H. Schobert
The Energy Institute
The Pennsylvania State University
University Park, PA 16802

KEYWORDS: Anthracite, Molecular Modeling, Coal Structure

INTRODUCTION

Four Pennsylvania anthracites were selected for analysis, based on their availability from currently active mines and presumed geological differences. A battery of experiments was performed on these samples to determine their physical and chemical properties. The data collected from these experiments was used as input for modeling the structure of anthracite using Cerius[2], a Molecular Simulations Incorporated (MSI) software package. Visualization of anthracite structure is useful in visualizing the reactions necessary to produce advanced carbon materials, such as graphite, from anthracite.

EXPERIMENTAL

The anthracites come from the Harmony, Jeddo, LCNN, and Summit mines, all of which mine the Eastern Middle Field of Pennsylvania. LCNN and Jeddo mine the Mammoth vein; Harmony, the Lykens Valley #2; and Summit, the Tracey vein. No blending of coals is done at these plants, ensuring repeatability of data collected on the anthracites. Approximately 1000 lbs. of each anthracite were collected and a subset homogenized using techniques outlined by Glick and Davis of the Penn State Coal Sample Bank and Data Base [1]. The end products of this process were aliquots of –20 and –60 (U.S. Standard Sieve) mesh anthracite stored in foil laminate bags under an argon atmosphere [1]. Next, chemical and physical data were collected using X-ray diffraction, ^{13}C NMR, proximate and ultimate analysis, maceral point counts, CO_2 surface area, and helium density. Values for aromaticity, H/C ratio, and interlayer spacing were used in generating possible anthracite structures using MSI software [2].

RESULTS

Ultimate and proximate analysis results are presented in Table 1 and Table 2, respectively. With increasing carbon content there is a decrease in the hydrogen content, as expected. This is indicative of ring condensation with concurrent loss of hydrogen. When normalized to 100 carbon atoms, Summit has the highest hydrogen content with 32 hydrogens per 100 carbon atoms while LCNN has the lowest with 19 hydrogen atoms per 100 carbon atoms. Table 2 shows relatively equal amounts of ash and volatile matter, except for the Summit anthracite, which has nearly twice the levels of ash in comparison to the other samples. High levels of mineral matter, as indicated by high levels of ash, are undesirable for graphite production [3]. The maceral compositions are shown in Table 3. The category "other inertinite" was used when the optical differences between fusinite and semi-fusinite could not be distinguished. Maceral composition is usually an important parameter as macerals are known to have different chemical structures which may lead to different levels graphitizability [4]. X-ray diffraction, diffractogram shown in Figure 1, was used to determine the distance between aromatic sheets in d-spacing. The XRD diffractogram of the Jeddo sample indicates d-spacings range from 12.91 to 2.57 nm in the identifiable peaks. ^{13}C Single Pulse NMR, Figures 2, was used to determine the aromaticity of the samples. All the anthracites studied where found to be 100% aromatic.

DISCUSSION

Using the chemical data, a hypothetical structure for the Jeddo anthracite was generated and minimized using molecular mechanics (Drieding force-field [5]), see Figure 3. The parameters utilized in generation of the model were %H, %N, %O, d-spacing, aromaticity, and number of rings in an aromatic, or pre-graphitic sheet. The atomic H/C ratio determined from the ultimate analysis (H/C=0.22) and calculated from the model (H/C=0.22) are in agreement. Unfortunately, the relative proportions of quartenary, pyrollic, and pyridinic nitrogen have not been determined for anthracite. Therefore it was assumed the nitrogen was present primarily in the quartenary form (9 of the 11 nitrogens are quartenary in Figure 3), presumably from the condensation of smaller pyridinic containing sheets. Oxygen was assumed to be in open or closed ethers with perhaps some carbonyl. As there are only 18 heteroatoms per 1010 carbons in the proposed anthracite, any errors in their assignments will have a minimal impact on the gross structure of the model. However, their assignments and placements may well have a bearing on the reactivity of the structure.

Past research has shown graphitized anthracites have crystallite heights of <36.8 nm, therefore the raw anthracite modeled here was generated with heights significantly lower than 36.8 nm [6]. The anthracite model shown in Figure 3 is approximately 45 Å across (plan view) and approximately 15 Å high. Average d-spacings between the sheets fall within the acceptable experimentally determined range, approximately 4 Å. However, the structure shown has not been subjected to molecular dynamics (thus may be trapped in a local minimum) nor does the force-field used contain an implicit π - π interaction term. Furthermore, the model was minimized in a vacuum and has not experienced high pressures or interactions with neighboring sheets, which may be important in the overall structural alignment. Hence the structural representation is a product of less accurate modeling methods (due to model size restrictions on quantum mechanics and computational expense).

Ring condensation in anthracite is believed to be between >10 and 100 (rings per sheet) [7], so the number of rings in a polycyclic sheets shown in Figure 3 is a maximum of 91 and minimum of 47 rings. Combining the chemical data with stated assumptions resulted in a simplistic structure for the Jeddo anthracite, Figure 3. The model contains five pre-graphitic planes with an average of 81 rings comprising a sheet. The beginnings of graphitic stacking are apparent, Figure 3. The aromaticity of the model is 99%, while the experimentally determined aromaticity is 100%. Recall that the model is in agreement with the elemental composition. Hence the model is in close agreement with the chemical data determined to date. Incorporation of physical data, such as helium density, and additional chemical data will further refine the structure [8].

CONCLUSIONS

The coals selected for this research are all in the anthracite range, yet exhibit varied chemical properties (mostly hydrogen content, maceral composition and degree of crystallinity) presumably as a result of different geological histories. It may be assumed that the graphitizability of these samples will vary with their constitution. These differences can be better presented through visualization of the anthracite's structure and its changes upon carbonization. A model structure for Jeddo anthracite is presented. Incorporation of additional physical and chemical data will further refine the proposed model.

REFERENCES

1. Glick, D.C. and Davis, A., Operation and composition of the Penn State Coal Sample Bank and Data Base. Organic Geochemistry 1991;17(4):421-430
2. MSI, Molecular Simulations Incorporated. Cerius^2 Version 3.5, San Diego CA 1998
3. Zeng, S. M., Rusinko, F, Schobert, H. H., Producing High-quality Carbon and/or Graphite Materials from Anthracite by Catalytic Graphitization, PEDA, 9303-4019, 1996
4. Taylor, G. H., Teichmuller, M., Davis, A., Diessel, C. F. K, Littke, R., Robert, P., Organic Petrology. Berlin Germany: Gebruder Borntraeger. 1998: 112
5. Mayo, S. L., Olafson W.L., Goddard W.A., Drieding: A generic force-field for molecular simulations. J. Phys. Chem. 1990;94:8897-8909
6. Atria, J., Novel Approach To The Production Of Graphite From Anthracite, The Pennsylvania State University, MS thesis, 1994
7. Schobert H.H. The Chemistry of Hydrocarbon Fuels. London UK: Butterworths. 1990:112
8. Faulon J.L., et al. Correlation between micropore and fractal dimension of bituminous coal based on computer generated models. Energy & Fuels 1994;8(2):408-415

Table 1. Ultimate Analysis Of Anthracite Samples*

Anthracite	% C	% H	% N	% S	% O (by diff.)
LCNN	95.7	1.5	1.2	0.5	1.0
Jeddo	95.2	1.8	1.1	0.6	1.3
Harmony	94.0	2.2	1.0	0.5	2.3
Summit	93.2	2.5	1.6	0.6	2.2

*dry ash-free basis

Table 2. Proximate Analysis Of Anthracite Samples

Anthracite	% Moisture	% Volatiles	% Ash	Fixed Carbon
LCNN	3.3	4.5	6.7	88.3
Jeddo	4.7	6.1	8.1	85.9
Harmony	4.6	7.5	6.6	86.2
Summit	2.6	11.1	17.6	71.2

Table 3. Maceral Percentages (from point counts)

Anthracite	Vitrinite	Fusinite	Semi-fusinite	Other Inertinite	Liptinite
LCNN	80	10	7	2	1
Jeddo	86	6	5	2	1
Harmony	60	24	14	1	1
Summit	80	15	4	0.5	0.5

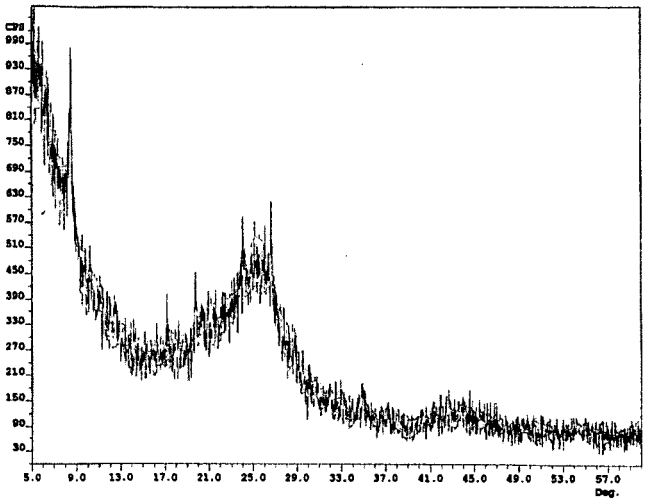

Figure 1. XRD Diffractogram Of Jeddo Anthracite

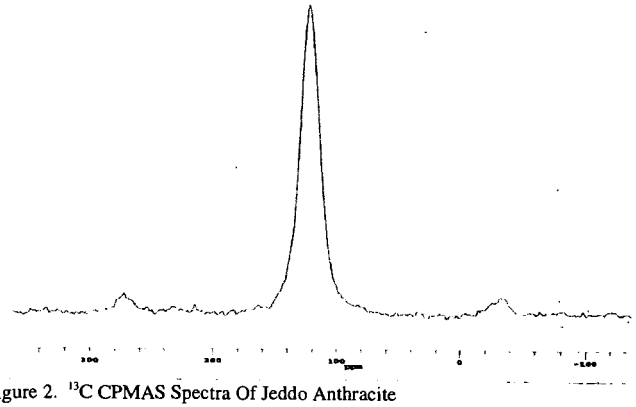

Figure 2. ^{13}C CPMAS Spectra Of Jeddo Anthracite

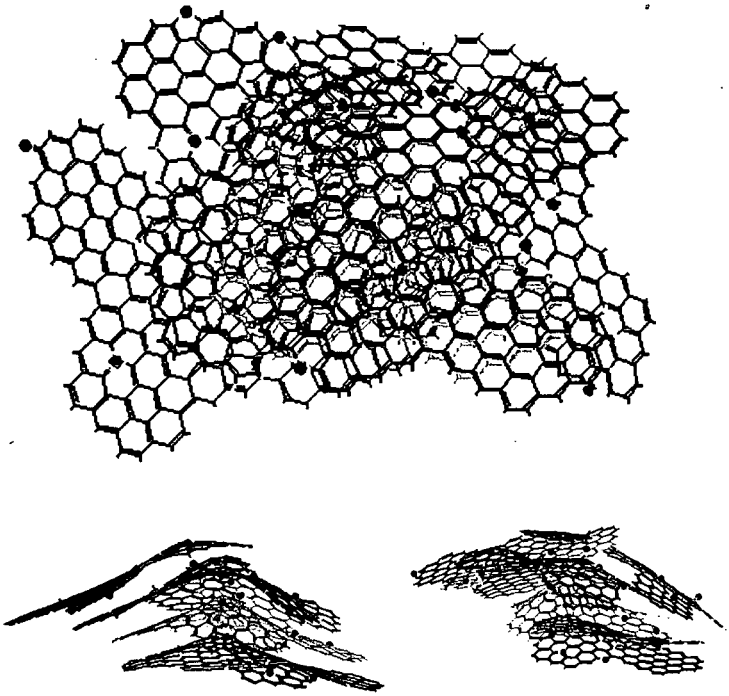

Figure 3. Plan And Side Views Of A Simplistic Model Of Jeddo Anthracite. $C_{1010}H_{223}O_9N_9$ Heteroatoms shown as spheres.

VERIFICATIONOF THE AIDA'S CHEMICAL DETERMINATION METHOD FOR OXYGEN-FUNCTIONALITY IN COAL AND COAL PRODUCT

Tetsuo Aida, Aiko Nishisu, and Issei Yamanishi
Department of Industrial Chemistry, Faculty of Engineering in Kyushu, Kinki University
11-6 Kayanomori, Iizuka, Fukuoka 820, JAPAN

Keywords: Coal, carboxylic acid functionality, phenolic hydroxyl functionality, non-aqueous titration

INTRODUCTION

Coal contains various type of chemical functionality. It is believed that the oxygen-containing functionality in coal plays very important role to control its physical and chemical properties. Particularly, since a carboxylic acid and phenolic hydroxyl functionality have a relatively strong acidic characteristic comparing with other functionality such as alcoholic hydroxyl functionality, they can induce strong cohesive forces like a hydrogen bonding, which seems to be responsible to determine many characteristics of coal based on the macromolecular network structure. Thus, it is critical to have the quantitative information about such functionality as carboxylic acid and phenolic hydroxyl functionality in coal or coal product in order to develop the efficient chemical transformation processes of coal such as a liquisaction, gasification, chemical desulfurization, etc..

It has long been a common sense in the coal science community that the hydrogen bonding contribution by carboxylic acid functionality to the chemical and physical property of coal could be almost negligible toward the high ranked coals like a bituminous coal, simply because of the very small amount of the functionality, which used to be determined by the chemical method developed by Blom et al.[1] about 40 years ago.

Although the recent development of sophisticated instrumentation such as FT-IR, ^{13}C-NMR, XPS, etc., has made it possible to provide quite reliable information about such hetero-atom-functionality as sulfur-, nitrogen- and oxygen-containing functionality, they still seem to fall into a common problem, that is, the low accuracy to determine a small amount of the functionality.

Recently, we had developed a chemical method [2], using following chemical reactions.

$$\text{R-COOH} + \text{n-Bu}_4\text{NBH}_3 \xrightarrow[\text{in pyridine solvent}]{} \text{R-COOn-Bu}_4\text{N} + \text{BH}_3 + \text{H}_2$$

(R = Aryl, Alkyl)

This method has several advantages compared to the conventional one mentioned above.

First of all, this reaction proceeds quantitatively with a single step in pyridine solution generating a gaseous product, H_2, which, gives us much better accessibility of the chemical reagent to the carboxylic acid functionality buried into macromolecular network structure of coal than in aqueous solution reaction(cf. Blom's method) based on the swelling behavior, and also a reasonable accuracy due to the volumetric determination of the gaseous product (H_2).

Secondly, this reaction exhibits a significant difference of the reaction rate depending upon the acidity of functionality, which makes easy to distinguish other functional groups such as phenolic and alcoholic hydroxyl functionality by using more reactive chemical reagents. Figure 1 demonstrates one of the examples of our experiment [3], which were carried out by using $n\text{-Bu}_4\text{NBH}_4$, $LiBH_4$ and $LiAlH_4$ as reactants, and determined the distribution of oxygen functionality in the pyridine extract of coal. Although we have not enough data concerning the difference of functionality between coal and pyridine extract at present moment, 8.0fold difference between our data and previous one [4] seems to be too much and quite interesting.

Most striking experimental result came out from the –COOH determination for various kind of coals, as shown in Figure 2, which demonstrates the coal rank dependency of the –COOH content, comparing the data previously reported[5]. Very interestingly, there is a quite large discrepancy in the range of high rank coal. This fact convinced us that our approach to develop more reliable chemical determination method could be right, because the coal swelling in water used to be dramatically decreased over higher rank region than sub-bituminous coal.

As Niksa pointed out in his recent personal communication and paper [6], it was well-known contradiction that the most of the CO_2 released during the pyrolysis of sub-

bituminous and bituminous coals could not be rationalized with the uni-molecular decomposition chemistry of carboxylic acid functionality in coals. Because the amount of carboxylic acid functionality reported in the raw coal was too small to handle it.

In order to verify the analytical data obtained by our new methodology, we have conducted a non-aqueous titration as an alternative method. In this paper, we like to report the experimental results

EXPERIMENTAL

The chemical reagents were commercial products (Aldrich's gold label grade) which were used without further purification. Pyridine for the chemical determination of carboxylic acid functionality was dried over calcium hydride and distilled before use.

Coals from the Argonne National Laboratory (premium) and the Ames Coal Library were ground, seized, and dried with a silica-gel at room temperature under vacuum for three days, and stored under a dry nitrogen atmosphere. The pyridine extract of coal was prepared by means of the ultrasonic irradiation method [7].

A typical procedure of the non-aqueous titration of carboxylic acid and phenolic hydroxyl functionality in coal extract was as follows: 100mg of coal extract was dissolved in 5.0ml of dried pyridine, and placed into a Pyrex cell under N_2-atmosphere which has an Pt-electrode and magnetic stirrer. The solution was potentiometrically titrated with a pyridine solution of n-Bu_4NOH (0.1mol/l).

RESULTS AND DISCUSSION

1. Non-aqueous titration of model compounds

Benzoic acid and 2-naphthol were used as model compounds for carboxylic acid and phenolic hydroxyl functionality, respectively. The non-aqueous titration of each functionality was carried out in pyridine solution by using n-Bu_4NOH (0.1mol/l) pyridine solution as a titrant. The reaction is considered to proceed with following chemical equations.

$$\text{-COOH(or Ph-OH)} + \text{n-Bu}_4\text{N}^+\ \text{OH}^- \longrightarrow \text{-COO}^-\text{n-Bu}_4\text{N}^+ + \text{H}_2\text{O}$$

Figure 3 shows the dependence of a potential difference on the titrant volume observed in the determination of individual model compounds, benzoic acid and 2-naphthol, and that of these mixture is shown in Figure 4. Obviously, there are two inflection points on the titration curves of mixture, and it was confirmed that they were appearing at exactly right volume of the titrant corresponding to the concentration of carboxylic acid (the first inflection point) and the sum of both compounds (the second inflection point), respectively.

2. Non-aqueous titration of pyridine extract of coal

Based on the results obtained from the model compound experiment described above, the determination of carboxylic acid and phenolic hydroxyl functionality in the pyridine extract of Pittsburgh No.8 coal has been performed by using the same procedure. The results demonstrated in Figure 5 and 6

Comparing with model compounds experiments mentioned above, a characteristic feature seems to be the difficulty to judge one of the two inflection points, which is thought to be due to the carboxylic acid functionality in coal extract. Although the reason of this phenomenon is not clear at this moment, the indistinct pKa distribution due to heterogeneous carboxylic acid functionality in coal may be responsible for that.

Anyway, the concentration of carboxylic acid and phenolic hydroxyl functionality in the pyridine extract of Illinois No.6 coal was determined by the same manor as shown in Figure 6, and they are compared in Table 1with those obtained from our chemical method (Aida's method) previously reported[2].

It is quite interesting that the values calculated from the two infection points seems to be reasonably matched with those of the chemical determination. Particularly, we have convinced the matching between the sum of carboxylic acid and phenolic hydroxyl functionality determined by the chemical method ($LiBH_4$) and the value obtained from the second inflection point, which used to be clear and have no difficulty to find out.

3. Non-aqueous titration of pyridine extract of coal with internal standard

In order to verify the data obtained by the non-aqueous titration, we may be able to use an internal standard compound. Namely, the addition of a standard compound, such as phthalic acid into the coal extract solution will force to shift the two inflection points with the titrant volume corresponding to the amount of the standard compound, if the identification of two inflection points was correct.

In Figure 7, the experimental results obtained were shown. Expectedly, the inflection points were shifted with exact amount of the titrant volume corresponded to phthalic acid.

CONCLUSION

A chemical determination method (Aida's method) for the oxygen containing functionality in coal and coal product has been verified by using an alternative analytical technique, "non-aqueous titration".

It seems to be a very serious mischief concerning the content of the carboxylic acid functionality in higher rank coals than sub-bituminous coal in previous literatures, which used to be reported as a almost negligible amount. In according with our chemical determinations the content of carboxylic acid functionality in Illinois No.6 coal reach up to 5times more than previous data.

AKNOWLEDGEMENTS

A part of this research was supported by the grant from The Japanese Ministry of Education through The 148th Committee on Coal Utilization in The Japan Society of Promotion of Science (JSPS).

REFERENCES

(1) Blom, L., Edelhausen, L., and van Krevelen, D.W., Fuel, **36**, 135(1957)
(2) Aida, T, et al., Prepr. Am. Chem. Soc. Div. Fuel Chem., **41**(2), 744(1996)
(3) Yoneda, M., Yamanishi, I., Aida, T., Prepr., Sekitan Kagaku Kaigi (Japanese), 97(1998)
(4) For instance, the content in the Shinn's model, Fuel, **63**, 1187(1984)
(5) Jung, B., Stachel, S.J., and Aalkins, W.H., Pap. Am. Chem. Soc., Div. Fuel Chem., 36 869(1991)

(6) Niksa, Stephen, Energy & Fuels, **10**, 173(1996); Solomon, P. R., et al., Energy & Fuels, **4**, 319(1990)
(7) After irradiation with ultrasonic wave for 3hous at room temperature, the suspension of powdered coal and excess amount of piridine was filtrated by using the Memblem Filter (5μm) under pressure.

Table 1. Functionality analyses of pyridine extract of Illinois No.6 coal

Functionality	Aida's method	Non-aqueous titration
	(mmol / g)	
-COOH	0.83 (n-Bu4NBH4)	0.88 (1st inflection point)
Ph-OH + -COOH	2.90 (LiBH4)	2.76 (2nd inflection point)

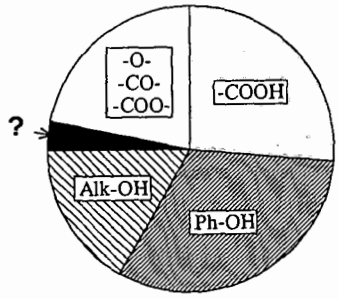

Figure 1. Distribution of oxygen functionality in pyridine extract of Illinois No.6 based on total oxygen

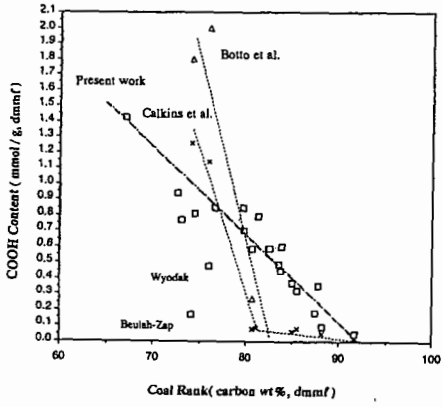

Figure 2. Correlation between content of carboxylic acid functionality and coal rank

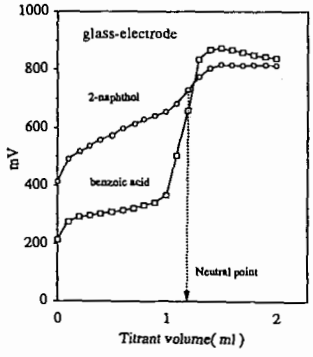

Figure 3. Non-aqueous titration of model compound

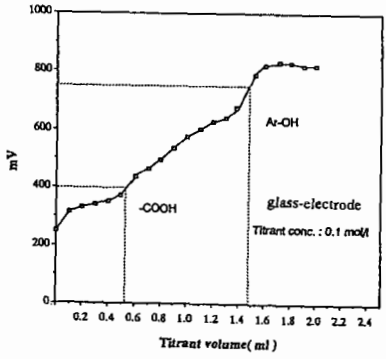

Figure 4. Non-aqueous titration of model compound mixture

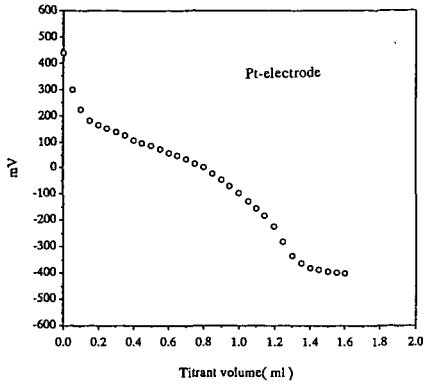

Figure 5. Non-aqueous titration of pyridine extract of Pittsburgh No.8

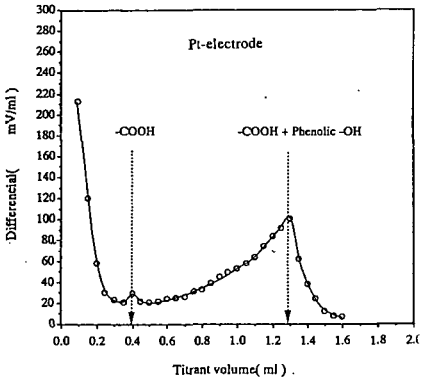

Figure 6. Non-aqueous titration of pyridine extract of Pittsburgh No.8

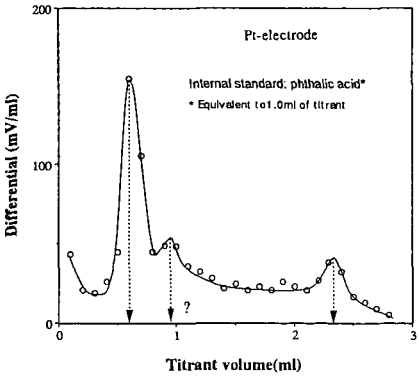

Figure 7. Non-aqueous titration of pyridine extract of Pittsburgh No.8 with internal standard

TIME RESOLVED SMALL ANGLE X-RAY SCATTERING REACTIVITY STUDIES ON COALS, ASPHALTENES, AND POLYMERS

R. E. Winans, S. Seifert, and P. Thiyagarajan[†]
Chemistry Division and [†]Intense Pulsed Neutron Source Division
Argonne National Laboratory, Argonne, IL 60439

Keywords: Argonne Premium Coals, pyrolysis small angle X-ray scattering

ABSTRACT

The objective of this study is to examine changes in the structures of coals, asphaltenes, and polymers in situ with small angle X-ray scattering (SAXS) during thermal treatments. We have built a SAXS instrument at the Basic Energy Sciences Synchrotron Radiation Center at the Advanced Photon Source that allows us to obtain scattering data on very small samples and in the millisecond time domain. The Argonne Premium Coal samples, petroleum derived asphaltenes, and polymers with functionality to model fossil fuels were used in this study. The information that can be derived from these experiments includes: changes in fractal dimensionality, surface topology, and size and type of porosity. The information is correlated with other methods on the same samples.

INTRODUCTION

Small angle scattering is a good method to observe features such as porosity and surface properties of disordered systems over broad length scales. This non-destructive technique is useful for in situ analysis and with the advent of third general light sources with high photon flux, rapid data acquisition is possible. The nature of the porosity of a suite of 15 coals has been studied by SAXS and the results compared to adsorption techniques.[1] Coal pyrolysis followed by gasification has been followed by SAXS. They found that upon pyrolysis there was an increase in micro and meso pores.[2] SAXS investigation of pore sizes of Canadian coals and their chars showed that reactive chars from low rank coals have greater pore volumes compared to the coals, while the opposite effect is seen for less reactive chars from higher rank coals.[3] The fractal pore structure of raw and heated brown coals was studied by SAXS.[4] All of these were done with lab instruments. Synchrotron sources allowed faster data acquisition such that in situ experiment are facilitated such as the dynamics of solvent swelling.[5] The Argonne coals have been looked at by a number of temperature programmed techniques such as TGA-FTIR,[6] TGA-MS,[7] Py-FIMS,[8] Py HRMS,[9] PMRTA,[10] and IGC.[11] These results will be used to help interpret data from temperature programmed (TP) SAXS of the Argonne Coals, resids, and polymers.

EXPERIMENTAL

The eight Argonne Premium Coal Samples were used without modification in this study.[12] The ethylene [I] and oxymethylene [II] linked polymers have been used as possible models.[13,14] More recent studies have looked at ethylene linked benzene with [III] and without carboxylic acid groups [IV].[15,16] The purpose of this later study was to examine the possible role of carboxylic acids to form crosslinks in low rank coal pyrolysis. The SAXS instrument was constructed at ANL and used on the Basic Energy Sciences Synchrotron Radiation Center CAT undulator beamline ID-12 at the Advanced Photon Source (http://www.bessrc.aps.anl/).

Quartz capillaries (1 mm) were used to sample 5 mg of -100 mesh coal or polymer. Scattering patterns were obtained as the sample is heated from 25-600 °C. Monochromatic X-rays (8.5 - 23.0 keV) are scattered off the sample and collected on a 19 x 19 cm^2 position sensitive two-dimensional gas detector. More recent data are taken using a 9-element mosaic CCD detector (15 x 15 cm) with maximum of 3000 x 3000 pixel resolution. An advantage of this new detector is that unlike the wire detector, the full beam from the undulator can be used which gives a factor of 1000 increase in intensity. The scattered intensity has been corrected for absorption, the empty capillary scattering, and instrument background. The differential scattering cross section has been expressed as a function of the scattering vector Q, which is defined as $Q = (4\pi/\lambda) \sin\theta$, where λ is the wavelength of the X-rays and θ is the scattering half angle. The value of Q is proportional to the inverse of the length scale ($Å^{-1}$). The instrument was operated with two different sample-to-detector distances, 68.5 cm to obtain data at $0.04 < Q < 0.7$ $Å^{-1}$ and 3740 cm to measure at $0.006 < Q < 0.1$ $Å^{-1}$.

Small Angle X-ray Scattering

A typical plot of the time temperature-resolved data for the pyrolysis of the Illinois No. 6 bituminous coal (APCS 3) is shown in Figure 1. These curves can be analyzed to determine size of features,

topology, and changes in total scattering. Power law slope from the data, such as is shown in Figure 1, are used to describe the topology of the system. Finally, the invariant Q_0 is calculated and is proportional to the fluctuation of the electron density in the system. Changes in the invariant are useful in monitoring topological changes in the sample, $Q_0 = \int_0^\infty I(Q)\, Q^2\, dQ$. For example, the invariant goes to zero for a homogeneous system that does not have any concentration fluctuation.

RESULTS AND DISCUSSION

The results from the TP SAXS are initially best understood by comparing them to results from other techniques and by looking at the various trends observed between the different rank premium coals. An example of the scattering curves as a function of Q is shown in Figure 1 for the Illinois bituminous coal (APCS 3). To avoid confusion, a few selected curves are drawn to represent the changes seen as the sample heats up. An obvious feature that is seen for the low rank coals but is most pronounced with the Illinois coal is the increase in scattering over an intermediate temperature range. This result is best observed in the changes of the invariant with temperature which is shown in Figure 2. There is a rapid increase in the Q_0 at ~130 °C where most likely water is being driven off. This could result from structural reorganization of the macromolecules in coal. These structural changes are common with the coals of < 80% carbon, but are not seen in the higher rank coals. However, the role of water release is not the only factor since the lignite and subbituminous coals have a greater water content and yet the effect is much less. The structure change is more than just a physical swelling of the structure since the free swelling index of this coal (4.8) is much less than, for example, the Upper Freeport (APCS 1), which has a FSI of 8.5.[12]

With the Upper Freeport, the increase in Q_0 is not observed, but instead shows the transitions at the softening and fluidity points. Normally the approaches used to look at these transitions are plasticity or fluidity measurements and inverse gas chromatography (IGC). A comparison of the SAXS and ICC data are shown in Figure 3. One expects the IGC transition to occur at a lower temperature since the heating rate was in hours compared to the total heating time of 10 min. for the SAXS data. However, note that the slope is the same (dashed line). In IGC, this slope is used to calculate the enthalpy of adsorption which for APCS 1 is 12.5 kcal/mole.[11] These values increase with rank of the coal in the bituminous range. The trend in Q_0 is also similar and is indicative of the increase in homogeneity of the system at these temperatures as the coals are becoming fluid. The low rank coals which do not become fluid show much different trends in Q_0 at these higher temperatures.

The changes in the power law slope can be correlated with TGA results under the same heating rates. For bituminous coals, such as the Illinois No. 6 and Pocahontas, there is a reasonable correlation as shown in Figure 4. However, for the low rank coals, the changes in d_f is much different and actually may have increased instead of decreasing with temperature as seen in the higher rank coals. One possible explanation for this is the fact that these coals are still early in the coalification process and what may be occurring is an accelerated coalification process. Part of this process may be the establishment of increased crosslinks instead of decreasing crosslinks, which normally occurs in the pyrolysis of bituminous coals. This has been suggested in other studies.[15] Recently, model polymers with carboxylic acid functionality have been studied to try to understand this crosslinking phenomena. Later, we will discuss the results of TP SAXS on the polymer.

In Utah coals (APCS 6), the d_f decreased at a much lower temperature than the other bituminous coals. This has also been observed for this coal by proton magnetic resonance thermal analysis (PMRTA). It has been suggested that the increased mobility observed is due to the liptinite macerals in this coal (which is rich with resinites, 75%) at lower temperatures. Our SAXS data would confirm this conclusion. The volatile release of the coal is not unusual but the increase in extractability with heating is much greater than other bituminous coals of similar rank. The resinite must have a synergistic effect on overall thermal degradation of the macromolecular matrix.

To better understand TP SAXS results for the coal samples, four polymers which represent various potential structures and functionality in coals have been examined under the same conditions as the coal pyrolysis. For both the naphthalene based polymers [I] and [II], the structure changes at much lower temperatures than coals. However, as expected, the oxymethylene linked polymer [II] is the most reactive. In both polymers, a broad feature between Q = 0.1 to 0.3 emerges at high temperature which would be the formation of larger polycyclic aromatics. The PyHRMS has shown that these polymers, especially [II] undergo secondary reactions to form strong Ar-Ar links which can lead to larger polycondensed aromatics.

The polymers from ORNL behaved much differently. For [III] with carboxylic acid functionality, the Q_0 did decrease but not nearly as much as seen in [I] and [II]. The structure seen by SAXS for

the hydrocarbon polymer [IV] appeared to be very stable over the temperature range studied even though it is known that the solubility increased with increasing temperature.[15] However, up to about 475 °C these polymers showed no weight loss in TG analysis. The most direct comparison is between I and IV, which have the same linkages but differ in the aromatic ring, where the naphthalene [I] appears to be much more reactive.

CONCLUSIONS

Structural changes upon pyrolysis are observed in the SAXS data for coals and polymers. These changes can be correlated and contrasted with a number of other thermal analytical methods on the same coal and polymer samples. The results are very rank dependent with the lower rank coals showing variations over the entire temperature range. The naphthalene based polymers are much more reactive than the benzene-ethylene linked polymers and appear to give more secondary transformations.

ACKNOWLEDGMENTS

This work was performed under the auspices of the Office of Basic Energy Sciences, Division of Chemical Sciences and Division of Materials Sciences, U.S. Department of Energy, under contract number W-31-109-ENG-38. The support of the BESSRC staff is appreciated, especially Jennifer Linton and Mark Beno.

REFERENCES

1. Kalliat, M.; Kwak, C. Y.; Schmidt, P. W. In *New Approaches in Coal Chemistry*; Blaustein, B. D., Bockrath, B. C., Friedman, S., Eds.; ACS Symposium Series 169; American Chemical Society: Washington, D.C., 1981; pp. 3-22.
2. Foster, M. D.; Jensen, K. F. *Fuel* **1990**, *69*, 88-96.
3. Xu, Yingnian; Koga, Yoshikata; Watkinson, A. Paul. *Fuel* **1994**, *73*, 1797-801.
4. Johnston, P. R.; McMahon, P.; Reich, M. H.; Snook, I. K.; Wagenfield, H. K. *J. Colloid Interface Sci.* **1993**, *155*, 146-51.
5. Winans, R. E.; Seifert, S.; Thiyagarajan, P. *Prepr. Pap. - Am. Chem. Soc., Div. Fuel Chem.* **1999**, *44*, 149-152.
6. Solomon, P. R.; Serio, M. A.; Carangelo, R. M.; Bassilakis, R.; Gravel, D.; Baillargeon, M.; Baudais, F.; Vail, G. *Energy Fuels* **1990**, *4*, 319-33.
7. Yun, Y.; Meuzelaar, H. L. C.; Simmleit, N.; Schulten, H.-F. *Energy Fuels* **1991**, *5*, 22-29.
8. Simmleit, N.; Schulten, H.-R.; Yun, Y.; Meuzelaar, H. L. C. In *Advances in Coal Spectroscopy*; Meuzelaar, H. L. C., Ed.; Plenum Press: New York, 1992; pp. 295-339.
9. Winans, R. E. In *Advances in Coal Spectroscopy*; Meuzelaar, H. L. C., Ed.; Plenum Press: New York, 1992; pp. 255-274.
10. Sakurovs, R.; Lynch, L. J.; Barton, W. A. In *Magnetic Resonance of Carbonaceous Solids*; Botto, R. E., Sanada, Y., Eds.; Adv. Chem. Series 229; American Chemical Society: Washington, D.C.; 1993; pp. 229-251.
11. Neill, P. H.; Winans, R. E. In *Inverse Gas Chromatography: Characterization of Polymers and Other Materials*; Lloyd, D. R., Ward, T. C., Schreiber, H. P., Eds.; ACS Symposium Series 391; American Chemical Society: Washington, D.C., 1989; pp. 290-305.
12. Vorres, K. S. *Energy Fuels* **1990**, *4*, 420-426.
13. Winans, R. E.; Hayatsu, R.; Squires, T. G.; Carrado, K. A.; Botto, R.E. *Prepr. Pap. - Am. Chem. Soc., Div. Fuel Chem.* **1990**, *35*, 423-429.
14. Squire, K. R.; Solomon, P. R.; Carangelo, R. M.; DiTaranto, M. B. *Fuel* **1986**, *65*, 833-43.
15. Mungall, W. S.; Britt, P. F.; Buchanan, A. C., III. *Prepr. Pap. - Am. Chem. Soc., Div. Fuel Chem.* **1997**, *42*, 26-30.
16. Britt, P. F.; Mungall, W. S.; Buchanan, A. C. III. *Energy Fuels* **1998**, *12*, 660-661.

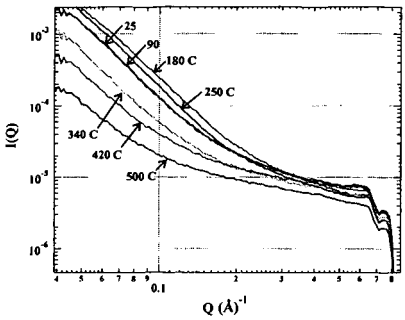

Figure 1. SAXS data from Illinois 6 pyrolysis at selected temperatures.

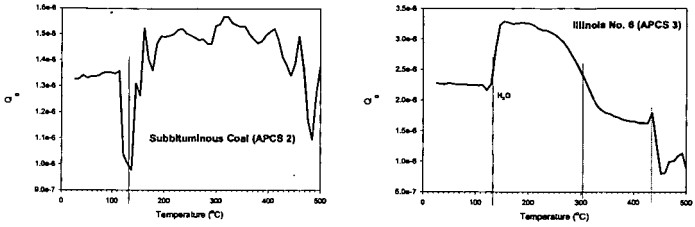

Figure 2. Invariant changes with pyrolysis.

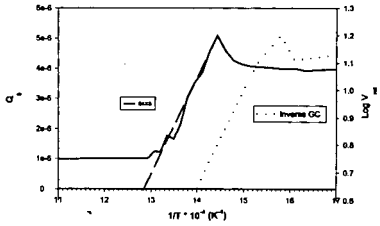

Figure 3. Comparison of SAXS with IGC data for the Upper Freeport coal (APCS 1).

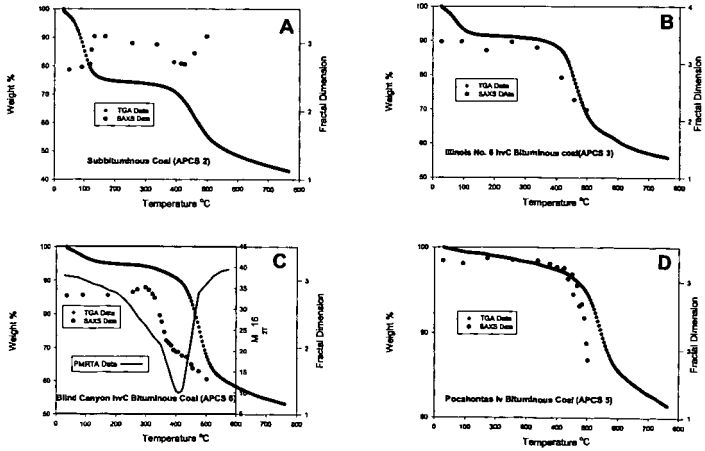

Figure 4. Comparison of TGA data with the d_f from SAXS.

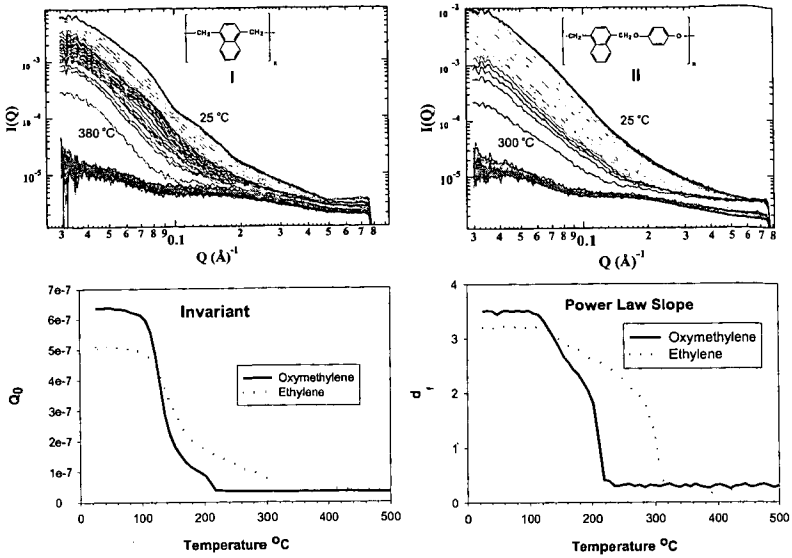

Figure 5. SAXS data for naphthalene polymers I and II with a comparison of invariants and power law slopes.

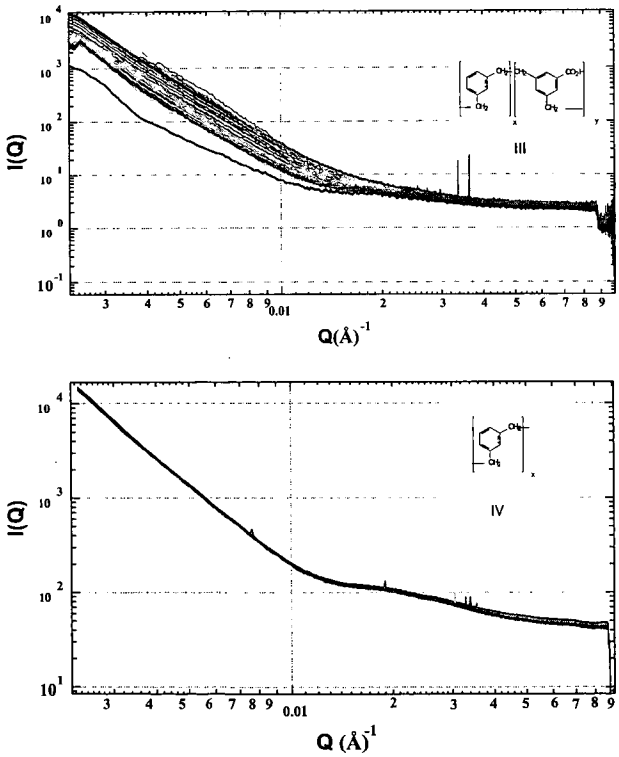

Figure 6. SAXS data for benzene polymers III and IV.

USE OF INTRA- AND INTER-MOLECULAR MODELS TO SIMULATE THE WIDE ANGLE X-RAY SCATTERING OF COALS. David L. Wertz, Department of Chemistry & Biochemistry, University of Southern Mississippi, Hattiesburg, MS 39406, USA.

INTRODUCTION. Hirsch et al.,[1] using the terminology of diffraction where $d = \lambda/2 \times \sin\theta$ for first order reflections in the x-ray experiments, assigned this peak to the average distance between layers which were proposed to contain the poly-cyclic units at the molecular level in coals. Using copper K_α Xrays, they found this peak (quite broad) to occur at $2\theta \approx 25°$, corresponding to $\langle d \rangle \approx 3.5$ Å. Their proposal of layering, at the molecular level in coals, has been verified, both by molecular modeling[2] and x-ray analysis using more modern equipment and several of the Argonne Premium Coals,[3] but their the use of ideal diffraction concepts to define structuring in coals is troubling because coals are not crystalline.

An alternative method for relating the measured x-ray intensities, which now may be accurately obtained using modern quantum counting equipment and computer-controlled data acquisition and processing method, has been utilized by our group.[4,5] This method correlates the measured intensity, which is a series of broad maxima and minima, with the average short-range structural unit in the coal and has been illustrated in the scattering studies of liquids, solutions, and amorphous solids. The Debye relationship correlates the structure of any molecular-level species, averaged of time and space, with the simulated wide angle phase interference curve caused by that species by:

$$j(q) = (\sum\sum q \times r_{ab})^{-1} \times \sum\sum n_{ab} \times \sin(q \times r_{ab});$$

where n_{ab} is the number of a-b atom pairs which occur at the distance r_{ab} in the structure, $f_a(q)$ and $f_b(q)$ are the scattering powers of atoms a and b, respectively, and $q = [4 \times \pi/\lambda] \times \sin\theta$.[6] For several of the Argonne Premium Coals, the average intra-molecular structural unit, (i.e., the average PC and its attachments) have been reasonably well identified;[7,8] so the n_{ab}'s and the r_{ab}'s for the average intra-molecular structural unit may be determined using three-dimensional geometry and then used to calculate the simulated phase interference curve for that coal using the Debye equation. This has been accomplished for several coals.[4]

The actual phase interference curve, i(q), may be obtained from the wide angle x-ray scattering (WAXRS) experiment. The comparison of j(q) to i(q) allows a judgement in the validity of the structural model used to calculate j(q), i.e., the array of n_{ab}'s and the r_{ab}'s that define that model. The comparison may be quantified by:

$$\tau^2 = \sum\{i(q) - j(q)\}^2/\sum i(q)^2.$$

The lower the value of τ, the better the agreement between the experimentally measured phase interference curve and the phase interference curve calculated from the model.

Solum et al propose that the average poly-cyclic unit in Pittsburgh #8 (PIT) coal is *ca.* C_{15} with four attachments.[7] Shown in Figure 1 is the simulated phase interference curve calculated for the C_{15} unit. Also shown in Figure 1 are the experimentally measured i(q)'s using both Mo K_α and Cu K_α Xrays.[3] As previously noted, the agreement between the experimentally determined i(q) and the j(q) calculated from the intra-molecular model based on C_{15} agree well at $q > 3$ Å^{-1}. The j(q) curve calculated from the C_{15} structural model is featureless in from 1.0 - 3.0 Å^{-1}; but the experimentally measured i(q) has a large maximum, centered at ca. 1.6 Å^{-1} with minima preceding and following this maximum. Similar results have been obtained for other coals.[3,4] Thus, it may be concluded that the dominant maximum in the measured x-ray intensity curves for coals, located at *ca.* 1.7 -1.9 Å^{-1}, is not due to structuring within the average PC unit.

Recently, an improved explanation of the measured x-ray intensities, expanding on the layering concept, has been proposed as the result of an x-ray scattering study of Beulah Zap lignite.[9] This procedure incorporates the concept of molecular-level layering in coals by calculating the distances between atoms in adjacent layers within the average short-range structural domain for that coal and correlating these distances with the structure curve calculated for each coal from wide angle x-ray scattering (WAXRS) experiments.

The objective of this study is to simulate the dominant peak in each experimentally determined i(q) using simplified structural models which approximate the average PC unit in the coal as a disc whose radius may be estimated from the NMR information available in the literature.

RESULTS. Shown in Figure 2 are several crude models of layering in the short-range domains in coals. The models differ, of course, in the number of layers in the average domain. To relate each of the models to coals, it has been assumed that the radius of the average PC unit (rad) is ca. 2.5 Å and average distance between the layers (<d>) is *ca.* 3.8 Å which is similar toe the average inter-layer distance reported for a number of the Argonne Premium Coals.[3] Shown in Figure 3 are the relative frequencies of the atom-pair distances (i.e., the structure curve) calculated from each model by:

$$F(r) = \sum \{rad^2 + [n \times \langle d \rangle]^2\}^{1/2};$$

where n describes the relationships between the layers in the model, and r is the distance between the atom in the various layers.

Using the Debye eq., each frequency function has been transformed into reciprocal space to produce its corresponding j(q). The simulated phase interference curve for each layer model is presented in Figure 4. Although the inter-layer structural models differ in the number of layers contained within each, their resulting phase interference curves are similar; with each featuring a maximum in the q = 1.8 $Å^{-1}$ region. Minima precede and follow this maximum. The sharpness of the maximum is related to the number of layers in the short-range structural domain.

In the three layer model, C–C atom-pair distances are expected to be centered at *ca.* 4.5 Å and at *ca.* 8.0 Å with a relative peak intensity of 2/1. The j(q) calculated for the three layer model is similar to the experimentally determined i(q) obtained for PIT. Shown in Figure 5 is the j(q) calculated from the three layer model compared to the i(q) measured for Pittsburgh #8 coal. For this comparison, $\tau = 0.021$ when <d> = 3.92 Å and rad = 2.6 Å. This very low structure correlation factor verifies the excellent agreement between i(q) and the J(q) calculated from the 3-layer model. The average interlayer distance determined by this method is similar to the average interlayer spacing distance reported by the earlier non-ideal diffraction interpretation of the secondary x-ray intensity reported for PIT.

The inter-molecular structure curve has been obtained by Fourier transform of the inter-molecular portion of the experimentally determined phase interference curve for PIT. This inter-molecular structure curve contains two maxima with relative intensities of 2/1. In Figure 6, this inter-molecular structure curve is compared to the atom-distance/frequency function calculated for the three layer model. The good agreement between these two functions indicates that the average short-range structural domain in PIT contains three layer units.

CONCLUSIONS. A simplified inter-layer model of the layering of the PC units in coals is consistent with both the phase interference curve obtained for Pittsburgh #8 coal by wide angle x-ray scattering a This model also predicts an atom-pair frequency curve which is consistent with the inter-molecular structure curve obtained for PIT.

REFERENCES

1. Hirsch, P. B., ***Nature (London),*** 1956, 177, 500-513 and numerous other publications.

2. Nakamura, K., Nakanoshashi, T., Iono, M., Sato, M., Yokoyama, S., and Sanada, Y., ***Energy Fuels***, 1995, 9, 1003-1010.

3. Wertz, D. L. and Bissell, M., ***Energy Fuels,*** 1994, 8, 613-617.

4. Wertz, D. L., ***Fuel***, 1995, 74, 1431-35; 1998, 77, 43-53.

5. Wertz, D. L., and Bissell, M., ***Adv. X-Ray Anal.,*** 1994, 37, 491 - 497.

6 Kruh, R. F., ***Chem. Rev.***, 1962, 62, 319 - 346.

7. Solum, M. S., Pugmire, R. J., and Grant, D. M., ***Energy Fuels***, 1989, 3, 187-193.

8 Munteen, J. V. and Stock, L. S., ***Energy Fuels,*** 1991, 5, 768 - 769.

9. Wertz, D. L. and Quin, J. L., ***Energy Fuels***, 1998, 12, 697-703: 1999, 13, 513-517.

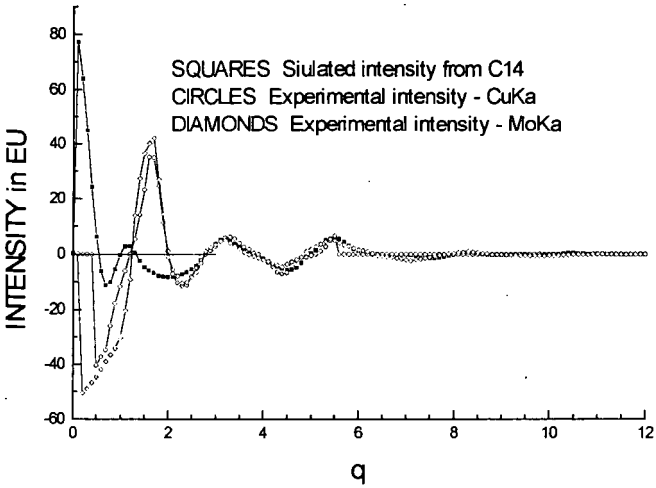

Figure 1. Comparison of the experimental phase interference curves for PIT with the simulated phase interference calculated for the C_{15} poly-cyclic unit.

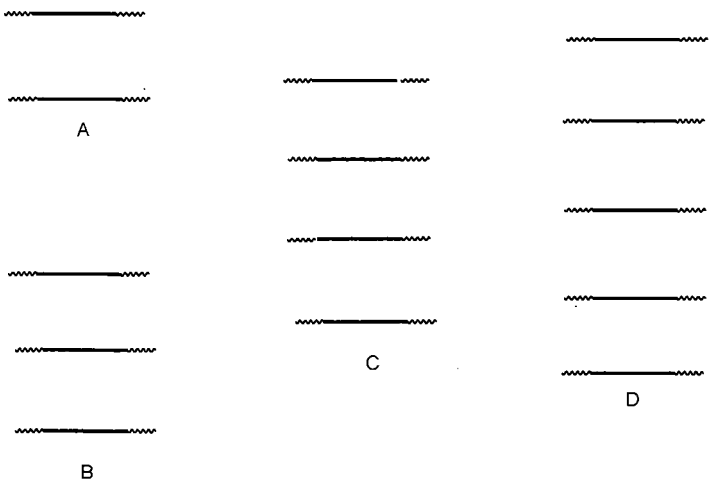

Figure 2. Models of molecular-level layering. Two layers (A), three layers (B), four layers (C), and five layers (D).

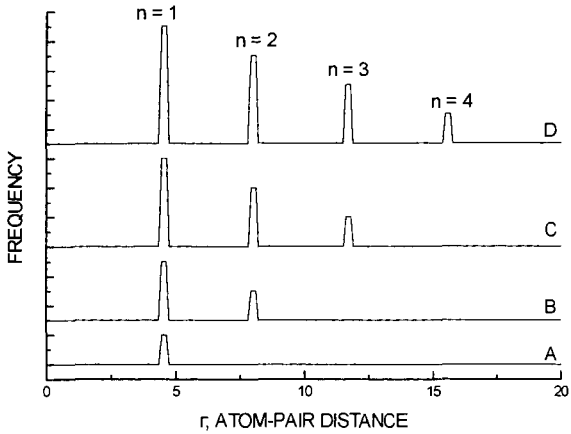

Figure 3. Frequency vs. atom-pair distance for the two-layer model (A), three-layer model (B), four-layer model (C), and the five-layer model (D).

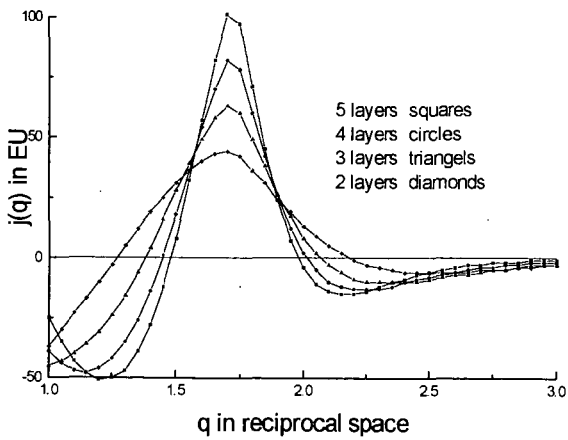

Figure 4. Simulated phase interference curves for the four inter-layer models.

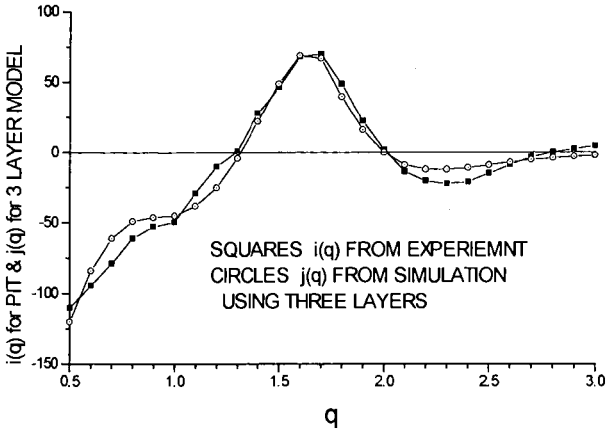

Figure 5. The i(q) for PIT compared to the optimized j(q) for the three-layer model.

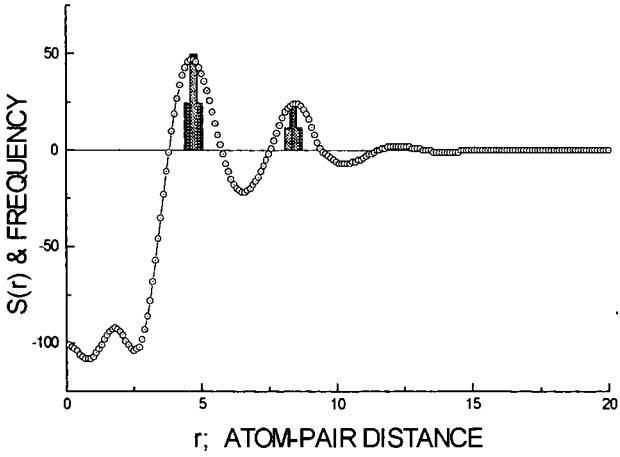

Figure 6. Inter-molecular structure curve for PIT compared to the frequency vs. atom-pair distance graph for the three-layer model.

STRUCTURAL PARAMETERS OF COALS FROM 002 LATTICE FRINGE IMAGES USING HRTEM

Atul Sharma, Takashi Kyotani and Akira Tomita
Institute for Chemical Reaction Science, Tohoku University,
Sendai, JAPAN.

Key words: Coal structure, Lattice image, HRTEM.

INTRODUCTION

Over the years several studies have been done using different techniques to get the insight into the coal structure. All these studies converge on one understanding that coal is heterogeneous in nature and made up of very small aromatic layers more or less randomly orientated. The layer size and stacking number increases with the rank of coal. Direct evidence about the arrangement of these aromatic layers, obtained by the electron microscope lattice imaging, is obviously an attractive complementary technique. Not much literature have been available on TEM observation of coals as such and most of the studies report about the heat treated coals. McCartney and Ergun [1] used electron microscopy to determine crystalline dimensions of meta-anthracite coal. Another attempt was made by Evans et al. [2] who observed anthracite coal and heat-treated coals. They found the coal samples to be completely amorphous and no evidence of any ordered layers. Millward [3] also reported that when coals were observed by electron microscope, no fringes which could be evidence of layered molecules was found. He highlighted the problems associated with instrument and irradiation damages which make it difficult to observe raw coals. Oberlin [4] developed dark field image technique to observe the coal structure. The electron microscope operation and theoretical consideration of image formation are now fully understood. With recent advances in electron microscope instrument like anti-contamination device which successfully preserve the specimen from irradiation damages during high-resolution observation, it is possible to image even the highly electron beam-sensitive materials like coals.

In this article we are presenting the structure of three different coals as observed by HRTEM. We also attempted to obtain stack distribution using image analysis technique developed by us and described elsewhere [5].

EXPERIMENTAL

Argonne Premium Coal Samples, Pocahontas no. 3 (POC) , Illinois no. 6 (IL) and Beulah-Zap (BZ), were selected for the investigation. The coal samples, ground in ethanol and sprayed on a copper microgrid, were observed under a TEM (JEOL-2010) operating at 200 kV for high resolution images. The transmission electron microscope was equipped with computerized imaging system and EDS for elemental analysis. To get a general view of the coal samples, nearly 7 to 8

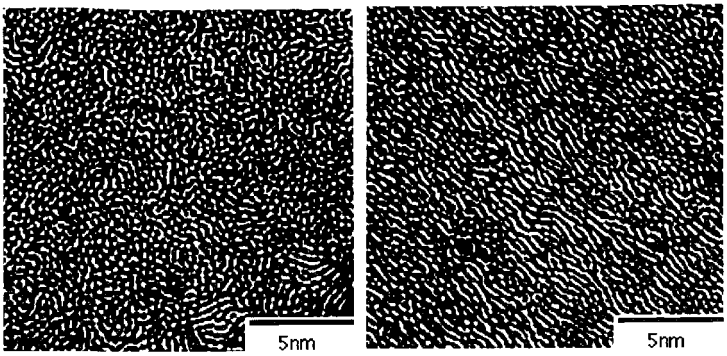

(a) (b)

Figure 1 HRTEM images of Beulah-Zap coal: (a) amorphous structure and (b) ordered structure.

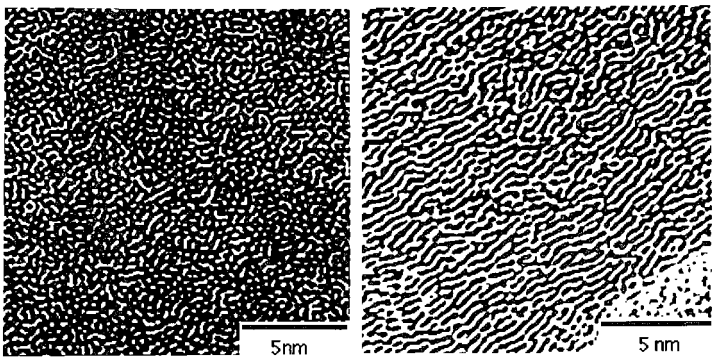

(a) (b)

Figure 2 HRTEM images of Illinois no.6 coal: (a) amorphous structure and (b) ordered structure.

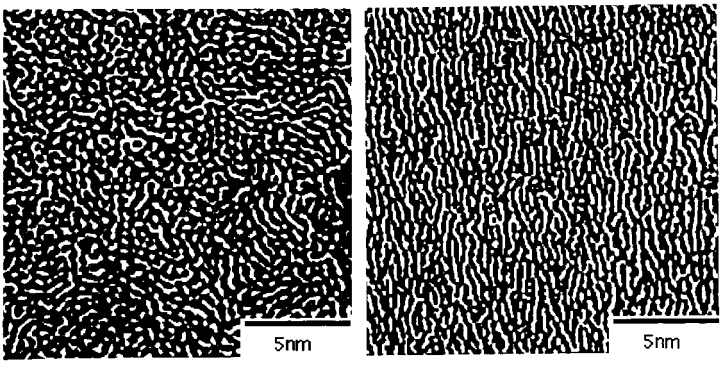

(a) (b)

Figure 3 HRTEM images of Pocahontas no.3 coal: (a) amorphous structure and (b) ordered structure.

different spots were observed. A quantitative analysis was done to evaluate stack distribution using our newly developed image analysis technique [5].

OBSERVATION OF COALS USING HRTEM

It is necessary first to ascertain that the TEM micrographs presented here are those of coals. In all cases, first a sub-micron size particle was selected for observation at a very low magnification and its diffraction pattern was taken and elemental analysis was carried out. The elemental analysis showed signatures of all the elements present in the coals as mineral matter which was also confirmed by the sharp spots observed in the SAD patterns. After confirming that this sub-micron size particle is coal, very thin edges of this particle were observed at a high magnification(x 500k). To prevent the sample from irradiation damages, the current density on the screen was kept at less than 1 pa/cm^2. At this illumination almost nothing can be observed on the fluorescent screen. However, the structure can be observed on the TV screen by increasing the aperture and sensitivity of the camera. By this approach we considerably reduced the number of electrons hitting the sample.

RESULTS AND DISCUSSION

In Figures 1 to 3, the HRTEM images from two different spots for BZ, IL and POC coals are shown. All three coals show the presence of both amorphous and ordered structure. Even in ordered structures, layers are not plane and show lack of mutual orientation. It is known that coals contain small condensed aromatic units. These units show a parallel stacking but lack orientation and planarity because of the presence of hetero-atoms or hydroaromatic portions. These fringes or layers observed from HRTEM images are in accordance with the above understanding, and hence these layers are not graphite-like layers. Figure 4 shows a typical example of extracted images from HRTEM images using the filtration technique [5] for quantitative analysis. The extracted images from five different spots were subjected to image analysis algorithm [5] to evaluate stack distribution and the results are shown in Figure 5. The distributions show that the fraction of single layers or amorphous part is higher in BZ coal than in POC coal and the fraction of highly stacked group is relatively large with POC. However, the number of photographs taken in this study are too less to discuss further on the difference among the three coals. Figures 6a-c show the presence of mineral matter in the three coals. BZ and IL show very clear lattice fringes from the mineral matter. To make the fringes more clear, we separeted these from the organic part by drawing a white line. In Figure 6a, these are enclosed by the white line while in Figure 6b, these are towards left of the white line. In POC coal, mineral matter is present as nearly circular dark spots. Figure 6d shows an onion-like structure similar to fullerene as suggested by Fang et al [6]. This was observed only in POC coal and only in one spot.

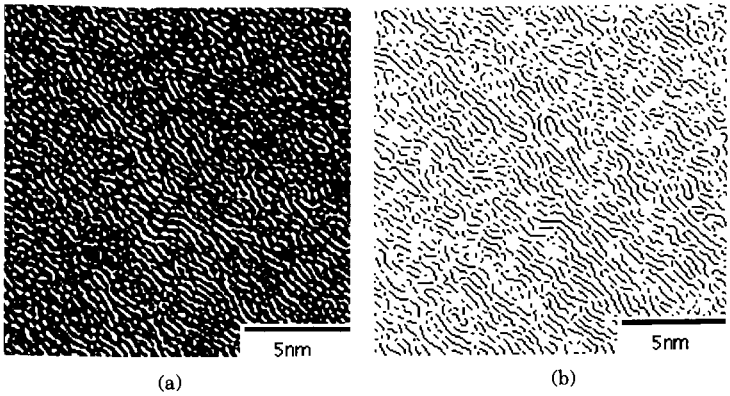

Figure 4: (a) HRTEM image and (b) corresponding extracted image.

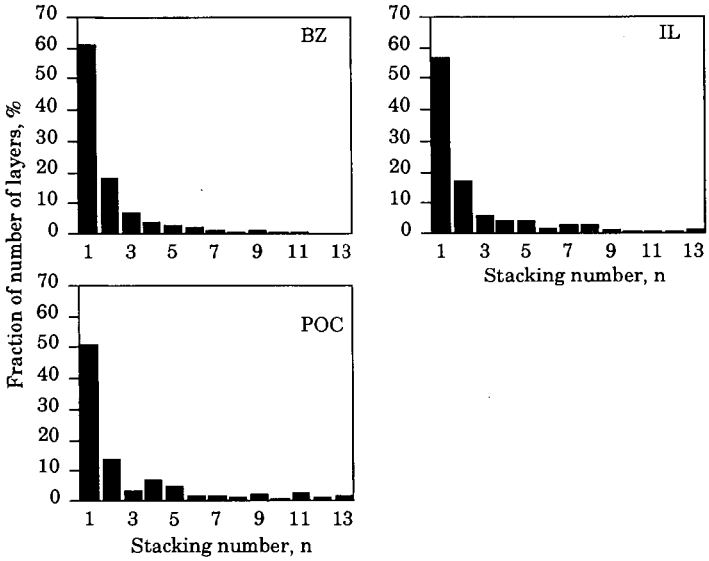

Figure 5 Fraction of number of layers occuring in *n* layers.

CONCLUSIONS

The HRTEM technique is powerful tool for extracting microstructure information of coals. Both amorphous and ordered structures were observed. Direct evidence of lattice fringes which can be ascribed to layers was found.

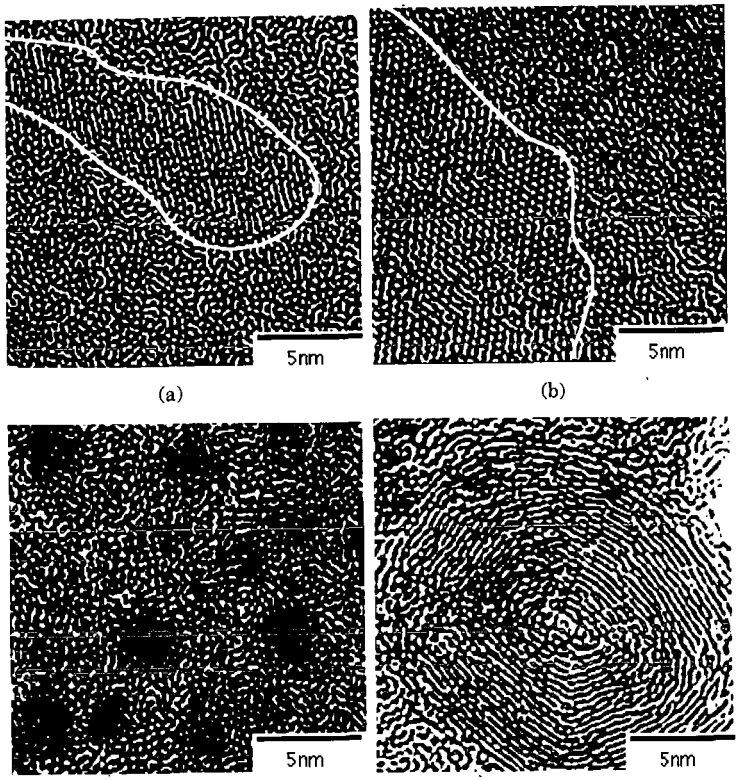

Figure 6 HRTEM images of: (a) mineral matter in Beulah-Zap coal, (b) mineral matter in Illinois no.6 coal, (c) mineral matter in Pocahontas no. 3 coal, and (d) onion-like structure in Pocahontas no. 3.

ACKNOWLEDGMENT

This study was part of "Research for the Future Program- Molecular Engineering of Coal" which was supported by the Japan Society for the Promotion of Science.

REFERENCES

1. McCartney, J.T., Ergun, S. *Nature*, 1965, 205, 962-964.
2. Evans, E.L., Jenkins, J.L., Thomas, J.M. *Carbon*, 1972, 10, 637-642.
3. Millward, G.R. In *Coal and modern coal processing: An introduction*, Pitt, G.J., Millward, G.R., eds., Academic press, 1979, pp. 94.
4. Oberlin, A. *Carbon*, 1979, 17, 7-20.
5. Sharma, A., Kyotani, T., Tomita, A. A new quantitative approach for microstructural analysis of coal char using HRTEM images. *Fuel*, in press.
6. Fang, P.H., Wong, R. *Mat. Res. Innovat.*, 1997, 1, 130-132.

MICROHETEROGENEITY OF SOLVENT-SWOLLEN COAL PROBED BY PROTON SPIN DIFFUSION

Koyo NORINAGA *,†, Jun-ichiro HAYASHI, Tadatoshi CHIBA, and Masashi IINO †
Center for Advanced Research of Energy Technology (CARET), Hokkaido University
N13, W8, Kita-ku, Sapporo 060-8628, Japan
† *Institute for Chemical Reaction Science, Tohoku University*
Katahira, Aoba-ku, Sendai, 980-8577, Japan

KEYWORDS: Coal, Swelling, Microphase separation

ABSTRACT

Phase separated structure of solvent swollen coal was characterized thorough its property of proton flip-flop spin diffusion. It is shown that the fashion of coal swelling is non-uniform on a segmental scale and a microscopic phase separation does take place on a scale from several to 20 nm even in good solvents like pyridine.

INTRODUCTION

The most convincing model of coal structure is that of a cross-linked macromolecular network. All attempts to relate the macromolecular network parameters such as the molecular weight between cross-link points to the degree of swelling in a good solvent have taken the Flory-Rehner theory [1] as a starting point for the swelling of macromolecular networks. The theory involves the assumption that the deformation is affine, i.e., that the primitive chain is deformed in the same way as the macroscopic deformation (swelling) of the sample. Accordingly, the premise is required that the swollen coal is uniform in the segmental scale when we relate the macroscopic swelling to the molecular characteristics such as cross-link density. Based on the ^{1}H NMR transverse relaxation characteristics, however, it was found that the hydrogens in pyridine-swollen coals could be divided into two groups: those whose relaxation was characteristic of solids and those whose relaxation was characteristic of liquids. Barton et al. [2] reported that the ^{1}H NMR transverse relaxation signals measured at ambient temperature for bituminous coals swollen by deuterated pyridine, show that up to ~60% of the coal molecular structures can be sufficiently destabilized to become mobile. Therefore, at least 40% of the coal hydrogen remains in rigid molecular structures and is characterized by an NMR signal component that is similar to the signal for the corresponding dry coal. This result demonstrates that the swollen coal can be recognized to have a phase separated structure involving solvent rich phase and apparently solvent impervious phase. However the scale of heterogeneity in the swollen coals is presently not fully understood.

In spite of its indirect character, measurements of ^{1}H spin diffusion by pulsed NMR have proven to be a useful technique for evaluating the compatibility of polymer blends [3-6] and the microdomain structure of multiphase polymers. [7-11] When a nuclear system is disarrayed from equilibrium in an NMR experiment, the excess spin energy acquired by the resonant nuclei can remain in the spin system for a long time compared to transverse relaxation time, T_2, before being transferred to the lattice. This follows directly from the fact that longitudinal relaxation time, T_1, is much larger than T_2 in solid materials. [12] During this time the spin energy can disperse between neighboring nuclei by energy-conserving "flip-flop" spin transitions. This process is termed spin diffusion and may provide observable energy transport over distances of several tens of nanometers. For the coal swollen by the saturation of deuterated pyridine, there exits at least two distinct morphological regions in the NMR sense. In such a case, owing to their state of motion, certain regions or sites responsible for the mobile phase provide exceptionally efficient transfer of energy to the lattice, while the rigid component weakly coupled to the lattice, can exhibit molecular motions that disfavor relaxation. It is possible, through the mechanism of spin diffusion, for the component that is tightly coupled to the lattice to relax other resonant nuclei in the spin system either totally or partially. By analyzing the spin diffusion process under an appropriate initial and boundary conditions, we can estimate the diffusive path length, and then get an information about the domain size of each phase.

In this study, the phase separated structure of solvent swollen coal is characterized thorough its property of proton flip-flop spin diffusion. Six coals of different rank swollen by the saturation of deuterated pyridine were subjected to ^{1}H NMR relaxation measurements. The NMR experiments provide transverse relaxation time, T_2, longitudinal relaxation time, T_1, and that in the rotating frame $T_{1\rho}$. The time dependency of the spin diffusion is also monitored by Goldman-Shen pulse sequence. The dimension of a heterogeneity of the swollen coal is evaluated by analyzing the spin diffusion process.

EXPERIMENTAL

Samples. Four Argonne Premium Coal Sample Program (PCSP) coals [13] and a brown coal were used as coal samples. Their particle sizes were finer than 150 μm. They were dried under a pressure of less than 1 Pa at 333 K for 48 h, which is long enough to attain a constant weight. The elemental composition, ash and water contents, and swelling ratios of the coal samples in pyridine or pyridine/CS_2 mixed solvent are listed in Table 1. The coal sample was weighed and transferred to an NMR tube with a 10 mm o.d. The mass of the sample was 0.3 g. A 0.5 g of fully deuterated pyridine, Py-d_5, (Aldrich, 99.99% atom D) was

then added to the sample and the tube was sealed under pressure of less than 2 Pa while frozen with liquid nitrogen. A mixture of Py-d_5 and CS_2 (1:1 by volume) was also used as a solvent for UF coal. The coal-solvent mixtures were stored at 303 K for at least 4 months before the NMR measurement. Styrene/divinylbenzene copolymers (St/DVB, crosslink density, 2, 4, and 8%) swollen in benzene-d_6 were also prepared.

^{1}H NMR. NMR measurements were carried out at 303 K using JEOL Mu-25 NMR spectrometer equipped with spin locking unit operating at a proton resonance frequency of 25 MHz. The solid-echo pulse sequence, $90°_x$-τ-$90°_y$ (90° phase shift) provided an approximation to the complete free induction decay (FID). Typical values for the pulse width, pulse spacing, repetition time and number of scans were 2.0 μs, 8.0 μs, 6 s and 32, respectively. The saturation recovery pulse sequence, $90°_x$-t-$90°_x$ was used to monitor the recovery of the magnetization with the pulse separation time, t and provided T_1. $T_{1\rho}$ was measured by the so-called spin-locking pulse sequence, that is $90°_x$ pulse is followed by a reduced amplitude pulse, sustained for a time t and phase shifted 90°. The magnetization remaining at time t is monitored by observation of the free induction signal. Rotating frame measurements were made at radiofrequency field of 6 G. Spin diffusion was monitored by the Goldman-Shen pulse sequence. [14] The original pulse sequence was modified as $90°_x$-t_0-$90°_x$-t-$90°_x$-τ-$90°_y$, according to Tanaka and Nishi [11] in order to avoid the dead-time effect after the pulse.

RESULTS AND DISCUSSION

Transverse relaxation characteristics. The natural logarithm of the FID curves for the dried and swollen YL coal are drawn as a function of decay time in Figure 1(a). Although the solvent swelling enhance the fraction of slowly decaying components, a portion of coal hydrogen remains rigid. The observed FID was assumed to be expressed by the following equations and numerically analyzed by nonlinear least squares methods.

$$I(t) = I_G(0) \exp[-t^2/2T_{2G}^2] + I_{L1}(0) \exp[-t/T_{2L1}] + I_{L2}(0) \exp[-t/T_{2L2}] \qquad (1)$$

where $I(t)$ and $I_i(t)$ are the observed intensity at time t, and that attributed to component i, respectively, and T_{2i} is the transverse relaxation time of the i th component. The fraction of hydrogen producing exponential decays, H_m, are listed in Table 2. H_m for the swollen coal samples range from 0.2 to 0.6, and T_{2G} value is similar to that for the corresponding dry coal. In contrast, when exposed to benzene-d_6, hydrogens in St/DVB crosslinked copolymer are entirely converted to mobile hydrogens producing exponential decays, regardless of cross link densities of St/DVB as illustrating in Figure 1(b). This indicates that solvent penetrates thoroughly into St/DVB and it is likely to be deformed in a more or less uniform fashion. For the swollen coal samples, it is clear that there are domains which do not swell and are not penetrated by solvent as shown schematically in Figure 2. The phase structures of the swollen coal are separated into at least two phase, i.e., solvent rich (SR) and solvent impervious phase (SI). Brenner [15] studied the changes in optical anisotropy of dry and solvent-swollen thin section samples of a bituminous coal. He found that the natural optical anisotropy was completely relaxed by immersion of the coal in pyridine. These different experimental techniques, i.e., ^{1}H NMR and optical microscopy, produce different conclusion on the phase structure in the solvent-swollen coal. This contradiction seems to be responsible for the difference in the spatial resolution between these experimental techniques. The optical microscopy technique can hardly detect heterogeneities whose spatial dimensions are less than the optical wavelength (400~700 nm). Therefore, the dimension of heterogeneities of the swollen coal must be smaller than ~700 nm.

Longitudinal relaxation characteristics and spin diffusion. To examine whether the spin diffusion process is active or not in the swollen coal samples, proton longitudinal relaxation was measured both in the laboratory and rotating frame. Figure 3 (a) shows the result of T_1 measurement for the swollen UF coal. T_1 is almost composed of one component while $T_{1\rho}$ can be analyzed by the sum of two exponential functions as shown in Figure 3 (b). From these results, one can clearly understand the effect of spin diffusion. T_2 signals are composed of three components without the effect of spin diffusion while $T_{1\rho}$ and T_1 measurements are affected strongly by spin diffusion and the number of the components decreases from $T_{1\rho}$ to T_1. The existence of at least two time constants for a rotating frame longitudinal relaxation process i.e., $T_{1\rho}$, in a system means that spin-diffusion processes cannot effectively average the different dynamical properties of protons in different spatial domains on the relevant time scale of the specific relaxation process. On the other hand, in the time scale of T_1 measurements, the distinctly separated spin systems were sufficiently averaged by the spin diffusion. The scale of spatial heterogeneities of the swollen coals can be estimated by evaluating the diffusive path length, L, i.e., the maximum linear scale over which diffusion is effective. The approximate expression is

$$L = (2dDt)^{1/2} \qquad (2)$$

where d is spatial dimension, i.e., the degree of freedom of diffusion, D is diffusion coefficient, and t is characteristic time for diffusion. d is one, two, and three corresponds to the domain shape of lamella, cylinder and sphere, respectively. It has been shown that in a regular lattice with lattice constant a, the spin diffusion coefficient due to dipolar spin flip is given

by [8]

$$D = 0.13a^2\sqrt{M_2} \tag{3}$$

where M_2 is the second moment of the NMR line shape. For both Gaussian and Lorentzian line shapes, $\sqrt{M_2} = T_2^{-1}$. For a regular lattice, D can be principally calculated from eq 3, but since the lattice constant is an ill-defined quantity for disordered materials like coals, a theoretical value can only be estimated by

$$D \approx 0.13\bar{a}^2/T_{2G} \tag{4}$$

where $\bar{a}^2$ is the average of the square of distances between adjacent protons in the solvent impervious domain. Because of the lack of information on the molecular structure of coal, it is impossible to accurately determine $\bar{a}^2$. However, $\bar{a}^2$ of the coal samples can be estimated semiquantitatively from the data of true densities evaluated by helium pycnometery [16] and hydrogen contents of the corresponding dry coal [13] by assuming a cubic lattice of hydrogens. In Table 2, the estimated values of D are listed. D range from 5.1×10^{-12} to 6.2×10^{-12} cm^2/s and have the same order in many organic polymer systems. The observed longitudinal relaxation time corresponds to the characteristic time t. By assuming d is 3, we can estimate L as 40 nm from eq 2 for UF/Py-d_5. Therefore the linear dimension of the structural heterogeneity in UF/Py-d_5 is certainly less than 40 nm on the basis of T_1 data. Following the same procedure for the $T_{1\rho}$ data the lower limits of the heterogeneity can be estimated to be 1 nm from the short $T_{1\rho}$. For UF/(Py-d_5 + CS_2), the limiting size in heterogeneity can be estimated as 1 - 20 nm. Recently, Xiong and Maciel [17] studied the proton longitudinal relaxation characteristics in dry coal using a solid state high resolution NMR technique. They found two $T_{1\rho}$ values for the three kind of bituminous coals, which indicates the existence of structural heterogeneity in the coals on a spatial scale of at least of 5 nm. While these estimates are crude they nevertheless provide some information of the maximum diffusive path lengths probed by the NMR experiment when spin diffusion is operative. The Goldman-Shen pulse sequence was thus employed to monitor the spin diffusion process. The advantage of the Goldman-Shen experiment is that the time for spin diffusion can be arbitrarily varied, and if this time is much less than T_1, the analysis is straightforward.

Goldman-Shen experiment. The Goldman-Shen experiment is a technique to put the separate spin systems at different spin temperatures and then sample them as a function of time so that their approach to equilibrium can be followed. The modified Goldman-Shen pulse sequence used in this experiment is shown in Figure 4. During time τ_0, the magnetization in the SI phase has decayed to zero, while there is still sufficient magnetization in the SR phase. During the pulse interval t, spin diffusion through the magnetic dipolar coupling occurs from the SR phase to the SI one. The third 90°_x pulse rotates the magnetization into the transverse plane for observation and the final 90°_y pulse creates the solid echo. The typical decaying signals after the Goldman-Shen pulse sequence observed in IL/Py-d_5 for various values of the pulse interval t are shown in Figure 5. The recovery of the fast decaying component is observed. The recovery factor, $R(t)$, of the magnetization of SI phase can be defined as

$$R(t) = \frac{M(t) - M(t \to 0)}{M(t \to \infty) - M(t \to 0)} \tag{5}$$

In Figure 6, $R(t)$ is plotted versus $\tau^{1/2}$ for the solvent-swollen BZ and PT coal. The time evolution of $R(t)$ is analyzed by the diffusion equation solved by Cheung and Gerstain [8] to get information on the domain size. The transfer of the magnetization in solids via dipolar spin flip interaction may be described by the spin diffusion equation

$$\frac{\partial}{\partial t} m(r,t) = D\nabla^2 m(r,t) \tag{6}$$

where $m(r,t)$ is the local magnetization density at site r and time t. The differential equation is then solved according to the appropriate boundary and initial conditions. The analytical solution of eq 6 due to Cheung and Gerstain is

$$R(t) = 1 - \varphi_x(t)\varphi_y(t)\varphi_z(t)$$
$$\varphi_\alpha(t) = \exp(Dt/\bar{b}^2_\alpha)\mathrm{erfc}(Dt/\bar{b}^2_\alpha)^{1/2} \text{ for } \alpha = x,y,z \tag{7}$$

where $\bar{b}$ is the mean width of domains in SR phase. The quantity $(D/\bar{b}^2_\alpha)^{1/2}$ was considered as an adjustable parameter. The solid curves in Figure 6 represent the nonlinear least squares fits to the data by using eq 7. The results for the analytical fits are listed in Table 2. These calculations indicate that the SR phase domain in the swollen coals have sizes ranging from several to 20 nm. The size seems to become smaller with decreasing coal

rank. The information on the morphologies of the domains is necessary to estimate the domain size adequately. However there is presently little information available on the shape of domains in the swollen coal. $\bar{b}$ is the mean width of domains in SR phase and would corresponds to the distance between the domains in SI phase. Cody and Thiyagarajan [18] estimated the interdomain spacing of a pyridine-swollen bituminous coal to be approximately 15 nm by the small angle neutron scattering technique. This value agrees well $\bar{b}$ of the swollen bituminous coals, i.e., IL, PT, and UF coals, which were evaluated under the assumptions that the domain shapes are cylinder or sphere.

ACKNOWLEDGMENT. The authors are grateful to Drs. Tadashi Yoshida and Masahide Sasaki of the Hokkaido National Industrial Research Institute for their useful advice on the NMR measurements. This work was supported in part by a "Research for the Future Project" grant from the Japan Society for the Promotion of Science (JSPS), through the 148th Committee on Coal Utilization Technology.

REFERENCES

(1) Flory, P. J. *Principles of Polymer Chemistry;* Cornell University Press: Ithaca: NY 1953.
(2) Barton, W. A.; Lynch, L. J.; Webster, D. S. *Fuel* **1984**, *63*, 1262.
(3) Kwei, T. K.; Nishi, T.; Roberts, R. F. *Macromolecules* **1974**, *7*, 667.
(4) Nishi, T.; Wang, T. T.; Kwei, T. K. *Macromolecules* **1975**, *8*, 227.
(5) Douglass, D. C.; McBrierty, V. J. *Macromolecules* **1978**, *11*, 766.
(6) McBrierty, V. J.; Douglass, D. C.; Kwei, T. K. *Macromolecules* **1978**, *11*, 1265.
(7) Assink, R. A. *Macromolecules* **1978**, *11*, 1233.
(8) Cheung, T. T. P.; Gerstain, B. C. *J. Appl. Phys.* **1981**, *52(9)*, 5517.
(9) Cheung, T. T. P. *Phys. Rev. B* **1981**, *23*, 1404.
(10) Cheung, T. T. P. *J. Chem. Phys.* **1982**, *76*, 1248.
(11) Tanaka, H.; Nishi, T. *Phys. Rev. B* **1986**, *33*, 32.
(12) Bloembergen, N. *Nuclear Magnetic Relaxation*, Benjamin, New York 1961.
(13) Vorres, K. S. *User's Handbook for the Argonne Premium Coal Sample Program*; Argonne National Laboratry, IL, 1993.
(14) Goldman, M.; Shen, L. *Phys. Rev.* **1966**, *144*, 321.
(15) Brenner, D. *Nature* **1983**, *306*, 772.
(16) Huang, H.; Wang, K.; Bodily, D. M.; Hucka, V. J. *Energy Fuels* **1995**, *9*, 20.
(17) Xiong, J.; Maciel; G. E. *Energy Fuels* **1997**, *11*, 866.
(18) Cody, G. D.; Thiyagarajan, P. *Proceedings of Adv. Energy. Thech.*, Sapporo, Japan 1998, p 31.

Table 1 Properties of Coal Samples.

Coal	(Symbol)	C	H	N	S	O [a]	ash	Swelling ratio [d]	
		[wt% daf [b] coal]					[wt% mf [c] coal]	Py[-]	Py/CS_2[-]
Yallourn	(YL)	65.0	4.6	0.6	0.2	29.6	57.5	2.7	
Beulah Zap	(BZ)	72.9	4.8	1.2	0.7	20.3	32.2	2.2	2.0
Illinois#6	(IL)	77.7	5.0	1.4	2.4	13.5	8.0	2.8	
Pittsburgh	(PT)	83.2	5.3	1.6	0.9	8.8	9.3	2.4	
Upper Freeport	(UF)	85.5	4.7	1.6	0.7	7.5	13.2	1.0	1.9

[a] by difference. [b] dry-ash-free. [c] moisture-free. [d] determined by the method proposed by Green et al.

Table 2 Domain Size of Solvent Rich Phase.

Sample	Solvent	S/C [a]	H_m [b] [-]	$D[10^{-12}cm^2/s]$	$\bar{b}$ [nm] 1-D	2-D	3-D
YL	py	1.75	0.56	-	-	-	-
YL	py	3.50	0.60	5.7	2	5	8
BZ	py	1.75	0.44	6.2	2	5	8
BZ	py/CS_2	1.81	0.34	-	-	-	-
IL	py	1.75	0.55	5.6	5	12	19
PT	py	1.75	0.51	5.5	5	12	21
UF	py	1.75	0.20	-	-	-	-
UF	py/CS_2	1.81	0.45	5.1	5	10	16
St/2%DVB	benz	4.75	1.00	-	-	-	-
St/4%DVB	benz	2.31	1.00	-	-	-	-
St/8%DVB	benz	2.31	1.00	-	-	-	-

[a] Mass ratio of solvent to coal or polymer. [b] Fraction of mobile hydrogen producing exponential decays.

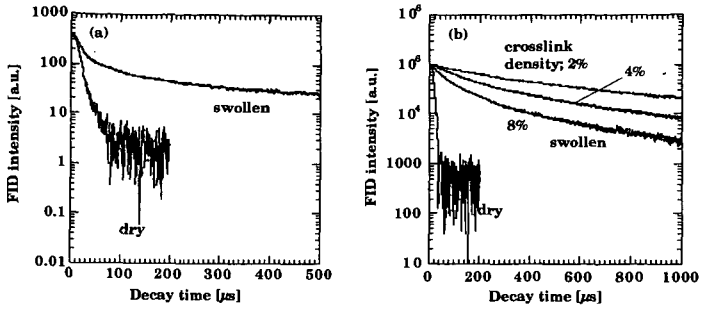

Figure 1 ^{1}H-NMR transverse relaxation signals.
(a) dried and swollen YL. (pyridine-d_5, S/C=1.75), (b) dried and swollen St/DVB. (benzene-d_6, S/C=2.31 for 4% and 8% crosslink densities, S/C=4.75 for 2%)

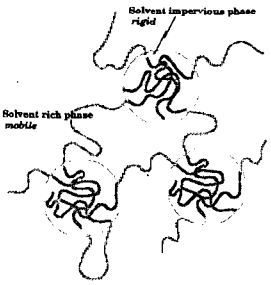

Figure 2 Conceptual model for microdomain structure of solvent-swollen coal.

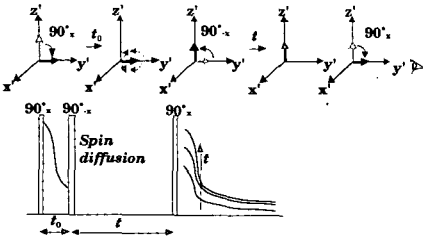

Figure 4 Schematic figure of the Goldman-Shen pulse sequence.

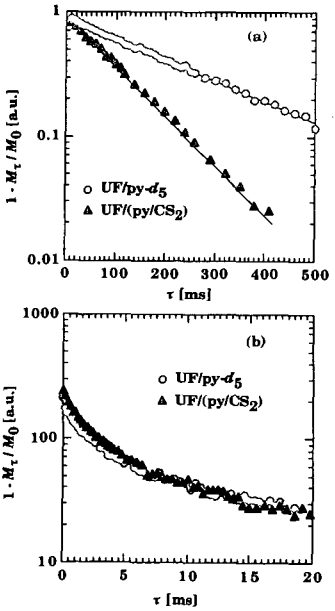

Figure 3 T_1 and $T_{1\rho}$ plots for solvent-swollen UF. (a) T_1, (b) $T_{1\rho}$

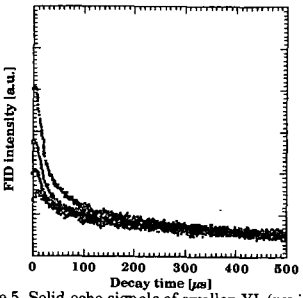

Figure 5 Solid-echo signals of swollen YL (pyridine-d_5, S/C=1.75) after the modified Goldman-Shen pulse sequence for various value of t. t is equal to 1, 25, 64 and 225 ms from the bottom

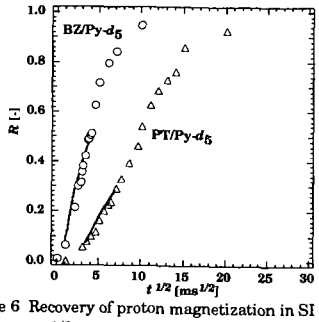

Figure 6 Recovery of proton magnetization in SI phase as a function of $t^{1/2}$ for the solvent-swollen BZ and PT coal. Solid lines represent the best fit to the data by using eq 7.

PHENOLIC RESINS AS MODELS FOR THE STRUCTURE OF COAL

Paul Painter, Pakorn Opaprakasit,
Maria Sobkowiak and Alan Scaroni
Energy Institute
Penn State University
University Park, PA 16802

KEYWORDS: Models for the macromolecular structure of coal: phenolic resins

INTRODUCTION

For many years the "standard model" for coal structure has essentially considered most coals to consist of covalently cross-linked networks with a cross-link density and sol fraction that varies systematically with rank (this model excludes arthracites and other high rank coals that are more graphitic in their structure). It has also been proposed that certain types of secondary forces, such as hydrogen bonds or charge-transfer complexes, can act as cross-links, although with respect to hydrogen bonds we disagree with this viewpoint (1). There is also an alternative model, proposed a few years ago, that places even more weight on the role of non-covalent interactions, proposing that most coals are associated structures held together by these secondary interactions acting in some undefined co-operative manner (2-6). These different views of coal structure remain to be resolved.

One of the problems with characterizing coal, particularly the nature of its network structure, is that crucial parameters such as the cross-link density can only be measured indirectly by techniques such as swelling and by recourse to a theoretical model. The most widely used model has been that originally proposed by Flory and Rehner, modified in various ways by different workers over the years to account for the specific character of coal (a high cross-link density, hence "short" chains between cross-linked points, and the presence of strong specific interactions such as hydrogen bonds, see reference 7 and citations therein). What is clearly needed is a model, highly cross-linked system where the cross-link density is known or can be measured directly, thus allowing an experimental test of the validity of various approaches. Here we will propose the use of phenolic resins and present preliminary results that demonstrates the close resemblance of the properties of these materials to coal.

RESULTS

The nature of phenolic resins

Ordinary phenol/formaldehyde resins were the first true synthetic polymers produced commercially (as opposed to chemically modified natural polymers) and were called Bakelite. Depending upon reaction conditions either novolak or resol resins can be produced, the former essentially consists of branched oligomers of phenol units, linked by methylene bridges at their ortho and meta (to the hydroxyl group) positions, as illustrated in figure 1. These materials are not cross-linked, in the sense of forming a densely interconnected network of units through covalent linkages. Resols, on the other hand, form methylol (CH_2OH) groups and their synthesis does lead to a densely cross-linked network, as illustrated in figure 2.

At least superficially one recognizes an immediate correspondence to the "standard model" structure of coal; aromatic clusters linked by methylene and some ether units. Coal, of course is far more heterogeneous, containing larger aromatic units, many of which are heterocyclic, and these are presumably linked

by a broader range of "bridge types" (e.g. ethylene). This is reflected in the infrared spectrum, as can be seen in figure 3, where the spectrum of a simple phenol formaldehyde resol is compared to that of a randomly chosen coal. The bands present in the coal spectrum are generally broader, the aromatic "ring-breathing" mode in the resol near 1600 cm^{-1} is much weaker, as is the aliphatic stretching modes near 2900 cm^{-1}. Methylene bridges between aromatic units clearly absorb very weakly (but it is well known that the absorption coefficient for CH_2 stretching increases as CH_2 units are linked to form longer aliphatic chains). However, the situation becomes much more interesting if we increase the level of complexity of the system just slightly.

Figure 4 compares the spectrum of a phenol/dihydroxynaphthalene/ formaldehyde copolymer (50:50, meaning 50% phenol and 50% dihydroxynaphthalene) to that of a coal. Because of the multiplicity of linkage sites on the naphthalene ring, we produce an apparently densely cross-linked network even under conditions used to synthesize novolaks based on phenol alone. The infrared spectrum of this resin is now strikingly similar to that of the coal, the principal differences being in the aliphatic CH stretching region (the bands in the synthetic resin are much weaker) and the C-O stretching region (1200-1300 cm^{-1}) where the resin absorbs more strongly than coal because of its higher OH content. The spectra can be made even more similar by chemical "tinkering". For example, if we copolymerize with p-cresol instead of phenol, bands in the CH stretching region become more prominent, and so on. However, space does not permit us to explore this here. Next we will briefly describe our synthetic procedure, which we used to produce a range of copolymers, then briefly summarize the results of solvent swelling and extraction experiments, which again bear a striking resemblance to those obtained from coal.

Synthesis

Appropriate quantities of phenol, 1,5-dihydroxynaphthalene and oxalic acid were first dissolved in water. The mixture was then stirred and preheated at 65^0C for 30 minutes. Formaldehyde was then added and the mixture was refluxed at 100^0C for 2-3 hours. As the polymerization proceeded the solution or suspension gradually changed color. Finally, water was then removed by heating under vacuum at a temperature of 200^0C. The resulting resin is a black solid copolymer, only partially soluble in solvents such as pyridine, THF and NMP.

The samples were characterized by ^{13}C nmr, FTIR and pyrolysis GC/MS. The latter results were particularly interesting because we have always been concerned that reactions leading to larger aromatic clusters could occur when this technique is applied to coal. We had no evidence for this in our studies of the synthetic resins. The details of this characterization work will be presented in a separate publication.

Extraction and Swelling Experiments

Extraction and swelling experiments were performed on the resins using the usual techniques applied to coal. In these initial experiments the solvent used was pyridine. Swelling experiments (measured on ground particles placed in a graduated cylinder) were performed on the extracted material. The results are presented in Table 1.

It can be seen that an ordinary resol has 32% pyridine soluble material and swells to approximately twice its original dimensions in pyridine, very similar to results obtained with coals like Illinois #6. Copolymers synthesized with dihydroxynaphthalene units behave similarly at low concentrations of this co-

Substituting p-cresol, which can only polymerize in a linear, non-branched fashion, for phenol, restores much of the extractability.

CONCLUSIONS AND RAMIFICATIONS

We have synthesized resins that mimic the spectroscopic, swelling and solubility characteristics of coal. The crucial point is that we start with a knowledge of the structure of these materials and whether or not they are covalently cross-linked. We are comparing the behavior of these materials in various solvents as a means to determine the role that association through secondary forces plays in swelling and solubility. Although the cross-link density of these resols is not known (but could possibly be estimated by the pattern of linkages revealed by the aromatic CH out-of-place bending modes in the IR spectrum), it is a relatively easy task to chemically cross-link initially oligomeric novolaks with labeled compound and measure this parameter directly. We believe this approach will prove valuable in sorting out various models of coal structure and the role of secondary interactions such as hydrogen bonds.

ACKNOWLEDGMENT

The authors gratefully acknowledge the support of the Office of Chemical Sciences, U.S. Department of Energy, under grant No. DE-F602-86ER1353.

REFERENCES

1. Painter, P.C. Energy and Fuels, 1996, **10**, 1273.
2. Nishioka, M., Gebhard, L.A. and Silbernagel, B.G. Fuel, 1991, **70**, 341.
3. Nishioka, M. Fuel, 1991, **70**, 1413.
4. Nishioka, M. Fuel, 1992, **71**, 941.
5. Nishioka, M. Energy and Fuels, 1991, **5**, 487.
6. Takanohashi, T., Iino, M. and Nishioka, M. Energy and Fuels, 1995, **9**, 788.
7. Veytsman, B. and Painter, P.C. Energy and Fuels, 1997, **11**, 1250.

Table 1

Sample	Extraction Yield in Pyridine %	Swelling Ratio
Resol (phenol formaldehyde	32%	2.06
PDHNF20	42%	2.01
PDHNF30	12%	
PDHNF40	6%	
PDHNF50	6%	1.74
PCDHNF50	35%	

PDHNFX = Phenol-co-dihydroxynaphthalene/formaldehyde copolymer with x wt% of dihydroxynaphthalene.

PCDHNFX = p-cresol-co-dihydroxynaphthalene/formaldehyde copolymer

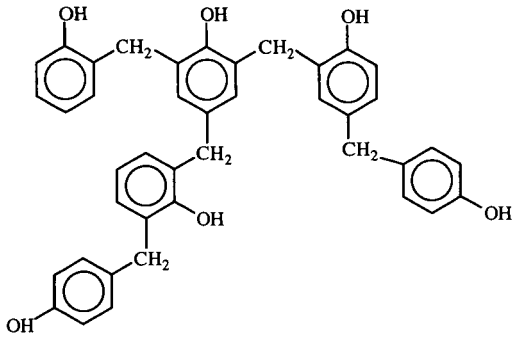

Figure 1. Typical oligomeric structure found in a novolac resin.

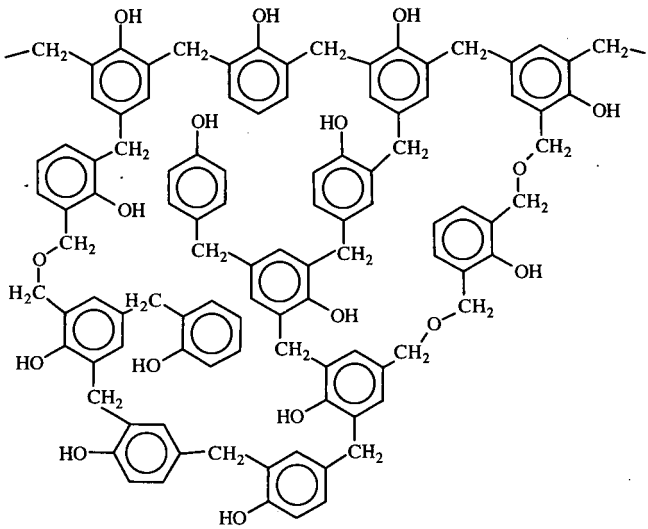

Figure 2. Schematic representation of part of the structure of a cured phenolic resin.

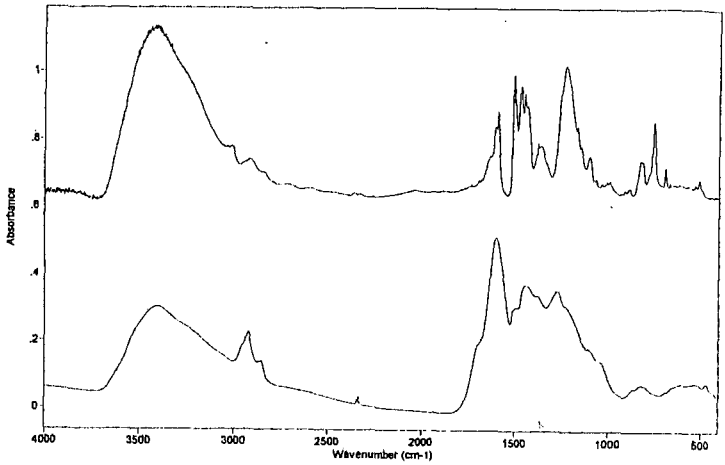

Figure 3. Comparison of the infrared spectrum of a cured resol (phenol-formaldehyde to a coal (PSOC 1423 P, 70% C)

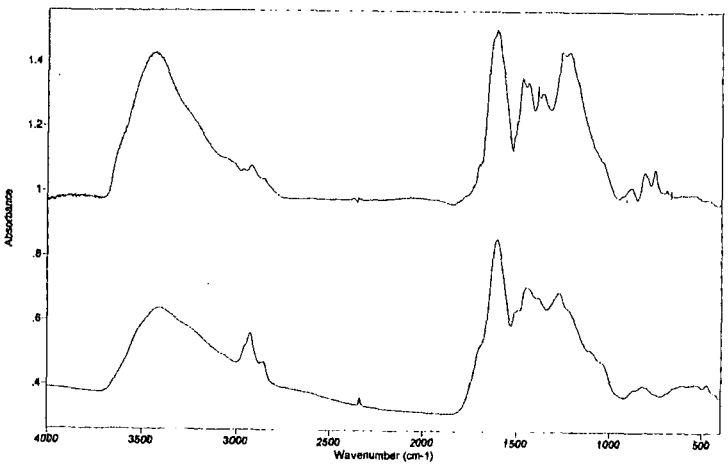

Figure 4. Comparison of the infrared spectrum of a cured phenol-co-dihydroxynaphthalene (50%) formaldehyde copolymer to that of a coal (PSOC 1423 P, 70% C)

EFFECT OF VARIOUS ADDITIVES ON SOLVENT EXTRACTION OF COALS

Masashi Iino[1], Toshimasa Takanohashi [2], E. Sultan Vayisoglu Giray[1], Chong Chen[1], Yoshihiro Masui[1], and Kazuhiro Takahashi[1]
[1]Institute for Chemical Reaction Science, Tohoku University, Katahira, Aoba-ku, Sendai 980-8577, JAPAN
[2]Energy Resources Department, National Institute for Resources and Environment, Onokawa, Tsukuba 305-8569. JAPAN

KEYWORDS: Coal extraction, additive, carbon disulfide / *N*-methyl-2-pyyrolidinone mixed solvent

INTRODUCTION

The extraction of bituminous coals with carbon disulfide / *N*-methyl-2-pyrrolidinone (CS2 / NMP) mixed solvent (1:1 by volume) was found to give very high extraction yields at room temperature (1). We have also found that the addition of a small amount of various additives such as tetracyanoethylene (TCNE) and *p*-Phenylenediamine(*p*-PDA) to the mixed solvent increases the extraction yields greatly(2,3). For example, the yield of the room temperature extraction of Upper Freeport coal with the 1:1 CS2 / NMP mixed solvent increases from 59 wt% (daf) to 85 wt% (daf) by adding only 5% (based on coal) of TCNE to the mixed solvent(2). Recently inorganic salts of chloride and fluoride are found to be also effective for the increase of the extraction yields.

We have also found (4) that when the extracts obtained with the CS2/NMP mixed solvent were fractionated with pyridine to yield pyridine-insoluble (PI) and –soluble (PS) fractions, part of PI became insoluble in the mixed solvent, though it is a part of the extracts with the mixed solvent. By the addition of a small amount of the additives such as TCNE, tetracyanoquinodimethane (TCNQ) or *p*-phenylenediamine to the mixed solvent, PI became soluble in the mixed solvent.

While, swelling and viscoelasticity behaviors of coal show that coal has a kind of macromolecular network structure. The changes of reactivity and product selectivity of coal by heat or solvent treatment were often explained by the changes of this network structure. But the nature of the macromolecular network structure are still unknown. Although covalently connected crosslinking structures are often assumed, the evidencces for them are not enough. Recent works, including our results, suggest that for some bituminous coals, large associates of coal molecules i.e., non-covalent (physical) network are a better network model than the covalent one. Coal extracts and coal derived liquids are known to readily associate between themselves to form complex associates (5-8).

Solubility limit of coals, i.e., how high extraction yields can be obtained without the breaking of covalent bonds is one of the key points to clarify a kind of network bonds, i.e., covalent or non-covalent (physical) networks. If coal consists of highly developed covalent networks and low molecular weght substances occuluded in them, coal extractability is low, as observed in the extractions with conventional solvents such as pyridine. However, 85wt% of the extraction yield obtained for CS2 / NMP / TCNE solvent system described above suggests that Upper Freeport coal has little covalent networks.

In this presentation the effect of various additives on extraction yield of coal, and solubility of the extract component (PI) in the mixed solvent was reviewed including recent results. Mechanisms for the enhancement of the extraction yield and the solubility by the additives are discussed.

EXPERIMENTAL

Extraction of coals with CS2 / NMP mixed solvent

The coals used in this study are shown in Table 1. A coal was extracted with CS_2 / NMP mixed solvent (1:1, volume ratio) under ultrasonic irradiation repeatedly at room temperature (1) with or without an additive. The extract obtained was fractionated with acetone and pyridine, respectively, to give acetone-soluble(AS), pyridine-soluble and acetone-insoluble(AI/PS), and pyridine-insoluble(PI) fractions. Solubility of PI in the mixed solvent was examined at room temperature under ultrasonic irradiation with or without an additive.

RESULLTS AND DISCUSSION

Effect of Additives on Extraction Yields of Coals

Tables 2 – 4 show the yields of the extractions of Upper Freeport coal with the CS_2/NMP mixed solvent with electron acceptors, donors (aromatic amines), and halogenide salts, respectively. Table 2 shows the effect of an electron acceptors, together with their electron affinity, which is a measure of the electron acceptability of electron acceptor. Table 2 shows that only TCNE and TCNQ gave high extraction yieldsas expected from their high electron affinities. However, other electron acceptors used here do not show the extraction yield enhancements. Table 3 also shows that the effectiveness of electron donors is not an order of their electron donatability, since *N,N,N',N'*-tetramethyl-*p*-phenylenediamine (TMPDA), which is the strongest electron donor, gave much lower yield than other donors. The results for halogenide salts in Table 4 indicate that a kind of halogenide anions affects the extraction yields, i.e., the yields increased in the order; F>Cl>Br>I, and little change between Li and tetrabutylammonium cations.

Table 5 shows the effect of the addition of tetrabutylammonium fluoride (TBAF) on the extraction of various coals. Upper Freeport, Lower Kittanning, and Stigler coals incresed their extraction yields with the CS_2 / NMP mixed solvent by the addition of TBAF, but for Pttsburgh No.8, Illinois No.6 coals the yields did not increase. For the addition of TCNE the same tendency of the extraction yields were obtained for the five coals above (2).

Effect of Additives on Fraction Distribution of Extracts

Table 6 shows the fraction distribution of the extracts obtained from the extraction of Upper Freeport coal with TCNE, *p*-PDA, and TBAF. Table 6 indicates that the increase in the extraction yields is mainly due to the increase of the heaviest extract fraction, i.e., PI, and little increase in the lighter fractions of AS and AI/PS.

Effect of Additives on Solubility of Extract Fraction

Tables 7 and 8 show the effect of electron acceptors and donors (aromatic amines) on the solubility of PI in the CS_2 / NMP mixed solvent, respectively. Table 7 shows a similar tendency as the effect of electron acceptors on the extraction yields (Table 2), i.e., only TCNE and TCNQ are effective for the increase in the solubility of PI. Table 8 shows that aniline and *p*-PDAincreased the solubility of PI greatly, and especially *p*-PDA is as effective as TCNE and 25mg (0.23mmol)/g-PI increased about 40% of the solubility.

Mechanisms for the enhancement of the extraction yield and the solubility by the additives

The solubility increase of PI by TCNE addition, and also the increase in the extraction yield are considered to be caused by the breaking of noncovalent bonds in aggregates among coal molecules(8), since the effect of TCNE addition is reversible, i.e., PI', which is considered to be free of TCNE by washing the TCNE-solubilized PI by pyridine, is again partly insoluble in the mixed solvent, and it becomes almost completely soluble by the re-addition of TCNE. From similar behaviors of the other additives toward a kind of coals and fraction distribution of the extracts as TCNE they also solubilize coal by the same mechanism as TCNE.

The 1:1 CS2-NMP mixed solvent can break the weak non-covalent bonds which are not broken convensional solvents such as pyridine. The additive such as TCNE and *p*-PDA in the mixed solvent, which has strong interaction with coal molecules, can break even the strong noncovalent bonds. A kind of interactions between the additives and coal molecules are not clear, but the results here suggest that charge-transfer (donor-acceptor) interaction may not be a main interaction.

The additives such as TCNE, *p*-PDA, and TBAF is very efficient for the extraction yield enhancement of Upper Freeport coal. For example, the addition of TCNE more than 0.05g to 1g of the coal reached an almost constant extraction yield of about 85 wt% (daf). Using the structural parameters of fa and degree of aromatic ring condensation for Upper Freeport coal reported by solum et al.(9), 0.05g of TCNE per 1g of coal is calculated to correspond to 1 molecules of TCNE per about 8 aromatic clusters of the coal. The reasons why these additives are so effective, and the effectiveness is depend on a kind of coals are not clear, though all the coals which increase their solubility remakably by the additives contain much of the heaviest extract fraction, PI.

These results obtained strongly suggest that at least some bituminous coals, which gave very high

extraction yields with the CS2/NMP/additive solvent, have chemical structure consisting of complex mixture of the aggregates among coal molecules, and having no giant covalently bound cross-linked network.

CONCLUSIONS

The effects of various additives on the extraction yield of coals and the solubility of extract fraction were investigated. The additives such as TCNE, *p*-PDA, and lithium and ammonium salts of fuloride and chloride are found to be very effective for the increase in the extraction yield and the solubility of the extract fraction. A mechanism that noncovalent bonds in the aggregates among coal molecules are broken by the additives is proposed.

ACKNOWLEDGMENT

This work was supported by "Research for the Future" project of Japan Society for the Promotion of Science.

REFERENCES

1. Iino, M., Takanohashi, T., Osuga, H. and Toda, K., *Fuel*, **1988**, 67, 1639-1647.
2. Liu, H., Ishizuka, T., Takanohashi, T. and Iino, M., *Energy Fuels*, **1993**, 7, 1108-1111.
3. Ishizuka, T., Takanohashi, T., Ito, O. and Iino, M *Fuel*, **1993**, 72, 579-580.
4. Sanokawa, Y.,Takanohashi, T. and Iino, M., *Fuel*, **1990**, 69, 1577-1578.
5. Sternberg, H. W., Raymond, R. and Schweighardt, F. K., *Science*, **1975**, 188, 49-51.
6. Stenberg, V. I., Baltisberger, R. J., Patel, K. M. et al., *Coal Science* (ed Gorbarty, M. L., Larsen, J. W., Wender, I.), Academic Press, New York, **1983**, pp 125-171.
7. Nakamura, K., Takanohashi, T., Iino, M. et al., *Energy Fuels*, **1995**, 9, 1003-1010.
8. Iino, M., Liu, H., Hosaka, N., Kurose, H. and Takanohashi, T., *Prepr. Pap. Am. Chem. Soc.,Div. Fuel Chem.* **1997**, 42(1), 248-252.
9. Solum, M. S., Pugmire, R. J., Grant, D. M., *Energy Fuels*, **1989**, 3, 187-192.

Table1. Analysis of coals

Coal	Ultimate analysis(wt%,daf)				Ash(wt%,db)
	C	H	N	O+S [a]	
Sewell'B'	88.4	5.3	1.4	4.9	4.6
Upper Freeport	86.2	5.1	1.9	6.8	13.1
Lower Kittanning	84.0	5.6	1.7	8.7	9.0
Lewiston Stockton	82.9	5.4	2.0	9.7	19.6
Pittsburgh No.8	82.6	5.5	2.1	9.8	8.7
Stigler	77.8	4.8	1.5	15.9	11.7
Illinois No.6	76.9	5.5	1.9	15.7	15.0

[a] By difference

Table 2. Effect of the addition of electron acceptors on extraction yields[a] of Upper Freeport coal together with their electron affinity

additive[b]	Ectraction yield (wt%)	Electron affinity (eV)
None	64.6	-
TCNE[c]	85.0	2.2
TCNQ[d]	80.0	1.7
DDQ[e]	49.8	1.95
1,2,4,5-Tetracyanobenzene	44.4	0.4
p-Benzoquinone	39.3	0.77
2,6-Dichloro-p-benzoquinone	49.7	1.2
p-Chloranil	45.5	1.37

[a] CS_2/NMP mixed solvent (1:1 by volume), room temperture

[b] 0.2mmol/g-PI of an election acceptor, [c] Tetracyanoethylene

[d] 7,7,8,8-Tetracyanoquinodimethane, [e] 2,3-Dichloro-5,6-dicyano-p-benzoquinone

Table 3.Effect of the addition of electron donors(aromatic amines)on extraction yields[a] of Upper Freeport coal together with their ionization potential

Additive[b]	Extraction yield (wt%,daf)	Ionization potential (eV)
None	51.4	
aniline	72.3	7.7
p-PDA[c]	81.3	6.87
TMPDA[d]	61.4	6.5
melamine	61.8	-

[a] CS_2/NMP mixed solvent(1:1 by volume), room temperature
[b] 25 mg/g-coal of an electron donor
[c] *p*-phenylendiamine, [d] N,N,N',N'-tetramethyl-*p*-phenylenediamine

Table 4. Effect of the addition of halogenide salts on extraction yields[a] of Upper Freeport coal

Additive (mmol/g-coal)	Extraction yield (wt%,daf)	Additive (mmol/g-coal)	Extraction yield (wt%,daf)
None	56.4, 59.8	$(n\text{-butyl})_4NH_4F$ (0.25)	83.9
LiCl (0.24)	81.7	$(n\text{-butyl})_4NH_4Cl$ (0.25)	78.8
LiBr (1.0)	68.7	$(n\text{-butyl})_4NH_4Br$ (0.25)	61.8
LiI (1.9)	60.9	$(n\text{-butyl})_4NH_4I$ (0.25)	59.3

[a] CS_2/NMP mixed solvent(1:1 by volume), room temperature

Table 5. Effect of the addition of TBAF on the extraction yields[a] of various coals and fraction distributions of the extracts

Coal	TBAF	Extraction yield (wt%,daf)	Fraction distribution(wt%,daf)		
			AS	PS	PI
Upper Freeport	None	60.1	8.2	25.0	26.9
	0.25mmol/g-coal	82.4	11.5	12.7	58.2
Lower Kittanning	None	38.7	6.3	27.1	5.3
	0.25mmol/g-coal	63.7	9.4	17.9	36.4
Pittsburgh No.8	None	43.5	12.3	30.0	1.2
	0.25mmol/g-coal	39.9	11.8	23.4	4.7
Stigler	None	21.2	6.1	14.5	0.6
	0.25mmol/g-coal	62.4	6.4	17.2	38.8
Illinois No.6	None	27.9	7.8	19.1	1.0
	0.25mmol/g-coal	27.4	10.0	16.8	0.6

[a] CS_2/NMP mixed solvent(1:1 by volume),room temperature

Table 6. Fraction distribution of the extracts obtained from the extraction[a] of Upper Freeport coal with the additives

Additive	extraction yield (wt%,daf)	fraction distribution of the extract (wt%,daf)		
		AS	AI/PS	PI
none	60.1	8.2	25.0	26.9
TCNE	85.0	10.5	28.5	47.0
p-PDA	81.3	9.8	23.1	48.4
LiCl	83.6	10.2	16.1	57.3
TBAF	82.4	11.5	12.7	58.2

[a] CS2/NMP mixed solvent(1:1 by volume), room temperature

Table 7. Effect of the addition of electron acceptors on solubility[a] of pyridine-insoluble extract (PI)

Additive[b]	Solubility of PI (wt%)		Electron affinity (eV)
	PI from Upper Freeport Coal	PI from Zao Zhuang Coal	
None	66.4	51.0	-
TCNE[c]	99.5	99.5	2.2
TCNQ[d]	94.3	81.0	1.7
DDQ[e]	88.8	53.8	1.95
1,2,4,5-Tetracyanobenzene	71.2	47.7	0.4
p-Benzoquinone	76.1	44.1	0.77
2,6-Dichloro-p-benzoquinone	67.4	37.0	1.2
p-Chloranil	51.8	34.8	1.37

[a] CS_2/NMP mixed solvent (1:1 by volume), room temperture

[b] 0.2mmol/g-PI of an electron acceptor, [c] Tetracyanoethylene

[d] 7,7,8,8-Tetracyanoquinodimethane, [e] 2,3-Dichloro-5,6-dicyano-p-benzoquinone

Figure 8. Effect of the addition of electron donors (aromatic amine) on solubility[a] of pyridine-insoluble extract fraction (PI) from Upper Freeport

Additive[b]	Solubility of PI (wt%)	Ionization potential (eV)
None	55.1	-
aniline	85.4	7.7
o-PDA	91.8	7.2
m-PDA	85.1	7.1
p-PDA	96.5	6.9

[a] In CS_2/NMP mixed solvent(1:1 by volume), room temperature

[b] 25mg/g-PI of an additive

ROLE OF SOLVENT IN THE INTERACTION OF TCNE/TCNQ WITH COAL

Chong Chen and Masashi Iino
Institute for Chemical Reaction Science
Tohoku University
Katahira 2-1-1, Aoba-ku, Sendai 980-8577, Japan

Keywords:additive, coal, solubility

INTRODUCTION

After N-methyl-2-pyrrolidinone(NMP)-CS_2(1:1, v/v) mixed solvent was found having the magic ability to dissolve coal up to about 60wt% based on daf coal[1], the seeking for higher solubility of coal has never stopped. Enhancement of the coal solubility by adding additives is our way. Up till now, more than 10 additives including electron acceptors and donors were examined[2-5]. Electron acceptors, Tetracyanoethylene(TCNE) and 7,7,8,8-Tetracyano-quinodimethane(TCNQ) were found to be two powerful additives. However, the mechanism is still not clear. Previous studies on the mechanism have been concentrated on the charge-transfer complex formation between additives and coal leaving the role of the solvents out of focus[2, 9-10]. However, the attempt to correlate the solubility of coal and the electron acceptor-ability was not successful. Therefore, other mechanism must be involved. In this work, solvent was found strongly related to the mechanism of TCNE/TCNQ to increase the coal solubility.

The conclusion of charge-transfer complex formation between coal and TCNE/TCNQ was drawn from the IR shift of ν_{CN} in TCNE/TCNQ when they were mixed with coal in solvent. We have reported that the coal containing TCNE deposited from NMP-CS_2(1:1, v/v) mixed solvents had a pair of IR band at 2200cm^{-1} and 1500cm^{-1} [2]. Initially, the band at 2200cm^{-1} had been proposed arising from charge-transfer complex between TCNE and coal[6]. However, further investigation found that the two IR bands arisen from the reaction product of TCNE and NMP, i.e., NMP 1,1,2,3,3-pentacyanopropene salt(NPCNP). TCNE does not exist as a neutral molecule in NMP, instead, an anion derivative of TCNE was formed, which may be the key component to enhance the coal solubility. Addition of NPCNP was found also effective for the coal solubility increase.

In the case of TCNQ, the interaction of TCNQ with coal aromatics seems to be related to the solvent used. TCNQ radical anion generated in NMP may be an intermediate of TCNQ interaction with coal aromatics. The extent of TCNQ interaction with coal aromatics depends on the structure of aromatics.

EXPERIMENTAL

UV spectral properties of TCNE/TCNQ in various solvents were measured on HITACHI U2000 UV spectrometer with 1 cm quartz cell. FTIR spectra were recorded on JASCO FT/IR-8300 spectrometer using KRS-5 or KCl cell(thickness of 0.1mm), 16 scans at resolution of 4cm^{-1}. NMR measurement was carried out on JEOL JNM-LA400 spectrometer. $CDCl_3$ was used as solvent. All the solvents used for spectral analysis are spectrophotometeric grade. "Anhydrous" NMP was dehydrated by 4Å molecular sieves overnight.

The procedure of the reaction of TCNE with NMP in the presence of water referred to that of TCNE reaction with pyridine in the presence of water[8], but it was carried out at room temperature. 30mL acetone containing 6.3g TCNE was added into 100ml NMP containing 10% water under N_2 protection. After the reaction, acetone and NMP were removed via a rotary evaporator at 40°C and large volume of diethyl ether was decanted into reactor. A yellow solid was obtained(yield, 58wt%, based on raw product). Recrystallization of a portion of the solid from diethyl ether gave a yellow crystal of **I**, mp 51-52°C: UV-visible(NMP) λ_{max} nm(log ε) 400(4.41), 418(4.40); FTIR(thin film, cm^{-1}) 1519($\nu_{C=C}$), 2203($\nu_{C\equiv N}$); (liquid film) 2199(in NMP, $\nu_{C\equiv N}$); ^{1}H-NMR($CDCl_3$) δ 3.70, 3.06, 2.77, 2.24ppm, a broad and weak peak at 7.5~11ppm downfield shift as the increase of concentration of **I**; ^{13}C-NMR($CDCl_3$) δ 178.32, 135.60, 116.70, 114.06, 113.78, 57.91, 51.95, 31.26, 30.46, 17.38ppm. Anal. Calcd for NMP-1,1,2,3,3-Pentacyanopropene salt(**I**, $C_{18}H_{20}N_7O_2$): C, 59.02%; H, 5.29%; N, 26.75%; O, 8.78%. Found: C, 59.18%; H, 5.46%; N, 26.78%; O, 8.74%.

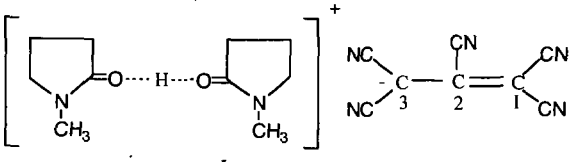

I

RESULTS AND DISCUSSION

Spectra properties of TCNE-NMP system

The shift of stretching frequency of $C\equiv N(v_{CN})$ of TCNE in some solvents indicates that TCNE may react or interact with solvents(Table 1). In acetone and THF, almost no shift was observed. The small shift in toluene is attributed to the formation of charge-transfer complex of TCNE with toluene. However, the large shift of v_{CN} in NMP indicates that TCNE does not exist as a neutral molecule in this solvent. Instead, a new substance may be generated by the reaction of TCNE with NMP. In dehydrated NMP, ν_{CN} shifts to 2338cm^{-1} arose from complex of TCNE-NMP, while in commercial NMP(used for extraction) containing very small amount of water(estimated from the hydroxyl band), the ν_{CN} band appears at 2199cm^{-1}, which indicates the presence of PCNP anion.

Figure 1 shows the change of UV spectra of TCNE in NMP of different water content. In dehydrated NMP, PCNP anion absorptions at 400 and 418nm are very weak. However, they are increasing but the peak of TCNE-NMP complex at 298nm decreasing as the increase of water content in NMP, indieating that PCNP anion is generated from the reaetion of TCNE with NMP in the presence of water.

The reaction of TCNE with pyridine[8] or pyridone[11-12] to generate PCNP anion was known 30 years ago, but the reaction of TCNE with NMP to generate the same anion is found first time.

Although this reaction needs water, commercial grade NMP used for extraction usually contains small amount of water. Based on our experimental procedure, 1 gram coal or PI was added 0.2mmol TCNE in 60 mL NMP-CS_2 mixed solvent(1:1, v/v), 0.012wt% water in NMP is enough for 0.2mmol TCNE to generate PCNP anion. Although we have not measured the water content of the NMP, it is quite possible that 97% commercial grade NMP used for extraction contains enough water for the reaction. Moreover, NMP is very easy to absorb water. It is very difficult to remove all the water from NMP. Even dehydrated NMP was used, PCNP anion band at 400 and 418nm is still observable(Figure 1) in TCNE-NMP system. This is probably due to incomplete dehydration by molecular sieves or re-absorption of water during the operation. It was also found that in commercial NMP, ν_{CN} of TCNE in NMP always shifts to 2199cm^{-1}. These results demonstrate that TCNE exists as PCNP anion in NMP but not neutral TCNE molecule.

Effect of 1,1,2,3,3-pentacyanopropene(PCNP) anion to increase the solubility of PI

Based on the spcctral study, TCNE does not exist as a neutral molecule in NMP as well as in the NMP-CS_2 mixed solvent. Instead, NPCNP is formed. The solubility of PI and its parent coal(UF) in the NMP-CS_2 mixed solvent was examined by adding small amount of NPCNP. Figure 2 shows that the addition of only 0.04mmol/g-PI NPCNP is enough to increase the solubility of PI from 54% to 96%; more NPCNP, 0.2mmole/g-PI, results in 99.9% solubilization of PI. The addition of 0.2mmol/g-coal NPCNP increases the UF coal solubility from 64.6% to 71.5%, which is closed to the increment by adding the same amount of TCNE[3]. Another PCNP anion contained compound, Pyridinium 1,1,2,3,3-pentacyanopropenide, which was synthesized from pyridine and TCNE in the presence of water[8], was also found effective to enhance the solubility of PI. The two experiments indicate that PCNP anion is the key component to enhance the solubility of coal.

The mechanism of PCNP anion to enhance coal solubility is believed to be attributed to breaking hydrogen bonding. NMR study confirms the possibility of this anion being able to break the hydrogen bonding formed between pyridine and phenol. The details will be reported in a paper submitted to Energy Fuels.

Spectral property of TCNQ in various solvents

The UV-visible spectra property of TCNQ depends on solvent, as shown in Figure 3. It is quite different in NMP and pyridine than in THF and chloroform. The peaks around 800nm, i.e., 752, 771 and 833, 854nm, were assigned to the TCNQ radical anion[13-14]. Figure 3 illustrates that TCNQ generates TCNQ radical anion in NMP and pyridine but not in THF and chloroform.

In the room temperature, the addition of aromatics into the NMP solution containing TCNQ results in the change of its UV-visible spectrum. As shown in the Figure 4, the absorption of TCNQ radical anion around 800nm disappeared as accompanied by appearing a new absorption at 490nm, which may be arisen from the complex formed between TCNQ and aromatics. However, when the aromatics were added into the mixture of TCNQ and chloroform, chlorobenzene or THF, no such change occurs. The spectra are just a summation of the TCNQ-solvent and aromatics. Accordingly, we can not deny the possibility that TCNQ reacts with aromatics by the TCNQ radical anion as an intermediate.

The extent of TCNQ reaction with the aromatics depends on the structure of aromatics. Phenanthrene reacts with TCNQ radical anion quickly, the peaks around 800nm disappeared in several minutes after it was added into the mixture of TCNQ-NMP and a new peak at 490nm appeared. However, anthracene, the isomer of phenanthrene, is hard to react with TCNQ anion radical at room temperature. The spectrum has no change even after 180min. The larger size

aromatics, pyrene, can react with the TCNQ radical anion, but it takes longer time than phenanthrene needed. The different distribution of π electrons on the aromatic ring may cause the difference. Coal from different source and rank contains aromatics of different ring size and structure, which may cause the selective effect of TCNQ for certain coal, e.g., TCNQ is effective for some coals but not effective for others.

When pyridine insoluble fraction(PI) from Upper Freeport coal extracts(extraction with CS_2-NMP mixed solvent, 1:1 by volume) was used instead of pure aromatics to repeat the experiment mentioned above, similar spectra changes were observed. As the reaction time increase, the absorption of TCNQ radical anion around 800nm decreased but the absorption at 490nm increased(see Figure 5). Based on the results of pure aromatics, aromatics in PI reacts with TCNQ radical anion to generate a new complex(around 490nm) is concluded.

CONCLUSIONS

The importance of solvent was noted in examination the mechanism of TCNE/TCNQ to enhance the coal solubility. TCNE was found not to be existed as a neutral molecule in NMP. Instead, it reacts with NMP in the presence moisture to generate 1,1,2,3,3-pentacyanopropene (PCNP) anion, which is considered a key component to enhance the coal solubility by breaking coal-coal interaction, e.g., hydrogen bonding. TCNQ generates TCNQ radical anion in NMP and pyridine, which is an intermediate of TCNQ interaction with coal aromatics.

ACKNOWLEDGMENTS

This work was supported by "Research for the Future" project of Japan Society for the Promotion of Science(JSPS). We are greatly grateful to Prof. John Larsen of Lehigh University for his valuable discussion and comments on this work.

REFERENCES

1. Iino, M.; Takanohashi, T.; Ohsuga, H.; Toda, K. *Fuel* **1988**, *67*, 1639-1647
2. Iino, M.; Kurose, H.; Giray, E. S.; Takanohashi, T. *PreprPap. Am. Chem.* Soc., Div. Fuel Chem. **1998**, 43(3), 712-716
3. Liu, H-T; Ishizuka, T.; Takanohashi, T.; Iino, M. *Energy Fuels* **1993**, 7, 1108
4. Ishizuka, T.; Takanohashi, T.; Ito, O.; Iino, M. *Fuel* **1993**, *72*, 579-580
5. Sanokawa, Y.; Takanohashi, T.; Iino, M. *Fuel* **1990**, *69*, 1577-1578
6. Schwager, I.; Kwan, J. T.; Miller, J. G.; and Yen, T. F. *PreprPap. Am. Chem. Soc., Div. Fuel Chem.* **1978**, *23*, 284-289
7. Thompson, R. L.; Rothenberger, K. S.; Retcofsky, H. L. *Energy Fuels* **1997**, *11*, 739-746
8. Middleton, W. J.; Little, E. L.; Coffman, D.D.; Engelhardt, V. A. *J. Am. Chem. Soc.*, **1958**, *80*, 2795-2806
9. Flowers, R.A.; Gebhand, L.; Larsen, J. W.; Sananda, Y; Sasaki, M.; Silbernagel, B. *Energy Fuels* **1994**, *8*, 1524-1525
10. Iino, M.; Liu, H-T.; Hosaka, N.; Kurose, H.; Takanohashi, T. *Prepr. Pap. Am. Chem. Soc. Div. Fuel Chem.* **1997**, *42*, 248-252
11. Thyagarajan, B. S.; Rajagopalan, K.; Gopalakrishnan, P. V. *Chem. Ind.* **1996**, *5*, 1887-1888
12. Thyagarajan, B. S.; Rajagopalan, K.; Gopalakrishnan, P. V. *J. Chem. Soc.(B)* **1968**, 300-303
13. Melby, L. R.; Harder, R. J.; Hertler, W. R.; Mahler, W.; Bensin, R. E. and Mochel, W. E., *J. Am. Chem. Soc.*, **1962**, *84*, 3374.
14. Shin, D-M.; Choi, K-H. and Park, J. S., et al., *Thin Solid Films*, **1996**, *523*, 284.

Table 1. List of TCNE in various solvent

solvent	ν_{CN}(cm^{-1})
blank	2260
acetone	2257
THF	2257
toluene	2252
NMP[a]	2338
NMP[b]	2199

[a]dehydrated by 4Å molecular sieves;
[b]commerical one(NMP content 97%) containing small amount water(estimated from the weak hydroxyl band in the spectrum).

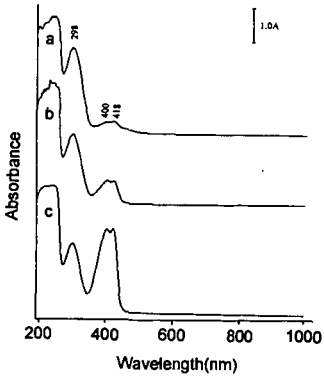

Fig. 1. UV-visibile spectra of TCNE in NMP containing water(mg/mL). a, 0; b, 15; c, 50

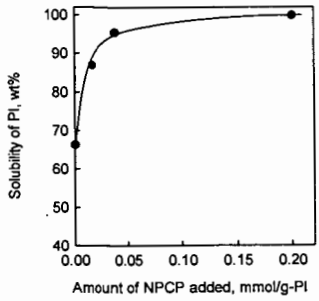

Fig. 2. Increase of the solubility of PI(pyridine insoluble fraction) form Upper Freeport coal in the NMP-CS_2 mixed solvent by adding NPCNP

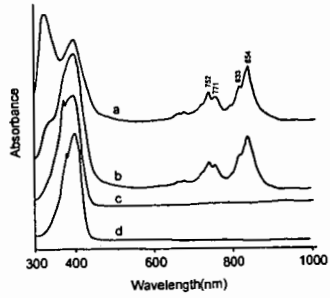

Fig. 3. UV-visible spectra of TCNQ in various solvents.

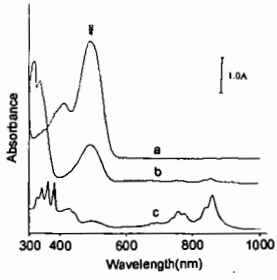

Fig. 4. UV-visible spectra of aromatics(1×10^{-5}moleL^{-1}) in 5×10^{-5}moleL^{-1} TCNQ NMP solution.
a, phenanthrene(reaction for 3 min); b, pyrene(40 min); c, anthacrene(180 min)

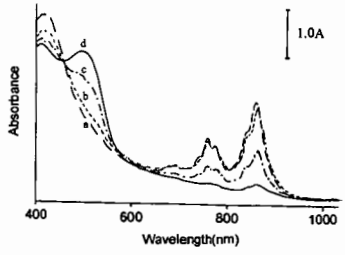

Fig. 5. UV-visible spectra of PI-TCNQ-NMP-CS_2(1:1, v/v) system.
a, 0 min; b, 30 min; c, 60 min; d, 90 min

Molecular Size and Structure in Pyridine Extracts of Upper Freeport Coal as Separated by M41S Sieving

Jerry E. Hunt, Randall E. Winans, Mike Ahrens, and Langqiu Xu
Chemistry Division
Argonne National Laboratory
9700 South Cass Ave.
Argonne, IL 60439

KEYWORDS: coal, extracts, sieving, separation, mass spectrometry

INTRODUCTION

The determination of the structure of coal has long been of interest due to its crucial importance in research on reactivity and processing. However, the chemically and physically heterogeneous nature of coals makes determination of the chemical nature of even the building blocks complicated, since the molecular structure and molecular weight distribution are not dependent on a single molecule or repeat unit as in technical polymers or biopolymers, but on a complex mixture of molecules and potential connections between them which may vary among coals.

Coal extracts have long been used to obtain coal material in solution form that can readily be characterized. However, what part of the total coal structure these extracts represent is not completely known. Pyridine has been a particularly good solvent for coal; for example, the extractability of Upper Freeport has been shown to be as high 30%.. Although pyridine extracts of coal have been referred to as solutions, there is good evidence that they are not truly solvated, but are dispersions which are polydisperse in particle size.[1] The particle sizes may span the size range from clusters of small molecules (a few Å) to extended clusters of large particles (a few hundred Å), not unlike micelles, where the functional groups of molecules which interact favorably with the pyridine solvent lie at the surface of particles.

Mesoporous silicates are attractive candidates for separations due to their high surface areas and porous nature. MCM-41 is one member of a new family of highly uniform mesoporous silicate materials introduced by Mobil, whose pore size can be accurately controlled in the range 1.5 Å-10 nm.[2,3] This recently discovered M41S class of zeolites should be useful to effect size separation, due to their large pore sizes and thus their potential for the separation of larger compounds or clusters. True molecular sieving on the size range of molecular and cluster types found in coal solutions should be possible with M41S materials by tuning the pore size.

We have synthesized a mesoporous silicate material with a surface area of approximately 1100 m^2/g and pore sizes of approximately 25 Å and 33 Å. The results of a study on the ability of this mesoporous materials (M41S) to be used as stationary phases for separations of coal complexes in pyridine is the subject of this paper.

EXPERIMENTAL

The coal used in this study is the mv bituminous Upper Freeport coal (APCS 1) of the Argonne Premium Coal Samples series.[4] We have used a new room temperature extractor, the Gregar extractor and traditional refluxing in pyridine to extract the coal. Approximately 10 g of coal was extracted in the Gregar extractor for one week. The extract was filtered and stirred with the M41S material for one week. This was then filtered and the zeolite-containing coal was extracted with methylene chloride. The extraction removed the coal material from the zeolite quantitatively.

A similar quantity of coal (10 g) was extracted by pyridine reflux for one week. The extract was divided and stirred for one week in 33 Å and 25 Å M41S material. After filtering, the zeolite material containing the coal was extracted with methylene chloride. Approximately 25% of the coal material was recovered from each zeolite by methylene chloride extraction. Further extraction with chlorobenzene resulted in only a few additional percent of coal.

Synthesis of MCM-41 was an approach combining the advantages of several literature works[2,3,5]. Different chain length of surfactants, ranging from dodecyltrimethylammonium to octadecyl-trimethylammonium bromide, were used as template to construct a periodic mesophase. The silica source used was tetramethyl orthosilicate. The synthesis was carried out at room temperature in the

solution of methanol and sodium hydroxide mixture. Pure silica versions of these zeolites were prepared to alleviate irreversible absorption by aluminum sites.

Mass spectra were recorded on a Kratos Maldi III instrument for laser desorption (LD) and a Kratos MS-50TA for low voltage high resolution mass spectrometry (LVHRMS). For the LD spectra, the laser intensity for the N_2 laser (337 nm) was kept at ion appearance threshold for all samples. The LVHRMS was recorded using low energy electron ionization (18eV) to maximize ionization of high mass compounds with minimal fragmentation. TGA-DTA (thermal gravimetric analysis and differential thermal analysis) measurements were obtained on a SDT 2960 from TA Instruments. For these samples, measured against an alumina standard in a 100 mL/min O_2 flow with a temperature ramp of 10°C/min to 800°C. The TGA data is also represented in its first-derivative or differential thermal gravimetry (DTG) format. Total organic loss were calculated by measuring the weight loss over the approximate temperature range of 200-600 °C. XRD analyses were carried out on a Rigaku Miniflex+ instrument using CuKα radiation, a NaI detector, a 0.05° step size, and a 0.50°, 2/min scan rate. XRD and SAXS showed pore sizes of 25 Å and 33 Å for the two M41S-class zeolites.

RESULTS AND DISCUSSION

The Gregar extractor extracted only 7.45% of the Upper Freeport coal into pyridine. The LD mass spectrum of the coal-zeolite extract showed only minimal ion intensity. The LVHRMS of this sample was used to estimate the number of aromatic rings present in the extracts. The results show that the largest mole % of hydrocarbon containing material was zero rings (5.5%), one ring (2.5%), two ring (0.8%) species. There is a small amount of material that can be attributed to multiple ring systems above three rings (2.87%). The reason for the low extractability using this technique may be a result of room temperature pyridine extraction as opposed to refluxing pyridine for the traditional technique. Although the amount of material is less, it is interesting that the majority of this is essentially aliphatic with very little aromatic character.

The refluxing pyridine extracted 29.6% of APCS 1, which is consistent with published results of extractabilities of this coal.

We used TGA to determine the weight loss as a function of temperature. From this data we can determine the total amount of organic material in the mesoporous zeolite. The TGA data shown in Fig 1 indicates that the 33 Å pore size material contains a larger amount of coal extract from the pyridine solution than the 25Å M41S mesoporous material. This is shown as the weight loss per cent of the total sample weight of 22.6% for the 33Å material versus 15.6% for the 25Å material (Fig. 1 & 2).

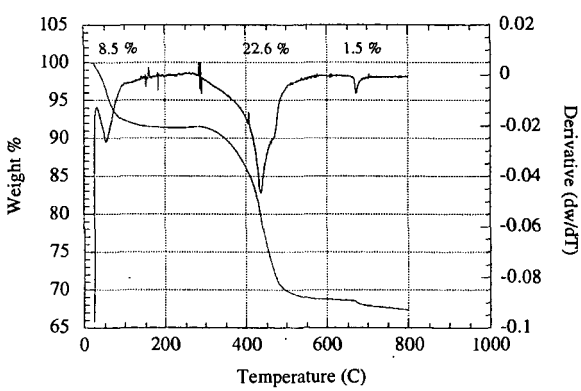

Fig. 1. The TGA of 33Å M41 S material with pyridine extract of Upper Freeport coals

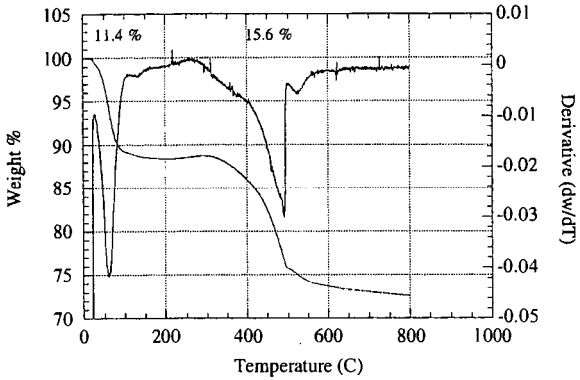

Fig. 2. The TGA of 25Å M41 S material with pyridine extract of Upper Freeport coals

Certainly, very polar material will bind to the silica. In the case of both M41S mesoporous materials only 25 % can be removed from the zeolite. The more nonpolar will be extracted in the washes of coal-infused M41S material. The TGA indicates that very low molecular weight material is evolved at about 60°C, which we assign to occluded pyridine. The major part of the organic material begins to come off at roughly 300°C and peaks at 440°C for the 33Å material and at 500 for the 25Å material. In addition, there is a distinct shoulder at 460 in the 33Å and at 520 in the 25Å which may indicate different organic compounds or clusters of compounds. The peak at 675 in the 33Å material is only 1.5% of the total weight, but may be related to very tightly bound (very polar) organic material on the silica.

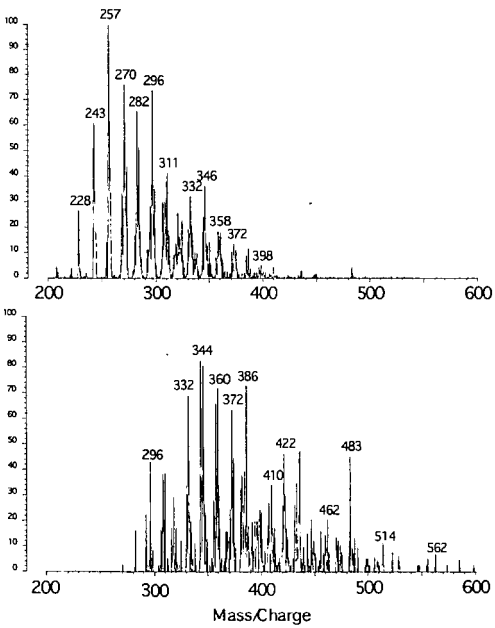

Fig. 3 The laser desorption mass spectrum of methylene chloride extract of APCS 1 imbibed M41S zeolite. 25 Å pore diameter (upper panel) 33 Å pore diameter (lower panel)

The laser desorption mass spectra of the extracts from the coal-containing mesoporous zeolites is shown in figure 3. Here there is a clear distinction in mass between the 25 Å and the 33 Å sieves. The average mass of the 33 Å extract is higher than that of the 25 Å extract by roughly 44 mass units. This would correspond to an additional ring system. Since LD chiefly accesses the aromatic content of a sample, we believe that this difference can be attributed to one additional ring in the 33 Å over the 25 Å extract. That is, the separation of the extract using mesoporous sieving by M41S-class zeolites is effectively differentiating small ring sizes. This suggests that one additional ring is responsible for the separation difference between 25 and 33 Å. Clearly, the average molecular size of an aromatic molecule of molecular weight 300 is much smaller than either pore size. This suggests that the separation takes place on larger clusters of molecules of similar ring sizes. We suggest that molecular clusters which are manifested in the LD spectra as relatively small aromatic molecular ions are separated as large clusters of molecules. Evidence from small angle neutron scattering of pyridine coal systems shows a high polydispersity in cluster size. We may be accessing one portion of that range in the 20-30 Å size range. Further experiments with larger pore size mesoporous M41S materials are underway.

The LVHRMS results comparing the 25 Å and 33 Å is shown in Figure 4. The average aromatic ring size is an estimate based on the number of double bond equivalents calculated from the high resolution data. The 33 Å shows an increased aromatic ring size over the 25 Å.

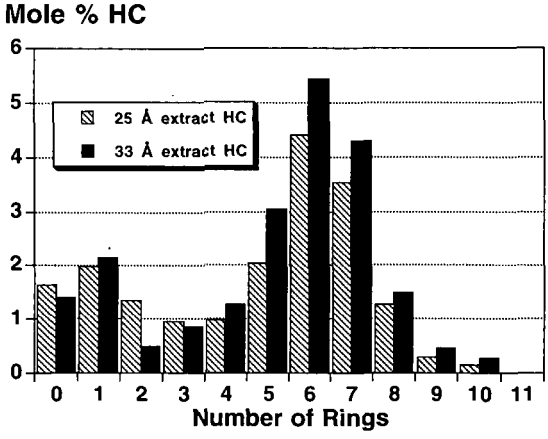

Fig 4. Comparison of aromatic ring size from HRLVMS of methylene chloride extracts of 25Å and 33Å M41S sieves loaded with pyridine extracts of Upper Freeport coal (APCS 1).

ACKNOWLEDGMENT

This work was supported by the Division of Chemical Sciences, Office of Basic Energy Sciences, U. S. Department of Energy, under contract W-31-109-ENG-38.

REFERENCES

1. Cody, G.D., Thiyagarajan, P., Botto, R. E., Hunt, J. E., Winans, R. E., Energy Fuels, 1994. **8**(6): p. 1370-8.
2. Beck, J. S., U.S. Pat., No. 5,057,296, 1991
3. Beck, J. S.; Vartuli, J. C.; Roth, W. J.; Leonowicz, M. E.; Kresge, C. T.; Schmitt, K. D.; Chu, C. T-W.; Olson, D. H.; Sheppard, E. W.; McCullen, J. B.; Higgins, J. B.; Schlenker, J. L., J. Am. Chem. Soc., 1992, 114, 10834-43
4. Vorres, K., Energy & Fuels 4, 420-426 (1990)
5. Pinnavaia, T. J.; Thorpe, M. F., Access in Nanoporous Materials, Plenum Press: New York,1995.

CONSTRUCTION OF MODEL STRUCTURES OF UPPER FREEPORT COAL EXTRACTS USING SOLID-STATE ^{13}C NMR CHEMICAL SHIFT CALCULATION

Hiroyuki Kawashima and Toshimasa Takanohashi
National Institute for Resources and Environment
16-3, Onogawa, Tsukuba, Ibaraki, 305-8569, Japan

KEYWORDS: Coal model structure, Solvent extraction, Solid-state ^{13}C NMR

INTRODUCTION

Many analytical techniques have been used for coal research and the analytical data have enabled the construction of model chemical structures of coal. The construction of model structure of coal is important in improving our understanding of the relationships between coal structure and its properties; this knowledge can lead to more effective and economical methods of coal conversion. Iino et al. investigated the extract fractions obtained from the extraction of Upper Freeport coal with a carbon disulfide/N-methyl-2-pyrrolidinone mixed solvent at room temperature and the fractionation with acetone and pyridine by using ^{1}H NMR, elementary analysis, SEC and hydroxyl group estimation.[1] Based on the structural parameters obtained, i.e., f_a(aromaticity), σ (the degree of substitution on aromatic rings) and H_{aru}/C_{ar} (the degree of condensation of the aromatic rings), Takanohashi et al. constructed the model structures of the extract fractions, as shown in Fig. 1.[2] Recently, for calculating the NMR chemical shifts of known molecular structures, several programs have been developed. We modified the chemical structure of Upper Freeport coal extracts constructed by Takanohashi et al. using the ^{13}C NMR chemical shift calculations. The purpose of the present work is to improve the model structures by comparison of actual and calculated solid-state ^{13}C NMR spectra.

EXPERIMENTAL

Sample: The extract (60 wt% on raw coal basis) from a carbon disulfide/N-methyl-2-pyrrolidinone mixed solvent extraction at room temperature for Upper Freeport coal was fractionated with acetone and pyridine into three fractions, i.e., acetone-soluble (AS), acetone-insoluble/pyridine-soluble (PS), and pyridine-insoluble (PI) fractions. These extract fractions of Upper Freeport coal were used as samples. Data on structural analysis of the extracts are summarized in Table 1.

NMR measurements: Solid-state ^{13}C NMR measurements were made by the SPE/MAS method using a Chemmagnetics CMX-300 NMR spectrometer. About 100 mg of sample were packed in the sample rotor. The measuring conditions were as follows: the 90° ^{1}H pulse width was 4 μ s; ^{13}C frequency, 75.46 MHz; spinning rate of MAS, 10 kHz; number of scans, 2000; and pulse repetition time, 60 s. Chemical shifts were calibrated with respect to tetramethylsilane using the hexamethylbenzene's methyl group peak at 17.4 ppm as the external standard.

Chemical shift simulations: Chemical shift calculations were carried out using ACD Laboratory CNMR predictor software. Thomas et al. calculated ^{13}C chemical shifts for some substituted pyridines using several NMR prediction programs and showed that the CNMR predictor gave the best results in their work.[3] Kohnert et al. evaluated and tested for prediction of NMR spectra of photosynthetic metabolites using the CNMR predictor.[4] The software allows treatment of molecules containing up to 256 carbon atoms. The software calculates chemical shifts by searching for similar sub-structural fragment with the corresponding experimental shift value in the internal database and evaluating the chemical shift value taking into account intramolecular interactions. Using the software, we calculated the chemical shifts of all carbons of each model structure constructed by Takanohashi et al.[2] Next, the calculated ^{13}C NMR spectra were obtained by considering an adequate line width to each peak and summing, supposing that all peaks were Gaussian peaks.(This process was performed by Spinsight ver.3.5.2 software.) The line width fitted to the actual spectra was adopted. For AS, PS and PI, the line width for aromatic carbon was 814 Hz, 1203 Hz and 1344Hz, respectively, and the line width for aliphatic carbon was 354 Hz, 460 Hz and 601Hz, respectively. As the fraction became lighter, the line width of each peak became narrower, with narrower lines for aliphatic than for aromatic carbon. Although, all aromatic or

aliphatic carbons may not have the same line width, it is time consuming to derive a line width for each carbon, so each one line width was used for aromatic or aliphatic carbon of the each extract fractions. By comparison with actual spectra, the model structures were modified. The chemical shifts were calculated again for the revised structures. By repeating this process, the best fitting structures were determined.

RESULTS AND DISCUSSION

Fig 2 shows the experimental NMR spectra of the extract fractions and the calculated NMR spectra for model structures of each fraction. For AS, with regard to the actual spectra, the model structure had high fractions for non-protonated aromatic carbon (125~140 ppm) and CH_2 carbon(15~25 ppm), and low fractions for protonated aromatic carbon(100~120 ppm), CH_2 carbon(30~45 ppm) and methyl carbon(0~15 ppm). We added methyl carbon to the model structure of AS and reduced the substituted aromatic carbon and β CH_2 carbon. The resulting structure of AS is shown in Fig. 3(a) and the calculated NMR spectrum for the revised model structure is shown in Fig.4(a) with the measured spectrum. For PS and PI, the model structures had high fractions for non-protonated aromatic carbon (125~140 ppm) and CH_2 carbon(35~50 ppm), and low fractions for methyl carbon(0~20 ppm). We added methyl carbon to the model structures of PS and PI and reduced the substituted aromatic carbon. Figs. 3(b) and (c) show the resulting structures of PS and PI that best fitted the actual spectra. Fig. 4(b) and 4(c) show the calculated NMR spectra of the revised model structures with the measured spectra. We modified all structures of extract fractions mainly by adding methyl and ethyl groups and reducing naphthenic ring structures. This indicates that the all initial structures lacked methyl and ethyl groups and were rich in naphthenic ring structures, which we could not distinguish by the previous analytical data. By these techniques, the correction of the model structures for the extract fractions could be made.

The chemical shift at 60 ~ 80 ppm corresponds to the aliphatic carbon connected with oxygen such as $-CH_2-O-$, which is thought to be important for the crosslink of coal. For the calculated spectra for PS and PI, the peaks appeared in this chemical shift range. Considering the crosslinks in coal, such oxygen containing methylene bonds possibly exist in coal, but the actual spectra showed no peak in this chemical shift range between aromatic and aliphatic carbon peak, and we cannot confirm the peaks. The amounts of the aliphatic carbon connected with oxygen may or can not be so large compared with the other forms of carbon, and the peaks may be overlapped, so in the actual spectra the peaks might not appeared.

Table 2 shows structural parameters of the revised model chemical structures. The values of f_a and H_{arv}/C_{ar} were almost similar between the initial and the revised model structures, but the values of σ and H/C were different. The values of σ were higher for the initial structures and the values of H/C were higher for the revised structures. This was because, in the modification process, we added some methyl and ethyl groups and reduced some naphthenic ring structures in order to fit the actual spectra. In this regard, further examination is required to coincide these data. However, relatively good agreement was obtained between the actual spectra and calculated ones by the new models.

CONCLUSION

The solid-state ^{13}C NMR spectra of the model structures for the three extract fractions were estimated using the NMR chemical shift calculation method. By comparison of the estimated spectra with the observed ones, some corrections were made to the chemical structure of models to fit their spectra, and we proposed the modified model structures based on NMR chemical shift calculations. The energy-minimum conformation will be calculated by the molecular mechanics and molecular dynamics

ACKNOWLEDGMENT

This work was supported by the Japan Society for the Promotion of Science("Research for the Future" Project).

REFERENCES

1.M.Iino, T.Takanohashi, S.Obara, H.Tsueta and Y.Sanokawa, Fuel, 68, 1588(1989)

2.T.Takanohashi, M.Iino and K.Nakamura, Energy Fuels, 12, 1168(1998)

3.St.Thomas, I.Bruhl, D.Heilman and E.Kleinpeter, J.Chem.Inf.Comput.Sci., 37, 726(1997)

4.R. L. Kohnert, B. Arbogast and L. S. Daley, Biotechnology Software and Internet Journal, June 1996, p. 17

Table 1. Structural parameters of extracts of Upper Freeport coal[2]

Sample	Ultimate analysis (wt%)[a]					Structural parameters					
	C	H	N	S	O[b]	M_n	f_a	H_{au}/C_{ar}	σ	H/C	molecular formula
Original coal	86.2	5.1	1.9	2.2	4.6					0.71	
AS	88.5	6.7	1.1	0.5	3.2	520	0.71	0.69	0.39	0.91	$C_{38}H_{34}NO$
PS	86.6	5.8	2.0	1.8	4.5	1270	0.78	0.72	0.51	0.75	$C_{92}H_{68}N_2O_5$
PI	85.8	5.0	2.1	1.1	6.0	2210	0.79	0.71	0.48	0.70	$C_{158}H_{110}N_3SO_8$

a)dry ash free

b)calculated as the difference

Table 2. Structural parameters of the revised model chemical structures

Sample	Structural parameters				
	f_a	H_{au}/C_{ar}	σ	H/C	molecular formula
AS	0.71	0.71	0.30	1.03	$C_{38}H_{39}NO$
PS	0.79	0.69	0.44	0.81	$C_{91}H_{74}N_2O_5$
PI	0.80	0.67	0.40	0.77	$C_{157}H_{121}N_3SO_8$

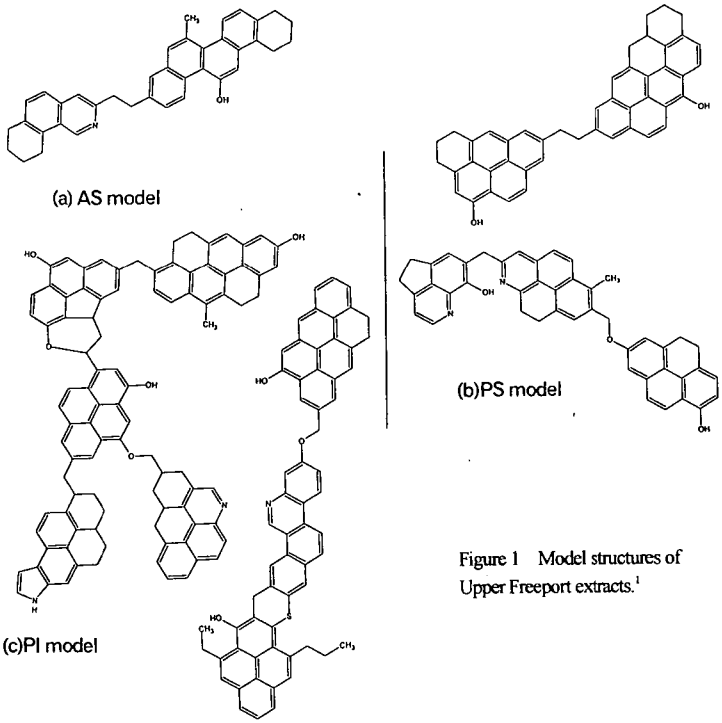

Figure 1 Model structures of Upper Freeport extracts.[1]

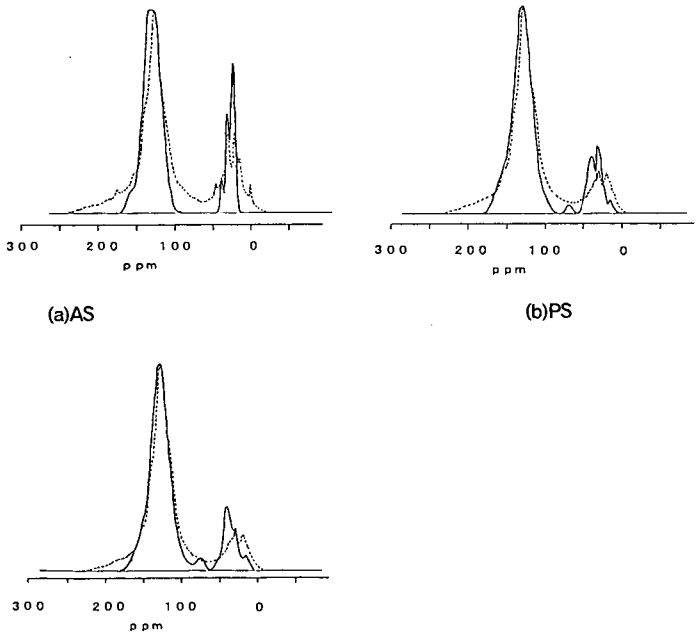

Figure 2 Measured SPE/MAS ^{13}C NMR spectra of solvent extracts(- - - - - -) and calculated NMR spectra of model chemical structures(——).

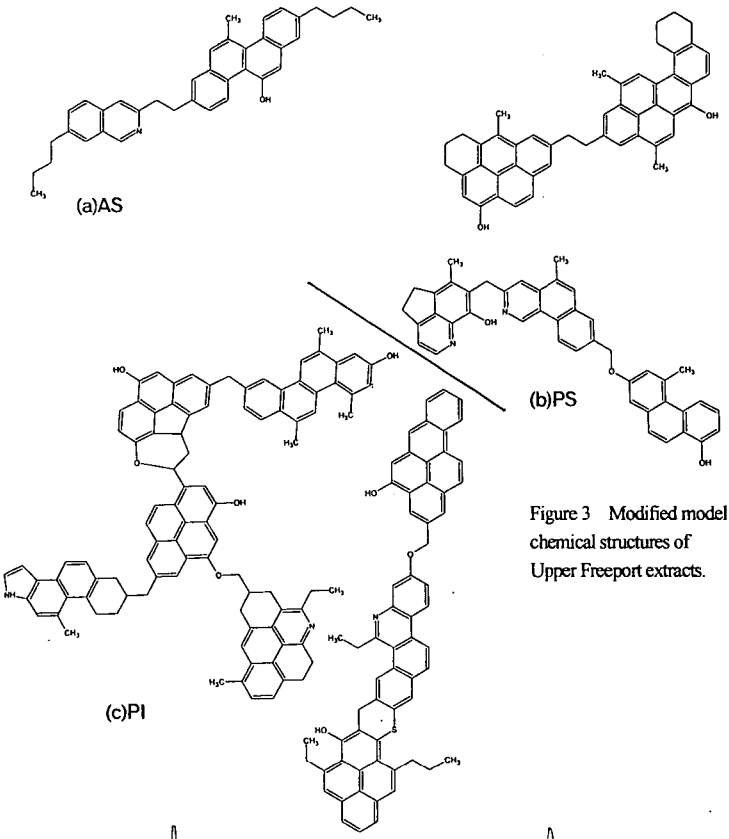

Figure 3 Modified model chemical structures of Upper Freeport extracts.

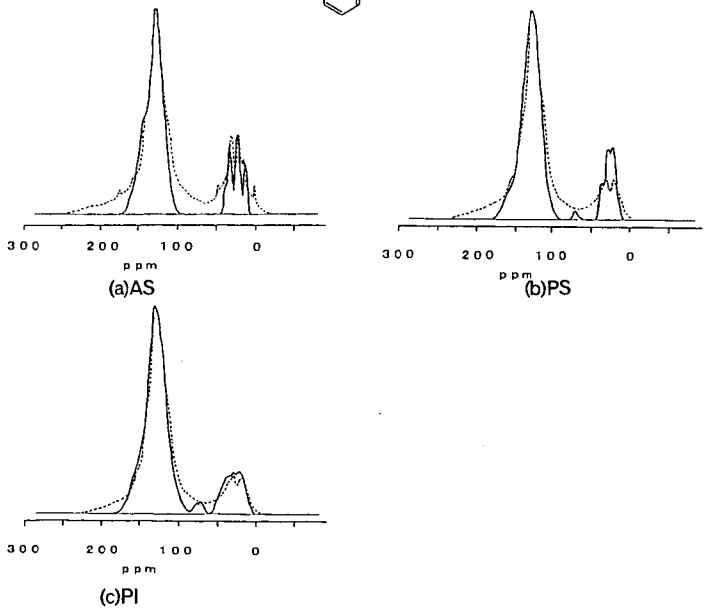

Figure 4 Measured SPE/MAS ^{13}C NMR spectra of solvent extracts(- - - - - -) and calculated NMR spectra of modified model chemical structures(——).

ADSORPTION AND DIFFUSION OF ALCOHOL VAPORS FOR ARGONNE PREMIUM COALS

Toshimasa Takanohashi
Energy Resources Department, National Institute for Resources and Environment,
Tsukuba 305-8569, JAPAN

Yuki Terao and Masashi Iino
Institute for Chemical Reaction Science, Tohoku University,
Sendai 980-8577, JAPAN

KEYWORDS: coal, sorption isotherm; sorption model

INTRODUCTION

Green and Selby reported [1] that pyridine sorption isotherms can be explained by a dual-mode sorption model that has been widely applied to the sorption of glassy polymers. This model is represented by two phenomena, adsorption on the surface described by a Langmuir isotherm, predominant at the initial portion of the plot of sorption isotherm, and diffusion (absorption) into the bulk structure described by Henry's law, the linear portion with relative pressures. Shimizu et al. [2] carried out research on organic vapor sorption using various ranks of coals and found that sorption data for Illinois No. 6 coal could be treated by the Langmuir–Henry equation regardless of a kind of the organic vapors (methanol, benzene, pyridine, and cyclohexane) used. Takanohashi et al. [3] reported that methanol sorption in the residues from coals with the high extraction yields greatly increased compared to the corresponding raw coals, suggesting that more microporosity has been developed by the extraction. In contrast, for coals with low extraction yields, sorption behavior of residues was similar to that of the raw coals, regardless of coal rank.

The steric effects on the kinetics of solvent swelling of coals have been reported.[4,5] Solvent swelling of coal involves diffusion of solvent molecules into the macromolecular structure of coals. Larsen et al. [4] reported the steric effects of various alkyl-substituted pyridines and anilines on equilibrium swelling ratio of coals. Aida et al. [5] determined the initial swelling rates in addition to the equilibrium swelling values of Illinois No.6 coal in various solvents, and showed that the rate retardation of diffusion of alkyl-substituted amines can be increased by almost a thousandfold by changing from *n*-butylamine to *tert*-butylamine. However, the swelling of coal in liquid phase also causes other structural changes such as extraction and relaxation of macromolecular structure, which can influence the swelling behavior.

To investigate the steric effect on alcohol vapor sorption for coals, the sorption isotherms of alcohols with different size of alkyl groups were measured for four Argonne premium coal samples. Data were analyzed using the Langmuir–Henry dual-mode sorption equation. Based on the adsorption and diffusion parameters from the model equation, micropore and cross-linking structures of the coals are discussed.

EXPERIMENTAL

Sample Preparation

Four Argonne premium coal samples (Pocahontas No.3, Upper Freeport, Illinois No.6, and Beulah-Zap coals) were obtained in ampoules (5 g of -150 μm). Because water and gases adsorbed on the coals prevent the measurement of sorption, samples were dried at 80 °C for 12 h *in vacuo*, just before the sorption measurements. Various alkyl-substituted alcohols were used without further purification as the sorbate.

Upper Freeport coal was extracted exhaustively with a carbon disulfide / *N*-methyl-2-pyrrolidinone (CS_2 / NMP) mixed solvent at room temperature.[6] The residue was washed with acetone and dried in a vacuum oven at 80 °C for 12 hr. The extraction yield was 60 wt% on the dry-ash free basis. The extraction residue was also used as the sorbent.

Sorption Experiments

Sorption isotherms were measured with an automatic vapor adsorption apparatus (BELSORP18, BEL JAPAN, INC) at 30 °C. Approximately 200 mg of sample was placed in the sample tube and weighed. The deaeration treatment of methanol in the solvent tank was carried out with liquid

nitrogen three times through freeze-thaw cycles. Samples were pretreated under vacuum ($< 10^{-4}$ Torr) at 80 °C for 12 h: The sorption isotherm was measured at the relative vapor pressures of $0.01 < p < 1$ at 30 °C by using the constant-volume gas adsorption method. Each sorption was measured when the change in the amount of sorption remained constant within 5% for 10 min.

RESULTS AND DISCUSSION

Sorption Behavior.

Sorption isotherms of methanol, ethanol, *n*-propanol and *n*-butanol (only for Upper Freeport coal) are shown in Figures 1. The amount of sorption is represented on the basis of each sample (g). Generally, the sorption increased exponentially at low vapor pressures and then increased linearly with pressure in the intermediate pressure range, although the total sorption was different among the coals used. The sorption by Upper Freeport raw coal was the smallest for all alcohols used. As the size of alkyl group increased, the total sorption became smaller for all coals, showing that alkyl groups prevent the alcohols from being sorbed by the coals. For lower rank coals, Beulah-Zap and Illinois No.6 coals, the sorption behaviors of methanol and ethanol were similar at vapor pressures more than 0.2, i.e., the slope of isotherm was almost the same. While, for high rank coals, Upper Freeport and Pocahontas No.3 coals, the slope of isotherms in the cases of *n*-propanol and *n*-butanol was relatively small, indicating that they would hardly be sorbed

Sorption Analysis Using the Dual-Mode Sorption Model

The results of curve fitting from the Langmuir – Henry dual mode equation (1) are also shown in Figure 1.

$$C = C_H + C_D = C'_H\, b\, p / (1 + b\, p) + k_D\, p \qquad (1)$$

where C is the total sorption (mmol/g-sample), C_H is adsorption on the surface, C_D is the amount of diffusion (absorption) into the bulk, C'_H is the pore saturation constant, b is the pore affinity constant, p is the relative vapor pressure (P/P_0), and k_D is the Henry's dissolution constant.

For all the cases except for Beulah-Zap – ethanol and *n*-propanol systems, data were fit by the Langmuir–Henry equation, suggesting that alcohol sorption can be explained by adsorption on the surface that occurred at low relative pressures and diffusion into the bulk that increased linearly with pressure. Since coals have many interacting sites such as functional groups on their surface, adsorption preferentially occurs at low vapor pressure. A steep increase of sorption observed for all coals at low vapor pressures, especially for low rank coals, can be due to the adsorption on oxygen functional groups of the surface, although in the case of *n*-propanol the rate of the sorption increase at low vapor pressures was small.

Constants of the Langmuir–Henry equation obtained by the fitting are listed in Table 1. The values for Beulah-Zap – ethanol and *n*-propanol systems were obtained by a different fitting method, i.e., the adsorption parameter was obtained by fitting in the low vapor pressure range less than 0.2 and the diffusion parameter by fitting in the intermediate pressure range more than 0.4, because a discontinuity point exists at around vapor pressure of 0.2. The C'_H (mmol/g-sample) for Upper Freeport coal was the smallest for all alcohols, showing that Upper Freeport coal has fewer pores on the surface than other coals. As the size of alkyl group increased, i.e., methyl, ethyl and propyl, the C'_H decreased, especially for high rank coals the rate of decrease was large. The result suggests that high rank coals have smaller micropore sizes. The b which is related to the ratio of the adsorption rate to the desorption rate, showed a tendency to decrease in the cases of *n*-propanol and *n*-butanol. The steric effect of alkyl group of alcohols may accelerate their desorption.

The Henry's dissolution constant k_D (mmol/g-sample), which represents the degree of diffusion into the bulk, was also the smallest for Upper Freeport coal in all cases. For low rank coals, the k_D values of methanol and ethanol were similar, while the value of *n*-propanol was small. In contrast, for high rank coals k_D greatly decreased in the order of methanol, ethanol and propanol, suggesting that the difference in the size of alkyl group on alcohols might greatly influence their diffusion into the bulk.

Effect of Extraction

Figure 2 shows the isotherms for Upper Freeport residue, with the Langmuir–Henry fitting curves. Constants of the Langmuir–Henry equation obtained by the fitting are also listed in Table 1. The C'_H of each alcohol for the raw coal and its extraction residue was almost similar in magnitude, although the value of methanol for the residue was smaller than that for the raw coal. The values of b increased by the extraction for all alcohols. In contrast, the k_D for the residue was quite larger than that for the raw coal in all cases. Even for bulky alkyl-substituted alcohols such as *n*-propanol

and *n*-butanol, high the k_D values were obtained, 1.6 for both. These results suggest that the adsorption sites on the surface did not change so much by the extraction, while a considerable amount of large void was formed in the bulk. Since the oxygen content of the Upper Freeport residue, 6.3 wt%, is much lower than those for Illinois No.6 and Beulah-Zap raw coals, the increase in the k_D for the residue may be due to increased physical diffusion into the formed voids.

CONCLUSIONS

Almost all sorption isotherms of various alcohols could be explained by the Langmuir-Henry dual-mode sorption equation, and adsorption and diffusion parameters could be estimated. Both pore saturation and dissolution constants were the smallest for Upper Freeport coal of all coals used. As the size of alkyl group increased, their constants decreased for all coals. Especially for high rank coals, Pocahontas and Upper Freeport coals, the dissolution constant greatly dropped. In contrast, the dissolution constant for the extraction residue from Upper Freeport coal was quite large for all alcohols, compared to those of the raw coal, although the pore saturation constant did not change so much. A considerable amount of micropores with relatively large sizes formed by the extraction may be responsible for the increased diffusion.

ACKNOWLEDGMENT

This work has been carried out as one of "Research for the Future" projects of the Japan Society for the Promotion of Science (JSPS) through the 148th committee on coal utilization technology of JSPS.

REFERENCES

1. Green, T.K. and Selby, T.D., *Energy Fuels*, **8**, 213 (1994).
2. Shimizu, K., Takanohashi, T. and Iino, M., *Energy Fuels*, **12**, 891 (1998).
3. Takanohashi, T., Terao, Y. and Iino, M., *Fuel*, in press.
4. Larsen, J.W. and Lee, D.Y., *Fuel*, **64**, 981 (1985).
5. Aida, T., Fuku, K., Fujii, M., Yoshihara, M., Maeshima, T. and Squires, T.G., *Energy Fuels*, **5**, 79 (1991).
6. Iino, M., Takanohashi, T., Ohsuga, H. and Toda, K., *Fuel*, **67**, 1639 (1988).

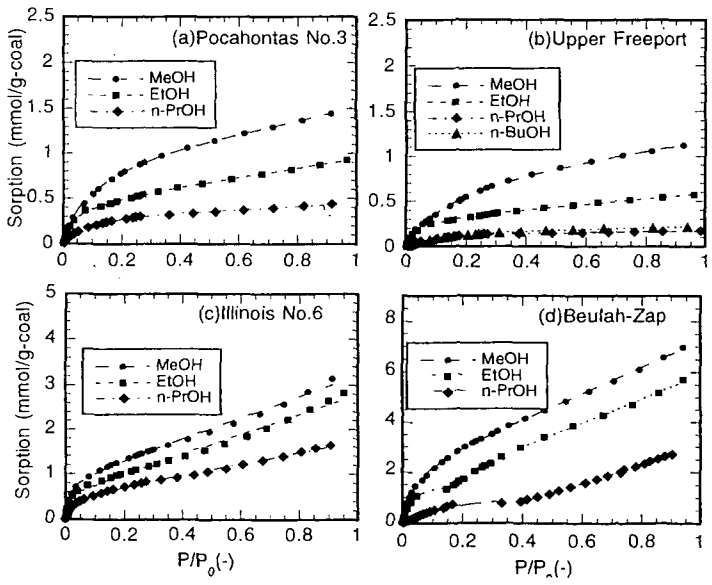

Figure 1 Sorption isotherms of various alcohols at 30 °C for Pocahontas No.3 (a), Upper Freeport (b), Illinois No.6 (c) and Beulah-Zap (d) coals, with the fitted lines with the Langmuir-Henry dual mode equation.

Table 1 The adsorption and diffusion parameters by Langmuir–Henry dual-mode sorption equation for the raw coal – alcohol systems and Upper Freeport extraction residue

coal	sorbate	C'_H [a] (mmol/g-coal)	b [b] (-)	k_D [c] (mmol/g-coal)
Pocahontas No.3 raw	methanol	0.98	10	0.61
	ethanol	0.46	26	0.49
	n-propanol	0.35	12	0.12
Upper Freeport raw	methanol	0.81	35	0.79
	ethanol	0.30	30	0.29
	n-propanol	0.18	9	0.01
	n-butanol	0.20	7	0.05
Upper Freeport residue	methanol	0.58	55	3.1
	ethanol	0.33	69	2.3
	n-propanol	0.35	35	1.6
	n-butanol	0.37	13	1.6
Illinois No.6 raw	methanol	0.97	58	2.9
	ethanol	0.66	108	1.9
	n-propanol	0.58	32	1.1
Beulah-Zap raw	methanol	2.3	29	5.0
	ethanol	1.7	39	4.8
	n-propanol	1.3	6	3.7

[a] Pore saturation constant. [b] Pore affinity constant. [c] Dissolution constant.

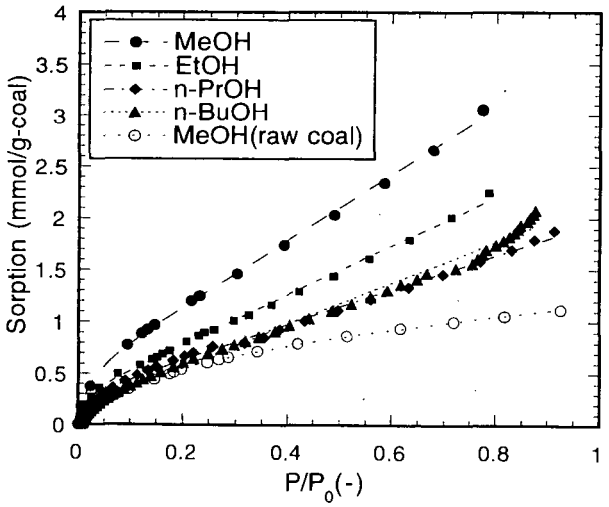

Figure 2 Sorption isotherms of various alcohols at 30 °C for Upper Freeport residue, with the fitted lines with the Langmuir-Henry dual-mode equation.

SYNERGISTIC EFFECT ON SOLVENT SWELLING OF COAL

Tetsuo Aida, Eisaku Suzuki, issei yamanishi, and Masaki Sakai
Department of Industrial Chemistry, Faculty of Engineering at Kyushu
Kinki University, 11-6 Kayanomori, Iizuka, Fukuoka 820, JAPAN

Keywords: coal, solvent swelling, synergistic effect

INTRODUCTION

It has long been curious question why the coal swelling exhibited a synergistic effect in a certain binary solvent system. In 1986, Hombach[1] observed a significant synergistic effect on the solvent swelling of coal in the mixed solvent such as amine and methanol, and tried to rationalize with a hypothesis which the change of the solubility parameter of the mixed solvent was responsible for that phenomena.

In the meantime, Iino et al.[2] also found a quite interesting binary solvent system on the coal extraction, that is, the mixture of CS_2 and N-methyl pyrrolidinone(NMP) gave a maximum extraction yield at their 50:50(vol-%) mixing conditions. This solvent system is well-known as a " ***Magic*** " solvent for the coal extraction, of which detailed mechanism has not yet been clarified.

In the course of our studies on the coal swelling, we have learned that the coal has an significant steric requirement[3] toward the penetrating solvent molecules due to the cross-linking macromolecular network structure. Also, the maximum swelling ratio of coal swelling was very much depending on the donorability of the swelling solvent, as previously pointed out by Marzec[4]› probably because of the specific interaction between the solvent molecule and the cross-linking network structure formed by the relatively weak bonding interactions, such as hydrogen bonding, charge transfer bonding, $\pi-\pi$ bonding and even the van der Waals bonding interactions. These findings are now extending to our new sight of the coal chemistry, the elucidation of synergistic effects on coal swelling and the empirical determination of a "Coal Affinity Parameter".[5] Eventually, we could categorize the synergistic effects on the solvent swelling into the three types of the mixed solvent systems.

In this paper, we present our recent experimental results concerning the mechanism of synergistic effect appeared on the solvent swelling of coal, especially focusing on Type-I and Type-II.

EXPERIMENTAL

The chemical reagents were commercial products (Gold label grade) which were used without further purification. Solvents used in this study were dried over appropriate drying agents and distilled before use. Coals from the Ames Coal Library and Argonne National Laboratory were ground, seized in N_2 atmosphere, dried at 110°C under vacuum overnight, and stored under a dry nitrogen atmosphere.

The measurement of the solvent swelling of coal was carried out by means of our hand-made instrument, and the experimental procedures were same as previously reported.[6]

RESULTS AND DISCUSSION

1. Synergistic effects on coal swelling in mixed solvent

As reported by Hombach, a coal swelling in a mixture of methanol and tertially amine, such as dimethylaniline, trimethylamine, or trimethylamine affords a significant synergistic effect on its equilibrium swelling values(Q).

Figure 1 shows the typical example obtained our swelling measurements which is exhibiting the relationship between Q-value and the swelling rates (V-value) vs. concentration of methanol on the Illinois No.6 coal swelling in triethylamine/methanol mixed solvent.

It is quite interesting that in spite of the large synergistic effect on the Q-value there was almost no effect on the V-value (swelling rates). This fact strongly suggests that the synergistic phenomena appearing on this solvent system will not very much depend on the specific molecular interaction between tri-methylamine and methanol. We like to categorize this type of swelling system, as "Type-I".

Meanwhile, it has long been well-known phenomenon in the coal chemistry that the benzene-methanol mixed solvent enhanced its coal extractability. Actually, as far as our swelling measurements, both individual solvent can not give us a large amount of Q-

value, but the mixed solvent system has demonstrated completely different figures on their swelling parameters (Q & V) as shown in Figure 2. In this case, not only the Q-value, but also the V-value exhibited large synergistic effects on the solvent composition.

Obviously, there are several interesting features on this swelling behavior, suggesting the different swelling mechanism from the Type-I synergistic effect described above. Namely, in this case, both the Q-value and the V-value showed large synergistic effects on the solvent compositions. This means that some specific interactions will exist between each solvent molecule toward the macromolecular network structure of coal. We can categorize this type of swelling, as "Type-II".

Almost ten years ago, Iino et al.[2] reported so-called "magic solvent system" on a coal extraction. Since then, any detailed information concerning the extraction mechanism did not come out in the literatures. We have initiated a study on the rationalization of the mechanism of the ***Magic solvent extraction*** by means of the solvent swelling technique.

In Figure 3, a solvent swelling phenomena of Illinois No.6 coal in CS_2-NMP system measured by our instrument was demonstrated.

As expectedly, the significant synergistic effect was observed on both the Q-value and the V-value like a Type-II swelling system described above. As far as the swelling data shown in Figure 2, and 3, it seems to be quite difficult to rationalize the difference on the swelling mechanism between them. However, there are quite interesting data suggesting different type of a specific molecular interaction between both solvents like a kind of an electron donor-acceptor complex formation, of which detailed discussions will appear in our next paper.

Anyway, we like to categorize this type of synergistic effect as "Type-III".

2. "Type-I" synergistic effects on coal swelling

Some years ago, we had revealed the steric requirement of coal towards penetrating solvent molecules.[3] Coal exhibits a significant steric restriction to the penetrating molecules probably because of their cross-linking network structure like a "molecular sieve". For example, the initial swelling rates of Illinois No.6 coal in n-, sec-, iso- and tert-butylamine were 3.7×10^{-1}, 6.8×10^{-2}, 3.1×10^{-2}, and $6.2 \times 10^{-3} (min^{-1})$, respectively. This means that the swelling rate (V-value) of Illinois No.6 coal in a sterically bulky t-butyl amine was 600times slower than that of a less sterically hindered n-butylamine.[3] Therefore it is quite difficult to evaluate the accurate equilibrium swelling value (Q) in the bulky molecule solvent system, because of the very slow swelling rate, i.e., in the case of t-butyl amine its swelling was still continuing even after 10 days.

Meanwhile, as shown in Figure 4, we have found that this steric requirement of coal could be dramatically relieved in a mixed solvent system such as a methanol solution. Namely, in this solvent system, the equilibrium swelling value (Q) of the sterically hindered molecule seems to be increased by the addition of a small amount of methanol, and the further increase of the methanol concentration results the exactly same Q-values of the less hindered molecule.

In order to confirm this speculation, we had conducted a dynamic swelling measurements of Illinois No.6 coal in the 20%-MeOH / Et_3N solution. The result is demonstrated in the Figure 5 comparing with the one in CS_2/NMP mixed solvent.

In the case of MeOH/Et_3N solvent system, a strange behavior was observed at the initial stage of the coal swelling. Namely, a rapid penetration of solvent molecules into the coal matrix was induced within a minute after the mixing of coal and solvent, and then a slow but steady swelling was followed it.

It will be quite interesting to examine the solvent composition change at the initial stage of such coal swelling as shown above, because we can assume what kind of solvent molecule predominantly penetrated into the coal matrix. For this experiment we had carefully arranged the experimental condition as follows: The ratio of the coal and solvent was determined by a calculation from their ratio at the equilibrium swelling, which will make us easy to determine a small change of the solvent compositions in the supernatant by means of gas-chromatography. The initial contact between coal and solvent was performed by the introduction of the mixed solvent into the previously evacuated test tube in which the coal sample was placed. The results obtained are shown in Figure 6.

Very interestingly, the MeOH-concentration in the mixed solvent significantly decreased at early stage of swelling, which seemed to be comparable to the change of swelling volume of coal.

All of these experimental data strongly suggest that the coal swelling in the binary

solvent system composed by a sterically hindered molecule and a less hindered molecule will result an initial coal/solvent-gel formation induced by the predominant penetration of the less hindered solvent molecule. Actually, in according with our previous swelling measurement in the neat solvent system, Illinois No.6 coal swelled in methanol 60times faster than in t-butyl amine.[3] Thus in the binary solvent swelling system a methanol molecule has to predominantly penetrate into the coal, inducing a significant relaxation of a steric requirement due to the cross-linking network structure of coal, which will make the sterically hindered molecule like a triethylamine easy to penetrate into the coal matrix. We would like to call this type of steric relaxation as "Wedge Effect" of the mixed solvent demonstrating in Figure 7.

Actually, the solvent swelling was always involved with a sterically hindered molecules as a counter part of methanol, like a trimethylamine or dimethyl aniline.

In order to verify our speculation discussed above, we took another advantage to use a cross-linked synthetic polymer (styrene-divinylbenzene co-polymer: Bio-bead SX, BIO-Rad Ltd.), which had the known covalent cross-linking density and chemical structures.

Figure 8 shows our experimental data, which was obtained by using a hexamethyl phosphoramide (HMPA) as a sterically hindered component and a dimethylformamide (DMF) as a less bulky component. Obviously, there is a dramatic increase of the Q-value of HMPA by the addition of small amount of DMF.

All of these experimental data discussed above seems to be consistent with that the Type-I synergistic effect will be induced by the relaxation of the steric requirement of coal resulted by the initial formation of the coal-gel due to the predominant penetration of the less hindered solvent molecule.

3. "Type-II" synergistic effects on coal swelling

Just recently, we had developed a reliable chemical determination of the oxygen functionality in coal,[7] and learned that there were significant amount of carboxylic acid functionality, phenolic hydroxyl and alcoholic functionality in even bituminous coal like Illinois No.6 coal. Based on our preliminary analysis of coals by means of this new technique, the content of these acidic hydroxyl functionality in Illinois No.6 coal (pyridine-extract) reached up to 1.5, 12, and 10units over 100carbon atoms, respectively.[8] This means that the density of the functionality in the macromolecular network structure of coal is approximately one unit per 16 carbon skeleton. This is just an amazing fact, because the most of these oxygen functionality in coal are potentially capable to form a hydrogen bonding which is thought to play a major role for inducing the apparent cross-linking, as illustrating in Figure 9.

This modeling is our standpoint to understand the mechanism of the "Type-II" synergistic effect on coal swelling.

There may be at least two key factors for distinguishing Type-II from Type-I synergistic effects. Namely, the Type-II can be observed even in the mixed solvent composed of less hindered molecules, and also exhibits a significant synergistic effect on the swelling rate (V-value in Figure 2).

If the coal had such polar hydroxyl functionality as mentioned above, a benzene molecule must have a big trouble in its initial stage of the penetration, because of the blocking by the polar cross-inking like a hydrogen bonding, even if there were some comfortable spaces inside of the macromolecular network structure. In this case, very naturally, the coexistence of a polar and small sized molecules like a methanol in the solvent will induce a destruction of an apparent cross-linking structure constructed by a hydrogen bonding with same manor as Type I synergistic effect discussed above.

It will be also true that the polar solvent like a methanol could be in trouble to penetrate into the macromolecular network structure, because of the apparent cross-linking due to $\pi-\pi$ interactions between aromatic rings. In this case, the coexistence of benzene in the solvent must help its penetration by breaking such non-polar bonding interactions in macromolecular network structures.

This speculation, "Co-operative Swelling" can be verified by the same treatments as applied to the Type-I synergistic effect shown in Figure 6. The solvent compositions during the coal swelling in a benzene/MeOH mixed solvent were analyzed by using the same technique as described in Type-I synergistic effect. The results obtained are summarized in Figure 10.

It is obvious that there is an interesting difference between the Type-I and Type-II synergistic effects on the solvent composition change during a coal swelling, that is, in the case of the Type-II synergistic effect, both solvent systems, 20vol%-benzene/MeOH and 20vol%-MeOH/benzene, exhibited the predominant penetration of benzene and MeOH

molecule into the macromolecular net work structure of coal, respectively. These phenomena can result in a synergistic effect because of their cooperative destruction toward apparent cross-linking structure formed by polar and non-polar bonding interactions in the coal matrix.

Actually, we often experience a curious solvent dependency of the solubility of the condensed aromatic compounds, for example, benzene can dissolve anthracene very nicely, but a methanol, even DMF can not dissolve it. This phenomenon is suggesting that the aromatic-aromatic interaction in coal may be far larger than our imagination.

Anyway, in this solvent system, the major role of the methanol molecule is thought to be the relaxation of the apparent cross-linking structure caused by destruction of the hydrogen bonding. If so, the combination with a molecule which has more stronger hydrogen bonding ability than methanol, like trifloroacetic acid (pKa=2.5) must induced a more larger synergistic effect. The same idea will be applicable to the swelling experiment, in which a strong base like a tetra-butylammonium hydroxide ($n\text{-}Bu_4NOH$) is used as a destruction agent of a hydrogen-bonding cross-linking in the macromolecular network structure of coal.

These facts can be rationalized with the decreasing cross-linking due to hydrogen bonding in the macromolecular network structure of coal. Under these circumstances the equilibrium swelling value (Q) and the swelling rate(V-value) of the coal swelling must be increased by their cooperative destruction of the apparent cross-linking structure of coal.

CONCLUSION

The synergistic effect observed on the coal swelling in binary solvent were categorized three types, Type-I, Type-II, and Type-III. The Type-I can be rationalized by the relaxation of the steric requirement of coal induced by the initial formation of coal-gel. The Type-II synergistic effect consistent with the cooperative destruction of the apparent cross-linking structure, such as hydrogen bonding or a $\pi-\pi$ bonding interaction.

AKNOWLEDGEMENT

A part of this research was supported by the grant from The Japanese Ministry of Education through The 148th Committee on Coal Utilization in The Japan Society of Promotion of Science (JSPS).

REFERENCES

(1) Hombach, H.P., Fuel **59**, 465(1980)
(2) Iino, M., Matsuda, M., Fuel, **62**, 744(1983)
(3) Aida, T., Fuku, K., Fujii, M., Yoshihara, M., Maeshima, T., Energy & Fuels, **5**, 79(1991)
(4) Szeliga, J., Marzec, A., Fuel, **62**, 1229(1983)
(5) Aida, T., Yamanishi, I., Prepr. Sekitan Kagaku Kaigi(Japanese), 169(1998)
(6) Aida, T., Squires, T.G., Prepr. Pap.-Am. Chem. Soc., Div. Fuel Chem, **30**, 95(1985)
(7) Aida, T., Yoshinaga, T., Yamanishi, I., Tsutsumi, Y., Proceedinggs of 9th International Conf. on Coal Science, Essen(Germany), 179(1997); Aida, T., Hirama, N., Tsutsumi, Y., Prepr., Pap.-Am. Chem. Soc., Div. Fuel Chem, **42**, 218(1997) ; Yoneda, M., Yamanishi, I., Aida, T., Prepr., Sekitan Kagaku Kaigi(Japanese), 97(1998)
(8) Aida, T., unpublished results

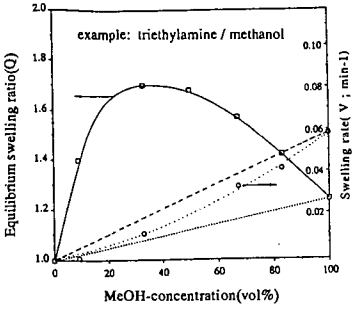

Figure 1. Swelling of Illinois No.6 in binary solvent (Et3N/MeOH)

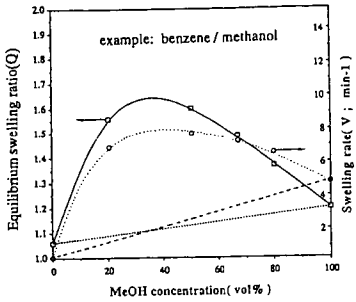

Figure 2. Swelling of Illinois No.6 in binary solvent (benzene/MeOH)

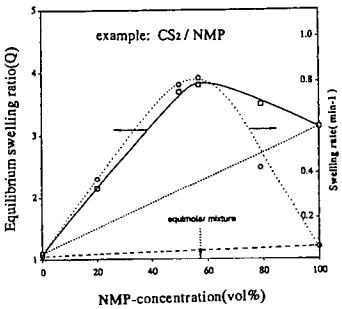

Figure 3. Swelling of Illinois No.6 in binary solvent (CS2/NMP)

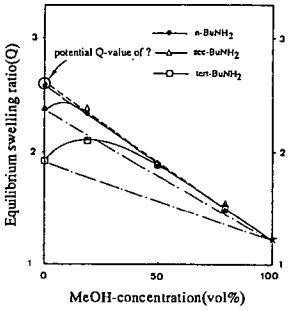

Figure 4. Swelling of Illinois No.6 in binary solvent (BuNH2/MeOH)

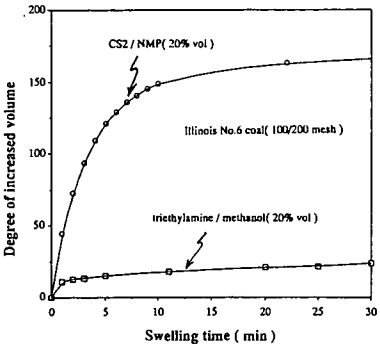

Figure 5. Swelling behavior of Illinois No.6 in binary solvent

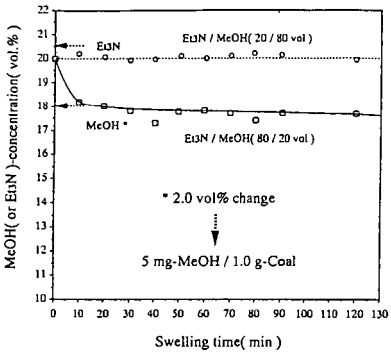

Figure 6. Composition change in binary solvent during coal swelling

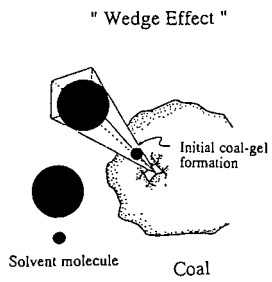

Figure 7. Penetration model of mixed solvent into macromolecular network structure of coal

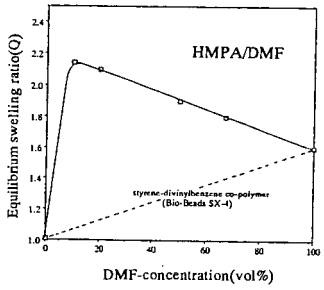

Figure 8. Solvent swelling of cross-linked synthetic polymer in HMPA/DMF mixed solvent

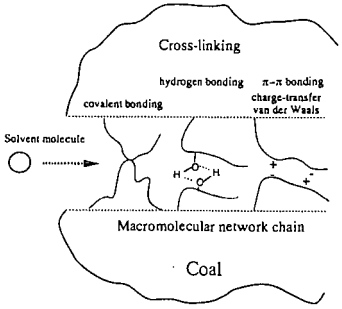

Figure 9. Penetration model of solvent molecule into macromolecular network structure of coal

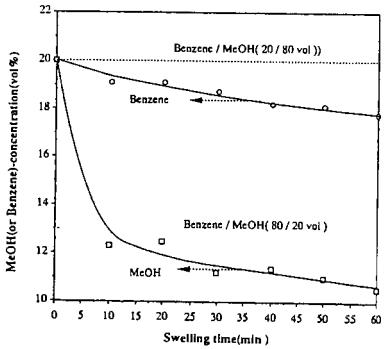

Figure 10. Composition change in binary solvent during coal swelling

STRUCTURE OF COALS REVEALED BY SLOW STEP SCAN XRD AT THEIR SWELLING

Kinya Sakanishi, Izumi Watanabe, and Isao Mochida

Institute of Advanced Material Study, Kyushu University, Kasuga, Fukuoka 816-8580, Japan

Keywords: Argonne coal samples, step scan XRD, solvent swelling

ABSTRACT

Argonne coal samples were treated in dilute acetic acid aq. or polar solvents such as DMF and pyridine, and analyzed by high resolution slow step scan XRD to clarify the effects of such pretreatments on the secondary aggregate structure in the coals caused by non-covalent bonds interactions. Solvent swelling ratios of the lower ranked Beulah-Zap and Wyodak coals with pyridine and DMF increased significantly by the mild acid treatment, suggesting that the coal aggregate structure may be rearranged to more mobile and weaker forms through the removal of ion-exchangeable cations. The slow step scan XRD profiles of the coals showed that the peaks for the organic components can be classified into two parts; one is ascribed to the aromatic plane stacking interactions (around 26 °), the other is probably due to the interactions among aliphatic side chains (around 20 °, that is called γ-band). The solvent-swollen coals with polar solvents such as pyridine or DMF intensified the peaks for the γ-band even after the removal of the solvent by washing with methanol. The solvent-impregnated coal gel (solvent/coal weight ratio of unity) also showed the intensified γ-band, suggesting that the solvent itself may contribute to the rearrangement of the ordered packing in the coal aggregate structure probably due to the aliphatic side chain entanglement and hydrogen bond.

INTRODUCTION

Coals consist of primary macromolecular structure and its secondary network, latter of which is caused by aromatic ring stacking, aliphatic side chain entanglement, and hydrogen bonds, cation bridges, charge transfer interactions through oxygen functional groups.[1-5]

Coal pretreatments have been developed to modify the coals for their easier transportation, grinding, drying, storage and the following conversion processes such as pyrolysis, liquefaction, and gasification.[6-9] Flotation and washing treatments with water, acid or basic solution are one of the conventional procedures for the removal of mineral matters and contaminants by a simple gravimetric separation and filtration, respectively. The former process can be performed to the demineralization of coals by the aid of oil agglomeration or air-bubble flotation. The selected solvents for the latter procedure can dissolve a part of water-soluble mineral matters and ion-exchangeable cations during the storage, transportation or grinding procedures.

Solvent swelling and impregnation treatments of the coals have been the one of the most classical methods for the modification of the coal macromolecular structure induced by the non-covalent bonds interactions such as hydrogen bond, electrostatic interactions, and aromatic plane stacking.[10-15] Selection of solvent and its amount required for the swelling or impregnation should be carefully optimized for the design of the most efficient and adequate solvation of the coals. Polar solvents such as pyridine, THF, and DMF have been reputed to be quite effective for the liberation of the non-covalent bonds interactions in the coal macromolecular network. It was reported that the impregnation of a small amount of pyridine enhanced the coal fusibility and the following carbonization reactivity even after the extraction of the soluble fraction, because pyridine played an important role in the liberation of hydrogen bond and the favorable rearrangement of the coal aggregate structure during the heat treatment and carbonization.[16]

X-ray diffraction(XRD) have been applied to the characterization of carbonaceous materials including coals for the better understanding of their molecular-level structuring and ordered packing extent of their unit structure.[17-21] Slow step scan XRD analyses have been reputed to give the higher resolution of the diffractograms, classifying the carbon-related peak around 20 - 26 ° into two parts ; one is derived from aromatic ring stacking around 26 °, and the other is derived from aliphatic chain entanglement around 20 °. The ratio of the two peaks depends on the coal rank, and hence the secondary macromolecular network in coals is influenced by their ratio.

In the present study, four coals in the Argonne Premium Coal Bank were treated in diluted acetic acid or polar solvents such as DMF and pyridine for the modification of the secondary aggregate structure of the coals. A preliminary measurement of the slow step scan XRD indicated that the XRD patterns of the coals may change by the mild acid treatment and/or solvent swelling treatment.[22]

EXPERIMENTAL

Coals

Four coals (100 mesh under) of Beulah-Zap(BZ), Wyodak(WY), Illinois No.6(IL), and Upper Freeport (UF) in the Argonne Premium Coal Bank were used in the present study.

Acid Pretreatment

1.5 g of the coal was treated in aqueous 1.6 mol acetic acid or methoxyethoxy-acetic acid with 10wt% ethanol at room temperature under atmospheric nitrogen flow for 26 - 46 h. After the filtration, the acid-treated coals were dried overnight at 60 °C under vacuum. The filtrates were analyzed by Inductively Coupled Plasma(ICP; SP1500, Seiko Electronics) to quantify the eluted metal cations by the acid treatment. The degrees of the demineralization were calculated based on the difference in the elemental compositions between original and treated coals. The removal ratio of respective metal was calculated based on the ash analysis data supplied from Argonne Premium Coal Bank.

Solvent Swelling and Impregnation

0.4 g of the coal was mixed with a prescribed amount of solvent in a graduated test tube, and settled at 40 °C under nitrogen flow for a few days to measure the swelling ratio by some solvents. Pyridine, DMF, methanol and benzene were used as solvents for the swelling of coal. The swelling ratio (Q) was calculated as follows;

$Q = h_t/h_o$

h_t: height of swollen coal layer in the tube

h_o: height of coal particle layer without solvent

The solvent impregnation treatment of the coals with pyridine, DMF, or THF was performed by mixing the coal powder with solvent at the weight ratio of unity at 40 °C. The solvent-swollen coal was washed with methanol to remove the solvent.

XRD Measurements

The slow step scanning XRD (Rigaku Geigerflex) of coals before and after the acid pretreatments was measured by the scanning speed of 0.4 sec/0.01° at room temperature. The solvent-colas were analyzed by the step scan XRD with or without the removal of solvent.

RESULTS AND DISCUSSION.

Change of Coal Aggregate Structure by the Acid Pretreatment

Figure 1 illustrates slow step scan XRD patterns obtained for coals before and after the acid treatment. In all coals, a broad diffraction profile was obtained around 20 °. The acid treatment intensifies the diffraction in lower-ranked coals of BZ and WY coal. In contrast, a higher-ranked coal of IL did not change its diffraction patterns before and after the acid treatment. It is suggested that ordered packing in the lower ranking coals can be rearranged by the liberation of aggregate structure due to the removal of cation bridge.

Solvent Swelling Behaviors of the Coals

Figure 2 illustrates the swelling ratio in coals of different ranks by four solvents. The extent of swelling of original coal was in the order of pyridine > DMF > methanol > benzene. The acid treatment significantly increased the swelling ratio of the lower rank coals of BZ and WY, while the swelling ratio of IL coal did not change so much by the acid treatment.

Non-treated lower-ranking coals are very refractory against the swelling by the polar solvents such as pyridine and DMF probably due to the strong cation-bridging through the oxygen functional groups. The aggregate structure of a higher-ranked coal IL, is essentially not changed by the acid treatment because of its lower contents of both ion-exchangeable cations and oxygen functional groups, resulting in the insensitivity to the swelling with polar solvents. Less and non-polar solvents showed much smaller swelling of which extent appears rather independent on their ranks.

Figure 3 shows the XRD profiles of BZ coal before and after the solvent swelling treatment with DMF or pyridine followed by washing with methanol. The peak around 20 ° was intensified by the solvent treatment even after the washing with methanol, indicating that solvent swelling treatment with polar solvents

may rearrange the aggregate structure caused by aliphatic chain entanglement to more oriented form. It is noted that such effect with DMF is more significant than that with pyridine.

Figure 4 illustrates the XRD profiles of DMF-treated BZ coal before and after the acid treatment. The acid treatment slightly intensified the peak around 26 °, indicating that the aromatic ring stacking may be rearranged to a small extent by the removal of bridging cations. In other words, the solvent treatment of BZ coal with DMF may contribute to the aliphatic chain entanglement, while the acid treatment may be more sensitive to the aromatic ring stacking caused by newly formed hydrogen bonds.

Figure 5 shows the XRD patterns of Beulah-Zap and Wyodak coals before and after the solvent-swelling treatments with and without the removal of DMF. The solvent-swollen coals with polar solvents such as pyridine and DMF intensified the peaks for the γ-band even after the removal of the solvent by washing with methanol. It is noted that the solvent-impregnated coal gel (solvent/coal weight ratio of unity) also showed the intensified γ-band peak without the removal of solvent, suggesting some contribution of the solvent itself to the rearrangement of the coal aggregate structure. It is also suggested that the interaction of polar solvent with coal macromolecules through the oxygen functional groups may survive and influence the secondary aggregate structure in the lower ranked coals even after the removal of solvent.

Figure 6 shows the XRD profiles of IL and UF coals before and after the impregnation treatment with DMF. The DMF-impregnated coals of the higher rank gave a intensified peak around 20 °, although the extent was much smaller than that with the lower ranked coals of BZ and WY. It is suggested that DMF may interact more weakly with the higher ranked coals which have less oxygen functional groups but with more and larger aromatic rings.

Based on the above results, the interactions between coal and solvent can be controlled by changing the combinations of coals of different rank with solvents of different polarity. The slow step scan XRD measurements is effective for the detection of the change in coal aggregate structure caused by the non-covalent bonds interactions such as aliphatic chain entanglement, aromatic ring stacking, charge transfer, and/or hydrogen bonds.

ACKNOWLEDGMENT

This work has been carried out as one of the "Research for the Future" projects of the Japan Society for the Promotion of Science (JSPS) through the 148 committee on coal utilization technology of JSPS.

REFERENCES

1. Solum, M.S.; Pugmire, R.J.; Grant, D.M. *Energy Fuels* **1989**, 3, 187..
2. Cody, G.D.; Davis, A.; Hatcher, P.G. *Energy Fuels* **1993**, 7, 455.
3. Carlson, G.A. *Energy Fuels* **1992**, 6, 771.
4. Nakamura, K.; Takanohashi, T.; Iino, M.; Kumagai, H.; Sato, M.; Yokoyama, S.; Sanada, Y. *Energy Fuels* **1995**, 9, 1003.
5. Larsen, J.W.; Gurevich, I. *Energy Fuels* **1996**, 10, 1269.
6. Evans, D.G. *Fuel* **1973**, 52, 186.
7. Miura, K.; Mae, K.; Morozumi, F. Prep. *ACS Div. Fuel Chem.* **1997**, 42, 209.
8. Mochida, I.; Sakanishi, K.; Sakata, R.; Honda, K.; Umezawa, T. *Energy Fuels* **1994**, 8, 25.
9. Mochida, I.; Sakanishi, K. *Advances in Catalysis (Academic Press, Inc.)* **1994**, vol.40, 39.
10. Suuberg, E.M.; Otake, Y.; Yun, Y.; Deevi, S.G. *Energy Fuels* **1993**, 7, 384
11. Otake, Y.; Suuberg, E.M. *Fuel* **1998**, 77, 901.
12. Otake, Y.; Suuberg, E.M. *Energy Fuels* **1997**, 11, 1155.
13. Hall, P.J.; Larsen, J.W. *Energy Fuels* **1993**, 7, 47.
14. Cody, G.D.; Eser, S.; Hatcher, P.; Davis, A.; Sobkowiak, M.; Shenoy, S.; Painter, P.C. *Energy Fuels* **1992**, 6, 716.
15. Aida, T.; Nawa, Y.; Shiotani, Y.; Yoshihara, M.; Yonezawa, T. *Proc. Int. Conf. Coal Sci.*, **1993**, pp.445.
16. Korai, Y.; Torinari, Y.; Mochida, I. *Cokes Circular, Jpn.* **1992**, 41, 232.
17. Cartz, L.; Diamond, R.; Hirsch, P.B. *Nature* **1956**, 177, 500.
18. Shiraishi, M.; Kobayashi, K. *Bull. Chem. Soc. Jpn.* **1973**, 46, 2575.
19. Wertz, D.L.; Bissell, M. *Energy Fuels* **1994**, 8, 613.
20. Wertz, D.L.; Quin, J.L. *Energy Fuels* **1998** 12, 697.
21. Wertz, D.L. *Energy Fuels* **1999**, 13, 513.
22. Mochida, I.; Sakanishi, K. *Fuel* in submission.

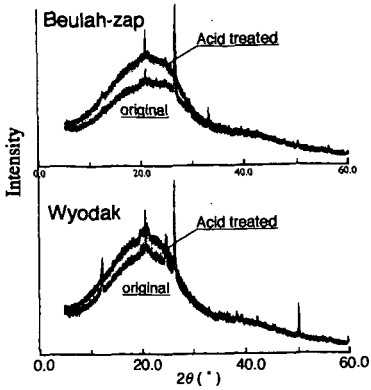

Figure 1 Effect of acid treatment on XRD patterns of BZ and WY coals

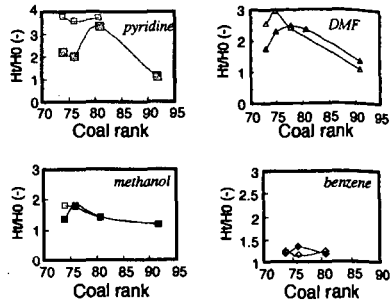

Figure 2 Swelling behavior of coals with various solvents

Opened symbol is acid treated coal
Closed symbol is original coal

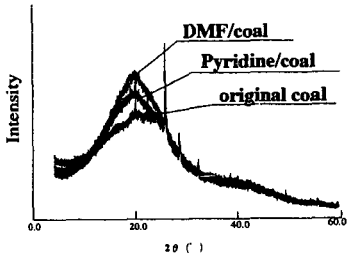

Figure 3 Effects of swelling by DMF and pyridine on XRD patterns of BZ coal with MeOH washing

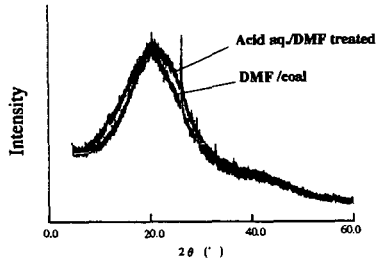

Figure 4 Effect of acid treatment on XRD of DMF-treated BZ-coal with MeOH washing

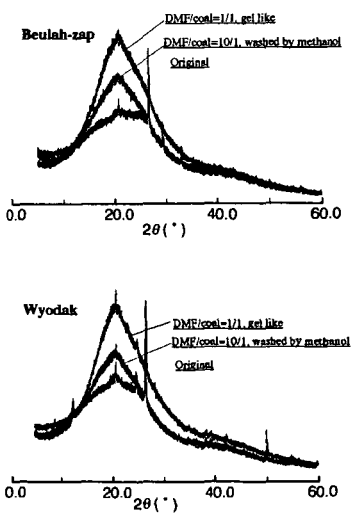

Figure 5 XRD patterns of BZ and WY coals before and after treatment with DMF

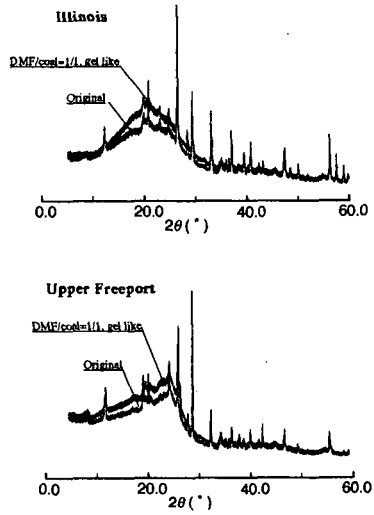

Figure 6 Effct of swelling with DMF on XRD patterns of IL and UF coals

CHANGE IN PHYSICAL AND CHEMICAL CHARACTERISTICS OF BROWN COAL ALONG WITH A PROGRESS OF MOISTURE RELEASE

Haruo Kumagai[1], Tadatoshi Chiba[1], Kazuo Nakamura[2]
[1]Center for Advanced Research of Energy Technology, Hokkaido University, Sapporo 060-8628, Japan
[2]Fundamental Research Laboratories, Osaka Gas Co., Ltd., Osaka 554, Japan

Keywords : moisture release, macromolecular structure, CAMD

INTRODUCTION

Low rank coals, such as lignite and brown coal, have high residual moisture contents in the range of 30-70wt% [1]. Due to such a high moisture content of the coal, moisture removal is the first and essential step in almost any process for upgrading or utilizing them. Since the moisture removal is known to have a significant effect on the physical and chemical properties of dried coal, fundamental understanding of moisture removal is of some consequence. It would be easy to imagine that the effects are brought about by the change in macromolecular structure of coal along with moisture release [2]. Although it is considerable that the physical change of coal during drying process is caused by the change in macromolecular structure of the coal, the natures of macromolecular structure of coal have not been fully understood. Recently, computer-aided molecular design (CAMD) technique has applied to the area of fuel chemistry to obtain insight into the structure, properties and interactions of macromolecules. Carlson has determined three-dimensional minimum-energy conformation of four bituminous coal models, and indicated that nonbonding interactions, in particular, van der Waals and hydrogen bonding interactions, are strong driving forces to form and stabilize the three-dimensional structure of the coal models [3]. Takanohashi and co-workers determined the minimum-energy conformation of bituminous coal by CAMD and reported that the bituminous coal has a possibility to have associated structure of coal molecules which have a continuous distribution of molecular weight [4,5]. In the present study, the conformational change in macromolecular structure of an Australian brown coal with its moisture removal process was simulated by means of a CAMD method.

EXPERIMENTAL

CAMD calculation method

The CAMD study was carried out using PolyGraf software. The software allows treatment of relatively large molecules containing up to 20 000 atoms and is capable of calculating the most stable structures with the minimum conformational energies using AMBER, MM2 and DREIDING force fields. In this study, the DREIDING force field was used. The energy for model molecule was evaluated from forces of bonded interactions (bond; E_b, angle; E_a, torsion; E_t, inversion; E_i), and forces of non-bonded interactions (van der Waals; E_{vdW}, electrostatic; E_{el}, hydrogen bond; E_{hb}); as follow:

$$E = (E_b + E_a + E_t + E_i) + (E_{vdW} + E_{el} + E_{hb})$$

The structure of Yallourn brown coal (YL) was modeled by two oligomers, namely a tetramer (Mw=1540) and a pentamer (Mw=1924), of unit structure. The unit structure which was constructed on the basis of the data from elemental analysis and ^{13}C-NMR spectroscopy of the coal is shown in figure 1. Each oligomer was specially arranged so as to have no interaction with others. Simulations of moisture removal process were initiated by generating 360 water molecules (65.25wt%, wet basis) surrounding the model molecule and the minimum energy conformation (MEC) for the model with water molecules was calculated based on molecular mechanics and molecular dynamics methods. After MEC was obtained, the potential energies and volume were calculated individually for the model molecule with water and model molecule alone. The volume was defined as the void volume using water as a probe molecule. The

calculation was repeated decreasing the number of water molecules step by step to 0, and finally MINEC for model molecule with 0 water, i.e., completely dried coal was obtained. Re-adsorption of water onto the completely dried coal was also simulated in the same manner by generating 360 water molecules surrounding the model molecule with 0 water.

Coal Sample

Yallourn brown coal (YL, Moisture;60.0wt% wet basis, ash; 1.1wt% dry basis, C;62.6wt%, H;4.6wt%, N;0.7wt%, S;0.3wt%, O;31.6wt% diff.) was selected and used as a sample. The moisture content of the sample coal was controlled by varying the relative humidity in a vessel from 0 to 84% at 303K using conc. H_2SO_4 and aqueous solutions saturated by selected salts.

Volumetric Change Measurements

For coal drying process, partially and completely dried brown coal samples were placed in constant diameter tubes (8 mm i.d.), then centrifuged for 5 min at 4 500 rpm. After which the height of the coal particle bed was measured by caliper. For volumetric recovery measurement, water was added in the tube containing completely dried sample, then the contents were vigorously stirred. The tube was sealed and placed in an oven kept at 303K for 7 days. The tube was centrifuged again for 5 min at 4 500 rpm, then the height of coal bed was measured. The volumetric shrinkage of sample during moisture release process was determined by referring to the initial volume of as received sample. The volumetric recovery of dried sample was determined by referring to the initial volume of as received sample.

RESULTS AND DISCUSSIONS

The volumetric change of the YL during moisture release process was determined. The results are shown in figure 2 as a function of the extent of moisture removal. During moisture release process, the volume decreases monotonously with moisture removal, and reaches nearly a half of initial volume at the final stage. The volumetric recovery for completely dried brown coal was also determined. The volume of the completely dried sample is not recoverable with moisture re-adsorption. These results reveal that the volumetric change of YL is irreversible when the moisture is removed completely from the coal and imply that the irreversibility is caused by conformational change in the macromolecular structure of the coal during moisture release process. In order to elucidate the conformational change, CAMD technique has been applied for simplified brown coal model molecule.

Volumetric change in MEC of YL model molecule during moisture release process obtained with CAMD calculation is shown in figure 3. The MEC were extracted after 100 pico-second molecular dynamics calculation. The calculated volume for MEC of YL model molecule with water molecules, here after defined as ***COAL/WATER***, shows monotonous decrease with moisture removal. The volumetric changes of ***COAL/WATER*** well corresponded to the experimentally observed volumetric changes of YL. The conformation for MEC of YL model molecule alone, defined as ***COAL***, showed an extensive shrinkage of the size from the initial expanded to the contracted as well as deformation of the shape with a decrease in the number of water molecules. The volume for ***COAL*** remains constant with the extent of moisture removal up to 60%. A significant decrease in ***COAL*** volume is observed with the extents higher than 80%, resulting in a completely dried COAL with a volume being 80% of the initial one. For re-adsorption of water molecules onto the completely dried coal, ***COAL/WATER*** recover its volume by 85% of the initial one. The volume of ***COAL***, however, is not affected by moisture re-adsorption. These CAMD calculation results indicate that removal of water molecules is responsible for the volumetric change of ***COAL/WATER*** with progress of moisture release, and change in the conformation of ***COAL*** proceeds in the final stage of moisture release. Also, the conformational change is irreversible and re-adsorption of water molecules causes an increase in coal volume without affecting the coal conformation.

The total potential energies for ***COAL/WATER*** ($E_{C/W}$) can be assumed as a sum of three potential energies, *i.e.* ***COAL*** (E_C), water molecules (E_W) and interaction between brown coal model

molecule and water molecules (E_{INT}), as follow;

$$E_{C/W} = E_C + E_W + E_{INT}$$

Figure 4 shows the change in $E_{C/W}$ and E_C as a function of moisture removal. Monotonous increase in $E_{C/W}$ clearly indicates the marked contribution of water molecules on the stabilization of ***COAL/WATER***. The stabilization could be attributed to the non-covalent interactions among water molecules and between YL model molecule and water molecules. E_C decreased drastically for the extent of moisture removal of 80% and the change corresponded well to the volumetric change of ***COAL***. The decrease of E_C suggests the stabilization of ***COAL***, whereas the increase of $E_{C/W}$ means that ***COAL/WATER*** becomes unstable along with moisture release process. For moisture re-adsorption, E_C shows incomplete recover, since $E_{C/W}$ reverts completely to its initial value. This means that the YL model molecule has most stable conformation at completely dried state. While the effects of moisture release on the conversion reactivity thought to be due to a physical change, such as collapse of pores, the stabilization of the macromolecular structure also makes contributions to the conversion reactivity. In summary, the change in conformation for YL model molecule with its moisture release process could be successfully simulated by using the CAMD method. Although the coal model molecule employed in this study is rather simple, the results appear to represent the characteristics of the brown coal, at least volumetric change with moisture release process.

CONCLUSIONS

1. *Change in conformation* of Yallourn coal model simulated by CAMD method well correspond to the observed volumetric changes of the coal
2. Removal of water molecules results in a drastic conformational change in the final stage of moisture removal.
3. Re-adsorption of water molecules causes increase in coal volume without affecting the coal conformation.

REFERENCE

1. Allardice, D. J. In The Science of Victorian Brown Coal; Durie, R. A., Eds., Butterworth-Heinemann: Oxford, 1991; Chapter 3, pp 104-150.
2. Vorres, K. S.; Kolman, R.; Griswold, T. Prepr. Pap. Am. Chem. Soc., Div. Fuel Chem. 1988, 33 (2), 333.
3. Carlson,G.A. Energy Fuels 1992, 6, 771.
4. Takanohashi,T.; Iino,M.; Nakamura,K. Energy Fuels 1994, 8, 395.
5. Nakamura, K.; Takanohashi, T.; Iino, M.; Kumagai, H.; Sato, M.; Yokoyama, S.; Sanada, Y. Energy Fuels 1995, 9, 1003.

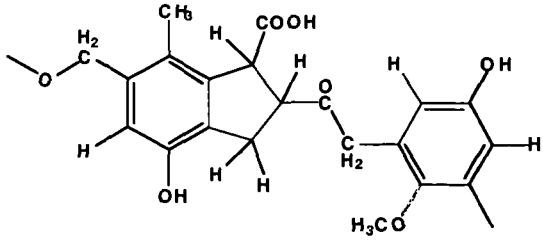

C:65.6, H:5.2, O:29.2 wt%
Mw:384.37
H-bond acceptor:7, H-bond donor:3

Figure 1 *Unit structure assumed for YL model molecule.*

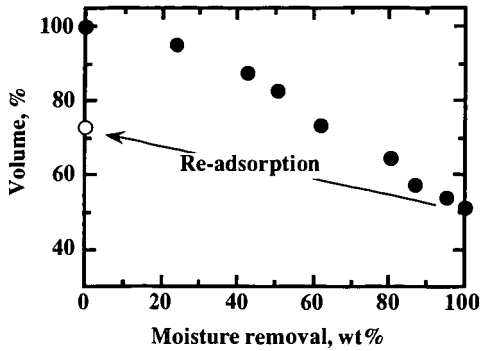

Figure 2 Volumetric change of YL during moisture release and re-adsorption process.

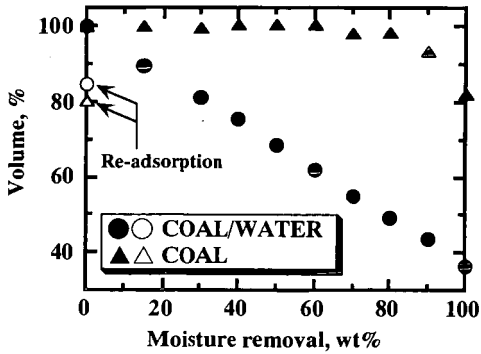

Figure 3 Volumetric change in YL model molecule with (COAL/WATER) and without (COAL) water molecules obtained with CAMD calculation.

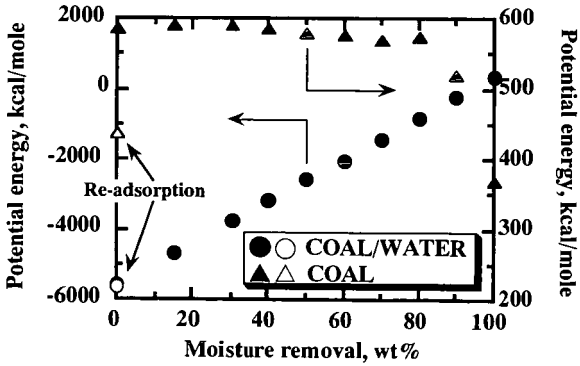

Figure 4 Variation in potential energies for YL model molecule with (COAL/WATER) and without (COAL) water molecules as a function of moisture removal.

ELECTRIC CHARGE REDISTRIBUTION INDUCED BY HYDROGEN BONDING IN LOW RANK COALS

Erik Kroo
Hydrocarbons Group. Advanced Fuel Research Inc.
87 Church Street, East-Hartford, CT 06108-3742

Keywords: hydrogen bonds, IR absorbance, apparent density

ABSTRACT

The nature of hydrogen bonds is predominantly electrostatic and strongly coupled to the environment in such a way, that formation or breaking of hydrogen bonds is accompanied by redistribution of electric charge among the participants. The intensity of infrared absorptions is related to charge separations along a particular bond. Therefore Fourier-Transform Infrared (FT-IR) spectroscopy is a promising tool to study the question whether charge separation in hydrogen bonding is important in coal. The objective of this study is to observe trends in infrared absorption intensities of hydrogen bonds, and in addition free OH and aliphatic deformation modes, as a function of moisture content in low rank coals, where hydrogen bonding is significant. FT-IR spectra of Zap lignite with varying moisture (0-22%) content were collected using the KBr pellet technique, and the spectra were curveresolved in the 3700-1900 cm^{-1} spectral region. The Mie theory of scattering was used for baseline correction and to calculate apparent density of coal particles. The data suggest that, in this particular lignite, charge redistribution as a result of hydrogen bonding is significant. It was observed that all of the measured quantities, i.e. the intensities of free OH, weak, medium and strong hydrogen bonds, aliphatic deformation modes as well as apparent density are influenced by the water monolayer buildup below 10% moisture, and that the direction of this influence reverses after saturation of the monolayer. A qualitative explanation of the charge redistribution mechanism involving polarization by hydrogen bond is given.

INTRODUCTION

Model calculations concerning quantitative aspects of hydrogen bonding in coal require that other noncovalent interactions, such as van der Waals forces, ionic and charge transfer type interactions, be more or less separable from hydrogen bonding. However, considering the nature of hydrogen bonds, this might not be true for coal. It is widely accepted that the nature of hydrogen bond is strongly electrostatic [1,2]. Consequently, the formation or breaking of hydrogen bonds is accompanied by redistribution of charge among the participants. Hydrogen bonds are also strongly coupled to the environment. For example, it was shown that in polypeptide chains hydrogen bonding and π-π stacking reinforce each other [3]. Quantum mechanical calculations reveal that a small change in the interaction potential originating from the vicinity of the hydrogen bond may lead to large-scale change in the bonding [4,5]. This interaction may be enhanced by the cooperative behavior of certain electric charges in coal. As a result this charge redistribution may well be extended beyond the participating coal molecules. Perhaps a good example of this is that coal can sustain and stabilize free electrons by delocalization along a larger condensed aromatic segment. Moreover, Flowers and coworkers [6] reported that the electron transfer to coal was a bulk property. If secondary effects of hydrogen bonding in coal are significant, it concerns important aspects of volumetric swelling theories like the separation of physical intermolecular interactions from hydrogen bonding interactions [7,8], and also dynamic properties of hydrogen bonding [8]. Another question is whether coal swelling can properly differentiate between free and hydrogen bonded OH functionalities [9] and/or inter and intramolecular hydrogen bonds. Since the intensity of infrared absorptions are related to charge separations along a particular bond, infrared spectroscopy seems to be a suitable tool to study this question. As a bonus to this approach, the apparent density of the coal particles can be calculated by applying Mie theory of scattering on the infrared spectra [10]. Water is natural to the coal structure and it was assumed that its presence in varying concentrations would invoke gradual changes in hydrogen bonding. A low rank coal (Zap lignite, Argonne Premium Coal Bank) was chosen in this work to study this question because of its capability to absorb significant amounts (up to about 26%) of moisture.

EXPERIMENTAL

The Zap lignite was dried in vacuum oven for 24 hours at 107 C° to decrease the moisture content to about 1.5%. The residual moisture was estimated by the TG-FT-IR technique [11]. The samples with varying moisture content were prepared by mixing wet (26%) and dried (1.5%) samples, and equilibrating them in sealed vials for one month. Fourier Transform Infrared (FT-IR) spectra were collected using the KBr pellet technique [12]. It was found that the

moisture equilibration between the coal particles and KBr at room temperature was very slow. However, at 107 C^o in vacuum the moisture content of the coal particles in the KBr pellet could be decreased below 1.5%. A typical coal spectrum is shown in Fig.1. The sloping baseline is the result of light scattered by coal particles, and it can be corrected using the Mie theory [10] where the adjustable parameters are n (index of refraction), D (average particle size, μm) and d(particle density, g/cc). There are two regions with only scattering (above 3700 cm^{-1} and between 1800 – 1900cm^{-1}) to occur and scattering vanishes below ≈ 800cm^{-1}. Therefore the values of the d, n, and D could be determined iteratively through minimizing the integral functions

$$\int (I_{Mie}(d,n,D) - I_{Spectr.})d(d,n,D) \qquad 1.$$

All three adjustable parameters are known [10] to fall between 1≤ d,n,D ≤2 , I is the sum of adsorbances in the 3700-4500 and 1800-1900cm^{-1} region for the calculated (Mie) and measured (Spectr.) spectra with I_{Mie}= 0 below 800cm^{-1}. The errors of the adjustable parameters, Δ_d, Δ_n and Δ_D, were obtained through setting Δ_d=0.05, and than estimating the corresponding errors of n and D (Δ_n = 0.01 and Δ_D = 0.01). This approach is valid, because the fit with the d, n, D parameters is excellent. n and D was constant within the error bar for all samples with n=1.64 and D=1.50.

The baseline-corrected spectrum of the 1.5% moisture sample is shown in Fig.1. It is also seen from this figure, that the pellet drying of this sample resulted in decreased hydrogen bond band intensities (3600-3000cm^{-1} region) but significantly increased the scattering. The additional scattering occurred on microcraks in the KBr pellet as a result of pellet drying. Therefore the Mie theory is not applicable to dried pellet samples without proper modifications. A rectilinear baseline correction [12] approximation was used in this particular case.

The conventional spectral deconvolution techniques usually fail if applied to spectra with highly overlapping bands [13,14]. An alternative approach used in this work is to choose available literature band assignments as the input parameters for the active IR bands in the 3700-1900cm^{-1} spectral envelope. The input band positions were: free OH (3618cm^{-1}) [15], weak (3560; 3495cm^{-1}), medium (3450; 3409; 3300; 3204; 3122cm^{-1}) [14-19] and strong hydrogen bonds (2741; 2555; 2372; 2215; 2043; 1902cm^{-1}) [20], aromatic stretching vibrations (3040cm^{-1}) [20] and aliphatic stretching and deformations (2960; 2935; 2900; 2870; 2840cm^{-1}) [20,21]. The aromatic and strong hydrogen bond bands were broadbend (bandwidths in the 100cm^{-1} order) contributions, and the band shapes were Voigt functions [21]. The final band positions and shapes can be optimized by the curve-resolving routine (Spectra Calc., Galactic Ind.), but curve-resolving does not work well if narrow and broad bands overlap, which is the case for the aliphatic modes as seen in Fig.1. (between 3000cm^{-1} and 2800cm^{-1}). Therefore, the aliphatic absorptions were stripped off from the spectra and the two spectral fragments were curve-resolved separately.

RESULTS AND DISCUSSION.

Infrared intensity data. The total line intensity of a given i →j vibrational transition can simply be given as

$$I_{i,j} = \frac{N\pi}{3c}[(\mu_x^{(k)})^2 + (\mu_y^{(k)})^2 + (\mu_z^{(k)})^2] \qquad 2.$$

where N is the Avogadro number, c is the speed of light and $\mu^k_{x,y,z}$ are the coefficients of the normal coordinate Q_k in the expansion of the electric moment

$$\mu_x = \mu_x^o + \sum_{k=1}^{3N-6} \mu_x^{(k)} Q_k + \text{higher terms} \qquad 3.$$

where the higher terms are thought to be small. The same can be written for the y and z components. The x component of the electric moment possessed by the molecule in its equilibrium position, μ^o_x, is practically equal to the x component of the permanent electric moment and only vibrations that cause change in the electric moment are IR active. Since almost every molecule possesses sufficient symmetry, practically only one of the x,y z components is different from zero. IR absorption of an intermolecular bond of the type A – A may vanish because no dipole is generated by the vibration, but the IR absorptions in intramolecular hydrogen bonds may also vanish in molecules possessing sufficient conjugation in the vicinity of the hydrogen bond [22]. The same reduction occurs in stretching intensities of CH_3, CH_2 and CH groups adjacent to double bonds [23]. Thus, the weakness of the IR intensity of a particular band is not necessarily connected with symmetry. Rather, charge transfer or conjugation compensates dipoles induced by the vibration. For this reason, trends in hydrogen bond and aliphatic stretching mode intensity changes can reflect charge redistribution in highly unsaturated materials like coal. On the contrary, free (non hydrogen-bonded) OH intensity is fairly proportional to the free OH concentration and is less effected by conjugation. It was found, that in lignites with increasing moisture content first a water monolayer is formed which is saturated at around 10% water [24,25]. Than a simple scenario for the coal macromolecule can be

described as follows. If water is added, the specific sites of the molecule will form hydrogen bonds with water, and the sites may be either hydrogen donor or acceptors depending on the electronegativity difference between water and the macromolecule. After the monolayer is filled up, hydrogen bonding between the second and first layer of water decreases the actual donor or acceptor character of the first layer, thereby changing the trend of charge transfer between water and coal as further water molecules are added. However, in heterogeneous complex aggregates like coal, these trends might be scrambled. The results are summarized in Table1, and it is seen that samples with around 10% moisture are indeed distinct.

The free OH concentration is very low below 1.5% and it is maximum at 1.5% moisture. As a result of hydrogen bond formation with water, the free OH gradually decreases with filling up the water monolayer. Glass and Larsen [26] also observed the reaction of free OH with a number of organic bases. Free OH in coal can be stabilized sterically if there is no reacting partner in the immediate vicinity to form a hydrogen bond, or an existing hydrogen bond can be destabilized to form free OH through polarization by neighbors [5]. If the diminishing IR intensities below 1.5% water (see Table 1) were caused by partial decomposition of OH groups or other functionalities, it would not decrease significantly the free OH concentration, because the remaining OH groups will have an increased chance to remain free from interacting neighbors. A more suitable mechanism is intramolecular hydrogen bond formation coupled with increased conjugation. This supports a coal swelling model proposed by Painter and coworkers [27,28]. According to the model, the swelling of coal is associated with topological reorganization of the network rather than changing chain dimensions. Favoring intramolecular hydrogen bonding requires special folding of the macromolecules of which plenty of examples, especially among helical structures, exists in nature.

The change of aliphatic intensities (see Table 1.) as a function of water content is a proof, that the charge transfer as a result of hydrogen bond formation with water extends to, at least, a larger section of the coal molecule being involved in the hydrogen bonding. An intensity minimum was observed at around the monolayer saturation. The aliphatic stretching intensities decrease with electron transfer towards the aliphatic functionalities. With hydrogen bond formation the electron density increases at the donor site. Therefore a qualitative explanation is that the coal is the donor in the hydrogen bond with water.

The reduction, rather than the increase, of hydrogen bond intensities with the water monolayer buildup can also be related to the water monolayer buildup. As additional hydrogen bonds are formed, the donor strength of coal is decreased reducing the electronegativity difference between coal and water and increasing the symmetry of the hydrogen bonds.

Apparent density data. Fig. 2 shows the calculated apparent (or particle) densities as a function of moisture. Using the linear relationship established by Suuberg and coworkers [29] for the swelling of Zap lignite with water, the proportional decrease of apparent density with moisture content can be predicted. The same trend is expected from comparing the true (He) density (1.55 g/cc) [30] with water density (1.31 gr/cc, measured in our lab). Note, that the "water density" which is the true density of coal saturated with water (in place of He), is an approximation of the apparent density of water saturated coal. The apparent "swelling" densities in Fig.2 were calculated from the linear relationship (Suuberg) by normalizing the actual value at 1.5% moisture to 1.09, which is the average "Mie" density between 1.5 and 10% water. It is seen that, while the apparent "Mie" density is identical with the "swelling density at 1.5 and 21.8% water content, the change with water is not gradual, but rather abrupt at the monolayer saturation point. It is possible, that this is due to the particle size difference between the two type of experiment. The size of coal particles in the KBr pellets was 1.5 μm, therefore the presence of macropores larger than about half of that (≈ 0.6 μm) could be excluded. If the ratio of larger than ≈0.6μm pores abruptly changes after the monolayer fill-up, this would explain the discrepancy between the scattering and macroscopic measurement techniques.

CONCLUSIONS

Infrared absorption intensities in the 3700-1900 cm^{-1} spectral region have been measured as a function of moisture in Zap lignite. The trends in absorption intensity changes as a function of moisture content can be related to water monolayer and subsequent secondary layer buildup. The polarization of hydrogen bonds changes direction at the monolayer saturation (≈ 10% water). These data suggest that the electric charge redistribution resulting from hydrogen bond formation and/or breaking in low rank coals is significant.

ACKNOWLEDGMENTS

The author is thankful to E.M. Suuberg and M. Serio for helpful criticism. The help of S. Charpenay in providing the Mie scattering software is gratefully acknowledged. The FT-IR spectra utilized in this work were collected under the U.S.Department of Energy contracts DE-AC22-88C88814 and DE-FG05-93-ER81593.

REFERENCES

1. Baur,W.H .Acta Chryst. **1965**, 19, 909.
2. Yamabe,S.;Morokuma,K. J.Am.Chem.Soc. **1975**, 97, 4458.
3. Schall,O.F.;Gokel,G.W .J.Org.Chem. **1996**, 61, 1449.
4. Hall,G.G. Theor.Chim.Acta **1985**, 67, 439.
5. Schmidt,P.P. J.Phys.Chem. **1993**, 97, 4249.
6. Flowers,II,R.A.;Gebhard,L.;Larsen,J.W.;Sanada,Y.;Sasaki,M.;Silbernagel,B. Energ.Fuels **1994**, 8, 1524.
7. Panauiotou,C.;Sanchez,I.C. J.Chem.Phys. **1991**, 95, 10090.
8. Painter,P.C. Energ.Fuels **1996**, 10, 1273.
9. Larsen,J.W.;Gurevich,I. Energ.Fuels **1996**, 10, 1269.
10. Solomon,P.R.;Carangelo,R.M.;Best,P.E.;Markham,J.R.;Hamblen,D.G. Fuel **1987**, 8, 897.
11. Carangelo,R.M.;Solomon,P.R.;Gerson,D.J. Fuel **1987**, 66, 960.
12. Solomon.P.R.;Carangelo,R.M.; Fuel **1982**, 61, 663 and **1987**, 67, 949
13. Jackson,R.S.;Griffiths,P.R. Anal.Chem. **1991**, 63, 2557.
14. Pierce,J.A.;Jackson,R.S.;Van Every,K.W.;Griffiths,P.R. Anal.Chem. **1990**, 62, 447.
15. Painter,P.C.;Sobkowiak,M.;Youtcheff,J. Fuel **1987**, 66, 973.
16. Solomon,P.R.;Hamblen,D.G.;Carangelo,R.M. ACS Symp.Ser. 205 **1982**, 4, 77.
17. Gethner,J.S. Fuel **1982**, 61, 1273.
18. Malhotra,V.M.;Jasty,S.;Mu,R. Appl.Spectr. **1989**, 43, 638.
19. Karsen,J.W.;Baskar,A.J. Energ.Fuels **1987**, 2, 232.
20. Solomon,P.R.;Hamblen,D.G.;Carangelo,R.M. in Fuel Science ACS Symp.Ser. **1982**, 205, 77.
21. Friesen,W.I.;Michaelian,K.H. Appl.Spectr. **1991**, 45, 50.
22. Detoni,S.;Hadzy,D.;Juranji,M. Spectrochim.Acta **1974**, 30A, 249.
23. Bellamy,L.J. The Infrared Spectra of Complex Molecules. Chapman and Hall, London, **1975**, pg.20.
24. Suuberg,E.M.;Otake,Y.;Deevi,S.C.;Yun,Y. Int.Conf.on Coal Sci.Proc. Butterworth-Heinemann Ltd. **1991**, pg.36.
25. Lynch,L.J.;Barton,W.A.;Webster,D.S. Int.Conf. on Coal Sci.Proc. Butterworth-Heinemann Ltd. **1991**, pg.8.
26. Glass,A.S.;Larsen,J.W. Energ.Fuels **1994**, 8, 629.
27. Painter,P.C.;Graf,J.;Coleman,M.M. Energ.Fuels **1990**, 4, 393.
28. Painter,P.C.;Shenoy,S.L. Energ.Fuels **1995**, 9, 364.
29. Suuberg,E.M.;Otake,Y.;Langner,M.J.;Leung,K.T.;Milosavljevich,I. Energ.Fuels **1994**, 8, 1247.
30. Smith,K.L.;Fletcher,T.H.;Pugmire,R.J. The Structure and Reaction Processes of Coal. Plenum Press, New York, **1994**, pg.164.

Table 1. Infrared intensities. Peak areas, arbitrary units.

wt% water	Free OH*	Partial sum of hydrogen bonds Weak**	Medium**	Strong**	Aliphatic CH_3*	CH_2*	CH*
< 1.5	0	7.1	55.0	46.1	1.5	4.3	2.1
1.5	11.8	36.8	133.7	66.0	1.6	4.9	1.9
4.3	10.2	45.7	131.1	148.4	1.8	4.8	1.9
8.9	9.2	44.9	125.5	62.9	0.7	3.8	1.2
10.3	5.2	20.3	93.3	63.8	1.4	3.5	1.7
16.2	5.8	31.8	95.9	53.1	1.7	4.6	2.0
21.8	2.2	11.3	85.9	12.2	2.3	5.1	2.6

* Dry coal basis
** Wet coal basis

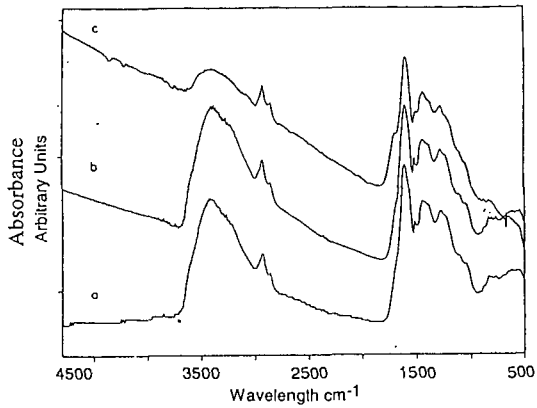

Figure 1. FT-IR spectra of Zap (1.5% moisture) a) after baseline correction; b) before pellet drying; and c) after pellet drying.

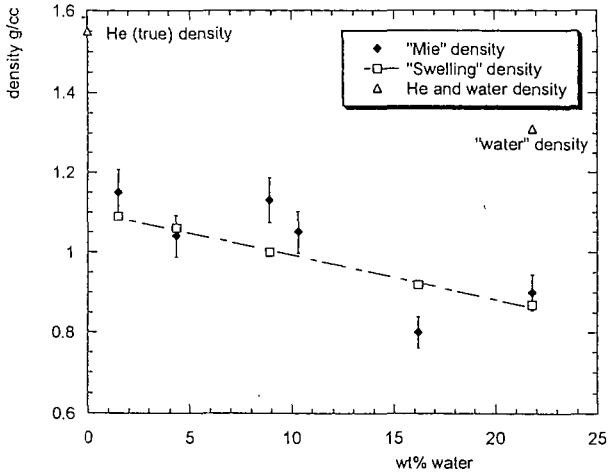

Figure 2. Comparison of calculated apparent densities. The "swelling" densities were derived from literature swelling data (Suuberg et.al. [29]) and normalized to 1.09 at 1.5% moisture, while the "Mie" density was calculated from FT-IR scattering data using the Mie theory of scattering and the KBr pellet technique. In addition the true (He) density [30] (dry coal) together with the water density (wet coal) is also shown.

In Situ F.T.I.R. MEASUREMENT OF THE CHANGE IN HYDROGEN BONDING OF COAL THROUGH HEAT TREATMENT

Kouichi Miura*, Kazuhiro Mae, Li Wen, Takumi Kusakawa and Akiko Kumano
Department of Chemical Engineering, Kyoto University, Kyoto 606-8501, Japan

INTRODUCTION

It is well known that hydrogen bonding plays an important role to keep the macromolecular structure of coal.[1-5] Several attempts have been made to estimate the amount and the strength of hydrogen bonding in coal. However, no definite methods have been presented for the estimation. One of the difficulties encountered for the estimation is the distribution of hydrogen bonding, and another problems associated with the estimation is the effect of adsorbed water. F.T.i.r. is believed to be a most powerful and convenient method to estimate the hydrogen bonding.[6-11] The water problem can not be completely overcome when the KBr pellet method was used, although the method is said to be suitable to quantitative studies.[9] Fuller and Smyrl[10] showed that the *in-situ* diffuse reflectance i.r. Fourier transform (DRIFT) technique with neat, undiluted, coal samples can be well utilized to trace the *in-situ* reactions such as oxidation, dehydration, etc. Painter *et al.*[7] clarified the attribution of hydrogen bonded absorption bands ranging from 2800 to 3600 cm^{-1}. It is known that the absorption wave number of hydrogen bonded OH stretching vibration shifts from that of free OH by $\Delta\nu_{OH}$, and that the $\Delta\nu_{OH}$ value increases with the increase of the strength of hydrogen bonding.

In liquid phase hydrogen-bonded adduct formation reactions between phenolic OH groups and various bases (B) have been examined in detail:[12-15]

$$\text{Ph-OH} + \text{B} \rightarrow \text{Ph-OH}\cdots\text{B} \quad ; \quad \Delta H \qquad (1)$$

where ΔH (< 0) is the enthalpy change of the reaction, and $-\Delta H$ is regarded as the strength of hydrogen bonding in general. $\Delta\nu_{OH}$ (>0) for this reaction is the wave number difference between the free OH in Ph-OH and the hydrogen bonded OH in Ph-OH···B. Through separate measurements of ΔH [kJ/mol] and $\Delta\nu_{OH}$ [cm^{-1}] for many phenol-base combinations a linear relationship was found to hold between them by many investigators. The relationship obtained by Drago et al.[13], for example, is given by

$$-\Delta H = 0.067\Delta\nu_{OH} + 2.64 \qquad (2)$$

For solid-gas interactions, Kiselev[16] found that a linear relationship between the heat of adsorption, ΔQ_a [kJ/mol], and the $\Delta\nu_{OH}$[cm^{-1}] for a hydroxylated silica surface and various vapors including steam. It was represented by

$$\Delta Q_a = 0.064\,\Delta\nu_{OH} - 1.16 \qquad (3)$$

These works clarified that the OH wave number shift caused by the formation of hydrogen bonding is well related to the enthalpy change of the hydrogen bonding formation. However, neither the distribution nor the amount of hydrogen bonding were not taken into account in these works.

Recently Miura and his co-workers[17] have presented a method to estimate the strength distribution of hydrogen bonding (HBD) in coal by use of F.T.i.r. and DSC. The method was developed by combining and extending the works of Drago *et al.*, Painter *et al.*, and Kieslev. They found the following $-\Delta H$ *vs.* $\Delta\nu_{OH}$ relationship for water free coals:

$$-\Delta H = 0.069\Delta\nu_{OH} \qquad (4)$$

In their analysis, however, F.T.i.r. measurements were performed using the KBr pellet technique, and hence the water effect might not be completely eliminated. Furthermore, the absorption coefficients for different hydrogen bonded OH were assumed to be same as the first approximation. The latter assumption affects the amount of hydrogen bonding but does not affect the $-\Delta H$ *vs.* $\Delta\nu_{OH}$ relationship given by eq 4.

To overcome these weak points in the former analysis, an *in-situ* diffuse reflectance F.T.i.r. (DRIFT) technique was employed for the measurement of spectra, and the change in absorption coefficients was taken into account in this paper. The improved method was applied to estimate the change of hydrogen bonding during the heating of the Argonne premium coals from 30 to 290 °C.

ANALYSIS METHOD

The method to obtain the HBD was originally presented in a previous work.[17] The method was improved in this paper by taking into account the change in absorption coefficients for different hydrogen bonded OH groups. The procedure to obtain the HBD by the improved method is summarized as follows:

1. Divide F.T.i.r. spectrum ranging from 2200 to 3700 cm^{-1} into several hydrogen bonded peaks by a curve fitting method as schematically given in Fig. 1(a). The Gaussian distribution was assumed for each absorption band in this work. Three peaks associated with aromatic and aliphatic CH stretch vibrations are easily eliminated from the spectrum.
2. Estimate the amount of OH for the j-th peak, $(n_{OH})_j$, by the Beer law as follows:

$$(n_{OH})_j = \alpha_j A_j \qquad (5)$$

where A_j and α_j are respectively the integral intensity and the absorption coefficient of the j-th peak. In this analysis α_j was assumed to be represented by the equation presented by Detoni et al.[18] for the hydrogen bonded NH groups

$$\alpha_j = \frac{\alpha_0}{1 + 0.0141(\Delta\nu_{OH})_j} \qquad (6)$$

where α_0 is the absorption coefficient of the stretch vibration of the free OH. Then the amount of the OH corresponding to the j-th peak, $(n_{OH})_j$, is given by

$$(n_{OH})_j = \frac{\alpha_0}{1+0.0141(\Delta\nu_{OH})_j} A_j \quad (7)$$

3. Calculate the strength of j-th hydrogen bonding, $(-\Delta H)_j$ by eq. 3 as

$$(-\Delta H)_j = 0.069\,(\Delta\nu_{OH})_j \quad (8)$$

4. $(n_{OH})_j$ *vs.* $(-\Delta H)_j$ relationship gives the distribution of the strength of hydrogen bonding as shown schematically in Fig. 1(c).

Table 1. Ultimate analyses and oxygen distribution of 8 Argonne premium coals used [wt%]

Coal (abbre.)	Ultimate analysis [d.a.f.]				Oxygen content [d.a.f.]			
	C	H	N	O(diff.)	as COOH	as OH	as C=O	as Ether
Beulah-Zap (ND)	72.9	4.8	1.2	20.1	3.81	9.16	1.96	2.28
Wyodak (WY)	75.0	5.4	1.1	21.0	3.33	7.68	0.74	2.56
Illinois #6 (IL)	77.7	5.0	1.4	13.5	0.23	5.86	0.93	0.57
Blind Canyon (UT)	80.7	5.8	1.4	13.5	0.23	5.22	0.63	3.68
Lewinston-Stockton (ST)	82.6	5.3	1.6	9.8	0.20	2.70	0.18	2.67
Pittsburg#8 (PITT)	83.2	5.3	1.6	8.8	0.16	4.32	0.18	2.08
UpperFreeport (UF)	85.5	4.7	1.6	7.5	0.14	1.96	0.44	0.36
Pocahontas (POC)	91.1	4.4	1.3	2.5	0.05	0.98	0.32	0.24

EXPERIMENTAL

Coals samples. Eight Argonne premium coals were used as samples. The ultimate analyses and the amount of OH and COOH oxygen[19] are given in Table 1. Coal samples -200 mesh were further ground for 1 minute in a mortar just before measurement.

Apparatus and procedure. All the IR spectra were measured at 4 cm^{-1} resolution on a JEOL JIR-WINSPEC50 F.T.i.r. spectrometer with a microscope stage. A Mettler 84HPT hot stage, shown schematically in Fig. 2, was attached to the microscope stage for the *in-situ* measurement. A mirror, which is believed not to absorb water, was used as a background. About 0.5 mg of neat coal samples were leveled and pressed on the mirror by hand using a spatula. It is essential to make a flat surface for obtaining good and reproducible spectra. The coal samples were equilibrated at 30 °C in a flowing nitrogen stream. Then they were heated at the rate of 5 K/min up to 300 °C during which nitrogen was continually supplied at the rate of 100 cc/min to prevent any possible leakage of air into the chamber and to keep the stability of the temperature. A BaF_2 disc was put on the pin hole from where the light passes though. The light source was a heated Ni-Cr wire and the detector was MCT (mercury cadmium-tellurium). F.T.i.r. spectrum was collecteded by acquisition of 100 scans at every 20 °C of interval.

RESULTS AND DISCUSSION

Change of spectra with heating. Figure 3 shows the *in-situ* F.T.i.r. spectra ranging from 2200 to 3650 cm^{-1} for four coals measured at every 20 °C. One of the problems encountered by many investigators in using *in-situ* F.T.i.r. was the spectra quality at high temperatures due to change in refractive index. Very beautiful and reproducible spectra could be obtained by use of the proposed measurement technique for all the coals in this work. Very flat base lines were obtained at all the temperatures, and the spectra for POC were almost same above 70 °C. This suggested that the spectra were not affected by the heating. Separate experiments were performed using kaolinite to check the change of spectra with increasing temperature up to 350°C. The mirror backgrounds at 30°C and at corresponding temperatures were used respectively to get the F.T.i.r. spectra. The spectra do not change with the background at different temperatures. Then all the spectra shown in this work were obtained using the background at 30°C. This made the *in-situ* measurement convenient, fast and reliable.

To get accurate information of hydrogen bonded OH groups, it is essential to ensure that the artifact does not exist during experiments and/or during the data processing after experiments. It is easily checked by tracing the change in the aliphatic and aromatic C-H bands. Because the C-H bond is hard to decompose or to form below 300°C, we can easily know whether some artifact exists or not from the variation of the 2890 and 2930 cm^{-1} bands (the absorption of aliphatic C-H bond), and 3050 cm^{-1} band (the absorption of aromatic C-H bond). It was found that these intensities were not affected by the temperature up to 300 °C. Therefore, all the changes in the OH spectra were really what happened in coal during the heating. Now, significant changes in the OH spectra were judged to occur for ND and WY coals, whereas very little change was judge to occur for PITT and POC coals during the heating for the four coals given in Fig. 2.

Change in strength distribution of OH associated with hydrogen bondings. All the spectra measured for the eight coals were analyzed by the procedure given above to estimate the change in HBD through the heating. Figure 4 shows the result of peak division and the HBD distributions obtained for ND as an example. The spectra ranging from 2200 to 3650 cm^{-1} were divided into 9 peaks by a curve-fitting method. The peak assignments were determined as follows by referring to the work of Painter *et al*[7]: six hydrogen bonded bands (HB1 at 3516 cm^{-1}; OH-π, HB2 at 3400 cm^{-1}; OH-OH, HB3 at 3280 cm^{-1}; OH-ether, HB4 at 3150 cm^{-1}; cyclic OH-OH, HB5 at 2940 cm^{-1}; OH-N, and HB6 at 2650 cm^{-1}; COOH-COOH) and three C-H bands (3050, 2993, and 2920 cm^{-1}). No free OH band was detected for all the coals. In actual peak

division the peak positions were slightly changed, depending on the sample by referring to the second derivative of each spectrum. The bands for the C-H bonds did not change during the heating, then they were easily separated from the hydrogen bonded bands. The amount of OH and the strength of each hydrogen bonding were calculated from each peak intensity, A_j, and the OH wavenumber shift, $\Delta\nu_{OH}$, with the aid of eqs 7 and 8, where the total OH value given in Table 1 was used as the value at 150 °C to estimate α_0 in eq 7. The strength distributions of hydrogen bonding thus estimated, $(n_{OH})_j$ vs. $(-\Delta H)_j$ relationships, for ND are shown in the right of Fig. 4. It is clearly shown that the amount of weakly hydrogen bonded OH preferentially decreases with the increase of temperature.

Quantitative analysis of change in hydrogen bonding during the heating. The changes of the amounts of the six hydrogen bonded OH with increasing temperature are shown for four coals in Fig. 5. As is expected from the spectra shown in Fig. 4, the amounts of HB1 to HB4 decrease significantly with increasing temperature for ND and WY, whereas all the hydrogen bondings do not change with increasing temperature for POC. The decrease in the total amount of OH with increasing temperature is related to the formation of H_2O. It is noteworthy that only the distribution changes without affecting the total amount of OH for PITT above 230 °C. This means that stronger hydrogen bonding, HB5, shifted to weaker hydrogen bondings, HB1 and HB2, above 230 °C.

To examine the change in the hydrogen bonding in more detail, total enthalpy for the formation of all OH associated hydrogen bondings, $(-\Delta H)_{total}$ (< 0), at each temperature was calculated by

$$(-\Delta H)_{total} = \sum_j (n_{OH})_j (-\Delta H)_j \quad \text{[kJ/kg]} \qquad (9)$$

Utilizing $(-\Delta H)_{total}$ and the total amount of OH groups, $(n_{OH})_{total}$, the average strength of hydrogen bonding, $(-\Delta H)_{av}$, can also be calculated by

$$(-\Delta H)_{av} = \frac{(-\Delta H)_{total}}{(n_{OH})_{total}} = \frac{\sum_j (n_{OH})_j (-\Delta H)_j}{\sum_j (n_{OH})_j} \qquad (10)$$

The $(-\Delta H)_{total}$ values and the $(-\Delta H)_{av}$ values are shown in Fig. 5 and Fig. 6, respectively. $(-\Delta H)_{total}$ decreases with the increase of temperature due to the changes in the hydrogen bondings. When the number of total OH groups does not change, the decrease in $(-\Delta H)_{total}$ is due to the rearrangement of hydrogen bondings. When H_2O is produced during the heat treatment, the number of OH groups decreases by the two mechanisms, and consequently $(-\Delta H)_{total}$ decreases. The first mechanism is the desorption of adsorbed water and the other is the formation of H_2O by the decomposition of two OH groups. For ND and WY, both $(-\Delta H)_{total}$ and $(n_{OH})_{total}$ decreased with increasing temperature, indicting that the change in $(-\Delta H)_{total}$ is brought about by the formation of water. On the other hand, for PITT above 230 °C, only the $(-\Delta H)_{total}$ value decreased without affecting the value of $(n_{OH})_{total}$. This indicates that the rearrangement of hydrogen bondings occurred at above 230 °C as stated above. This rearrangement may be associated with the glass transition as detected by DSC by several investigators.[20,21]

The changes in the average hydrogen bonding strength, $(-\Delta H)_{av}$, in Fig. 6 are also informative. The $(-\Delta H)_{av}$ values are around 20 to 24 kJ/mol-OH and kept almost constant during the heating for ND, WY, UT and IL. The $(-\Delta H)_{av}$ value for PITT is around 23 kJ/mol-OH below 230 °C, but it decreases to 20 kJ/mol-OH above 230 °C, indicating that the glass transition occurred between 230 to 270 °C. For high rank coals of UF and POC, the $(-\Delta H)_{av}$ values are 28 to 30 kJ/mol-OH, which are larger than for the other coals by 4 to 8 kJ/mol-OH. The $(-\Delta H)_{av}$ value for UF also decreased to 23.7 kJ/mol-OH above 230 °C, again indicating the occurrence of the glass transition. The $(-\Delta H)_{av}$ values estimated here are rather close to the values reported as the strength of hydrogen bonding in the literature.[1-3] A little bit larger $(-\Delta H)_{av}$ values for UF and POC are associated with the relative abundance of OH-N hydrogen bonding in these coals. It was clearly shown that the glass transition behavior can be detected from the change in $(-\Delta H)_{av}$ value for higher rank coals.

What we would like to stress here is that the value of α_0 is not required to calculate $(-\Delta H)_{av}$ as can be found from eqs 7, 8, and 10, which means that only F.T.i.r. spectra measurements are enough to obtain $(-\Delta H)_{av}$. This is a great merit of the proposed analysis method. Then the accuracy of the $(-\Delta H)_{av}$ values are well expected.

Differentiation between adsorbed water and decomposed water. It has been rather difficult to distinguish the chemisorbed water and the water formed by decomposition reaction, which made it difficult to define the dried state of coal. In this analysis we could estimate the changes in the amount of OH , $(n_{OH})_{total}$, and the enthalpy related to hydrogen bonding, $(-\Delta H)_{total}$, as shown in Fig. 5. Then we can estimate the change in the enthalpy related to hydrogen bonding with the formation of water by using the values of $(-\Delta H)_{total}$ and $(n_{OH})_{total}$ as

$$(\Delta H)_{H2O} = 2\frac{d(-\Delta H)_{total}}{d(n_{OH})_{total}} \qquad \text{[kJ/mol-H}_2\text{O]} \qquad (11)$$

where 2 in the r.h.s. was included to account for the fact that one H_2O molecule contains two OH groups. The magnitude of $(\Delta H)_{H2O}$ thus estimated is well expected to be dependent on the mechanism of water

formation. Then the $(\Delta H)_{H2O}$ values calculated by eq 11 with the aid of eqs. 7, 8, and 9 are shown against temperature in Fig.7. The values obtained for an Australian brown coal (Morwell; MW) and a lignin are also included in the figure for comparison. The $(\Delta H)_{H2O}$ vs. temperature relationships were so close each other, and there was a distinct jump at about 140 °C: the $(\Delta H)_{H2O}$ values below 140 °C were close to or slightly smaller than the heat of vaporization of water, ΔH_{vap}, whereas the $(\Delta H)_{H2O}$ values above 140 °C were significantly larger than ΔH_{vap}. These results suggest that the water detected below 140 °C is the chemisorbed water and that formed above 140 °C is the water formed by some decomposition reaction. Thus the HBD estimated by the proposed method is found to be utilized to distinguish the type of water formed. Finally we would like to stress that the value of α_0 or the value of $(n_{OH})_{total}$ is not required to obtain $(\Delta H)_{H2O}$, as was the case to calculate $(-\Delta H)_{av}$. Only F.T.i.r. spectra measurements are enough to obtain $(\Delta H)_{H2O}$. This is a great merit of the proposed method and it simplifies the procedure to obtain $(\Delta H)_{H2O}$.

CONCLUSION

In situ F.T.i.r. measurements were performed for the Argonne premium coals to estimate the change in hydrogen bonding through heat treatment. Neat, undiluted, coal samples were placed in a specially designed cell and they were heated from room temperature up to 300 °C in an inert atmosphere. F.T.i.r. spectra were collected in every 20 °C using the diffuse reflectance infrared Fourier transform (DRIFT) technique and the spectra ranging from 2200 to 3650 cm^{-1} were divided into 6 hydrogen bonded OH peaks and other peaks. The strength distribution of hydrogen bonding (HBD) at each temperature was well estimated through the analysis of the divided peaks by the propses method. By utilizing the HBD the changes in enthalpies associated with the desorption of water, the glass transition, and the decomposition of OH groups were well estimated. Only F.T.i.r. spectra measurements were found to be enough to obtain such enthalpies. This greatly simplified the calculation procedure and increased the accuracy of the enthalpies. The validity of the proposed *in situ* F.T.i.r. measurement method and the analysis method for obtaining HBD was well clarified.

ACKNOWLEDGEMENT

This work was supported by "Research for the Future" project of the Japan Society for the Promotion of Science (JSPS) through the 148 committee on coal utilization technology of JSPS.

REFERENCES

1. Larsen, J. W.; Green, T. K.; Kovac, J., *J. Org. Chem.*, **1985**, 50, 4729-4735.
2. Glass, A. S.; Larsen, J. W., *Energy &Fuels*, **1987**, 1, 230-232.
3. Larsen, J. W.; Baskar, A.J, *Energy &Fuels*, **1994**, 8, 284-285.
4. Arnett, E.M.; Tanweer, A., *Fuel*, **1993**, 72, 1169-1176.
5. Miura, K.; Mae, K.; Takebe, S.; Wakiyasu, H.; Hashimoto, K., *Energy &Fuels*, **1994**, 8, 874-880.
6. Solomon, P. R.; Carangelo, R.M., *Fuel*, **1982**, 61, 663-669.
7. Painter, P.C.; Sobkobiak, M.; Youtcheff, J., *Fuel*, **1987**, 66, 973-978.
8. Mu, R.; Malhotra, V. M., *Fuel*, **1991**, 70, 1233-1234.
9. Sobkobiak, M.; Painter, P.C., *Energy &Fuels*, **1995**, 9, 359-363.
10. Fuller, E.L. Jr.; Smyrl, N., *Fuel*, **1984**, 64, 1143-1150.
11. Chen, C.; Gao, J.; Yan, Y., *Energy &Fuels*, **1998**, 12, 446-449.
12. Purcell, K.F.; Drago, R.S., *JACS*, **1967**, 89, 2874-2879.
13. Drago, R.S.; Epley, T. F., *JACS*, **1969**, 91, 2883-2890.
14. Arnett, E. M.; Mitchel, E. J.; Murty, T. S. S. R.; Gorrie, T. M.; Schleyer, P. V. R., *JACS*, **1970**, 92, 2365-2377.
15. Arnett, E. M.; Mitchel, E. J.; Murty, T. S. S. R., *JACS*, **1974**, 96, 3875-3891.
16. Kiselev, A. V., *Surface Science*, **1965**, 3, 292-293.
17. Miura, K.; Mae, K.; Morozumi, F., *Am. Chem. Soc., Div. Fuel Chem.*, **1997**, 42(1), 869-876.
18. Detoni, S.; Hadzi, D.; Smerkolj, R., *J. Chem. Soc. (A)*, **1970**, 2851-2859.
19. Jung, B.; Stachel, S.; Calkins, W. H., Preprint, *Am. Chem. Soc., Div. Fuel Chem.*, **1991**, 36(3), 869-876.
20. Lucht, L.M.; Larson, J.M.; Peppas, N.A., *Energy &Fuels*, **1987**, 1, 6-58.
21. Yun, Y.; Sunberg, E. M., *Fuel*, **1993**, 72, 1245-1254.

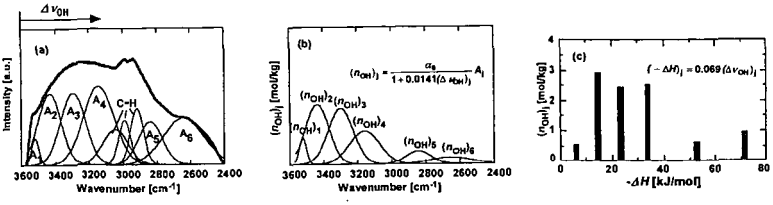

Figure 1 Procedure to obtain HBD from the spectra ranging from 2200 to 3650 cm^{-1}.

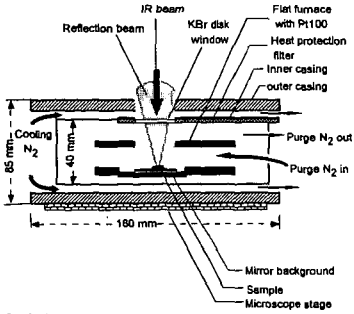

Figure 2 Schematic of a modified Metler 84HPT hot stage used for *in-situ* F.T.i.r. measurements.

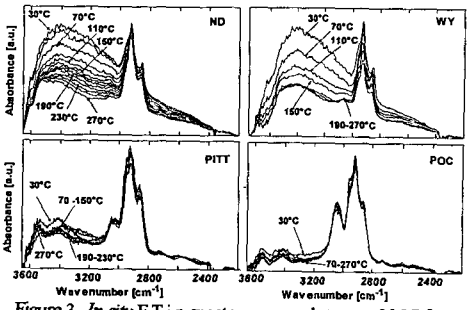

Figure 3 *In-situ* F.T.i.r. spectra measured at every 20 °C for four Argonne premium coals.

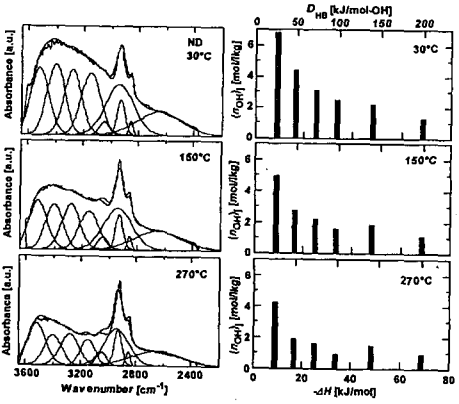

Figure 4 Typical examples of peak division of spectra and the HBDs estimated (ND coal).

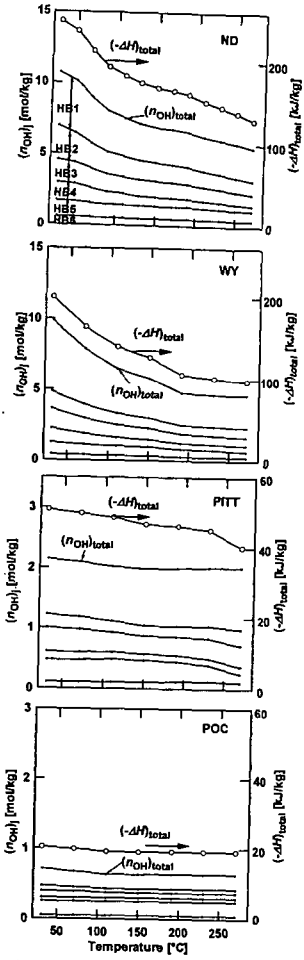

Figure 5 Change of $(n_{OH})_i$, $(n_{OH})_{total}$ and $(-\Delta H)_{total}$ with increasing temperature for four Argonne premium coals

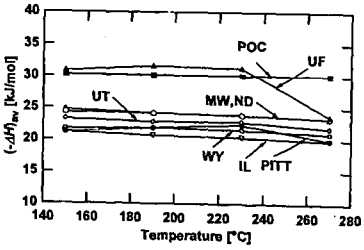

Figure 6 Change of $(-\Delta H)_{av}$ with increasing temperature for seven Argonne premium coals.

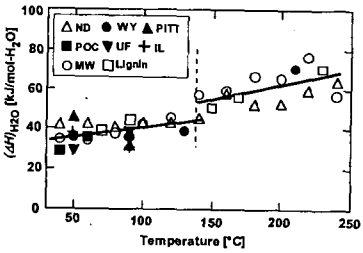

Figure 7 Change of $(\Delta H)_{H2O}$ with increasing temperature for Argonne premium coals, MW coal and a lignin.

QUANTITATIVE DESCRIPTION OF OXIDATIVE DEGRADATION OF BROWN COAL IN AQUEOUS PHASE BASED ON LATTICE STATISTICS

Jun-ichiro Hayashi and Tadatoshi Chiba
Center for Advanced Research of Energy Technology, Hokkaido University
N13-W8, Kita-ku, Sapporo 060-8628, Japan

Keywords: Bethe lattice, O_2 oxidation, degradation

INTRODUCTION

Some recently developed pyrolysis models[1-3] reasonably combine the kinetics of bridge breaking/formation with the Bethe lattiee statistics[4,5] that reeognizes aromatic clusters and bridges as *sites and bonds*, respectively. The assumption of coal as a lattice can be examined by analyzing the characteristics of its degradation, which provides the measurable structural changes of coal, namely, the decrease in the bridge concentration and corresponding increase in the fraction of low-molecular-mass components released from the network. The relationship between these changes may be quantitatively described by assuming coal as a lattice having a particular chain configuration. The authors[6,7] found that an O_2 oxidation in weakly alkaline aqueous phase solubilizes low rank coals to considerable extent. The oxidation increased the mass fraction of solvent-extractable material in a brown coal from 0.15 to 0.97. Analyses of the products revealed that aromatic carbon was selectively oxidized into carboxyls in the residual solid as oxidized coal, water-soluble non-aromatic acids and carbon dioxide, while aliphatic carbon was minimally involved in the reaction. Considering that the coal consists of aromatic clusters and inter-cluster bridges, they proposed a reaction mechanism that the oxidation converted aromatic carbons bonded to bridges into peripheral carboxyl groups on the neighboring clusters, and did the other aromatic carbons into non-aromatic acids or carbon dioxide. According to this mechanism as illustrated in Figure 1, the oxidation decomposes the macromolecular network of the coal by eliminating clusters as *sites* and converting bridges as *bonds* into peripherals. If the mechanism is valid, the extent of the degradation can be quantified by determining the amounts of lost bridges and clusters from those of formed carboxyls and oxidized aromatic carbon, respectively. In addition, the number of carboxyls formed as peripherals is expected to be equal to that of bridges which were bonded to eliminated clusters. The present paper examines the validity of the above-described mechanism of the oxidation and the applicability of general lattice statistics to the analysis of the degradation characteristics.

EXPERIMENTAL

Acid washed Morwell brown coal was oxidized at 85 °C for 1 – 12 h in an aqueous solution of Na_2CO_3, into which atmospheric oxygen gas was continuously bubbled. Details of the experimental procedure were described elsewhere[7]. The oxidized coal obtained through the oxidation for X h is hereafter referred to as SX. The oxidized coals were analyzed by a CP/MAS ^{13}C-NMR, and the carbon type distributions of the individual samples were determined. Details of the measurements, peak assignment and curve resolution of spectra were reported previously[7]. The concentrations of carbonylic, carboxylic and phenolic groups were measured by means of oximation, ion exchange and acetylation, respectively. The samples were also subjected to exhaustive extraction with various single and mixed solvents at ambient temperature under ultrasonic irradiation. For the all samples, the mass fraction of solvent-extractable material was defined as that of material extracted with DMF that gave the greatest fractions among the solvents employed[7]. Molecular mass distribution of the extracts was measured by a laser desorption-ionization spectrometry (LD/MS) on a spectrometer (Japan Perseptive, model Voyager™ RP-DE). The spectra were observed in a linear mode under the following conditions: accelerating voltage; 25 kV, mass range; 50 – 100000, pressure; $1 - 2\cdot10^{-7}$ torr. Pulses of a nitrogen laser operating at 337 nm was used for the laser desorption.

RESULTS AND DISCUSSION

The structural analyses determined the fractions of different types of carbon found in the oxidized coals: f_{CO} (carbonylic carbon), f_{COOH} (carboxylic carbon), f_{OH} (phenolic carbon), $f_{a\text{-}e}$ (aromatic C bonded to ether), $f_{a\text{-}C}$ (aromatic C bonded to carbon), $f_{a\text{-}H}$ (protonated aromatic C), $f_{a\text{-}O}$ (aliphatic C bonded to O other than methoxy carbon), $f_{al\text{-}OCH3}$ (methoxy), $f_{al\text{-}\alpha CH2}$ (methylene or methin at α position to aromatic C), $f_{al\text{-}CH2}$ (methylene at β position), $f_{al\text{-}\alpha CH3}$ (methyl at α position) and $f_{al\text{-}rCH3}$ (methyl at remote position). These fractions are indicated in the unit of mol-C per 100-mol C in S0. The fractions of total aromatic and aliphatic carbons, referred to as f_a and f_{al}, respectively, are defined as

$$f_a = f_{a-e} + f_{a-OH} + f_{a-C} + f_{a-H}$$

$$f_{al} = f_{al-O} + f_{al-OCH3} + f_{al-\alpha CH2} + f_{al-CH2} + f_{al-\alpha CH3} + f_{al-rCH3} + f_{al-acids}$$

$f_{al\text{-}acids}$ is the fraction of aliphatic carbon contained in non-aromatic acids. $f_{a\text{-}e}$ was calculated by the difference between the fraction of oxygen-bonded aromatic carbon that was determined by the NMR and $f_{a\text{-}OH}$. Figure 2 shows f_a, f_{al} and f_{COOH} as a function of oxidation time. f_a decreases monotonously with time while f_{al} remains unchanged. It is also seen that f_{COOH} increases as the oxidation progresses. Here, the differences of f_a and f_{COOH} from those of S0 are defined as Δf_a and Δf_{COOH}, respectively. The figure also shows the change in the fraction of aromatic carbon bonded to bridges, $f_{a\text{-}b}$, which was calculated according to Solum et al.[8].

$$f_{a-b} = f_{a-C} + f_{a-e} - \left(f_{COOH} + f_{al-OCH3} + f_{al-rCH3} + f_{al-\alpha CH3}\right)$$

The decrease in f_{a-b} with time indicates the loss of bridges by the oxidation. The total amount of bridges is calculated from a simple stoichiometry.

$$N_b = f_{a-b}/2$$

The loss of bridges, ΔN_b, is here defined as

$$\Delta N_b = N_b \text{ (for S0)} - N_b \text{ (for SX)}$$

When aromatic clusters are eliminated by the oxidation of aromatic carbon involved in them, the amount of eliminated clusters (ΔN_c) is expected to have a linear relationship with the loss of aromatic carbon *leading to the elimination*, defined as Δf_a*. ΔN_c and Δf_a* are expressed in the units of mol-cluster/100 mol-C in S0 and mol-C/100 mol-C in S0, respectively. They are related as

$$\Delta N_c = \Delta f_a{}^* / n_a$$

where Δf_a* is the loss of aromatic carbon accompanied with the loss of an aromatic ring, and is a little smaller than the observed loss, Δf_a, due to the formation of a small amount of quinones that never contributes to the elimination of clusters. The calculation of Δf_a* was described in our previous report[7]. n_a is the average number of aromatic carbon atoms per cluster. The number can be estimated from the abundance of bridgehead carbon relative to total aromatic carbon[8]. As reported previously, for S0 – S12, f_{b-ah} was found to account for at most 4 % of f_a. Such appreciably small values of f_{a-bh} indicate that the assumption of monoaromatic rings, in other words, n_a is 6 mol-C/mol-cluster, is reasonable for the all samples.

Figure 3 shows ΔN_b and Δf_{COOH} as a function of ΔN_c. ΔN_b is seen to be in good agreement with Δf_{COOH} as expected by the proposed mechanism of the oxidation, although some deviations are seen. Also, ΔN_b and Δf_{COOH} can be related linearly with ΔN_c at a slope of about 2.2. This means that 2.2 bridges are lost when an aromatic cluster is eliminated by the oxidation, and hence that each of the lost clusters was bonded to the same number of bridges in average. Moreover, the linear relationship itself should be noted when the mechanism of the oxidation is considered. As illustrated in Figure 1, the elimination of a cluster accompanies the formation of carboxyl groups at the chain ends of the neighboring clusters. As we described in the previous paper[7], aromatic rings carrying carboxyls generally have oxidation reactivities orders-of-magnitude smaller than do those without carboxyls. Therefore the neighboring clusters may behave as inert ones after carboxyls are formed, while they also lose bridges initially connected to them. Thus, the elimination of clusters would occur non-randomly, producing deactivated clusters that accumulate as the oxidation progresses. Here, let us consider the degradation of a macromolecular network or lattice consisting of clusters and bridges, of which initial concentration of inter-cluster bridges is $n_{b,0}$ (= $2 \cdot N_{b,0}/N_{c,0}$). The degradation is supposed to be caused by the elimination of clusters (or sites). In the case of a degradation involving deactivation processes as described above, the average number of bridges bonded to a remaining 'reactive' cluster is independent of $N_c/N_{c,0}$, and equals to the initial bridge concentration, namely $n_{b,0}$. Then, when a cluster is eliminated, $n_{b,0}$ bridges are always lost, and the following relationship holds.

$$n_b = 2N_b/N_c = 2\left\{N_{b,0} - n_{b,0}\left(N_{c,0} - N_c\right)\right\}/N_c = n_{b,0}\left\{2\left(N_c/N_{c,0}\right) - 1\right\}/\left(N_c/N_{c,0}\right) \qquad (1)$$

where $N_c/N_{c,0}$ is the fraction of remaining clusters to that before degradation and is a measure of the extant of cluster elimination. Figure 4 shows the observed n_b as a function of $N_c/N_{c,0}$ together with lines drawn on the basis of Eq.(1) assuming $n_{b,0}$ = 2.23. The observed change of n_b is seen to be well explained by the equation, i.e., the non-random degradation. Eq.(1) can apply to any lattices having different dimensions, coordination numbers and bridge densities. Thus, the results shown in Figures 2-4 reveal that the changes in f_{COOH}, N_c and N_b are reasonably explained on the basis of the proposed oxidation mechanism, and are also quantitatively described by the assumption that the coal is a lattice with $n_{b,0}$ of 2.2, while other parameters such as the coordination number are so far unknown.

The above explanation of the change in n_b by Eq.(1) not only provides the initial bridge concentration but also allows us to analyze other characteristics of the degradation assuming that the coal is a lattice. Bethe pseudo lattices are statistical lattices, each of which has infinite number of sites and is defined by the coordination number (Z) and site occupation probability (p, $0 \le p \le 1$) that is the number fraction of occupied sites to the total number of sites. When two sites neighboring to each other are both occupied, they are recognized to be linked by a bridge. Another characteristic of Bethe lattices is that no loops are allowed in them. The absence of loops provides analytical solutions of states of the lattices by only giving the parameters, Z and p, and this is the reason why the coal is assumed to be a Bethe lattice in the models described below. For a Bethe lattice with Z and p, n_b is expressed as

$$n_b = Z \times p$$

When the degradation of the lattice occurs with a random site-elimination mechanism, a given probability p^* and corresponding bridge concentration n_b* are related as follows.

$$n_b^*/n_{b,0} = p^*/p_0 \qquad (2)$$

where p_0 is the site-occupation probability of the initial lattice with $n_{b,0} = Z \times p_0$. The lattice statistics can also provide the distribution of degree of polymerization. The possibility of that an occupied site belongs to m-mers, each of which consists of m sites and $(m-1)$ bridges, is given as

$$F_m\left(p^*\right) = mb_m p^{(m-1)}\left(1-p^*\right)^{\{m(Z-2)+2\}}$$

where mb_m is the total number of configurations possible for m-mers. $F_m(p^*)$ is essentially the same as the fraction of m-mer with regard to the occupied-sites. Figure 5 shows the fractions of finite-sized m-mers as a function of p^* for the Bethe lattice with $Z = 3$. $F_{i-j}(p^*)$ seen in the figure is defined as

$$F_{i-j}(p^*) = \sum_{m=i}^{m=j} F_m(p^*)$$

Further details of the Bethe lattice statistics are well described in literature[4-5], and are therefore not done here. Eq.(2) that gives the relationship between the changes in n_b^* and p^* is applicable to the description of Bethe lattice degradation only when the elimination of sites occurs randomly (Case-I). In another case (Case-II) that the elimination of a site accompanies the deactivation of the neighboring sites as seen in the present oxidation, the elimination of a site results in the loss of $n_{b,0}$ bridges. Then, n_b at a site occupation probability, p, is expressed as

$$n_b / n_{b,0} = \{1 - 2(p_0 - p)/p_0\} / (p/p_0) \qquad (3)$$

Eq.(3) is directly derived from Eq.(2), since $p/p_0 = N_c/N_{c,0}$. As shown in Figure 6, n_b in Case-II is smaller than n_b^* in Case-I when $p = p^*$. Essentially, degradation of lattice/network is brought about by the elimination of bridges, and in this sense, the extent of degradation could be evaluated on the basis of the decrease in the bridge concentration, *i.e.*, n_b. Considering the above, p can be converted into another probability, p^{**}, that gives n_b equivalent to n_b^*. p^{**} is then calculated as

$$p^{**} = p_0\{1 - 2(p_0 - p)/p_0\} / (p/p_0)$$

Thus, if the chemical network of the coal can be assumed to be a Bethe lattice, its degradation caused by the oxidation would be approximately described by a random degradation using p^{**}.

Here, a structural model of the coal are proposed and examined on the applicability to quantitative explanation of changes in the fraction of extractable material caused by the oxidation and molecular mass distribution of the material. The first model assumes the followings:

1. S0 consists of solvent extractable material and a fully developed network. The extractable material comprises of m-mers with m ranging from 1 – 40, while the network is described as a Bethe lattice with $p_0 = 1$ and thus $n_{b,0} = Z$.
2. The fractions of the network and extractable material in S0 are 0.85 and 0.15, respectively, which is based on the observed Y_{DMF} for S0, 0.15.
3. The concentration of bridges for the extractable material (referred to as $n^e_{b,0}$) is 1.8, which was determined by analyzing a CP/MAS ^{13}C-NMRspectrum of DMF extract from S0.
4. When a site is eliminated, the probability of that the site belongs to the network is 0.85. This is based on the assumption that the network and extractable material have equivalent reactivity to the oxidation.
5. The solvent extractable material, given as DMF extract, consists of molecules whose degree of polymerization ranges from 1 to 40. The basis of this assumption is mentioned below.

In addition to the above, the second assumption for the model A is also considered in the model B. Figure 7 compares calculated $F_{1\text{-}40}(p)$ as a function of p^{**}/p_0 with Y_{DMF}. It should be noted that $F_{1\text{-}40}(p)$ strongly depends on Z and also agrees well with Y_{DMF} at Z = 2.18. In the model B, the bridge concentration of S0, namely $n_{b,0}$ is given as

$$n_{b,0} = 0.85Z + 0.15n^e_{b,0}$$

and then $n_{b,0}$ is calculated as 2.1 using $Z = 2.2$. This value of $n_{b,0}$ is in good agreement with that determined from the results shown in Figure 5, i.e., 2.2. This is, however, not enough to demonstrate the validity of the model B. The predicted distribution of molecular mass or degree of polymerization of the solvent extractable material should also be in agreement with that observed. Figure 8 illustrates LD/MS spectra of DMF extracts from S0, S3, S6, S9 and S12. The spectra reveal that the features common among the extracts from different oxidized coals; that the molecular mass distributes widely over the range from 100 up to 8,000 and that compounds with molecular mass of around 300 are the most abundant. Moreover, the distribution seems not to vary significantly with the extent of the oxidation. The distribution of molecular mass could be converted into that of degree of polymerization, by giving the average molecular mass of the monomeric unit. The average molecular mass, M_m, was calculated as about 200 by considering the carbon content, n_a and f_a. The value of M_m means that the degree of polymerization of the extracts ranges from 1 to approximately 40. This is the basis of that $F_{1\text{-}40}(p)$ is considered in the above-described models. Figure 9 shows the molecular mass distribution predicted by the model B assuming $M_m = 200$. The calculated distribution is little sensitive to the probability p^{**} as seen for the mass spectra of DMF extracts. It should also be noted that the distribution agrees well with that observed, although the quantitative comparison of them is difficult at present, due to that the molecular mass per monomeric unit itself should more or less distribute due to variety of chemical structure of peripherals and bridges.

CONCLUSIONS

The oxidation depolymerizes the coal by eliminating aromatic clusters. When a cluster is eliminated, the bridges that have been connected to the cluster are converted into peripheral chains of the neighboring clusters, and carboxyl groups are formed at the ends of the peripherals. The elimination of the cluster also accompanies the deactivation of the neighboring clusters due to the formed carboxyls. The mechanism of the oxidation allows us to describe the following relationships;

$\Delta f_{COOH} \approx \Delta N_b$ and $\Delta f_{COOH} / \Delta N_c \approx \Delta N_b / \Delta N_c = n_{b,0} \approx 2.2$

The model B, which assumes that coal is a mixture of a fully developed Bethe lattice with $Z = 2.2$ and $p_0 = 1$, and solvent extractable material with $n^{e}_{b,0} = 1.8$, reasonably predicts the observed increase in the fraction of DMF extractable material. The model can also predict the extract's molecular mass distribution semi-quantitatively as a function of p^{**}, the corrected.

ACKNOWLEDGMENT

This work was supported by a "Research for the Future Project" (Coordinator; Prof. M. Iino, Tohoku University) grant from The Japan Society for the Promotion of Science (JSPS), through The 148th Committee on Coal Utilization Technology.

REFERENCES

1. Niksa, S.; Kerstein, A.R. *Fuel* 1987, **66**, 1389.
2. Grant, D.M.; Pugmire, R.J.; Fletcher, T.H.; Kerstein, A.R. *Energy Fuels* 1989, **3**, 175.
3. Fletcher, T.H.; Kerstein, A.R.; Pugmire, R.J.; Solum, M.S.; Grant, D.M. *Energy Fuels* 1992, **6**, 414.
4. Stauffer, D. "*Introduction to Percolation Theory*" 1985, Tailor & Francis, London.
5. Stockmayer, W.H. *J. Chem. Phys.* 1943, **11**, 45
6. Hayashi, J.-i.; Matsuo, Y.; Kusakabe, K.; Morooka, S. *Energy Fuels* 1997, **11**, 284.
7. J.-i. Hayashi, Aizawa, S.; Kumagai, H.; Chiba, T.; Yoshida, T.; Morooka, S. *Energy Fuels* 1999, **13**, 69.
8. Solum, M.S.; Pugmire, R.J.; Grant, D.M. Energy Fuels 1989, 3, 187.

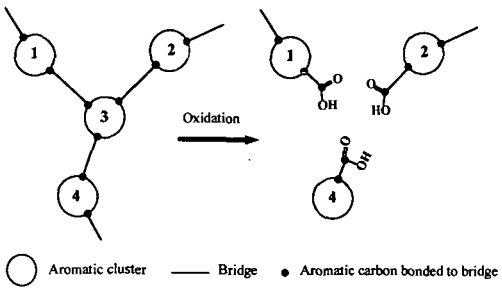

Figure 1. Elimination of aromatic cluster and conversion of inter-cluster bridge into carboxyl group by oxidation.

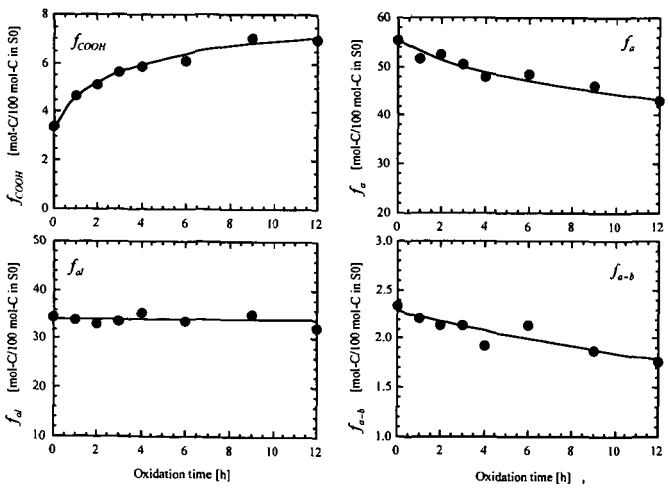

Figure 2. Fraction of different types of carbon, f_a, f_{al}, f_{COOH} and f_{a-b}, as a function of oxidation time.

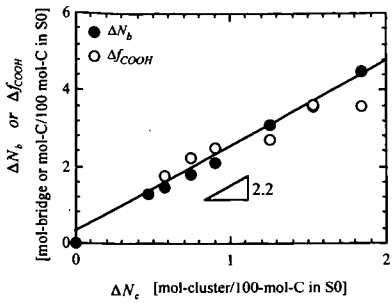

Figure 3. Δf_{COOH} and ΔN_b as a function of loss of aromatic clusters, ΔN_c.

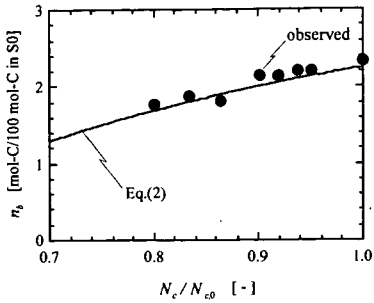

Figure 4. Observed and calculated n_b as a function of $N_c/N_{c,0}$.

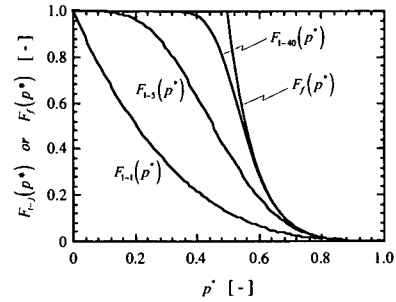

Figure 5. Fraction of site belonging to m-mers as a function of site-occupation probability, p^*.

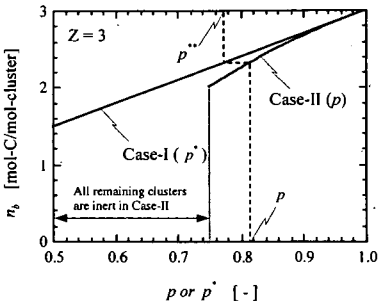

Figure 6. n_b^* as a function of p^* in random degradation (Case I), n_b as a function of p in non-random degradation (Case II) and p^{**} calculated from relationship between n_b^* and n_b.

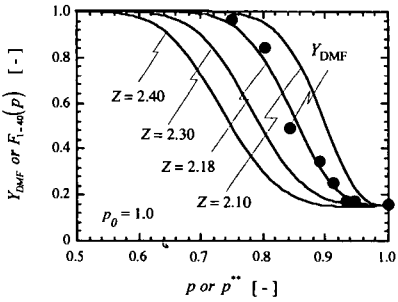

Figure 7. Fraction of DMF-extractable material, Y_{DMF}, as a function of normalized probability p^{**}/p_0 and its comparison with $F_{1\text{-}40}(p)$ predicted by model-B assuming different values of Z.

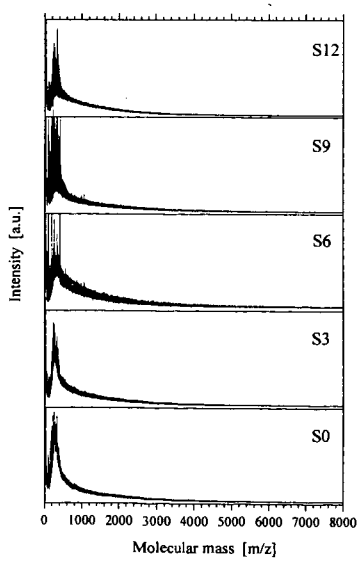

Figure 8. MALDI spectra of DMF extracts.

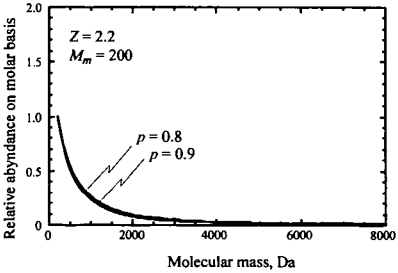

Figure 9. Molecular mass distribution predicted by model assuming $M_m = 200$.

COAL DEGRADATION THROUGH EXTRACTION AND DEPOLYMERIZATION IN A FLOWING SOLVENT UNDER PRESSURE

Kouichi Miura*, Kazuhiro Mae, Hwang Yoo Seock, Ryuichi Ashida, and Masato Morimoto
Department of Chemical Engineering, Kyoto University, Kyoto 606-8501

INTRODUCTION

Solubilization and/or depolymerization are the initial steps of coal liquefaction, coking, or pyrolysis. Most of the solubilization/depolymerization experiments performed at rather high temperature in relation to coal liquefaction utilized a batch reactor, the so-called autoclave, where the interaction between the solubilized small molecules and the insoluble macromolecules can not be neglected. Furthermore, it is almost impossible to know the actual extraction yield at a high temperature using autoclave, because we can not separate the fraction which is soluble at the high temperature but is precipated at room temperature from the residue. The solid recovered at room temperature after experiments is the mixture of the residue and the precipitated solid. Blessing and Ross[1] used a specially designed autoclave which is equipped with a basket assembly. Solvent can penetrate the basket through the glass frits fitted at the top and the bottom of the basket. Coal samples were placed in the basket assembly, and the extract was expected to come out from the basket through the glass frits. Unfortunately this trial was unsuccessful, because the diffusion rate of the deposit through the frit was very small. Flow reactors have been used by several investigators for examining the solubilization/depolymerization behavior of coal at a rather high temperature. Aida et al.[2] tried to extract coal in a flowing stream of solvent with an UV spectrometer as a detector. This enabled them to monitor the products continuously, but detailed analysis of the products has not been performed because of the experimental difficulty. Kandiyoti et al.[3-6] have heated coal up to 450 °C in a flowing stream of solvent to avoid the secondary reaction. They have examined the effect of operating conditions in detail. Their interest was, however, the hydrogenation reaction above 400 °C, because their main research target was to examine the coal liquefaction mechanism.

We have recently found that some bituminous coals can be extracted up to 75 % in a flowing non-polar solvent at 350 °C without appreciable decomposition.[7] At room temperature about a half of the extract were still soluble in the solvent and the rest half precipitated as solid. Both the soluble fraction and the precipitated solid were almost free from mineral matters, suggesting the possibility of preparing clean fuel from coal in high yield.

In this paper the solubilization/depolymerization experiments of eight Argonne premium coals were performed at 350 °C in a flow type reactor, where coal samples were heated in a flowing stream of tetralin. The purposes of this work were to examine the coal structure through detailed analyses of the extract and the residue, and to examine the possibility of preparing clean fuels and/or raw materials for the subsequent conversion. The possibility to decompose further the soluble, the precipitated solid and the residue recovered from Pittsburgh #8 coal was also examined.

EXPERIMENTAL

Coal Samples. Eight coals of the Argonne premium coals were used in this work. The analyses of these coal samples are given in **Table 1**.

Experimental Procedure for extraction/depolymerization. **Figure 1** shows a schematic diagram of the apparatus used for extraction and/or depolymerization. 100 to 200 mg of coal samples were placed between two filters (11.2 mm OD and 0.5 mm opening) in a reactor made of Swagelok. Tetralin was supplied continuously using a high pressure pump at the flow rate of 1 ml/min. The pressure was regulated using a pressure regulating valve (TESCOM) at 10 MPa. The reactor was heated at the rate of 5 K/min to 350 °C where it was kept for 0 to 90 min, then it was cooled immediately by a sufficient amount of water to terminate the solubilization and/or depolymerization. The coal fraction extracted and/or depolymerized at the reactor temperature became soluble in the solvent and came out from the reactor with the flowing solvent, but a part of the solubilized components precipitated as solids when the solvent flow was cooled to room temperature. The solid thus precipitated, called "deposit" in this paper, was collected by 3 filters (20, 10, and 2 μm openings) placed in series just before the pressure regulating valve. The deposit which passed these filters were collected in a separation trap with the soluble components at room temperature. The components soluble at room temperature are called "soluble" here. Product gas was collected in a gas bag, and analyzed using a gas chromatograph for the components smaller than C6 hydrocarbons in molecular weight. Thus each coal sample was separated into the residue that is not extracted or depolymerized, the deposit, the soluble, and gaseous components. The weights of the residue and the deposit were directly measured after drying them in vacuo at 70 °C. The weight of gaseous components was calculated from the analysis using the gas chromatograph. The rest of the product was regarded as the soluble.

Decomposition of soluble and deposit. The deposit prepared from PITT was served to the flash hydro-pyrolysis and the pyrolysis in a liquid tetralin to examine the possibility to decompose the deposit further. The flash hydropyrolysis was performed using a small scale of batch reactor at 700, 800, and 900 °C at the residence time of 60 s. The decomposition of the soluble, the deposit and the residue in liquid tetralin was performed using a small batch reactor (6 ml in volume). About 50 mg of sample was placed with 5 ml of tetralin in the batch reactor. The whole reactor was immersed in a sand bath regulated at a temperatures between 380 to 450 °C, and kept there for 60 min. The products were separated into hexane-soluble fraction (HS), hexane-insoluble and tetralin soluble fraction (Tets-HI), residue and gas components by a similar procedure presented above.

Analyses of the products. The soluble, the deposit and the residue were characterized through various analyses. Ultimate analysis and SPE/MAS ^{13}C solid NMR analysis[8] of the deposit and the residue were performed using a CHN corder (Yanaco, CHN-500) and a NMR spectrometer (Chemagnetics, CMX-300), respectively. The gel permeation chromatography (GPC) was used to estimate the molecular weight distribution of the deposit, because the more than 95 % of deposit could be solubilized in dimethylformamide (DMF). The packed column used is a Shim-pack GPC-8025 (Shimadzu), and an eluent DMF was supplied at the flow rate of 0.5 ml/min. The matrix-assisted laser desorption/ionization time-of-flight mass spectrometry (MALDI-TOFMS; Shimadzu/Kratos KOMPACT-MALDI-II) was used to estimate the molecular weight distributions of the soluble, the deposit, the residue, and the raw coal.

RESULTS AND DISCUSSION

Changes in yields of soluble and deposit with increasing temperature and extraction time. **Figure 2** shows the changes in the yields of the soluble, the deposit, and the residue with increasing temperature and extraction time for IL coal. The soluble yield increased with the increase of temperature, reached 25% at 350 °C, and finally reached more than 30 % at the holding time (t_f) of 30 min at 350°C. On the other hand, the deposit yield was very small up to 350 °C while temperature is increased, but it increased gradually with the increase of holding time at 350°C and finally reached about 40% at t_f = 60 min or so. The increase of the soluble yield is judged to be brought about through the relaxation of coal structure upon heating in solvent, because most of the soluble was produced below 300 °C, in other words, the soluble was not produced through decomposition reaction. By keeping the coal for extended time at 350°C relatively large molecule components that are soluble in tetralin at 350 °C gradually came out from the coal particles. It would be because the intraparticle diffusion rate of the deposit is not so fast.

Figure 3 compares the ultimate product yields at 350 °C, which were arbitrarily defined as the yields at t_f = 60 min, for eight Argonne premium coals. The yields of soluble and deposit for bituminous coals, IL, PITT, and UF coals, were very large. The extrct yields for these coals are as follows: 80 % (soluble: 41 %, deposit: 39 %) for UF, 67 % (soluble: 29 %, deposit: 38 %) for PITT, and 63 % (soluble: 27 %, deposit: 36 %) for IL. Surprizingly, 80 % of UF coal were extracted at 350 °C. For the lowest rank coal, ND, the deposit yield was very small and appreciable amount of gaseous components were produced. Both the soluble and the deposit yields were small for the highest rank coal, POC. These results indicate that decomposition reaction occurred for the lowest rank coal ND, but little decomposition reaction occurred for the other higher rank coals. Therefore, most of the soluble and the deposit for the higher rank coals are judged to be relatively small molecule components existent in the original coal. The small molecules could come out because the macromolecular network of coal was relaxed through the heat treatment in the solvent.

These results suggest that the structure of the bituminous coals used in this work is rather close to the model B of Nishioka (physically associated model).[9,10] The soluble and the deposit are assumed to be physically associated each other and/or with the residue in the raw coal.

Ultimate analysis and ^{13}C NMR analysis. The above discussion clarified that 50 to 80 % of coal can be extracted with little decomposition by tetralin at 350 °C for bituminous coals. Then the solid products, the deposit and the residue, were characterized by various analyses to examine the change accompanying the extraction. **Table 2** compares the ultimate analysis and ash content of the raw coal, the residue, and the deposit prepared at t_f= 60 min at 350°C for PITT and IL coals. Since the soluble concentration was very small and hence could not be subjected to the analyses, the numbers for the soluble in Table 2 were calculated by the proportional allotment from the data for the raw coal, the residue and the deposit using their yields given in Fig. 3. Although the ultimate analyses were not significantly different among the raw coal, the deposit, and the residue, the hydrogen content and the atomic H/C ratio of the residue were appreciably smaller than those of the raw coal and the deposit. As a result of this difference, the atomic H/C ratio of the soluble was the highest. This indicates that the soluble is richer in hydrogen than the other fractions. The most distinguishing result is that the soluble and the deposit contain little ash, which means most of ash remains in the residue. This presents the possibility to prepare clean fuel or clean raw materials in a high yield from bituminous coals by simple extraction.

Figure 4 compares the ^{13}C NMR spectra among the raw coal, the residue, and the deposit prepared at t_f= 60 min at 350°C for PITT. The carbon distributions estimated from these spectra are given in **Table 3**. Again the carbon distribution for the soluble was calculated by the proportional allotment from the distributions for the raw coal, the residue, and the deposit by assuming that no decomposition reaction occurred during the extraction. Although the distributions for the raw coal, the residue, and the deposit are rather close, the proportions of methyl groups ($-CH_3$) and methylene bridge ($-CH_2-$) are smaller and the proportions of the bridgehead carbon (Bridgehead) are larger in the deposit and the residue than in the raw coal. These differences reflected on the the difference in the values of the aromaticity index, f_a, of the raw coal, the residue, and the deposit: they are 0.733, 0.785 and 0.782, respectively. The calculated carbon distribution for the soluble shows that the soluble is rich in methyl groups and methylene bridge and the the proportions of the bridgehead carbon is small, resulting in the small f_a value of 0.650. These results are consistent with the ultimate analyses shown in Table 2.

Above results suggest that soluble is the fraction consisting of small and more aliphatic molecules in the original coal, and that the average chemical structure of the raw coal, the residue, and the deposit are very close. This circumstantially supports the above discussion concluding that bituminous coals were extracted with little

decomposition below 350 °C. Then the detailed analyses of the soluble, the deposit, and the residue will give us a more realistic picture of bituminous coals.

Molecular weight distribution of soluble, deposit and residue. We have clarified that the molecular weight distribution (MWD) can be well estimated by the MALSI-TOFMS method for molecules less than 5000 in molecular weight by comparing the MALDI and the GPC measurements for a deposit solubilized in dimethylformamide (DMF).[7] Then **Figure 5** compares the MWDS measured by the MALSI-TOFMS method for the soluble, the deposit and the residue prepared from PITT at t_f= 60 min at 350 °C with the MWD of the raw PITT coal. The MWDs for the raw coal, the residue and the deposit are all bimodal having peaks at M_W = ca. 300 and ca. 2200. The M_W of the peak position for the larger molecules in the deposit seems to be slightly smaller than that in the residue. On the other hand, the soluble consists of only small molecules of less than 600 in M_W, and the peak position almost coincides with the peaks of smaller M_W in the raw coal, the residue and the deposit. These results again support the model B of Nishioka for the structure of PITT. The deposit and the residue still contain the small molecule components which could not be dissociated at 350 °C.

Decomposition of soluble, deposit and residue in tetralin. The soluble, the deposit and the residue prepared from PITT were heated in tetralin at 380 to 450 °C in the batch reactor to decompose them further. **Figure 6** shows the product distribution through the decomposition for the deposit. The yields of oil (HS) and TetS-HI fraction increased with increasing temperature up to 420 °C monotonously and the sum of the two yields reached 78 wt %. By further increasing the temperature up to 450 °C a part of the TetS-HI fraction were decomposed into oil fraction, and the yields of oil and TetS-HI reached 56 wt % and 22wt%, respectively. **Figure** 7 compares the MWDs of the products at 450 °C, which were measured by the MALDI-TOFMS method. Comparing with the MWDs of the soluble and the deposit, the oil fraction consists of the components smaller than these in the soluble, the components in TetS-HI fraction are similar to those in the soluble, and the TetI fraction consists of the components smaller than those in the deposit. These results show that the deposit can be further decomposed into small molecule compounds just by heating it in tetralin at 450 °C. **Figure 8** enlarges the MWD of the oil fraction so as to identify the components more easily involved. Most of the oil fraction consists of the components of M_w = 250 to 350. These components were judged to be dimers of two aromatic ring components from the ^{13}C NMR analysis.

Figure 9 compares the product distributions through the decomposition of the soluble, the deposit and the residue at 450 °C. Since 72 wt % of the soluble consisted of oil, the oil yield increased by only 9 % for the soluble through the decomposition. A small amount of gaseous components (CH_4 and CO are main components) were simultaneously produced. This indicates that the soluble fraction is hardly decomposed at 450 °C. The residue was converted into 32 wt % of oil, 1 wt% of gaseous components and 67wt % of TetI and residue. Figure 11 shows that more than 52 wt % of PITT coal (d.a.f. basis) are converted into oil fraction through the combination of extraction at 350 °C and the decomposition at 450 °C in tetralin. This is very attractive as a coal conversion process, since this conversion process does not require expensive gaseous hydrogen. These results with the detailed analyses of the soluble, the deposit, and the residue given above clearly show that the unit components composing the soluble, the deposit, and the residue are similar.

Flash hydropyrolysis of deposit. The above results and discussion showed that the unit structures of the deposit produced from PITT coal are two aromatic ring components. Thent the flash hydropyrolysis of the deposit was performed to examine the possibility to convert most of the deposit into two aromatic ring components such as naphthalene, methylnaphthalenes, etc. **Figure 10** shows the effect of temperature on the product yields for the flash hydropyrolysis of the deposit. Main products were, unexpectedly, CH_4 and benzene, and the total conversion to volatiles was less than 50 % even at 900 °C. Flash hydropyrolysis over 700 °C seems to be too severe to preferentially obtain two aromatic ring components. We are now examining the possibility of milder hydropyrolysis conditions for this purpose.

CONCLUSION

Eight Argonne premium coals were extracted in a flowing stream of tetralin under 10 MPa at 350 °C. Bituminous coals, Illinois #6, Pittsburgh #8, and Upper Freeport, were extracted by 65 to 80% at 350°C, and the extract was divided into about 30 to 40 % of soluble (soluble) at room temperature and 25 to 40% of precipitated solid (deposit) at room temperature. The contribution of the decomposition reaction on the extraction yield is judged to be neglected for these coals. The extraction yields of lower rank coals, Beulah-Zap was not so large as those for the bituminous coals. At 350°C appreciable gas formation was observed, indicating that the decomposition reaction as well as the extraction proceed for these coals. The extraction yield of the highest rank coal, Pocahontas, was also small reflecting its structure. Since both the soluble and the deposit were almost ash free, they will be well utilized as a starting material of subsequent upgrading processes such as liquefaction, pyrolysis, and coking.

The treatment of the extraction products prepared from PITT coal were performed in tetralin at 380 to 450 °C to examine the possibility to decompose the fractions under mild conditions. Through the extraction and the heat treatment at 450 °C Pittsburgh #8 coal was converted into 52 wt % of oil (hexane soluble). This is very attractive as a coal conversion process, since this conversion process does not require expensive gaseous hydrogen. The detailed analyses of the extraction and the decomposition products clearly showed the structure of PITT coal is represented by the model B of Nishioka (physically associated model).

ACKNOWLEDGEMENT

This work was supported by "Research for the Future" project of the Japan Society for the Promotion of Science (JSPS) through the 148 committee on coal utilization technology of JSPS. The authors thank to Prof.

M. Nomura of Osaka University for measuring ^{13}C NMR spectra in Fig. 4.

REFERENCES

1. Blessing, J.E.; Ross, D.S., *Organic Chemistry of Coal, ACS Symposium Series 71*, Larsen, J., Ed., 1978, pp 171-185.
2. Aida, T.; Slomka, B.; Squires, T.G. *Proc. the 25th Conf. Coal. Sci.* (Japanese), 175-178, 1988 (Tokyo).
3. Gibbins, J. R.; Kandiyoti, R., *Fuel* **1991**, 70, 909-915.
4. Zhang, S.-F.; Xu, B.; Moore, S.A. ; Herod, A.A. ; Kandiyoti, R., *Fuel* **1996**, 75, 597-605.
5. Zhang, S.-F.; Xu, B.; Moore, S.A.; Herod, A.A.; Kimber, G.M.; Dugwell, D.R.; Kandiyoti, R., *Fuel* **1996**, 75, 1557-1567.
6. Zhang, S.-F.; Xu, B.; Moore, S.A.; Herod, A.A.; Kandiyoti, R., *Energy Fuels* **1996**, 10, 733-742.
7. Miura, K.; Shimada, M.; Mae, K., *1998 International Pittsburgh Coal Conf.*, Paper No. 30-1.
8. Artok, L.; Schobert, H. H.; Nomura, M.; Erbatur, O.; Kidena, K., *Energy Fuels* **1998**, *12*, 1200-1211
9. Nishioka, M., *Fuel* **1992**, 71, 941-948.
10. Nishioka, M., *Fuel* **1993**, 71, 1719-1724

Table 1. Ultimate and proximate analyses of coals used [wt%]

Coal	Ultimate analysis [d.a.f.] C	H	N	O(diff)	Prox. analysis [d.b.] FC	VM	Ash
Beulah-Zap (ND)	72.9	4.8	1.2	20.1	45.3	44.9	9.7
Wyodak (WY)	75.0	5.4	1.1	18.5	46.5	44.7	8.8
Illinois#6 (IL)	77.6	5.0	1.4	16.0	44.4	40.0	15.4
Blind Canyon (UT)	80.7	5.8	1.6	11.9	49.5	45.8	4.7
Lewinston-Stockton (ST)	82.5	5.3	1.6	10.6	49.9	30.1	19.8
Pittsburg#8 (PITT)	83.2	5.3	1.6	9.9	52.9	37.8	9.3
UpperFreeport (UF)	85.5	4.7	1.6	8.2	59.3	27.4	13.1
Pocahontas (POC)	91.0	4.4	1.3	3.3	76.6	18.6	4.8

Table 2. Analyses of the deposit and the residue produced from PITT.

	Ultimate analysis [wt%, daf] C	H	N	O(diff)	Ash [wt%]	Atomic ratio[-] H/C	O/C
PITT							
Raw	80.6	5.4	1.8	12.2	7.3	0.81	0.11
Residue	80.8	4.8	2.0	12.4	21.3	0.71	0.12
Deposit	81.4	5.4	2.2	11.0	0.8	0.80	0.10
Soluble (Calculated)	79.8	5.9	1.3	12.4	=0	0.89	0.12
IL							
Raw	77.6	5.0	1.4	16.0	15.5	0.77	0.15
Residue	77.4	4.6	1.5	16.6	32.1	0.71	0.16
Deposit	79.2	5.3	1.8	13.7	0.1	0.80	0.10
Soluble (Calculated)	75.7	5.1	0.7	18.2	0.3	0.81	0.18

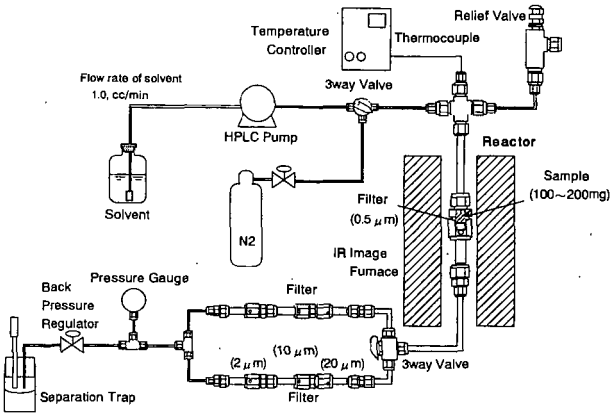

Figure 1. Schematic of experimental apparatus used for extraction/depolymerization in a flowing solvent.

Table 3. Carbon distribution in the raw coal, the residue, and the deposit prepared at 350 °C (t_f=60 min) for PITT.

Carbon type	Raw Coal	Residue	Deposit	Soluble (Calculated)
Aliphatic carbon				
$-CH_3$	0.069	0.047	0.049	0.103
$-CH_2-$	0.168	0.154	0.158	0.188
$-OCH_3$	0.013	0.008	0.010	0.020
C-O-C, R-OH	0.017	0.006	0.001	0.039
Aromatic carbon				
Ar-H	0.328	0.336	0.323	0.325
Bridgehead	0.299	0.336	0.337	0.238
Ar-OH, -OCH	0.092	0.105	0.120	0.054
-COOH	0.014	0.008	0.002	0.028
Aromaticity index, f_a	0.733	0.785	0.782	0.650

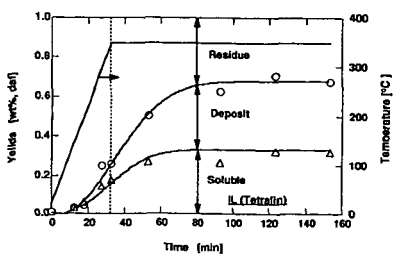

Figure 2. Change in the yields of soluble, deposit and residue with the increase of the holding time at 350 °C for IL.

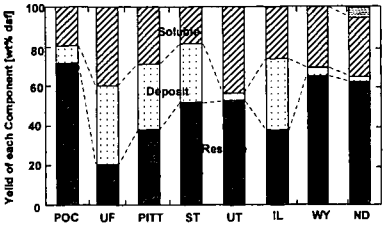

Figure 3. Yields of soluble, deposit and residue for Argonne premium coals (350 °C, t_f = 60 min).

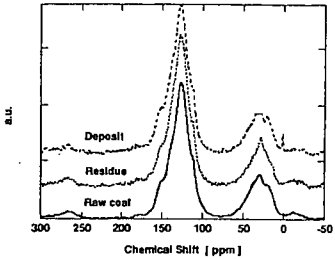

Figure 4. ^{13}C NMR spectra for the raw coal, and the deposit and the residue prepared at t_f = 60 min at 350 °C for PITT.

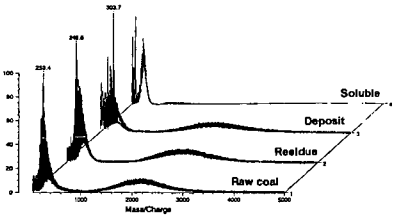

Figure 5 MWDs of the raw coal, and the residue and the deposit prepared at t_f = 60 min at 350 °C for PITT (MALDI-TOFMS).

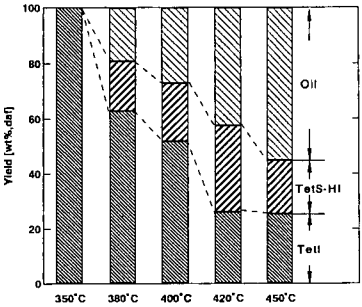

Figure 6. Product distributions through the decomposition of the deposit at different temperatures (PITT).

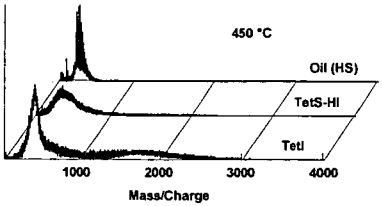

Figure 7. Comparison of the MWDs of the decomposition products from the deposit at 450 °C (PITT).

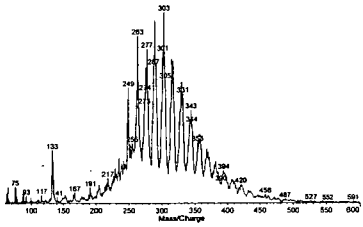

Figure 8. MWD of the oil fraction produced by the decomposition of the deposit at 450 °C (PITT).

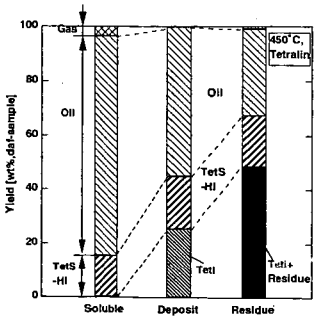

Figure 9. Product distributions through the decomposition of the soluble, the deposit and the residue at 450 °C (PITT).

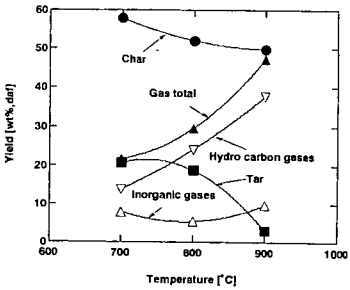

Figure 10. Effect of temperature on the product yields for the flash hydopyrolysis of the deposit (PITT).

HYDROGEN TRANSFER BETWEEN COAL AND TRITIATED ORGANIC SOLVENT

Atsushi Ishihara, I Putu Sutrisna, Masaru Saito, Weihua Qian and Toshiaki Kabe
Department of Applied Chemistry, Tokyo University of Agriculture and Technology, 2-24-16 Nakacho, Koganei, Tokyo 184-0012, JAPAN.

Keywords: hydrogen transfer, coal, tritiated tetralin

INTRODUCTION

To develop coal conversion techniques into useful fuels and chemicals by thermolysis and hydrogenation, it is important to elucidate the coal structure.[1,2] Although coal has a complex structure which includes various aromatics and functional groups, it can be considered that the reactivities of hydrogen in coal could reflect the coal structure since each hydrogen in aromatics, aliphatics, functional groups with heteroatoms etc. has the different reactivities. Therefore, the determination of reactivities of hydrogen in coal will provide significant information for coal structure.

Useful methods to measure hydrogen in coal are to utilize isotopes such as deuterium and tritium tracers.[3-11] A deuterium tracer was effective to trace reactive sites in coal and coal model compounds, however, there were few examples which enable quantitative analysis of the hydrogen mobility in coal because of the poor solubility of coal products and the difficulty of quantification of the deuterium tracer.[3-7] In contrast, we have reported that tritium tracer techniques were effective to trace quantitatively hydrogen in the coal liquefaction.[8-11] In these works, it was shown that the quantitative analysis of hydrogen transfer in coal could be given through the hydrogen exchange reactions among coal, gas phase and solvent as well as hydrogen addition. However, the method under coal liquefaction conditions includes destruction of the original structure of coal. In the course of our study, we were interested in the direct non-destructive determination of hydrogen in coal with its original form. Recently, we have reported that the tritium tracer methods are effective to determine the amount of hydrogen in the functional group of coal and examine the reactivities of hydrogen in coal through the reaction of coal with tritiated water and gaseous hydrogen in a pulse flow reactor or a batch reactor.[12-14]

In this study, we investigate the hydrogen transfer between coal and tritiated organic solvent to estimate the reactivity of hydrogen in coal. A hydrogen donor solvent tetralin was tritiated with tritiated water. To avoid significant destruction of the coal structure, reaction was performed in the range 200-300 °C below usual coal liquefaction conditions. After the reaction of coal with tritiated tetralin, the reaction of the tritiated coal and water was carried out to remove tritium in functional groups and to obtain the information for the position of hydrogen exchanged in coal.

EXPERIMENTAL

Reaction of Coal with Tritiated Tetralin

Four kinds of Argonne Premium Coal Samples (Beulah-Zap (ND), Illinois No. 6 (IL), Upper Freeport (UF), and Pocahontas #3 (POC)) were obtained in 5 g of ampules (< 100 mesh). The samples of Wandoan coal (WA) were ground to -150 mesh particles. Coal samples were dried for 2 h at 110 °C under 10^{-1} Torr. The analytical data of coals are shown in Table 1. Coal rank increases in the order ND<WA<IL<UF<POC and the oxygen content decreases in the same order. Tritiated tetralin was prepared by modifying the reported method.[15] Tritiated water (2g, 10^8 dpm/g), tetralin (1.2g), and sodium carbonate (0.005g) were added into a stainless tube reactor. After argon purge, the reactor was kept for 1 h at 420 °C under supercritical condition of water. After separation of tritiated water, tritiated tetralin was diluted to about 10^6 dpm/g. Coal (0.5 g) and tritiated tetralin (0.5 g, 10^6 dpm/g) was packed into a stainless tube reactor (6 mL). After the reactor was purged with argon, the reactions were performed under the conditions, 200-300 °C and 5-360 min. After the reaction, coal and tetralin were separated under vacuum at 200 °C for 2 h and the tritiated coal was washed with n-hexane, dried and oxidized by an automatic sample combustion system (Aloka ADS-113R) into tritiated water to measure its radioactivity. Every tetralin sample was dissolved into a scintillator solvent (Instafluor, Packard Japan Co. Ltd.) and measured with a liquid scintillation counter (Beckman LS 6500). The tetralin sample was also analyzed by gas chromatography equipped with FID

(Shimadzu GC-14A).

Procedure of Hydrogen Exchange Reaction between Tritiated Coal and Water.
In order to predict locations of exchangeable hydrogen in coal, the hydrogen exchange reactions of coal that reacted with tritiated tetralin, i.e., tritiated coal, with water were performed. The tritiated coal and water were added into a glass reactor. The reactor was immersed into an oil bath with stirring. The reaction was performed at 100 °C for 24 h. After the reaction, suction filtration was performed and tritiated coal was washed with hot water. Further, the separated coal was dried under vacuum (< 10^{-1} Torr) at 120 °C for 1 h. After the coal was dried, it was oxidized by a method similar to the above using the combustion of coal.

Calculation of Hydrogen Transfer Ratio.
Hydrogen transfer includes both hydrogen addition and hydrogen exchange. The Hydrogen Transfer Ratio (HTR) estimated in this paper means the ratio of the amount of hydrogen transferred into coal (H_{tr}) to the total amount of hydrogen in an original coal (H_{coal}). HTR between coal and tetralin was calculated on the basis of eq 1:

$$HTR = H_{tr} / H_{coal} \quad (1)$$

H_{coal} was calculated with the analytical data presented in Table 1. The amount of hydrogen transferred from tetralin into coal (H_{tr}) was calculated on the basis of eq 2:

$$R_{coal} / H_{tr} = R_{tet} / H_{tet}\,; \quad H_{tr} = H_{tet} \cdot R_{coal} / R_{tet} \quad (2)$$

H_{tet} is the amount of hydrogen contained in tetralin and R_{tet} is the radioactivity of tritium contained in tetralin after the reaction. In eq 2, it was assumed that the hydrogen transfer reaction between tetralin and coal is at equilibrium. Thus after the reaction, the ratio of the radioactivity in coal to the amount of the hydrogen transferred in coal (R_{coal} / H_{tr}) is equal to the ratio of the radioactivity in tetralin to the amount of hydrogen in tetralin after the reaction.

RESULTS AND DISCUSSION

Figure 1 shows the change in hydrogen transfer ratio (HTR) of coal with reaction time at 300 °C. Total HTR increased with reaction time and reached constant value at 180 min. At this time, it can be considered that hydrogen transfer reaction has reached the equilibrium state. After hydrogen transfer reaction, the hydrogen exchange between the tritiated coal sample and water was performed to remove tritium in the functional group of coal and know the extent of hydrogen exchange of functional group in the reaction of coal with tritiated tetralin. As shown in Figure 1, HTR corresponding to the hydrogen exchange between hydrogen in functional group of coal and tetralin increased with reaction time similarly and reached the constant value at 180 min.

Figure 2 shows the change in HTR of coal with reaction temperature at 180 min. Although HTR was observed for each coal at 200 or 250 °C, this may be due to the sorption of tetralin molecule into coal as well as the hydrogen exchange. HTR remarkably increased in most of coals with increasing temperature from 250 °C to 300 °C, while HTR for POC coal increased only slightly. Total HTRs for all coals and HTRs corresponding to hydrogen exchange of hydrogen of functional group in coal with tritiated tetralin are listed in Table 2. The result shows that at lower temperature, 200 and 250 °C, hydrogen exchanges between hydrogen in functional group and tetralin were very low. These results were significantly different from those for the reaction of coal with tritiated gaseous hydrogen, where most of hydrogen in functional groups exchanged with tritiated gaseous hydrogen at the same lower temperature in the presence of catalyst.[14] However, HTR for functional group of coal with tritiated tetralin also remarkably increased with a rise from 250 °C to 300 °C.

Figure 3 shows the change in tetralin conversion to naphthalene with temperature at 180 min. The trend of increase in tetralin conversion with temperature was similar to that in HTR. In the cases of lower rank coals, ND and WA, tetralin conversion increased with increasing temperature from 200 to 300 °C. In the cases of higher rank coals, IL, UF and POC, tetralin conversions were very low at temperatures 200 and 250 °C. However, those remarkably increased with a rise in temperature from 250 to 300 °C. The result suggests that, since lower rank coals, ND and WA, generated larger amount of radical species even at lower temperature, tetralin conversion

to naphthalene, that is hydrogen addition into coal was enhanced. For higher rank coals, however, it seems that a large amount of radicals were generated at 300 °C. Tetralin conversion for IL coal was highest at 300 °C and this may be due to the catalysis by a larger amount of pyrite included in IL coal.

In Figure 4, total HTR of coal with tritiated tetralin and HTR corresponding to hydrogen exchange for functional group in the reaction with tritiated tetralin at 300 °C and 360 min were compared with HTR corresponding to hydrogen exchange between coal and tritiated water at 100 °C which was previously reported. Except for ND coal, HTR corresponding to hydrogen exchange for functional group of coal in the reaction with tetralin was very similar to HTR of functional group between coal and tritiated water. The results shows that at 300 °C most of hydrogen in functional group of coal exchanged with tritiated tetralin. In the reaction of coal with tritiated tetralin, HTR decreased in the order IL>UF>WA>ND>POC which was different from that of the reaction of coal with tritiated water where HTR decreased with increasing coal rank.[14] There might be the decomposition of coal structure in lower rank coals at 300 °C which seems to affect the hydrogen transfer.

CONCLUSIONS

Hydrogen transfer reaction between coal and tritiated tetralin significantly proceeded at 300 °C and the amount of hydrogen transferred increased in the order POC<ND<WA<UF<IL. The trend for temperature dependence of hydrogen transfer between coal and tetralin was very similar to that of tetralin conversion to naphthalene. Except for ND coal, most of hydrogen of functional group in coal exchanged with hydrogen in tetralin at 300 °C. In contrast, at lower temperatures, 200 and 250 °C, hydrogen transfer from tetralin to coal was very low for each coal and hydrogen in functional group only slightly exchanged.

ACKNOWLEDGMENT

This study was supported by the Research for the Future Project of the Japan Society for the Promotion of Science (the 148 Committee on Coal Utilization Technology) under Contract JSPS-RFTF96R14801.

REFERENCES

1) Solomon, P. R., Hamblen, D. G., Yu Z., and Serio, M. A., *Fuel*, **1991**, *70*, 754.
2) Kelemem, S. R., George S. N., and Gorbaty, M. L., *Fuel*, **1990**, *69*, 939.
3) Franz, J. A. and Camaioni, D. M., *Am. Chem. Soc. Div Fuel Chem. Prepr.*, **1981**, *26*, 106.
4) Cronauer, D. C., Mcneil, R. I., Young, D. C., and Ruberto, R. G., *Fuel*, **1982**, *61*, 610.
5) Wilson, M. A., Vassalo, A. M., and Collin, P. J., *Fuel Processing Technology*, **1984**, *8*, 213.
6) Collin, P. J. and Wilson, M. A. *Fuel*, **1983**, *62*, 1243.
7) Skowronski, R. P., Ratto, J. J., Goldberg, I. B., and Heredy, L. A., *Fuel*, **1984**, *63*, 440.
8) Kabe, T., Kimura, K., Kameyama, H., Ishihara, A., and Yamamoto, K., *Energy & Fuels*, **1990**, *4*, 201.
9) Kabe, T., Horimatsu, T., Ishihara, A., Kameyama, H., and Yamamoto, K., *Energy & Fuels*, **1991**, *5*, 459.
10) Kabe, T., Ishihara, A., and Daita, Y., *Ind. & Eng. Chem. Res.*, **1991**, *30*, 1755.
11) Ishihara, A., Morita, S., and Kabe, T., *Fuel*, **1995**, *74*, 63.
12) Ishihara, A., Takaoka, H., Nakajima, E., Imai, Y., and Kabe, T., *Energy & Fuels*, **1993**, *7*, 362.
13) Qian, W., Ishihara, A., Fujimura, H., Saito, M., Godo M., and Kabe, T., *Energy & Fuels*, **1997**, *11*, 1288.
14) Kabe, T., Saito, M., Qian, W., and Ishihara, A., *Fuel*, **1999** in press.
15) Yao, J. and Evilia, R. F., *J. Am. Chem. Soc.*, **1994**, *116*, 11229.

Table 1 Ultimate analysis of coals used (% daf)[a)]

Coal	C	H	N	S	O	
ND	72.94	4.83	1.15	0.70	20.38	(L)
WA	76.9	6.7	1.1	0.3	15.0	(SB)
IL	77.67	5.00	1.37	2.38	13.58	(HVB)
UF	85.50	4.70	1.55	0.74	7.51	(MVB)
POC	91.05	4.44	1.33	0.50	2.68	(LVB)

a) Abbreviations: ND: Beulah-Zap, WA: Wandoan, IL: Illinois No.6, UF: Upper Freeport, POC: Pocahontas No.3; L: lignite, SB: subbituminous coal, HVB: high-volatile bituminous coal, MVB: medium-volatile bituminous coal, LVB: low-volatile bituminous coal. Except for WA, samples are coals of the Argonne Premium Coal Sample Program.

Table 2 HTRs of coals with tritiated tetralin

Coal	200 °C		250 °C		300 °C	
	Total HTR	HTR of OH[a)]	Total HTR	HTR of OH[a)]	Total HTR	HTR of OH[a)]
ND	4.4	1.7	4.6	-	8.1	3.8
WA	2.5	0.3	3.3	1.0	9.0	4.6
IL	4.5	1.6	5.7	0.9	14.4	6.2
UF	2.8	1.4	3.5	-	11.7	2.0
POC	2.3	0.1	2.9	-	4.2	0.5

a) Hydrogen transfer ratio of functional groups such as hydroxyl group which was determined by the reaction of tritiated coal with water at 100 °C.

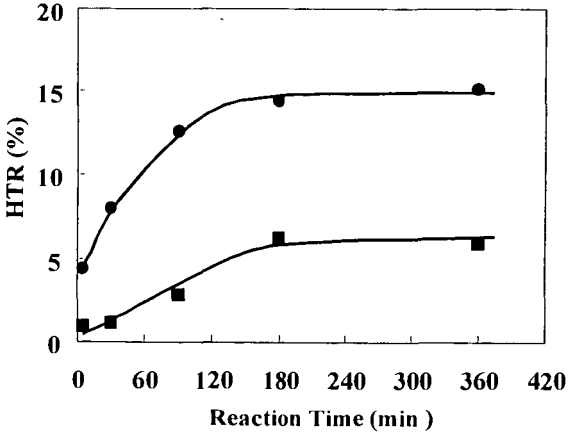

Figure 1. HTRs of Illinois No. 6 with [^{3}H]tetralin at 300 °C
●: Total HTR; ■: HTR for functional group in coal

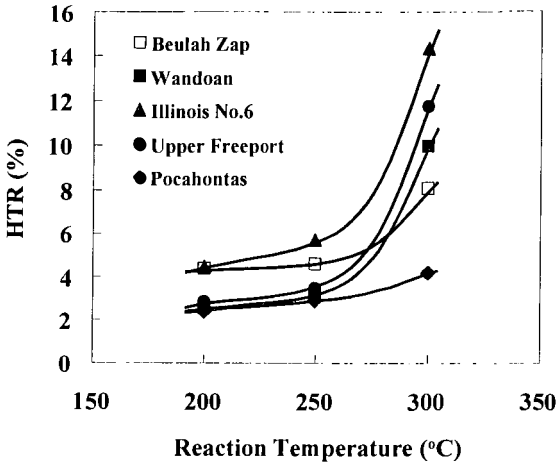

Figure 2. Effect of temperature on HTR of coal with [^{3}H]tetralin for 3 h.

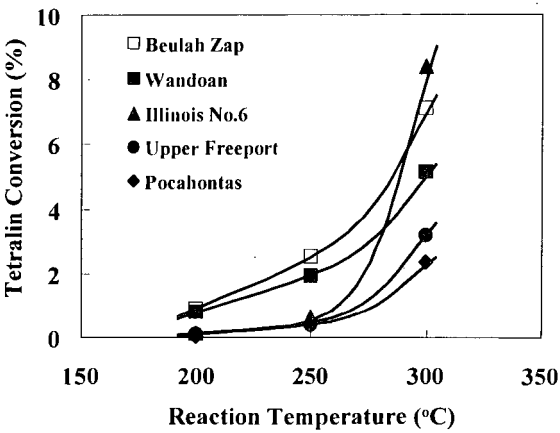

Figure 3. Effect of temperature on tetralin conversion in the reaction of coal with tetralin (3h).

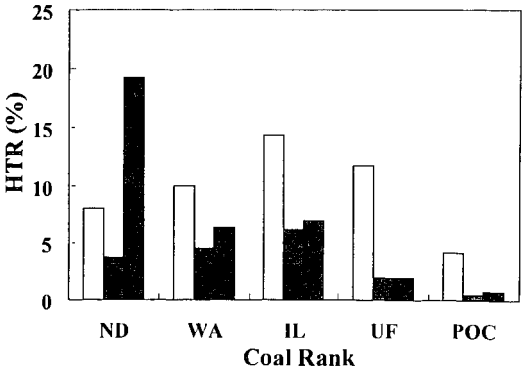

Figure 4. Comparison of HTRs of coals
□: Total HTR of coal with [^{3}H]Tetralin at 300 °C for 3 h
□: HTR of functional group in coal with [^{3}H]Tetralin at 300 °C for 3 h
■: Total HTR of functional group in coal with [^{3}H]H_2O at 100 °C for 6 h

EVALUATION OF COAL TAR PITCH FRACTIONS AS FEEDSTOCKS FOR THERMALLY STABLE JET FUEL

Suchada Butnark, Mark W. Badger, Harold H. Schobert
The Energy Institute
The Pennsylvania State University, University Park, PA 16802

Keywords: Coal tar pitch, hydrogenation, thermal stability, jet fuel, tetralin.

INTRODUCTION

Coal tar pitch, a by-product from the metallurgical coke industry, is made up of the volatile compounds evolved during coal carbonization. The inherent cyclic structure content indicates its ability to be upgraded into hydroaromatic and cycloalkane compounds that have been shown to contribute towards high fuel stability at elevated temperature [1,2,3]. Since 1960s coal tar pitch fractions have been successfully demonstrated to be a suitable feedstock for the production of jet fuels for high Mach aircraft [1,4], and have also been included in full-scale demonstrations in French fighter aircraft [5].

For the future development of high-performance jet aircraft flying at high Mach speeds, the fuel specifications have to be increased significantly due to the extreme operating conditions the fuel mat experience. The fuel may potentially be used as a heat sink in some parts of the aircraft and operated at temperature as high as 900°F. Under these conditions the fuel is stressed to temperatures above its thermal stability, which in turn leads to fuel degradation and coke formation [6,7]. It has been found that high thermal stability hydroaromatic and cycloalkane compounds are desirable components for advanced jet fuels [1,2,3]. As a result, coal tar pitch distillates, which can be converted to those structures under hydrotreatment process, are chosen again for jet fuel production. However, current evaluations on coal tar production have shown that the production of raw coal tar in the US has declined significantly over the past 30 years due to the environmental issues. But, by incorporating with suitable petroleum refinery streams, the feasibility and desirability of coal tar blending as a viable route for the production of thermally stable jet fuel would increase. Thus, we would need to protect and extend the lifetime of coal tar as a resource for advanced thermally stable jet fuel production.

The blends of various coal tar pitch distillates and suitable refinery streams have undergone laboratory-scale catalytic hydrotreatment. Coal tar pitch streams – high quinoline insolubles and low quinoline insolubles, carbon black oil, creosote oil, naphthalene still residue (NSR) and refined chemical oil (RCO) – and refinery streams – kerosene and light cycle oils (LCO) – were selected. The majority of these were eliminated early on in the study because of poor processing ability. Difficulties arising from asphaltene and pre-asphaltene precipitation from the heavy fraction were the main cause. The problems included a loss in catalytic activity and a decrease in hetero-atom removal. However, RCO proved to be an excellent feedstock. RCO is a very narrow boiling fraction, which contains over 50 % naphthalene. The hydrogenated products from the blends of RCO and LCO have produced good jet fuel fraction yields and high tetralin production – tetralin has been shown to have high thermal stability. Variations in reaction condition, pressure and temperature, as well as catalyst used have been performed to maximize the jet fuel fraction yield and tetralin conversion.

EXPERIMENTAL

Analysis Performed. Ultimate analysis of carbon, hydrogen and nitrogen compositions are obtained from a LECO CHN-600 analyzer and a LECO SC-132 sulfur determination analyzer. The feedstocks and products were analyzed by high temperature simulated distillation (HT-SimDis) GC analysis using a Hewlett-Packard 5890 series II plus fitted with a Restek MXT-500 SimDis column. The boiling point distribution and the cut point of 200-260°C fraction, jet fuel range, were observed. Quantitative analysis and chemical specification were performed on the feeds and samples using a Hewlett Packard 5890 GC fitted with a 5971 mass selective detector (MSD) fitted with a J+W DB17 capillary column. The analysis of feedstocks is shown in Table 1.

Catalyst Preparation. $NiMo/Al_2O_3$ and $NiMoP/Al_2O_3$ catalysts from Criterion have been employed for this work. The catalysts were presulfided following the method used by Ueda and co-workers [8].

Sample Used. Refined chemical oil (RCO) was obtained from Koppers Industries Company. British Petroleum (BP) supplied light cycle oils (LCO): LCO^a light cycle oil feed, LCO^b hydrogenated light cycle oil and LCO^c deeply hydrogenated light cycle oil.

Methods for Hydrogenation. Hydrogenation experiments were performed in 25 ml microautoclave reactors following the methods used by Reddy *et al* [9]. The conditions for hydrogenation experiments included pressures between 500-1300 psig H_2 and temperatures between 325-375°C. Variations in the feedstock blending composition (LCO: RCO = 3:1, 1:1, 1:3 and 0:1) were assessed as well as the effect of the two catalysts, $NiMo/Al_2O_3$ and $NiMoP/Al_2O_3$. After collecting a small part of the reaction products from the reactor, the remainder was recovered with THF followed by filtration.

RESULTS AND DISCUSSION

First, we compared the basic blends between different LCOs (LCO^a, LCO^b and LCO^c) and RCO at varying compositions and catalysts, and under the baseline conditions. Figure 1 shows that the blend of different LCO with RCO gave different jet fuel yields. LCO^c blends gave the outstanding jet fuel yield whereas those of LCO^a and LCO^b were in the same low-range yield. This is mainly due to the presence of hydroaromatic compounds in the LCO^c that contribute to the higher conversion of the RCO through hydrogen donation and shuttling reactions.

The blending compositions of LCO^c: RCO also affected the jet fuel yield (see Figure 1). By increasing the RCO concentration and using the $NiMoP/Al_2O_3$ catalyst, we see an increase in the proportion of the sample boiling in the jet fuel fraction (200-260 °C). This is due in part to the increase in tetralin in the products, through the composition of high boiling material and subsequent hydrogenation. Tetralin conversion, during RCO hydrogenation using $NiMOP/Al_2O_3$ catalyst (see Table 1) was lower than those of 1:1 blends under baseline condition in Table 2. Therefore, there was some synergistic effect promoted by the blend of LCO^c and RCO. This again was probably due the hydrogen donation reactions.

Figures 2-3 show chromatograms of blends of LCO^c and RCO before and after hydrogenation. The conversion of a significant portion of the naphthalene to tetralin can be seen along with the formation of other products. For an indication of the tetralin conversion, the calculated value was based on saturation of naphthalene ring only. Therefore, the actual value would be higher due to the contribution of the tetralin from the decomposition and hydrogenation of the high boiling point compounds. Furthermore, other cyclic structures in jet yield fraction of LCO^c also play an important role in the production of potentially thermally stable compounds. Therefore, to optimize jet fuel yield, tetralin production and other thermal stable components, we need to blend RCO with LCO^c with RCO loadings greater than 50%.

In addition, the hydrogenation conditions have formed products that have shown great increases in the H/C ratio and effective removal of sulfur and nitrogen. Table 2 shows the analyses of hydrogenated products by varying pressure, temperature and catalyst used. The H/C ratio of hydrogenated products has been increased and their colors become lighter as the increase of temperature. Sulfur and nitrogen content were decreased more than 80% and 70% respectively. This result shows that the catalysts, especially $NiMOP/Al_2O_3$, have worked well in both desulfurization and denitrogenation reactions.

Figure 4-5 shows the effects of pressure and temperature on tetralin conversion and jet fuel yield with the use of $NiMo/Al_2O_3$. Increases in temperature greatly affected both tetralin production and jet yield. The effect of pressure shows that conversion to tetralin and the fraction boiling in the jet fuel range goes through a maximum around the baseline conditions of 1000 psig. For the reactions at high temperatures, cracking of heteroatoms and large aromatic compounds and the

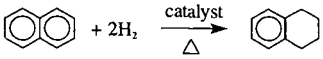

(1)

saturation of naphthalene molecules are more likely to occur. But at low-pressure condition, the reaction tends to shift chemical equilibrium to the right (Equation 1). This is why tetralin conversion is less likely to occur.

High-pressure condition also hindered the tetralin production as well as jet yield. Thus, it can be summarized that 1000 psig H_2 and 350-375 °C is the most suitable condition for hydrogenation of LCO^c: RCO blends.

CONCLUSIONS

The blend of LCO[c] and RCO under appropriate catalytic hydrogenation reaction can produce high quantities of tetralin, which indicates the potential high thermal stability, and an increase of sample boiling in the jet fuel fraction. The balance between jet fuel fraction yield, tetralin conversion and the production of other potentially thermally stable cyclic structures and can be controlled by blending composition and reaction conditions. The catalyst used plays an important role in tetralin conversion, desulfurization and denitrogenation processes.

ACKNOWLEDGEMENTS

The authors would like to express their gratitude to the Department of Defense and Air Force Wright-Patterson Laboratory for the support of this project under contract F33615-98-D2802 delivery order 3. Samples from Kopper Industries and BP Corporation are also gratefully appreciated.

REFERENCES

1. Letort, M. "Now-Make Jet Fuels from Coal", *Hydrocarbon Processing and Petroleum Refiner*, **41**(7), 1962.
2. Waiwright, H. W. "Coal's Place in Space Rocket Fuels from Tars", *Missiles and Rockets*, 43-48, October 1958.
3. Donath, E.E. and Hess, M. "Thermally Stable Hydrocarbon Fuels" *Chemical Engineering Progress*, **56**(4), 68-71, 1960.
4. Schlesinger, M.D. and Hiteshue, R.W. "Synthetic Fuel from Coal for Supersonic Aircraft", *US Bureau of Mines Report of Investigations No. 5902*, 1961.
5. Arnold, J. and Paul F.M. "Aviation Fuels from Coal", *Journal of the Institute of Energy*, 55-62, 1980.
6. Song, C., Eser, S., Schobert, H.H. and Hatcher, P.G. "Pyrolytic Degradation Studies of a Coal-Derived and a Petroleum-Derived Aviation Jet Fuel, *Energy and Fuels*, **7**(2), 234-243, 1993.
7. Heneghan, S.P., Zabarnick, S., Ballal, D.R. and Harrison III, W.E. "JP-8+100: The Development of High-Thermal-Stability Jet Fuel", *Journal of Energy Resources Technology*, **118**, 170-179, 1996.
8. Ueda, K, Matsui, H., Song, C. and Xu, W., " Catalytic Hydrocracking of Phenanthrene over $NiMo/Al_2O_3$, CoMo/ Catalysts and Metal-loaded Y-Zeolites", *Journal of the Japan Petroleum Institute*, **33**(6), 413-417, 1990.
9. Reddy, K.M., Wei, B. and Song, C., "Mesoporous Molecular Sieve MCM-41 Supported Co-Mo Catalysts for Hydrodesulfurization of Petroleum Resids", *Catalysis Today*, **1303**, 1-12, 1998.

Table 1: Ultimate analyses of LCO (a-c) and RCO.

Feed	% C	% H	% N	%S	H/C ratio	Jet range (200-260 °C)
LCO[a]	90.0	10.8	0.14	<0.05	1.44	18.5
LCO[b]	88.8	11.3	0.12	<0.05	1.53	28.8
LCO[c]	83.8	14.0	0.36	<0.05	2.00	32.5
RCO	91.7	6.5	0.43	0.42	0.84	52.1

Table 2: Analyses of hydrogenated products from refined chemical oil (RCO) and deeply hydrotreated light cycle oil (LCO) under varying conditions.

Reaction condition	NiMo				NiMoP			
	H/C ratio	%N	%S	%Tetralin Conversion	H/C ratio	%N	%S	%Tetralin Conversion
LCO: RCO = 1:1 at 1000 psig H_2								
325°C	1.50	0.12	0.042	57.0	1.50	0.13	0.053	63.1
350°C (baseline)	1.51	0.09	0.041	67.7	1.61	0.07	0.034	73.8
375°C	1.56	0.12	0.040	80.8	1.69	0.03	0.021	81.7
LCO: RCO = 1:1 at 350°C								
500 psig	1.47	0.13	0.011	63.9	1.54	0.08	0.017	74.6
1000 psig (baseline)	1.51	0.09	0.041	67.7	1.61	0.07	0.034	73.8
1300 psig	1.67	0.13	0.069	56.3	1.56	0.12	0.061	57.6

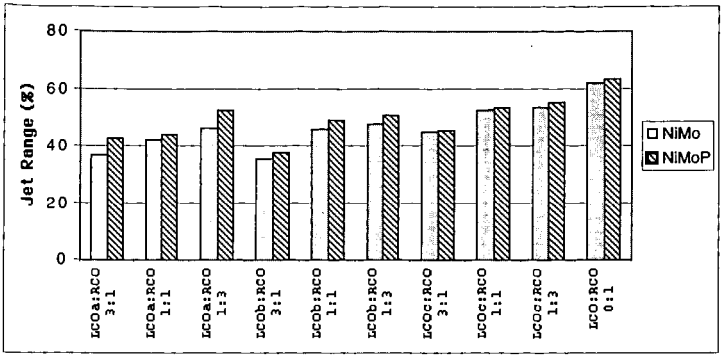

Figure 1: The effects of variation of blending types and composition on jet fuel yield.

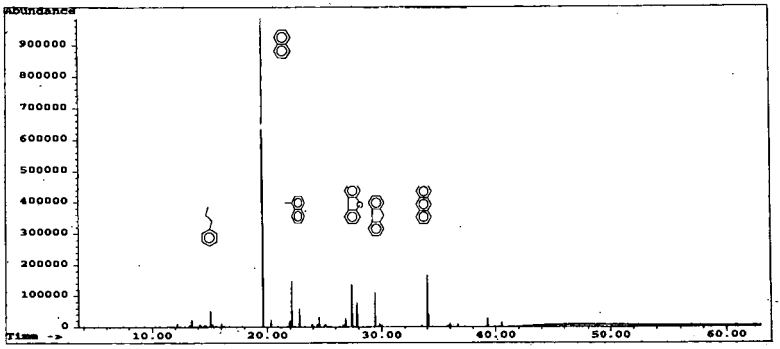

Figure 2: GC trace of the blend of LCO^c and RCO before hydrogenation reaction.

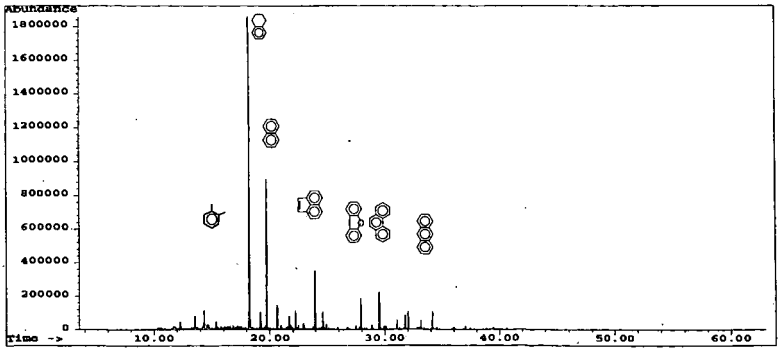

Figure 3: GC trace of hydrogenated product from the blend of LCO^c and RCO after hydrogenation at 50°C, 1000 psig H_2 by using NiMo/Al_2O_3).

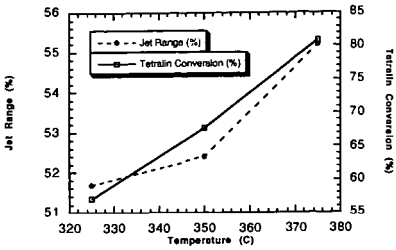

Figure 4: Temperature effects on jet fuel yield and tetralin conversion.

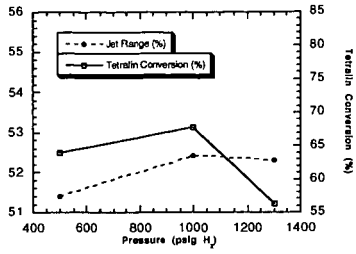

Figure 5: Pressure effects on jet fuel yield and tetralin conversion.

CARBON-CARBON BOND FISSION DURING HEAT TREATMENT OF COAL IN THE PRESENCE OF POLYCYCLIC AROMATIC COMPOUNDS

Satoru Murata, Koh Kidena, Nobuo Bandoh, Motoki Kouchi, and Masakatsu Nomura*

Department of Applied Chemistry, Faculty of Engineering, Osaka University,
2-1 Yamada-oka, Suita, Osaka 565, Japan

Keywords : Coal, Polycyclic aromatic compounds, C-C bond fission

INTRODUCTION

Coal liquefaction is believed to be one of the most important processes among coal utilization technologies in near future, which can convert solid coal to liquid fuel. In Japan, two coal liquefaction processes, brown coal liquefaction process (so called, NBCL process) and bituminous coal liquefaction process (NEDOL process), have been developed under financial support provided by NEDO. Many studies were conducted concerning the effects of the reaction temperature, residence time, the structures of recycle solvents, properties of iron catalysts, etc on the yield of liquid products.

Coal liquefaction had been thought to proceed via thermal cleavage of relatively weak bonds followed by stabilization of the resulting radicals by hydrogen donatable solvents, these mechanisms being described in the paper published in early 80's. In 1987, Malhotra *et al.* proposed another mechanism including radical hydrogen transfer (RHT) instead of thermal cleavage, with which they explained the experimental results of coal liquefaction and coprocessing of coal with heavy oil.[1] On the other hand, Franz *et al.*[2] and Savage *et al.*[3] proposed reverse radical disproportionation (RRD). The radical formed from RHT or RRD reaction, released alkyl radicals *via* β-cleavage, which will be stabilized by hydrogen donatable solvents. In this paper, we have investigated methyl groups generated from C-C bond fission of coal during heating in the presence of polycyclic aromatic compounds .

EXPERIMENTAL

Reagents and Coal Samples.

In the present study, about forty kinds of coal samples with carbon contents ranging from 67 % to 91 % (wt%, daf) were employed, which were provided by Nippon Steel Chemical Ltd., Center of Coal Utilization, Japan (CCUJ), the Iron and Steel Institute of Japan (ISIJ), and Nippon Brown Coal Liquefaction Co. Ltd. (NBCL). These coals were ground under 100 mesh and dried at 40 °C for a night before use. 9-Methyl-, 9-ethyl, and 9-methoxyanthracenes were prepared by the method reported previously. The other reagents employed in this study were commercially available and purified by conventional recrystallization or distillation prior to use.

Reaction of Coal Samples with Aromatic Compounds.

Details of reaction of coal samples with polycyclic aromatic compounds were described elsewhere.[4] Typical procedure was as follows: A mixture of 100 mg of a sample coal and 100 mg of anthracene was put in a pyrex tube (ø 6 mm x 100 mm long), then the tube being sealed. The resulting tube was put into an electric furnace preheated at 420 °C and kept for 5 min. After the reaction was quenched by removing the tube from the furnace, the products were recovered by washing the inside of the tube with methylene chloride and submitted to GC and GC-MS analyses.

MO Calculations.

All MO calculations were carried out on an Apple Macintosh computer by using a semiempirical molecular orbital calculation program, CAChe (Computer Aided Chemistry) MOPAC 94, which was purchased from CAChe Scientific Inc. The values of heat of formation for the polycyclic aromatic hydrocarbons were determined by solving the Schrödinger equations using the AM1 semiempirical Hamiltonians.

Solid State NMR Spectroscopy.

SPE/MAS ^{13}C NMR spectra were recorded on a Chemagnetics CMX-300 spectrometer under the following conditions; resonance frequency for ^{13}C 75.5 MHz; pulse width 45°; proton decoupling frequency 83 kHz (90° pulse width=3.0ms); scan number 1000; pulse delay 100 s; and MAS

frequency 10.5 kHz. Curve fitting was conducted on an Apple Macintosh computer with a data processing software, MacFID (TechMag Inc., Ver. 5.4). The classification of carbon types was as follows: carbonyl and carboxyl (the deconvoluted peak centered at 187 and 178 ppm), aromatic carbons attached to oxygen (167 and 153 ppm), aromatic carbons attached to carbon or hydrogen (140, 126 and 113 ppm), methoxy (56 ppm), methylene (40 and 31 ppm), α-methyl to aromatic ring and branched methyl (20 ppm) and terminal methyl in side chains (13 ppm).

RESULTS AND DISCUSSION

The Reaction of Coal Samples with Aromatic Compounds.

More than forty kinds of coal samples ranging from brown to semi-anthracite were employed in this study. The reaction of the coal samples (100 mg) with anthracene (100 mg) was conducted at 420 °C for 5 min in a pyrex tube. The main products containing anthracene skeleton were 9,10-dihydroanthracene (DHA), 1,2,3,4-tetrahydroanthracene (THA), and methylanthracene isomers (MA, mainly consisted of 9-methyl isomer along with minor amount of 1- and 2-methyl ones).

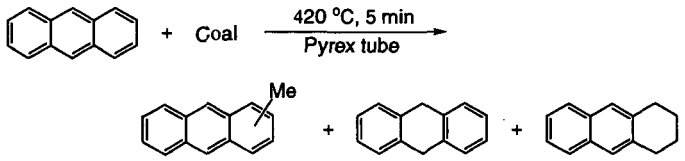

Although dimethylanthracenes and methyldihydroanthracenes were also detected, their yields were very small. In almost all runs, the recovery of anthracene derivatives was more than 90 mol%, which seems to be a reliable value for the following discussion. The results are summarized in Figure 1. DHA and THA were produced *via* hydrogen abstraction by anthracene from hydrogen donatable parts in the coal samples, while the formation of MA suggests that anthracene could capture the methyl radicals produced by C-C bond fission. Yields of DHA and THA became the highest from the reaction of the coal with *ca.* 86% of carbon (Figure 1a), while yield of MA showed different tendency, *i.e.*, the lower the coal rank was, the higher the MA yield was (Figure 1b). With elongation of reaction duration from 5 min to 30 min, MA yield increased monotonously.

We also conducted the reaction of the coal samples with pyrene and acridine, radical acceptability of which is known to be different from that of anthracene. Therefore, we would like to investigate correlation between radical acceptability and methylarene yields. The results are shown in Figure 2. In the every coals employed, yield of methylarenes obeyed the following sequence; pyrene < anthracene < acridine. We evaluated radical acceptability of these arenes according to the following equation using MO calculation program package (MOPAC 94):

$$\Delta\Delta H_f = \Delta H_f(\mathrm{ArHMe\bullet}) - \Delta H_f(\mathrm{ArH}) - \Delta H_f(\mathrm{Me\bullet})$$

where ΔH_f means standard heat of formation. The values of $\Delta\Delta H_f$ for pyrene, anthracene, and acridine were calculated to be +1.1, -4.8, and -28.6 kcal/mol, respectively. This indicates that using the arenes with higher radical acceptability, methyl radical migrates to the arenes more easily.

It is known that various kinds of carbon or methyl group are present in coal. The methyl migration reaction observed in this study should be caused by a certain type of methyl group. In order to get an information concerning the source of the methyl groups migrated, we measured solid state ^{13}C NMR spectra for the sample coals, the resulting spectra being divided into twelve curves and the carbon distribution was estimated as shown in experimental section. Figure 3 shows the plots of MA yield (wt%, from the reaction at 420 °C for 5 min) against concentration of methyl groups (methoxy, α-methyl, terminal methyl and their total) in the coals (mol%) estimated from the ^{13}C NMR spectra. The concentration of methoxy, terminal methyl and total methyl groups seemed to correlate weakly. Since the errors in the NMR measurements and estimation of carbon types were not so small, we could not determine what the origin of methyl groups migrated is. Only what we can say is larger amount of methyl gave higher yields of methylanthracenes in the reaction of coal with anthracene.

Migration of Methyl Groups from Methyl-Containing Compounds to Polycyclic Aromatics.

To discuss about the mechanism of methyl groups-migration reaction, we conducted the reaction of model compounds. We selected 9-methyl-, 9-ethyl-, and 9-methoxyanthracenes (abbreviated as 9-MA, 9-EA, and 9-MeOA, respectively). This reaction requires a hydrogen donatable solvent and a radical accepting compound, for which 9,10-dihydroanthracene (DHA) and acridine (Acr) were employed, respectively. The reaction was conducted at 420 °C for 5 min in a pyrex tube, the results being summarized in Table 1. The order of reactivity (judging from the conversion) of the anthracenes obeyed the following sequence; 9-MA ≈ 9-EA < 9-MeOA. The reaction of 9-MA afforded methylacridines (M-Acr), dimethylanthracenes (DMA), and methane in 18, 2.4, and 1.1 % yield, respectively, as the major methyl group-containing products. In the case of 9-EA, main products were ethylacridines (E-Acr, 15 %), diethylacridines (DE-Acr, 2.7 %), and ethane (3.9 %) along with small amount of methylacridines (2.2 %). In the reaction of 9-MeOA, the main products were M-Acr (44 %), methane (36 %), and anthrone (42 %).

Formation of light hydrocarbon gases and alkylacridines indicate that alkyl radicals participate this reaction and there are three possibilities for the fate of the radicals formed (Scheme1), *i.e.*, a) hydrogen abstraction to form alkanes, b) dimerization to alkanes, and c) capture with aromatics to form alkylarenes.

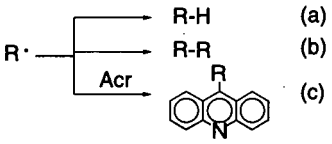

Contribution of these pathways a,b,c seemed to be varied depending on the functionality of methyl groups. Now, we are investigating the factors affecting the products distribution.

REFERENCES

1) McMillen, D. F.; Malhotra, R., Chang, S.-J.; Ogier, W. C.; Nigenda, S. E.; Fleming, R. H. *Fuel* **1987**, *66*, 1611; Malhotra, R.; McMillen, D. F. *Energy Fuels* **1990**, *4*, 184; McMillen, D. F.; Malhotra, R. *Energy Fuels*, **1991**, *5*, 179; Malhotra, R.; McMillen, D. F. *Energy Fuels* **1993**, *7*, 227; McMillen, D. F.; Malhotra, R.; Hum, G.P.; Chang, S. J. *Energy Fuels* **1987**, *1*, 193.
2) Autrey, T.; Alborn, E. A.; Franz, J. A.; Camioni, D. M. *Energy Fuels* **1995**, *9*, 420
3) Savage, P. E. *Energy Fuels* **1995**, *9*, 590
4) Kidena, K.; Murata, S.; Nomura, M. *Energy Fuels* **1998**, *12*, 782.

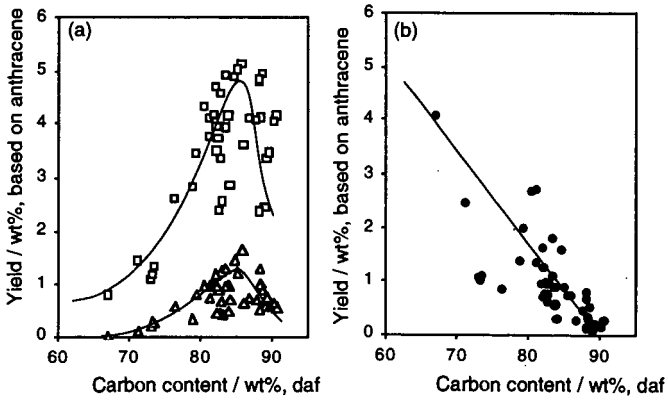

Figure 1 Plots of the yield of DHA (□, (a)), THA (△, (a)) and MA (●, (b)) from the reaction of coal with anthracene at 420 °C for 5 min against carbon content of the coals

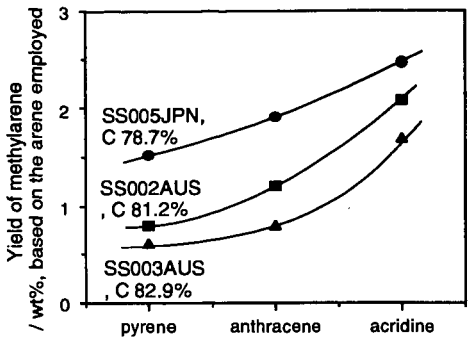

Figure 2. Yield of methylarenes from the reaction of coal with polycyclic aromatics (at 420 °C, for 5 min, in a pyrex tube)

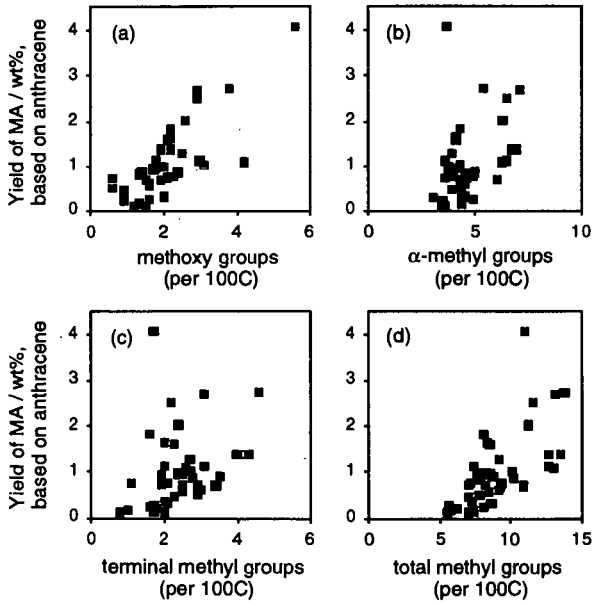

Figure 3. Plots of the yields of methylanthracene (MA) against concentration of each type of methyl group in the coal samples

Table 1. The reaction of methyl group-containing anthracene with acridine in the presence of DHA[a)]

Substrate	Conv. of Subst. (mol%)	Yield (mol%)				Yield of gas (mol%)		
		DMA	M-Acr	E-Acr	DE-Acr	H_2	CH_4	C_2H_6
9-MA	28	2.4	18	-	-	0.41	1.1	-
9-EA	28	-	2.2	15	2.6	0.37	-	3.9
9-MeOA	87	5.3	44	-	-	0.35	36	0.6

a) A mixture of substrate (0.25 mmol), Acr (0.25 mmol), and DHA (0.0625 mmol) was heated at 420 °C for 5 min in a pyrex tube.

Effects of Superacid Depolymerization and Catalytic Hydrogenation on Pyrolysis Reactivity of Illinois #6 Coal

Hideyuki TAKAGI, Takaaki ISODA, Katsuki KUSAKABE
and Shigeharu MOROOKA

Department of Materials Physics and Chemistry,
Graduate School of Engineering, Kyushu University,
Fukuoka 812-8581, Japan

KEY WORDS: coal, structural change, pyrolysis

INTRODUCTION

Pretreatments under mild conditions do not substantially alter the structure of coal and increase its extractability with organic solvents [1,2]. Up to 80 wt% of Yallourn coal, which had been oxidized at 60°C with aqueous H_2O_2 in the presence of 1-propanol, was solubilized in ethanol [1]. The ethanol soluble fraction was further hydrogenated using a Ru/Al_2O_3 catalyst in a mixed solvent of ethanol and acetic acid at 120°C for 12-72 h at a hydrogen pressure of 10 MPa [2], to give a yellowish white solid (hydrogenated white coal). This catalytic hydrogenation altered the aromatic structure of the coal, in part, and increased its reactivity with respect to pyrolysis. However, the H_2O_2 oxidation was not effective in increasing the extractability of bituminous coals.

Shimizu et al. [3,4] depolymerized a subbituminous coal using a superacid at 150°C. This was a unique process which greatly increased the solubility of coal. In the present study, Illinois #6 coal was depolymerized using the superacid, trifluoromethanesulfonic acid (CF_3SO_3H, hereafter, referred to TFMS), in the presence of solvents at 120°C, and the treated coal was then extracted with tetrahydrofuran (THF). The THF solubilized coal was then hydrogenated over a Ru catalyst at 120°C for 48 h under a hydrogen pressure of 10 MPa. Changes in coal structure and pyrolysis reactivity by the combination of superacid treatment and catalytic hydrogenation were then examined.

EXPERIMENTAL

Depolymerization via Treatment with Superacid Followed by THF Extraction: Figure 1 shows the procedure for superacid treatment and THF extraction of Illinois #6 coal. 1 g of the coal, which was pulverized to 74-125 μm in size, 3-5 mL of TFMS, and 13 mL of a solvent were mixed in an autoclave of 25 mL. Toluene, methylcyclopentane or isopentane were used as the solvent, and the suspension was stirred at 120°C for 3 h [3]. After the depolymerization, the product was neutralized with an aqueous solution (5 wt%) of Na_2CO_3. The precipitate was washed with water and extracted with THF under ultrasonic irradiation at room temperature. The mixture was then separated into THF-soluble (TS_d) and THF-insoluble (TI) fractions by centrifugation. The TS_d fraction was then subjected to hydrogenation. The raw coal was also

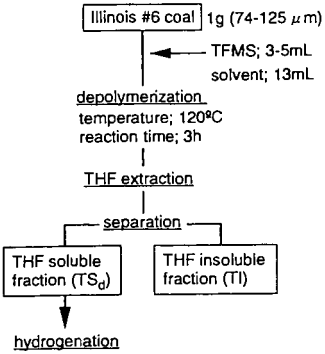

Figure 1. Deporimerization and fractionation procedure.

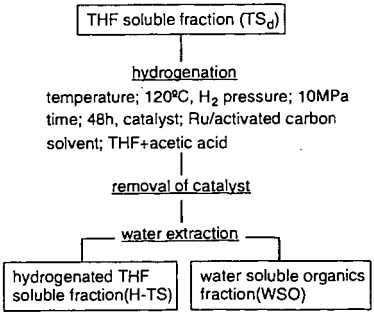

Figure 2. Hydrogenation and fractionation procedure.

extracted with THF, and the THF soluble fraction was subjected to further characterization. The TS fraction of the raw coal is hereafter referred to as the TS_r fraction.

Hydrogenation of THF Extract: Figure 2 illustrates the procedure used for the hydrogenation of the TS_d fraction. A ruthenium-supported activated carbon catalyst (metal content = 5 wt%, Wako Chemical) was used for the hydrogenation. 1 g of the TS_d fraction was dissolved in a mixture of 8 mL of acetic acid and 6 mL of THF in a 25 mL autoclave equipped with a magnetic stirrer, and hydrogenated using 1.5 g of the catalyst at 120°C for 48 h under a hydrogen pressure of 10 MPa. After the removal of the catalyst by filtration, the solvent was evaporated. The product was then extracted with water under ultrasonic irradiation, leading to a hydrogenated, THF-soluble (H-TS) fraction and a water-soluble organic (WSO) fraction. Each fraction was dried at 70°C for 6 h under vacuum, and the yields were determined gravimetrically.

Structural Analysis and Flash Pyrolysis of Products: The H/C atomic ratio of the coals was evaluated by elemental analysis, and the molecular weight was determined by GPC analysis described previously [2]. The hydrogen distribution and aromaticity (f_a) were estimated by H-NMR spectroscopy and elemental analysis using the Brown-Lander equation [5]. The thermal reactivity of the coals was evaluated by flash pyrolysis at 764°C under an inert atmosphere using a Curie-point pyrolyzer (CPP, Japan Analytical Industry, JHP-22). Inorganic gases (IOG; CO, CO_2, H_2O and H_2) and hydrocarbon gases (HCG; C_1-C_5) were analyzed using gas chromatographs (GC) equipped with TCD and FID detectors. The tar fraction was analyzed using a CPP connected to a GC interfaced with a mass spectrometer (GC/MS, Shimadzu, QP-5000) [6].

RESULTS

The TS_r and TS_d fractions were recovered as solids after the removal of the solvent, while the H-TS fraction was a viscous black liquid. Figure 3 shows the yields of the TS_r, TS_d and TI fractions. The yields are expressed in wt% of the mass of the dry raw coal. The TS yield, which was 14

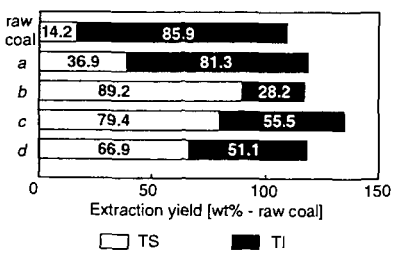

	solvent	TFMS (mL)
a	toluene	3
b	methylcyclopentane	3
c	isopentane	3
d	isopentane	5

Figure 3. Yields of TS and TI fractions by depolymerization using TFMS.

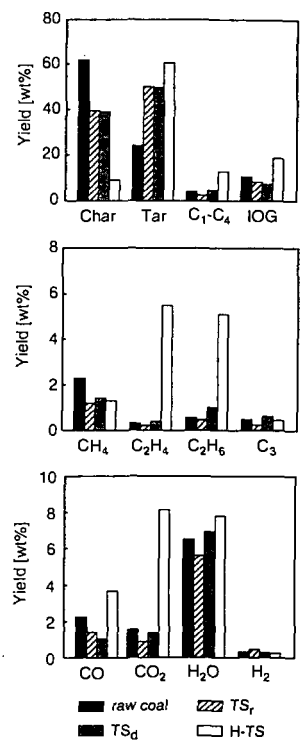

Figure 4. Product distributions of flash pyrolysis.

wt% for the raw coal, was increased by the depolymerization to 89 wt% for the case of methylcyclopentane, and 79 wt% for isopentane. Figure 4 shows the product distributions of the flash pyrolysis for the raw coal, the TS_r and TS_d fractions, and the H-TS fraction. The yields are expressed based on the initial mass of each sample used for pyrolysis. The char yield was 62 wt% for the raw coal, 40 and 38 wt% for the TS_r and TS_d fractions, respectively, and 5 wt% for the H-TS fraction. The tar yield was increased from 24 wt% for the raw coal to 61 wt% for the H-TS. The total yield of hydrocarbon gases, which were rich in ethylene and ethane, was increased as a result of the hydrogenation. The yields of CO, CO_2 and H_2O were increased, while the yield of H_2 remained unchanged by the hydrogenation.

Table 1 shows the elemental analysis of the raw coal and the TS_r, TS_d and H-TS fractions, as well as the molecular weight of the TS_r, TS_d and H-TS fractions. The H/C atomic ratio was increased from 0.89 for the raw coal to 1.52 for the H-TS fraction. The molecular weight of the H-TS fraction at the peak of the elution curve was approximately 1000. Table 2 shows the hydrogen distribution, as well as the aromaticity, of the TS_r, TS_d and H-TS fractions, as determined by H-NMR spectroscopy. The depolymerization resulted in an increase in the H_β and H_γ of the TS_r fraction. The hydrogenation of the TS_d fraction resulted in a decrease in the H_{ar}, H_α and f_a, and an increase in the H_β. The H_γ remained unchanged by the hydrogenation.

The tar component, obtained by the pyrolysis of the H-TS fraction at 764°C, contained approximately 40 components. The unit structures of 6 major components were analyzed by GC/MS, elemental analysis, molecular weight and hydrogen distribution. As shown in Figure 5, these species were composed of 1-3 rings, suggesting a partial hydrogenation of the coal structure. The yield of these species was 14 wt% for (A), 13 wt% for (B), 11 wt% for (C), 7 wt% for (D), 8 wt% for (E) and 4 wt% for (F) with respect to the initial mass of the H-TS.

DISCUSSION

The Illinois #6 coal, which was depolymerized using TFMS in the presence of methylcyclopentane, was solubilized in THF at a yield of 89 wt%. As shown in Table 2, the increase in the H_β and H_γ after superacid treatment suggests that alkyl groups, derived from the solvent, are introduced into the coal structure [3]. The decreases in H_{ar}, Ha and f_a indicate that the aromatic rings in the coal structure are hydrogenated over the Ru catalyst. The increase in H_β, which is assigned to methylene and alicyclic hydrogens, is also indicative of the hydrogenation of the aromatic structure of the coal. The H_γ, which is assigned to methyl hydrogens of the TS_d, remains unchanged by the hydrogenation, suggesting that side chains are not greatly decomposed during the hydrogenation.

No differences in pyrolysis reactivity were observed between TS_r and TS_d. The HCG yield is increased by only 2 wt% by depolymerization. Thus the superacid treatment leads to an increase in the amount of extracts without altering the pyrolysis reactivity of the TS_r fraction. The yield of volatile matters is increased by the hydrogenation from 62 wt% for the TS_d fraction to 95 wt% for the H-TS fraction. Assuming that the decrease in the f_a is caused by the hydrogenation of aromatic rings, 21 mol% of the aromatic carbons in the coal are converted to alicyclic carbons.

CONCLUSIONS

THF-solubilized coal was depolymerized with TFMS and then hydrogenated over a Ru catalyst in a mixed solvent of THF and acetic acid at 120°C. The pyrolysis reactivity of the THF-

Table 1. Elemental Analysis and Molecular Weight of the Raw Coal, TS_r, TS_d and H-TS Fractions

sample	C	H	N	$(O+S)_{diff}$	H/C	O/C	Mw [a]
	[wt% - d.a.f.]						
raw coal	74.5	5.5	1.5	18.5	0.89	0.19	
TS_r	75.3	5.5	1.4	17.8	0.88	0.18	3000
TS_d	77.2	6.3	0.9	15.6	0.98	0.15	1500~2000
H-TS	68.7	8.7	0.1	22.5	1.52	0.25	1000

[a] molecular weight

Table 2. Hydrogen Distribution and Aromaticity of TS_r, TS_d and H-TS Fractions

sample	mol/100 mol of hydorogen				f_a
	H_{ar}	H_α	H_β	H_γ	
TS_r	25.3	29.4	34.0	4.9	0.61
TS_d	19.9	22.5	39.8	11.2	0.60
H-TS	10.1	13.3	53.2	12.0	0.39

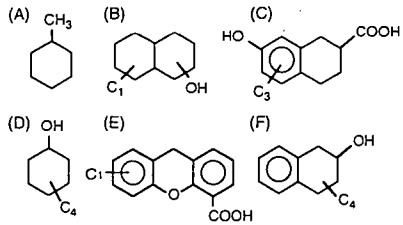

Figure 5. Unit structures of major compounds formed by pyrolysis of the hydrogenated TS fraction.

solubilized coal was increased by catalytic hydrogenation, which clearly altered the aromatic structure of the coal.

ACKNOWLEDGMENTS

This research was supported by Japan Society for the Promotion of Science (JSPS), Organization of New Energy and Industrial Technology Development Organization (NEDO), and Center for Clean Coal Utilization, Japan (CCUJ). The support by Research for the Future Projects (Coordinator; Prof. M. Iino, Tohoku Univ.) and International Joint Research Program (Coordinator; Prof. M. Nomura, Osaka Univ.) is especially acknowledged.

REFERENCES

[1] Isoda, T.; Tomita, H.; Kusakabe, K.; Morooka, S.; Hayashi, J.-i. *Proc. of Intern. Conference on Coal Science* **1997**, *2*, 581.
[2] Isoda, T.; Takagi, H.; Kusakabe, K.; Morooka, S. *Energy Fuels* **1998**, *12*, 503.
[3] Shimizu, K.; Karamatsu, H.; Inaba, A.; Suganuma, A.; Saitou, I. *Fuel* **1995**, *74*, 853.
[4] Olah, G. A.; Bruce, M. R.; Edelson, E. H.; Husain, A. *Fuel* **1984**, *63*, 1130.
[5] Brown, J. K.; Lander, W. R. *Fuel* **1960**, *39*, 87.
[6] Hama, H.; Matsubayashi, K.; Murata, S.; Nomura, M. *J. Jpn. Inst. Energy* **1993**, *72*, 467.

DETERMINATION OF STRUCTURAL VARIATIONS FOR A SERIES OF STEAM ACTIVATED ANTHRACITES

M. Mercedes Maroto-Valer, John M. Andrésen and Harold H. Schobert

The Energy Institute, The Pennsylvania State University,
405 Academic Activities Bldg, University Park, PA-16802, USA

Keywords: Activated carbon, anthracite, structural variations, porosity.

Although significant research has been conducted on the characterization of porosity, significantly less attention has been paid to the structural variations occurring during the activation process. Accordingly, this paper presents the structural characterization of a series of activated carbons using several analytical techniques. For this study, a Pennsylvania anthracite was steam activated in a vertical tube furnace for different periods of time. Solid yields below 60% enhanced the formation of mesopores. With increasing activation time, the atomic H/C ratios decrease and there is a significant rise in the condensation of the aromatic structures, regardless of the type of porosity developed.

INTRODUCTION

There is a continuous worldwide growing demand for the production of activated carbons, due to the increasing number of applications of these materials, especially those related to environmental protection [1]. The main reason for this expanding market is the ubiquitous use of activated carbons as adsorbent materials in a broad range of increasing applications, including both gas-phase and liquid-phase adsorption. In the US, the demand for activated carbon is forecast to increase 5-6% annually, and it is expected to reach 440 million pounds in the year 2002. The adsorptive properties of activated carbons are known to depend on both their porous and chemical structures. Although significant research has been conducted on the characterization of porosity, significantly less attention has been paid to the structural variations occurring during the activation process. Accordingly, this paper presents the structural characterization of a series of activated carbons by using several analytical techniques. For this study, anthracites were selected as precursors for the production of activated carbons. Their inherent fine pore structure makes them excellent raw materials for producing adsorbent carbons with molecular sieve properties for gas separation in pollution control technologies [2]. A Pennsylvania anthracite was steam activated in a vertical tube furnace for different periods of time. The chemical structures of the resultant series of activated samples were extensively characterized using elemental, solid state ^{13}C NMR and X-ray analyses. The structural variations determined by the above techniques were related to the adsorptive properties of the resultant activated carbons.

EXPERIMENTAL PROCEDURE

The Pennsylvania anthracite selected (Lehigh Coal & Navigation) contains ~ 6.8 % ash (db) and the atomic H/C ratio is 0.21. For this study, the anthracite was ground and sieved to generate particle size fractions of 150-250 μm and 1-3 mm. The activation set-up used consists of a vertical tube furnace, where a stainless steel tube reactor, containing around 5 g of sample, is placed. A thermocouple inserted in the reactor monitors the sample temperature. When the sample reaches the activation temperature (850°C), a flow of steam is introduced by pumping water into the reactor at low flow rates (~1.2 g/min). The porosity of

the samples was characterized conducting N_2 adsorption isotherms at 77K using a Quantachrome adsorption apparatus, Autosorb-1 Model ASIT, as previously described [3]. The elemental analyses were carried out on a Leco CHN analyzer. The solid state ^{13}C NMR measurements were conducted on a Chemagnetics M-100 instrument with a field of 2.4 T and a spinning speed of 3.5 kHz. For the quantitative single pulse excitation experiments (SPE) about 8000-14000 scans were acquired with recycle delays ranging from 60-100 seconds. As in earlier work [4], tetrakis(trimethylsilyl)silane (TKS) was used as an internal standard to determine the proportion of carbon observed by SPE. The dipolar dephasing (DD) SPE experiments were conducted using dephasing times between 1-400 μs.

RESULTS AND DISCUSSION

Development of porosity Table 1 lists the solid yields, BET surface area (SA), total pore volume (V_{TOT}) and micro- (Vmicro) and mesopore (Vmeso) volume for the activated anthracites. For the particle size fraction 150-250 μm, the solid yield decreases as the activation time increases, going from 59% to 33% after 60 and 90 minutes' activation, respectively. As expected, the larger particle size fraction presents a much higher solid yield, 79% for the 1-3 mm fraction at 90 minutes activation, compared to that of 33% for the 150-250 μm fraction. Thus, the solid yield is strongly dependent on the particle size of the precursor, with higher yields for the bigger particle size fractions. The anthracite fraction 150-250 μm activated for 90 minutes presents the highest SA and V_{TOT} (1037 m^2/g and 0.46 cc/g, respectively), while the fraction 1-3 mm activated for 90 minutes presents the lowest SA and V_{TOT} (284 m^2/g and 0.13 cc/g, respectively). These differences are strongly related to the solid yields [5]. A very good correlation has previously been obtained between the solid yields and the surface area and total pore volume, regardless of the particle size of the precursor [5].

The adsorption isotherms of the raw anthracite and the activated samples are Type I, corresponding to microporous systems. Table 1 also lists the micro- and mesopore volumes of the activated anthracites and Figure 1 shows the evolution of the micro- and mesopore volume with solid yield. For all the activated anthracites, the micropore volume is significantly larger than the mesopore volume. However, extensive gasification (solid yields < 60%) seems to promote the formation of mesopores, as illustrated by the rapid change of slope of the mesopore volume evolution (Figure 1). For instance, the mesopore volume accounts for only ~8% of the total pore volume at 59% solid yield (fraction 150-250 μm activated for 60 minutes), while the mesopore volume comprises ~19% of the total pore volume at 33% solid yield (fraction 150-1250 μm activated for 90 minutes). Previous studies have shown that the increasing formation of mesopores with decreasing solid yields are due to the removal of some pore walls and enlargement of some micropores [2].

Structural changes Table 2 lists the atomic H/C ratios for the parent anthracite and activated samples. As expected, the atomic H/C ratios decrease with activation, going from 0.21 for the parent anthracite to 0.07 for the sample activated for 90 minutes (150-1250 μm). Solid state ^{13}C NMR experiments were conducted in all the samples, using the quantitative Single Pulse Excitation (SPE) method [4]. Figure 2 shows the ^{13}C SPE spectrum for the anthracite (150-1250 μm) activated for 90 minutes. The internal standard (TKS) used for the quantitative SPE experiments gives a resonance at 3.2 ppm, while the aromatic carbon band is centered at ~122 ppm. The spectrum is dominated by the aromatic peak accounting for >99% of the total carbon. This is also the case for all the samples investigated, where the carbon aromaticity (fa) is ~1 (Table 2). The higher concentrations of paramagnetic centers expected in the activated samples did not affect the amount of carbon observed by SPE. For instance, for the anthracite (150-1250 μm) activated for 90 minutes, that is presumably the sample with the highest concentration of free radicals, over 90% of the carbon was observed by the SPE technique.

Additional structural information can be obtained by conducting NMR dipolar dephasing (DD) experiments to determine the proportions of non-protonated aromatic carbons ($f_{non-prot}$) and further calculation of bridgehead aromatic carbon [4]. Figure 3 shows the ^{13}C SPE-DD spectra for the parent anthracite, with dephasing times of 1, 40, 150 and 300 µs. The signal from protonated carbon has decayed after 40 µs, and the remaining signal is from the non-protonated aromatic carbon. The ratio of non-protonated to total aromatic carbon can be found by deconvoluting the decay of the NMR signal, as illustrated for the parent anthracite in Figure 4. The initial decay of the signal intensity is dominated by the dephasing of the protonated aromatic carbons and can be described with a Gaussian lineshape, while the longer decay is attributed to non-protonated aromatic carbon and is Lorentzian distributed. Table 2 lists the $f_{non-prot}$ for all the samples investigated. With increasing activation time, there is a significant rise in the $f_{non-prot}$ indicating an increase in the degree of condensation of the aromatic structures. The ^{13}C NMR structural data for all the activated anthracites will be correlated with X-ray data and the atomic H/C ratios.

CONCLUSIONS

Anthracites can easily be converted into activated carbons by steam activation. The particle size of the precursor strongly affects the solid yields of the resultant activated samples, with higher yields for bigger particle size fractions. For all the activated anthracites, the micropore volume is significantly larger than the mesopore volume. However, solid yields below 60% enhance the formation of mesopores. The SPE ^{13}C NMR experiments conducted show that with increasing activation time, there is a significant rise in the condensation of the aromatic structures, regardless of the type of porosity developed. Mechanisms that correlate the evolution of the porous structure with the chemical structure will be reported.

ACKNOWLEDGMENTS

The authors wish to thank the Consortium for Premium Carbon Products from Coal (CPCPC) at the Pennsylvania State University and the Research Council of the Basque Government for financial support. We also want to thank Lehigh Coal & Navigation Company for providing the anthracite sample.

LITERATURE CITED

1. Song, C.S. and Schobert, H.H., 1995, Fuel, **75**, 724.
2. Gergova, K., Eser, S. and Schobert, H.H., 1993, Energy & Fuels, **7**, 661.
3. Maroto-Valer, M.M., Taulbee D.N., and Schobert H.H., 1998, Prepr. Am. Chem. Soc. Fuel Division, **44**, 101.
4. Maroto-Valer, M.M., Andrésen, J.M., Rocha, D.C. and Snape, C.E., 1996, Fuel, **75**, 1721.
5. Maroto-Valer, M.M., Andrésen, J.M., and Schobert, H.H., 1999, 24th Biennial Carbon Conference, In Press.

Table 1: Yield, BET-surface areas, and total, micro- and mesopore volume for the activated anthracites [1].

	Activ. time min	Yield %	SA m^2/g	V_{TOT} cc/g	V_{micro} cc/g	V_{meso} cc/g
150-250 µm	60	59	613	0.32	0.30	0.02
150-250 µm	90	33	1037	0.46	0.37	0.09
1-3 mm	60	79	284	0.13	0.12	0.01

[1] The solid yields and surface areas are expressed in ash free basis.

Table 2: Atomic H/C ratios, carbon aromaticities (fa) and proportion of non-protonated aromatic carbon (fnon-prot) for the parent and activated anthracites.

	Activ. time / min	Atomic H/C	fa	fnon-prot
Parent	--	0.21	0.99	0.76
150-250 µm	60	n.d.	1.00	0.86
150-250 µm	90	0.07	1.00	0.93

n.d.: Not determined

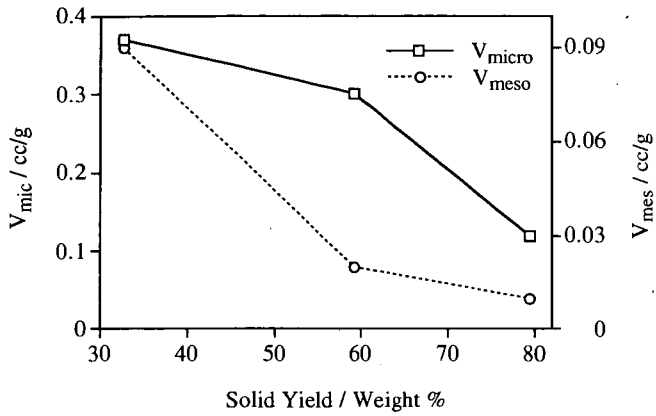

Figure 1 Evolution of the micro- and mesopore volume for the activated samples as a function of the solid yield.

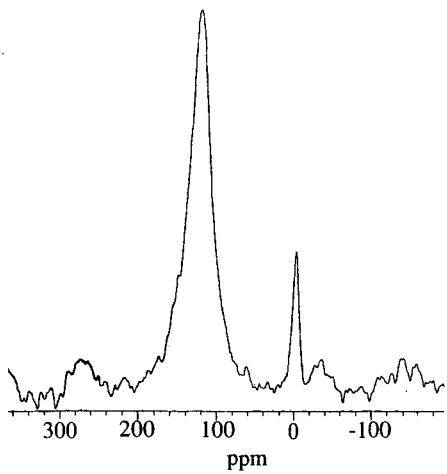

Figure 2 Solid state ^{13}C NMR spectrum for the anthracite (150-1250 µm) activated for 90 minutes using the quantitative SPE method.

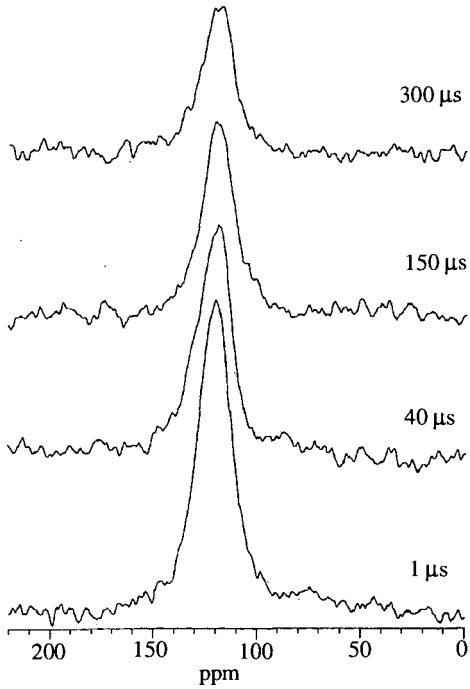

Figure 3 Spectra from SPE-DD ^{13}C NMR spectra for the parent anthracite (150-250 µm), with a dephasing time of 1, 40, 150 and 300 µs.

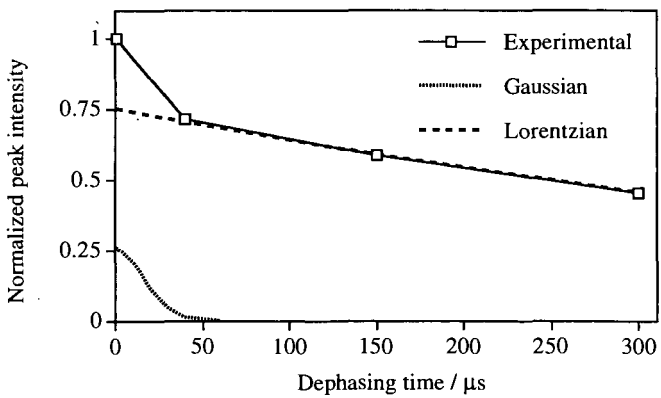

Figure 4 Plot of aromatic carbon peak intensity from the SPE dipolar dephasing experiments for the parent anthracite.

THE INVESTIGATION OF THE STRUCTURAL FACTORS FOR THE APPEARANCE OF COAL PLASTICITY

Koh Kidena[a], Masataka Hiro[a], Tsukasa Chikada[b], Satoru Murata[a], and Masakatsu Nomura[a]

[a] Department of Molecular Chemistry, Graduate School of Engineering, Osaka University, 2-1 Yamada-oka, Suita, Osaka, 565-0871, JAPAN
[b] Sumitomo Metal Industry, Kashima, Ibaragi 314-0255, JAPAN

Keywords: Coking coal, Coal plasticity, Heat-treatment

INTRODUCTION

Even now, about a half of coal consumption in Japan corresponds to coke production for steel making. Therefore, carbonization process is very important among coal utilization techniques. Much effort has been paied to the development of effective carbonization process and/or replacement of the present coking processes by new concept such as the direct ion ore smelting process because our country has been imported almost all the coking coals and worried about a precious resource exhausting problem. Therefore, a deep understanding of plastic phenomena of coal was desired earnestly. We have been studying the phenomena of fusibility of coals by the estimation of amounts of transferable hydrogen, the measurement of their solid-state ^{13}C NMR spectra and their thermogravimetric analyses (TGA)[1,2]. In those investigations, we found the relationship between R_{max}/WL (obtained from TGA) and Gieseler fluidity and also that solid state ^{13}C NMR can evaluate the amount of transferable hydrogen. We referred to the schematic illustration of the structural change during heating which was proposed by Spiro[3] in considering the mechanism of coal plasticity. Although Spiro's illustraion was based on the chemical structure of coal of 1980's, the structural analyses of coal and the detailed analyses of structural change during heating should be examined again in order to understand fusibility chemistry of coal at the level of molecule. Snape et al.[4] reported the characterization of partially carbonized coals based on solid-state ^{13}C NMR and optical microscopy: the change of aromatic cluster size with the heat-treatment was discussed. In the present study, we employed a typical coking and a non-coking coals, Goonyella and Witbank. Ruthenium ion catalyzed oxidation (RICO) reaction of two coals was performed to get information concerning aliphatic portion of these coals. At the same time, the sample coals were heat-treated in the electric furnace in order to observe the structural changes during heat-treatment at the level of molecule, and the resulting char fraction and the devolatilized tar fraction were analyzed by solid-state ^{13}C NMR and FT-IR spectroscopy, respectively.

EXPERIMENTAL SECTION

Samples.

The coal samples used in this study were Goonyella coal (GNY; C 88.1%, H 5.1%, N 1.9%, daf.) from Australia and Witbank coal (WIT; C 82.7%, H 4.5%, N 2.2%, daf.) from South Africa. WIT is called as non-coking coal in the field of coke industry, however, this coal shows a little degree of plasticity. The sample coals were provided by the Iron and Steel Institute of Japan, these being pulverized (-100 mesh) and dried at 60°C under vacuum for a night prior to use.

Ruthenium ion catalyzed oxidation (RICO) reaction of coal.

Coal sample (1 g), $NaIO_4$ (20 g) and $RuCl_3 \cdot nH_2O$ (40 mg) were put into a glass flask and stirred in the presence of mixed-solvent, H_2O (30 ml), CH_3CN (20 ml) and CCl_4 (20 ml), under the nitrogen flow at 40°C for 48 h. The resulting carbon dioxide was purged with N_2 flow through $CaCl_2$ and ascarite, and the yield of CO_2 was determined by the weight increase of ascarite. The details of the products workup and analysis were indicated elsewhere[5]. We could analyze the fractions containing lower carboxylic acids, higher carboxylic acids, aliphatic polyacids, and aromatic polyacids.

Heat-treatment of coal and analysis of the products.

Heat-treatment of coal was conducted by using a tubular electric furnace (Isuzu DKRO-14K with a temperature controller EPP-14) under 50 ml/min of nitrogen stream. One gram of coal sample was placed at the center of the quartz tube, and heated up to a determined temperature at a heating rate of 3 K/min. Final temperatures of heat-treatment were softening, maximum fluidity and resolidification temperatures of each coal (these were determined by Gieseler plastometry; 397, 456 and 498°C for GNY and 412, 432 and 446°C for WIT, respectively). The resulting char and tar fractions were recovered and weighed to obtain their yields. Tar fractions were analyzed by FT-IR spectroscopy (Shimadzu FTIR-8100M), and char fraction by ^{13}C NMR spectroscopy (Chemagnetics CMX-300).

RESULTS AND DISCUSSION

RICO reaction of two sample coals

In order to observe the structural differences between GNY and WIT at the level of molecule, we performed RICO reaction of these two coals. After the reaction, we recovered carbon dioxide, lower carboxylic acids, acids in organic layer and water layer, and residue with less solubility and high molecular weight materials. The yields of carbon dioxide reached around 50% of the whole product because of the high aromaticity of these coals, however, the carbon recovery of this reaction was excellent; 96% for GNY and ~100% for WIT. We determined the amount of a series of mono- and dicarboxylic acids from the analyses of lower acids fraction and organic layer. Figure 1 shows the distribution of mono- and dicarboxylic acids. Monoacids correspond to the side chains in coal, while diacids indicate the presence of bridge bonds between two aromatic moieties. From Figure 1a, we can recognize ~3 mol/100molC of acetic acid derived from methyl group in coal, and the amount of other acids derived from longer side chains decreased monotonously with the number of carbon. Diacids also showed similar tendency. As to the comparison of GNY and WIT, several differences were found: longer side chains and bridges were detected in larger amount for WIT than for GNY, and the longest side chains and bridges were found for WIT. As the other products derived from RICO reaction of coal, we obtained aliphatic polycarboxylic acids and aromatic polycarboxylic acids. The precursors of these acids were considered to be alicyclic structure attached to aromatic cluster and highly condensed aromatic cluster, respectively. However, the apparent differences of the amounts of these acids between two coals could not be observed. The results obtained by ^{13}C and ^{1}H NMR of two coals indicated that GNY had slightly larger aromatic cluster than WIT.

Structural changes during heat-treatment

We performed the heat-treatment of GNY and WIT in the electric furnace in order to investigate the structural changes during heating. The devolatilization started at about 300°C, and the deposition of tar fraction appeared around 400°C in the heat-treatment of coals. We recovered char and tar fractions after the end of heat-treatment. Other products were gases such as CH_4 and CO_2, and lighter hydrocarbons such as benzene. The yields of char and tar fractions obtained by the heat-treatment of coals at above three different temperatures were shown in Table 1. The weight loss (100% - char yield) at each heat-treatment temperature was similar to the data obtained from TGA, however, they were not exactly same because of the limitation for temperature control in the furnace during heat-treatment using an electric furnace. Atomic hydrogen/carbon ratio of char fraction decreased as the heat-treatment temperature increased. The decrease of H/C for a series of char samples may be due to the structural change during heating or the devolatilization of light fraction. In order to obtain more detailed information about the structural changes during the heat-treatment, we measured solid-state ^{13}C NMR spectra of the char samples. The spectra were shown in Figure 1 together with carbon aromaticity, f_a, evaluated from the ^{13}C NMR spectra for each sample. Although f_a of raw coal was different (0.83 and 0.79 for GNY and WIT, respectively), f_a values of the heat-treated samples became similar. Then, the ^{13}C NMR spectra were divided into 16 Gaussian peaks by referring to the assignment of carbon types in several model compounds, and we estimated the carbon distribution for each sample. We evaluated the change of amounts of each type of carbon based on the carbon distribution of char samples, their elemental analysis data and char yields. The data indicated the remarkable disappearances of the region of CH_2, CH_3 and oxygen or carbon substituted aromatic carbon. On the other hand, amounts of other type of aromatic carbon did not change. These results supported that elimination of alkyl side chains underwent during the heat-treatment at the temperature of coal plastic range but other structural changes such as the increase of aromatic cluster size did not occur. Furthermore, release of CH_4 was observed at temperature range of 400 - 600°C by TG-GC[2], and the decrease of H/C during heating could be explained by the release of aliphatic rich volatile fraction.

In the previous paper[2], we reported that the amount of volatile materials from coal at the temperature between maximum fluidity temperature and resolidification temperature was important for the appearance of coal plasticity. Furthermore, we analyzed the tar fractions from TG furnace by field desorption-mass spectroscopy to observe molecular weight distribution and aromaticity of the fractions, and indicated that the different rank coals provided volatile components with different composition. In this viewpoint, we analyzed tar fraction obtained from the heat-treatment of two kinds of coals by FT-IR and gas chromatography. For the materials which can be detected by gas chromatograph, a series of aliphatic hydrocarbons and complicated mixture of hydrocarbons were observed for WIT and GNY. The aliphaticity (evaluated from the ratio of peak intensity of 3040 cm^{-1} to that of 2956 cm^{-1}) of tar fractions for these coals seemed to be high in the FT-IR spectra (Figure 2). However, as the heat-treatment temperature increased, the aliphaticity of tar fraction evaluated from FT-IR spectra dropped. Therefore, the volatile materials in the plastic stage had higher aromaticity than those before softening. We can calculate apparent H/C ratio of the volatilized fraction (including lighter fraction than tar) based on the yield of char and elemental analysis data of raw coal and the char. It was higher for GNY than for WIT. FTIR results did not agree with them,

but we can explain this by the fact that GNY coal released more amount of CH_4 during the heat-treatment as reported previously[2].

SUMMARY

We obtained the information concerning about aliphatic portion of two sample coals by using RICO reaction, which oxidize aromatic carbon in coal, and we observed the structural changes during heat-treatment of two coals. As to the structural features of original coal, RICO reaction implied that longer aliphatic chains or bridges were existed in WIT than in GNY, and the size of aromatic cluster for GNY was evaluated to be somewhat larger than that for WIT according to the ^{13}C NMR data. The structural changes during heat-treatment were also observed. The increase of f_a and the decrease of H/C were observed in the char fraction, while the tar fraction has aliphatic carbons richly. The differences of structural feature and pyrolytic behavior between coking and non-coking coals were not so large, therefore, it is interesting to pay attention to the detailed analyses of both volatile fractions before softening and in the plastic range.

ACKNOWLEDGMENT

This work was partially supported by a Grant-in-aid provided by the Iron and Steel Institute of Japan.

REFERENCES

1. Kidena, K.; Murata, S.; Nomura, M., *Energy Fuels* **1996**, *10*, 672.
2. Kidena, K.; Murata, S.; Nomura, M., *Energy Fuels* **1998**, *12*, 782.
3. Spiro, C. L., *Fuel*, **1981**, *61*, 1121.
4. Maroto-Valer, M. M.; Atkinson, C. J.; Willmers, R. R.; Snape, C. E., *Energy Fuels* **1998**, *12*, 833.
5. Artok, L.; Murata, S.; Nomura, M.; Satoh, T. *Energy Fuels*, **1998**, *12*, 391.

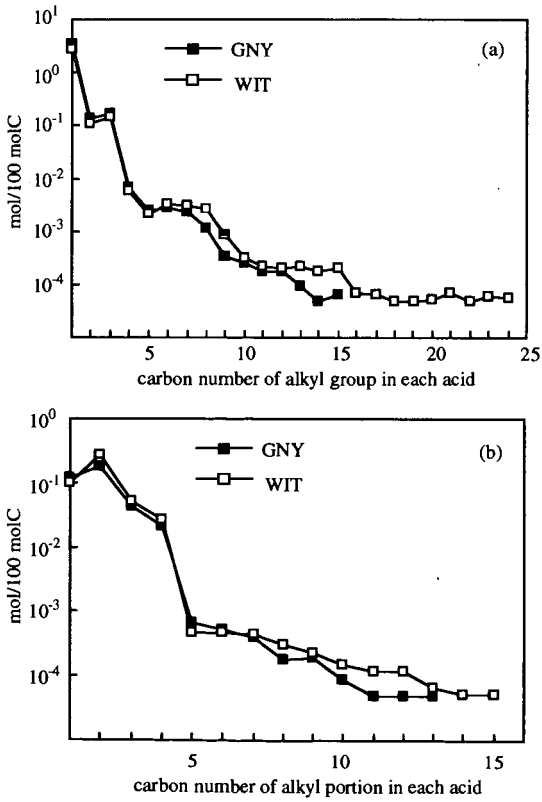

Figure 1. The yields of (a) monocarboxlic acids and (b) dicarboxylic acids from RICO reaction of GNY and WIT.

Table 1. The yields of char and tar after heat-treatment of coals and atomic H/C of char

Coal	Heat-treatment temperature (℃)	Yields (wt%, db.) Char	Tar	Atomic H/C ratio of char
GNY	raw coal	-	-	0.69
GNY	397	97.5	1.4	0.68
GNY	456	89.2	7.5	0.59
GNY	498	86.9	11.0	0.56
WIT	raw coal	-	-	0.65
WIT	412	90.0	4.8	0.63
WIT	432	87.0	6.9	0.60
WIT	446	85.6	6.4	0.59

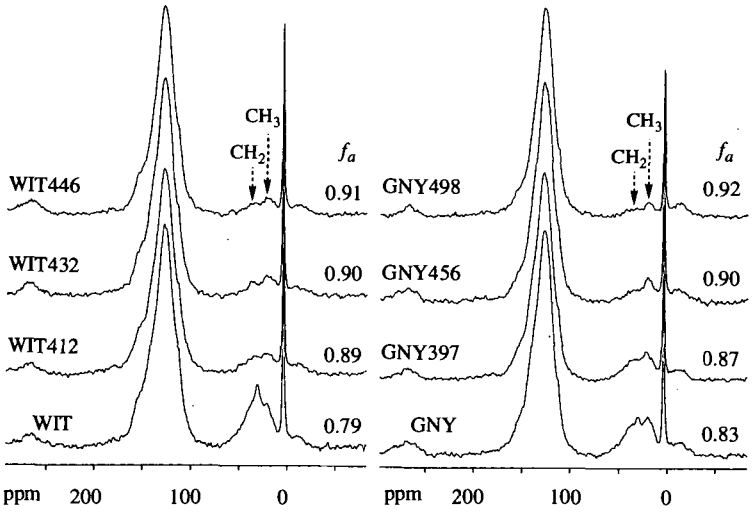

Figure 2. ^{13}C NMR spectra and their carbon aromaticity (f_a) of original coals and char samples after heat-treatment.

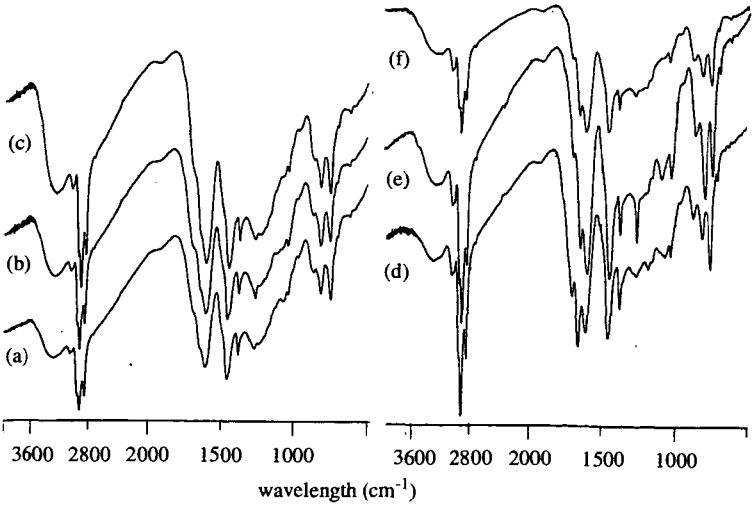

Figure 3. FT-IR spectra of the tar fraction obtained from the heat-treatment of WIT coal at (a)412, (b)432 and (c) 446 °C and GNY coal at (d)397, (e)456 and (f)498 °C.

THE CHARACTERIZATION OF PRODUCTS FROM COAL/RESID CO-COKING

Anne E. Fickinger, Mark W. Badger, Gareth D. Mitchell and Harold H. Schobert
The Energy Institute
Coal Utilization Laboratory
The Pennsylvania State University, University Park, PA. 16802

Keywords: Coal/resid co-coking, coal-derived jet fuels, coke formation.

Introduction

Co-coking is a novel process that incorporates the fundamentals of coal liquefaction and coal pyrolysis. The main motivation behind this novel process was to obtain coal-derived liquid products and carbon-rich solid products, by introducing coal and petroleum resid into a delayed coking operation and simultaneously upgrading them. The liquid products obtained would contain coal-derived material that is desirable because it would include cyclic structures, which when hydrotreated would produce a product that may have higher thermal stability than petroleum-based fuels in advanced aircraft applications. This is important since the next generation of aviation fuel may use the fuel as a heat sink, requiring the fuels to withstand the higher operating temperatures of high Mach aircraft.

In the past direct coal liquefaction processes satisfied the need for producing a feedstock for coal-derived jet fuel, that was a high yield of low-boiling aromatic hydrocarbons, which can be upgraded to hydroaromatic and cycloalkane compounds [1]. Coal liquefaction at present is not an economically viable solution. Coal pyrolysis is also a process that yields these coal-derived products using mild operating conditions. However, the main products obtained from coal pyrolysis are water, carbon oxides and light hydrocarbon gases while the desired coal-derived liquids are produced in low quantities [2]. In our approach to this study we wanted to see how we could adapt a well known and extensively used process for the production of coal-derived feedstocks for advanced jet fuel production. To this end we chose to study how we could utilize the delayed coking process.

Delayed coking is a process used commercially to obtain quality coke and light hydrocarbon fractions from low value petroleum resids and decant oil. This process typically operates in the temperature range of 450-500 °C [3]. Martin and co-workers researched the effects of simulating delayed coking conditions with the co-processing of resid and coal, on the overall products formed [4].

The work presented here represents a continuation of previous studies of co-coking [4,5,6], while focusing in on the characterization of the coal-derived products from this novel co-coking process.

Experimental

Three coals were selected from the Penn State Coal Sample Bank and Database based on their high fluidity, high volatile content and relatively low ash values. Two of the coals were high volatile bituminous coals from Virginia, while the third was a high volatile bituminous coal from the Pittsburgh seam. Table 1, displays the main characteristics of the three coals selected for co-coking. The samples were ground to a -60 mesh and vacuum dried at 110 °C for 2 hours prior to each of the experiments to remove excess moisture. The petroleum vacuum resid used was a coker feed supplied by BP America and was used as received.

Table 1. Properties of the coals used in this study

	POWELLTON	EAGLE	PITTSBURGH #8
RANK	hVAb	hVAb	hVAb
MOISTURE	6.5	6.8	2.4
ASH	5.0	5.5	10.0
%C	87.6	87.3	83.3
%H	5.8	5.6	5.7
%N	1.6	1.6	1.4
%S	0.9	-	1.3
%O	3.9	-	8.4
TEMP. MAX FLUIDITY (C)	448.0	437.0	438.0
FLUIDITY (DDPM)	30000+	30000+	20002

The reactions were carried out in vertical 25 ml microautoclave sealed reactors with *ca* 6 grams of coker feed and 3 grams of coal (resid/coal ratio of 2:1 by weight) at four temperatures (450, 465, 475, and 500 °C). The reaction length was 2 hours. The reactors were purged with nitrogen to remove any air within the reactors and left at ambient pressure. Once the reaction was complete, the reactors were cooled and the gases that evolved were vented. Any pourable liquid was collected through the stem and later included in the oils (hexane soluble fraction). The products were then removed from the reactor and subjected to a Soxhlet extraction using hexane to remove the oils, toluene to remove the asphaltenes, and finally THF to remove the preasphaltenes. The THF insolubles were then dried in a vacuum oven for 2 hours at 30 °C to remove any excess solvent so the coke product yield could be recorded on a dry weight basis.

The hexane-soluble fractions were subject to analysis using GC-MS and SimDis GC. Semi-quantitative analysis was performed using a Shimadzu GC 17A linked to a QP5000 MS and fitted with a Restek XTI-5 30 meter column. Boiling point distributions were measured using an HP 5890 II plus instrument with and FID and fitted with a 6 meter Restek MXT-500 SimDis column. Ultimate analysis was performed on the coke products using a LECO 600 CHN analyzer and a LECO MAC 400 was used for proximate analysis. Optical microscopy was also performed to determine how the coal and the resids interacted in the coke products.

Results and Discussion

Table 2 shows the overall distribution of the liquid and solid products obtained from co-coking experiments at temperatures of 450, 465, 475 and 500 °C respectively. From these results we can conclude the general trend that as the temperature increases the coke yield increases while the liquid products decreases. Similar conclusions were shown in the work carried out by Hossain and co-workers [7], in that the higher the internal pressures in the tubing bomb reactor the higher the solid carbon yield. In our system the higher temperatures promotes greater decomposition of the liquid phase to gaseous products, which in turn leads to higher internal pressure, and thus higher coke yields.

Table 2: Percent yields for the solvent fractions from co-coking experiments using Eagle, Powellton, and Pittsburgh coal plus coker feed at 450, 465, 475, and 500 °C

	PERCENT YIELDS					
TEMP (°C)	FEED	GAS	OILS	ASPHALTENES	PREASPHALTENES	COKE
450	CO-EAGLE	14.0	24.7	3.5	2.5	42.1
	CO-POWELLTON	12.1	32.2	17.2	4.0	37.1
	CO-PITTSBURGH	12.2	19.5	4.3	3.9	44.5
	COKER ONLY	16.9	52.5	5.0	1.6	21.2
	POWELLTON ONLY	19.2	2.3	1.1	20.0	86.2
465	CO-EAGLE	22.3	13.2	2.7	4.7	50.4
	CO-POWELLTON	22.5	7.1	0.3	0.8	25.91
	CO-PITTSBURGH	18.0	16.9	1.8	1.1	49.1
	COKER	16.1	47.7	7.9	1.9	14.5
475	CO-EAGLE	18.3	6.5	8.0	2.3	47.6
	CO-POWELLTON	9.1	7.7	0.6	2.4	36.5
	CO-PITTSBURGH	24.9	12.5	1.4	4.5	51.2
	COKER	37.2	28.2	1.6	6.9	25.9
500	CO-EAGLE	17.0	5.4	0.3	4.4	48.5
	CO-POWELLTON	28.3	6.7	0.3	2.2	50.6
	CO-PITTSBURGH	28.6	6.3	0.5	2.7	50.9
	COKER	47.1	16.9	0.4	6.0	35.3

Reactions preceded by a Co- indicates co-coking experiments.

GC-MS was performed on the hexane soluble fractions to obtain the specific compound distribution of the products from these experiments. The major peaks and volume percents were identified and based on the total area under the peaks. From Table 3, we can see that as the temperature of the reaction is increased, the presence of aromatic compounds increased. This would indicate that the coal conversion and the inclusion of coal derived material in the products was increasing. The coker feed on the other hand consisted of mainly saturated alkanes, which we see contributed to the high content of alkanes for the co-coking reactions at lower temperatures. It is also worth noting that the different coals produced coal-derived compounds at similar reaction temperatures. For example, co-coking experiments performed at 465 °C with Eagle produced high quantities of naphthenes, Pittsburgh produced high quantities of pyrenes, and Powellton had compounds that averaged out across the range of those identified. In addition we can see that in the identified products from co-coking, with the exception of Eagle at 465 °C, that no phenols have been identified. This suggests that their numbers have been sufficiently reduced under the reaction conditions, possibly due to their inclusion in the propagation reactions that lead to coke formation, and thus, their removal from liquid products. These compound distributions obtained from co-coking experiments showed similarities with the products derived from flash pyrolysis experiments by Nip *et al* [7].

Tables 4 shows the percentage yields of methyl substituted compounds that were identified in the oil fraction from co-coking experiments. C1, C2, C3, etc. correspond to mono, di, and tri substituted compound, respectively. It is clear to see that heat-treated coker feed does not contribute any significant quantities of substituted aromatic compounds to the oil fraction (see Table 3). Therefore all the aromatics identified come from coal-derived material.

Once again it can be seen that the different coals produced compounds with differing levels of substitution. Thus indicating the differences in the molecular composition of the coals, even though they are of the same rank classification. The most likely reason for this would be in the subtle structural differences in the reactive macerals, although this is difficult to prove. The increases in temperature are exemplified in the series of tests performed on Powellton coal between

450-500 °C. The general trend shown is that with an increase in temperature, there is a decrease in the amount of substitution in the compounds after the reaction is complete. This is due to the increased cleavage of the methyl groups from the ring at elevated temperatures, with formation of gaseous products. Although not reported, this does also contribute to a reduction in the H/C ratio in the products at higher temperature.

Ultimate analysis and optical microscopy was performed on the THF-insoluble to give an indication of the quality of the coke products being formed. Figure 1 shows that the H/C ratio for the products from co-coking have a lower value than the individual heat-treated feeds. If we calculated the H/C ratios for the products from co-coking from the results of the feeds coked individually, the estimated value is higher than the actual result from the co-coking experiments. This suggests that in co-coking we are enhancing coke formation and the formation of a more carbon-rich product. This is different from what other researchers, such as Tanabe and Gray [8], have seen. In their study the presence of fine particles such as clays, inhibited coke formation during the heat-treatment of vacuum resids.

The optical microscopy results indicated that the coal was contributing more to the mass of the coke product than the petroleum resid. The optical microscopy results also concluded that good mixing was occurring in the reactor between the resid and coal. Which was also a conclusion we gained from fluidity studies which were performed on the feeds and mixtures, that showed both the coals and coker feed were fluid over the same temperature range, and underwent devolatilization at the same rate. In addition optical microscopy gave a good indication of the fine mosaic structures formed during the co-coking conditions. Although there was little evidence to support the homogenizing of the two phases – coal and resid – the analyses showed interesting features. Amongst them were the influences of coal particle size on the degree mesophase formation and the elongated fluid structures from the coal, which were produced during the reactions.

Simulation distillation GC was performed on the hexane soluble fractions produced, to obtain boiling point distributions. For this research, the primary temperature range that was desired for the hexane soluble fraction to fall within was the jet fuel range. The jet fuel range is defined as liquids falling within the 200-260 °C temperature ranges. Figure 2, shows the boiling range for the three different coals with the coker feed, as well as the coker feed and heat-treated coals only, reacted at 465 °C. We can see the effect of combining both the coker feed and the coal lowers the yield of the jet fuels fraction by about half. It seems that the coal is acting as a catalyst for decomposition. When coal is present there is both in increase in gas and coke yields. Couple this with a decrease in liquids yields, we can assume the extra coke and gas come from the decomposition of the coker feed. One reason for this decomposition may be due to the presence of relatively high quantities of phenols being produced from the coal under the reaction conditions. Phenols are known to be good sources of radicals, which in turn can initiate retrogressive polymerization reactions, and the increased yield of coke.

Conclusions

From the work performed so far in the sealed batch reactor systems, we believe that 465 °C is the best temperature to produce the best quality oil fraction and carbon-rich product at reasonable yields. Further study will include feed ratio studies, alternative feeds and the effects of reaction length on yields. Future investigation of product characterization from this co-coking process will include the use of a vented reactor to increase the yield of liquid products at the optimum operating temperature of 465 °C, while still maintaining a relatively high yield of carbon-rich coke.

Acknowledgements

The authors would like to express their gratitude to the Department of Defense and Air Force Wright-Patterson Laboratory for the support of this project under contract F33615-98-D2802 delivery order 3.

References

1. Elliot, M.A.(Ed.), in "Chemistry of Coal Utilization Secondary Supplementary Volume", Wiley-Interscience Publication, New York, (1981).
2. Kural, O.(Ed.), in "Coal: Resources, Properties, Utilization, Pollution", Orhan Kural, Turkey, (1994).
3. Speight, J.G.(Ed.) in "The Chemistry and Technology of Petroleum. 2nd Edition", Marcel Dekker Inc., New York, (1991).
4. Martin, S.C., Tomic, J. and Schobert, H.H., ACS Div. Fuel Chem. **42**, 3, 121, (1997).
5. Badger, M.W., Fickinger, A.E., Martin, S.C., Mitchell, G.D., Schobert, H.H., AIE 8th Australian Coal Science Conference Preprints p. 245, December 1998
6. Fickinger, A.E., Badger, M.W., Mitchell, G.D., and Schobert, H.H, ACS Div. Fuel Chem.**44**, 1, 106, 1999.
7. Nip, M., de Leeuw, J.M., Crelling, J.C. Energy and Fuels **6**, 1, 125, (1992).
8. Tanabe, K. and Gray, M.R., Energy and Fuels, **11**, 5, 1040, (1997).

Table 3. Compound Distribution Yield in the Hexane Soluble Fraction

Feed	Oil Yield	Benzenes	Phenols	Alkanes	Napthenes	Fluorenes	Anthracenes/ Phenanthrenes	Pyrenes
Eagle 450	4.4	-	0.30	0.31	0.53	-	0.17	-
Pow 450	2.3	0.20	0.13	0.27	0.02	0.11	-	-
Coker 465	47.7	-	-	18.28	0.97	-	-	-
CoEagle 465	13.2	0.19	0.16	1.30	2.99	0.19	0.75	0.08
CoPitts 465	16.9	-	-	2.06	1.89	-	0.35	4.63
CoPow 450	32.2	-	-	11.34	-	-	-	-
CoPow 465	14.1	0.13	-	0.47	2.62	0.11	0.97	0.18
CoPow 475	7.7	0.32	-	-	1.84	0.11	0.77	0.13
CoPow 500	6.7	-	-	-	1.52	0.11	0.91	0.29

Table 4. Yield of substituted compounds in hexane soluble fractions from co-coking studies.

REACTION	Benzene			Phenols			Naphthenes			Fluorene	Anthracene/ Phenanthrene		Pyrene
	C1	C3	C4	C1	C2	C3	C1	C2	C3	C1	C1	C2	C1
Pow 450	-	-	-	0.07	0.09	0.04	0.08	0.14	0.06	0.02	0.09	-	-
Eagle 450	-	-	-	-	0.21	0.09	0.21	0.25	-	-	0.11	-	-
CoEagle 465	-	-	0.15	0.05	0.11	-	0.76	1.21	0.88	0.19	0.53	0.09	0.04
CoPitts 465	-	-	-	-	-	-	0.56	0.98	0.35	-	0.20	-	-
CoPow 450	-	-	-	-	-	-	-	-	-	-	-	-	-
CoPow 465	0.11	-	-	-	-	-	0.78	1.17	0.48	0.11	0.49	0.30	-
CoPow 475	-	0.04	0.27	-	-	-	0.61	0.74	0.29	0.11	0.45	0.15	0.05
CoPow 500	-	-	-	-	-	-	0.59	0.60	0.15	0.05	0.50	0.12	0.08

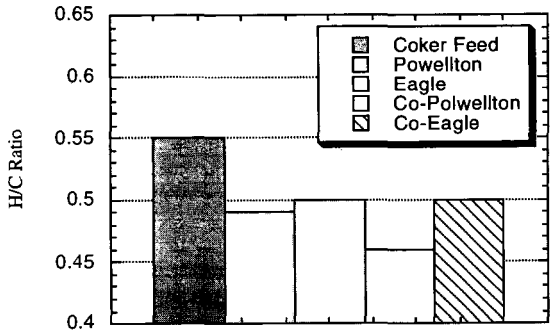

Figure 1. H/C ratios of THF insoluble products from coking experiments performed at 450 °C.

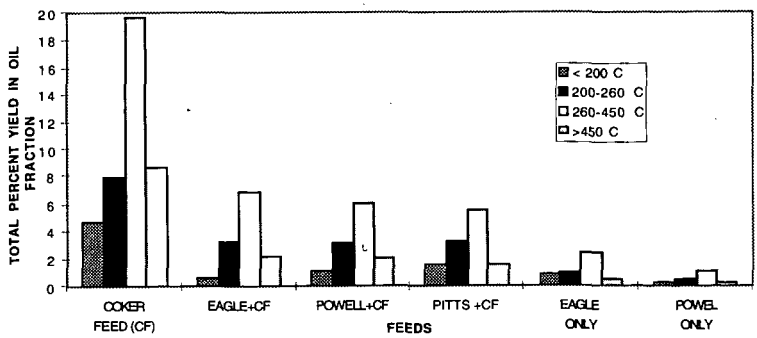

Figure 2. Boiling point distribution analysis of hexane soluble fraction from select co-coking experiments at 465 °C.